1-1-2007

Wear properties of substrates and coatings.

Hua Xu
University of Windsor

WEAR PROPERTIES OF SUBSTRATES AND COATINGS

By

Hua Xu

A Thesis

Submitted to the Faculty of Graduate Studies

through Engineering Materials

in Partial Fulfillment of the Requirements for

the Degree of Master of Applied Science at the

University of Windsor

Windsor, Ontario, Canada

2007

© 2007 Hua Xu

ABSTRACT

In this research, wear performance of five substrate materials and two hard coatings was comparatively studied using pin-on-disc sliding wear tests. Effects of hardness, counterface, load, and graphite of cast iron on the wear performance and wear mechanism were investigated. A micro-abrasion tester was designed and constructed. Micro-abrasion wear properties of those substrates and coatings were tested using the built tester. With respect to abrasive wear, the correlation between two testing methods was studied.

It is found that hardness, counterpart materials, and testing loads have significant influences on wear performance and behavior. D2 displays the best wear resistance in general. The designed micro-abrasion wear test system can be effectively used for abrasive wear study. The coatings exhibit much better sliding and micro-abrasive wear resistance than the substrates. The substrates and coatings have a similar abrasive wear performance in ranking during the micro-abrasion and sliding wear tests.

To

my dear parents, Shuxian And Hongxiang

for their endless love and encouragement

and

my dear husband and son, Yanwu and Percy

for their grateful devotion and support

IV

ACKNOWLEDGEMENTS

Sincere thanks have to be expressed to Dr. Xueyuan Nie (Associate professor, Department of Mechanical, Automotive and Materials Engineering), for his excellent supervision, great encouragement and endless support for the research.

I would like to extend my sincerest gratitude to my committee members for their useful comments that helped to improve the final copy of the thesis. I would like to acknowledge Dr. Ronghua Wei, of Southwest Research Institute, for the coating deposition and coating sample preparations.

Mr. John Robinson and Mr. Andrew Jenner are acknowledged for their generous help in technical assistance, machine building, and sample preparation. Special thanks are extended to Ms. B. Denomey for her most valuable assistance.

Sincere thanks are extended to the group members, Ms. Linlin Wang and Mr. Peng Zhang for their help and advice. Thanks also to everyone in the MAME Dept. who has offered me encouragement and support during the course of my study.

University of Windsor Tuition Scholarship and Ontario Graduate Scholarship in Science and Technology (OGSST) are greatly appreciated.

TABLE OF CONTENTS

VIII

LIST OF TABLES

LIST OF FIGURES

XVI

XVIII

XXVIII

CHAPTER 1 INTRODUCTION

Cast iron and steel have been used widely in many applications, especially in automotive industry. Many engines parts, such as engine blocks, cylinder heads, crankshafts, cylinder liners and pistons etc., are made from cast irons and steels. They are also widely used as tool materials, such as stamping die/mould materials. The wear resistance properties of cast irons and steels are very important for long service life for engine parts or tools. As commercial cast irons and steels are produced by different companies, it is necessary to evaluate their wear properties to direct the customer's selection of materials and benchmark the newly developed tribological materials.

The sliding wear test is the most popular and useful method to evaluate the wear resistance of materials,. In sliding contact, wear can occur due to adhesion, surface fatigue, tribochemical reaction and/or abrasion. Many factors influence the prevailing wear mechanism. The type of contact, namely elastic or plastic, is a function of the tangential traction on the surface, the contact area and material properties such as the yield strength. Besides the type of deformation, the properties of the solid body and of the counterbody, the interfacial element and the loading conditions determine the wear mechanisms [1]. Riahi and Alpas [2] measured the sliding wear resistance of an A30 type grey cast iron against AISI 52100 type steel within a load range of 0.3-50.0N, and a sliding speed range of 0.2-3.0m/s using a block-on-ring wear machine. A wear map was built to relate the wear rate and the wear mechanisms. Three wear regimes were described as Ultra-mild, mild, and severe wear [2]. Lim and Ashby explored wear maps

1

in a broad scope focusing on (a) pure iron and low carbon ($C \leq 0.3$ wt%) steels; (b) medium carbon ($0.3 < C \leq 0.7$ wt%) steels; (c)high carbon ($C > 0.7$ wt%) steels; (d) low alloy (2-5 wt%Cr, Mo, V and Ni) steels; (e) high alloy (typically 18wt% Cr, 8 wt% Ni) steels; and (f) tool (typically 20wt%of W, Co and Ni, 1.5wt%C) steels. The map of wear mechanisms was also constructed. Four main areas were described as (a) seizure; (b) melt-dominated wear; (c) oxidation-dominated wear (mild- and severe-oxidational wear); and plasticity-dominated wear (including delamination wear) [3].

Surface modification technologies such as laser heating, induction heating, flame hardening, gas, plasma nitriding and electrolytic plasma nitriding (EPN) have been used to improve the wear property of cast irons and steels [4-10]. For further advancement of wear properties, surface coating technologies are widely employed.

By applying an appropriate coating, many functional properties can be optimized separately for the bulk materials and the surface [11-50]. Being one of the first generation hard coatings, TiN coatings have been investigated extensively [12-16, 19-22, 24-25, 33-34, 43-50]. To meet the industrial demands for coatings with lower friction, a longer lifetimes, a better wear resistance or an improved thermal stability in different environments, improved coatings are developed. The different properties of a coating can be tuned to a desired value by alloying with suitable elements. Composite materials such as multilayer coatings and isotropic nanocomposite coatings, having structures in the nanometer range, can even show properties which can not be obtained by a single coating material alone[11]. Alloying of a coating during deposition, while maintaining the

2

deposit as a single phase, introduces the possibility of changing most of the properties of a coating. Hardness, toughness and the chemical properties are of prime interest for applications. Examples of alloyed coatings could be TiAlN, TiCN, TiBN, TiAlBN, Ti-DLC and Si-DLC etc, which are widely studied [11, 17-18, 21-25, 43, 45, 48]. Composite coatings are prepared and used as multilayers or as nanocomposites. The increased hardness of these biphased materials is a consequence of additional interfaces between different materials which hinder dislocation movement and which are places of energy dissipation and crack deflection. Some multilayer coatings include TiN/Al_2O_3 /TiC, TiN/TiCN/TiC, TiN/NbN, TiN/VN, DLC/DLC and Ti-DLC/DLC. Typical nanocomposite thin films with outstanding properties are TiSiN, TiC/DLC, TiC/a-C and TiN/MoS2 [11]. Quaternary TiSiCN coating is a newly developed composite coating which properties including wear resistance are only reported by a few papers [26-32].

Besides the sliding wear test, the micro-abrasion test is becoming popular as a method for the abrasion testing of substrate and surface coated materials. It is estimated that approximately 50-150 micro-abrasion test systems of the different types have been set up in the last few years at a number of coating suppliers, users and research establishments [35]. The reasons for this considerable interest are: (a) The test equipment is relatively cheap to purchase or manufacture. (b) Test samples can be quite small as the size of the wear scar that is produced is small. (c) It has the potential to be developed into an on-site test system. (d) The test system seems simple and is thus attractive. (e) The test system can also be used for thickness measurement [35]. Some researchers have done some

3

studies on the micro-abrasion testing system [35-41] and have tested micro-abrasive wear of materials [42-47].

According to the discussion above, it is understandable that different substrate materials from different suppliers, surface modification technology, and coating materials have significant influences on wear performance of components and tools. Particularly, there is lack of experimental comparison study tested shoulder by shoulder in terms of wear properties of various stamping die materials provided from different suppliers. Thus, in this study, 5 cast iron and steel substrate materials, named as 0050A, G3500, CarmoCast, CC2 and D2 collected from different companies have been selected. These materials have been hardened by quenching heat treatment. A classic TiN coating and an innovative TiSiCN coating as examples was deposited on stainless steel by a Plasma Enhance Magnetron Sputtering (PEMS) process [49]. The tribological and wear (sliding and micro-abrasive) properties of the substrates and coatings were investigated through pin-on-disc tribological tests and micro-abrasion wear test.

This thesis consists of seven chapters. Following the introduction, literature review mainly regarding sliding wear mechanism, micro-abrasion wear characteristics and coating performance are included in Chapter 2. Chapter 3 describes the experimental procedures. Chapter 4 demonstrates the tribological testing results of sliding wear for substrates 0050A, G3500, CarmoCast, CC2 and D2. The performance of these materials is evaluated. The effects of loads and counterface materials on the tribological performance of substrates are studied. The wear mechanisms under different loads and

4

against different counterpart materials are identified. Chapter 5 presents the mechanical and tribological property testing results of TiN and TiSiCN coatings. The effects of counterpart materials and environmental conditions are studied. The wear mechanisms under different environmental conditions and against different counterpart materials are discussed. The advantages of coating materials over substrate materials are recognized. Chapter 6 shows the micro-abrasion wear testing results of substrates 0050A, G3500, CarmoCast, CC2 and D2, and TiN and TiSiCN coatings. The anti-abrasive wear property of substrate and coating materials is evaluated. The correlation of pin-on-disc abrasive sliding wear test (against alumina pin) and micro-abrasion wear test is analyzed. The micro-abrasion wear mechanism is studied. Chapter 7 summarizes the results and recommends the future work.

5

CHAPTER 2 LITERATURE REVIEW

2.1 Introduction

Friction and wear are phenomena as old as the human race. What the modern engineer knows that the ancients did not is there are many mechanisms of wear: wear caused by adhesion, by abrasion, by oxidation, by delamination, by melting, and more [3].

Friction and wear are not intrinsic material properties but are characteristics of the engineering system (tribosystem). Usually the tribosystem consists of four elements: solid body, counterbody, interfacial elements and environment. The counterbody may be a solid, a liquid, a gas or a mixture of these. The interfacial elements could be lubricants, adsorbed layers, dirt, or, in general, a solid, a liquid, a gas or a combination of these. Sometimes, the interfacial element may be absent. The action on the elements or the interaction between them may vary widely. According to the motion, wear processes could be identified as sliding wear, rolling wear, oscillation wear, impact wear and erosive wear. Related to the interfacial element, wear processes are called dry or lubricated, or 2-body and 3-body wear. In 3-body wear, solid particles are trapped between two bearing surfaces [1].

Depending on the structure of a tribosystem, physical and chemical interactions occur between the elements that result in detaching material from the surface of the counterbody and /or the surface of the solid body. The formation of wear debris is

6

described by the wear mechanisms. Related to the wear mechanisms, wear processes could be classified as abrasive wear, adhesive wear, surface fatigue wear, oxidational wear etc [1, 51].

2.2 Sliding wear

2.2.1 Mode of wear

Sliding wear can be defined as a relative motion between two smooth solid surfaces in contact under load, where surface damage during the translational sliding does not occur by deep surface grooving due to penetration by asperities or foreign particles. The surfaces could be metallic or nonmetallic, and lubricated or unlubricated [1].

In sliding contact, wear can occur due to adhesion, surface fatigue, tribochemical reaction and abrasion. Many factors including the type of contact, the properties of the solid body and of the counterbody, the interfacial element and the loading conditions determine the wear mechanisms [1].

Different physical processes which occur during sliding wear are illustrated in Figure 2.1. Fig. 2.1(a) shows that welded junctions are built on clean mating surfaces due to adhesion. As a result of relative motion, material is detached or transferred which can lead to grooving of softer asperities by the work hardened transfer material. As shown in Fig. 2.1(b), sheet-like wear particles are formed, due to surface fatigue, during repeated plastic formation by a harder counterbody. Surface traction in sliding contact can lead to cracking of brittle materials such as ceramics (Fig. 2.1(c)). Loose wear particles, as the

7

result of cracking of surface films formed by tribochemical reactions, can act abrasively if they are harder than the base materials [1]. Three main factors that control wear of sliding surfaces are mechanical stresses, temperature, and oxidation phenomena. They may be influenced by normal load and sliding velocity. The Archard wear equation is the most frequently referenced "law" of sliding wear:

$$Q = \frac{KW}{H} \tag{2-1}$$

where Q is the volumetric wear rate. The main variables that influence sliding are W, the normal load and H, the indentation hardness of the softer surface. Severity of wear is described by means of the wear coefficient, K [52].
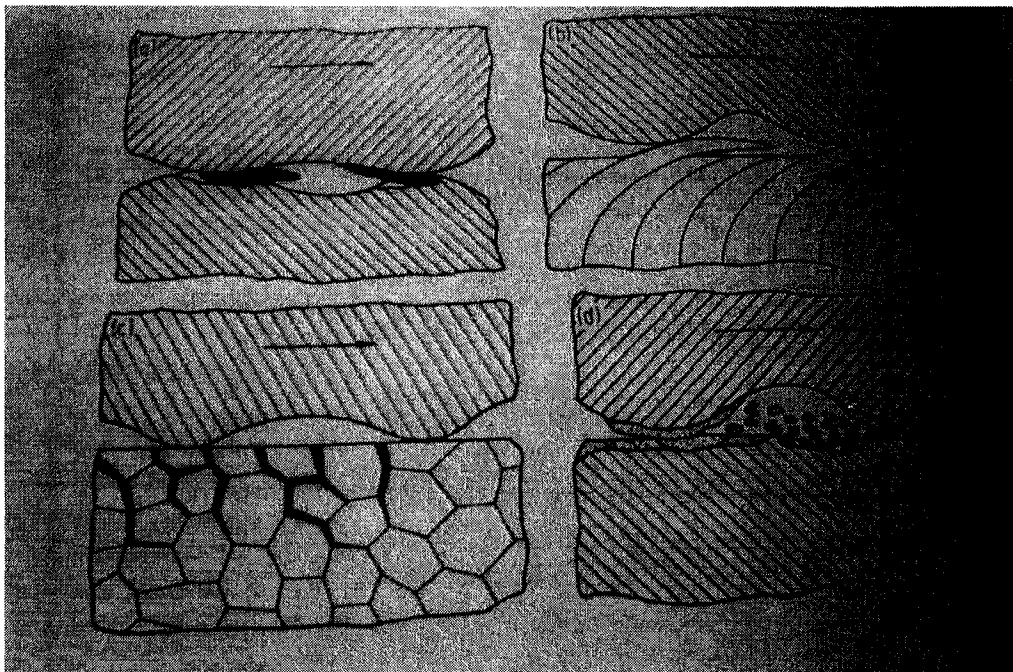
Fig. 2.1 Mechanisms of wear during sliding contact a) adhesive junctions, material transfer and grooving, (b) surface fatigue due to repeated plastic deformation on ductile solids, (c) surface fatigue results in cracking on brittle solids and (d) tribochemical reaction and cracking of reaction films [1].

8

2.2.2 Mild and Severe Wear

The formation of tribochemical reaction products is a well known phenomenon in the sliding contact of metallic surfaces. Sliding wear can be divided into mild wear and severe wear. The terms of mild wear and severe wear are used to describe conditions on the either side of transition [1]. Severe wear is due to metal-to-metal contact or contact between partners of material which involves such events as adhesion, plastic deformation, formation of junctions, transfer and back-transfer of materials. Severe wear results in roughening of the surfaces of the sliding pair and in a coefficient of wear at least one to three orders of magnitude greater than that in mild wear [1]. Mild wear occurs during the sliding contact of surfaces covered by oxide layers or surface layers produced by certain tribochemical reactions. Usually, theses surface layers only build up at load-bearing areas and their formation and structure depend on the contact temperature due to frictional heating [1]. Mild wear usually is associated with low wear rate, smooth surface, a steady friction trace and usually occurs at low loads and velocities. This type of wear is characterized by the formation of finely divided wear particle (debris) as well. Mechanical damage, which is accompanied by high load and velocity, and therefore high contact surface temperatures lead to severe wear. A practical way to distinguish between the mild wear and the severe wear is to observe the change in magnitude of the wear rates with load, sliding velocity, and/or sliding distance [1, 3].

9

2.2.3 Sliding Wear Mechanisms

Besides the general description of the wear mode of sliding wear, some researchers tried to Figure out the dominant wear mechanisms under different conditions. Lim and Ashby [3] considered four broad classes of mechanism in the sliding wear of steels: (1) seizure, (2) melt wear, (3) oxidational-dominated wear, and (4) plasticity-dominated wear. Plasticity-dominated wear is caused by adhesion and/or delamination [3]. Seizure occurs mostly because of plastic indentation, large-scale mass flow, and metallic transfer following a period of severe wear or immediately upon contact under high load [3]. The temperature increase caused by high relative velocity between the sliding surfaces may reach to the melting point of one or both sliding surfaces. If melting of surfaces occurs, it causes a decrease in the coefficient of friction and an increase in wear rate as the strength of metal drops rapidly [3, 52].

2.2.4 Delamination wear mechanism

This theory is based on the sub-surface crack and void formation. Cracks join by shear deformation and reach the surface [1]. The following sequential or independent events may lead to the ultimate failure of the surface due to the wear [1]: i) During sliding, normal and tangential forces are transmitted through contact prints by adhesive and ploughing actions from one surface to the other. Asperities of the softer surface are easily deformed. And some are fractured by the repeated loading action. Smoothing of the softer surface occurs due to deforming and/or removing of asperities. ii) Each point along the softer surface experiences cyclic loading. The harder asperities induce plastic shear deformation on the softer surface, which accumulates with repeated loading. iii)

10

Increasing subsurface deformation leads to nucleation of cracks below the surface. Pre-existing cracks and voids, or new cracks formed, are extended by further loading and deformation. The cracks tend to propagate parallel to the surface, at a depth depending on the material properties and the coefficient of friction. iv) At certain weak points, the cracks are finally able to shear to the surface, which results in long and thin wear sheets. Fig. 2.2 shows subsequent steps which result in flat, extended wear sheets. According to the study of Zhang and Alpas [53], thin flake-shaped debris of A356 aluminium-silicon were observed by the delamination wear mechanism. In their investigation, void and micro-crack nucleation, and subsurface crack growth were detected at the area near the surface. The subsurface crack propagation in A356 alloy is shown in Fig 2.3.
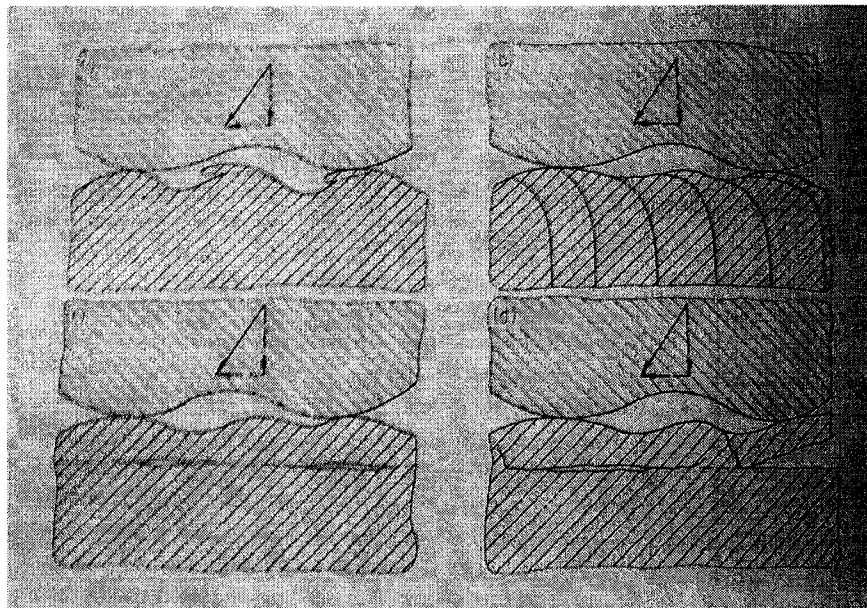
Figure 2.2 Formation of wear sheets due to delamination: (a) smoothing of the softer surface; (b) strain accumulation below the surface; (c) initiation of subsurface cracks; (d) formation of sheet-like wear particles [1].

11
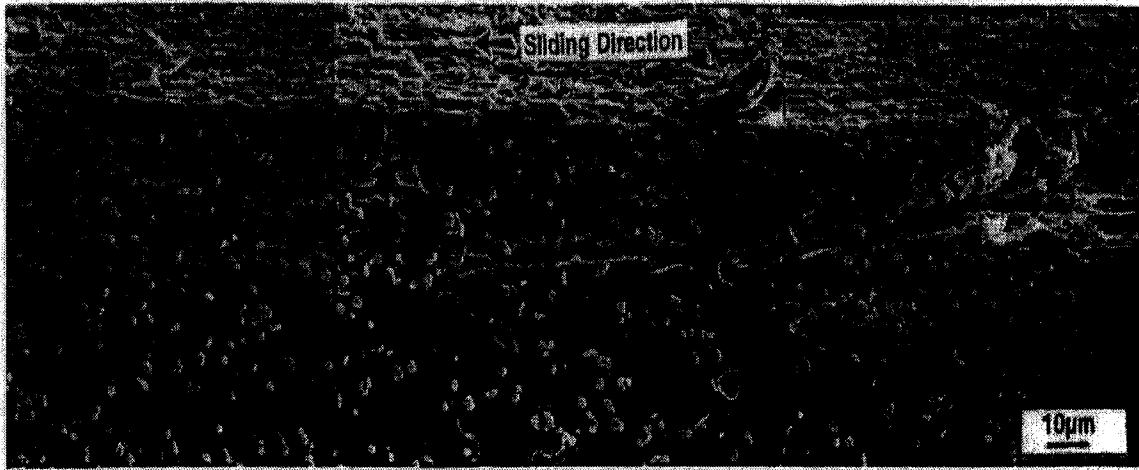
Figure 2.3   Subsurface crack propagation in A356 alloy [53].

2.2.5   Oxidation Wear Mechanism

It is widely known that the tribological functions of oxides formed during friction are as

follows:

1. Oxide films prevent the metallic contact between sliding surfaces.

2. Oxide films serve as a supplementary and effective lubricant.

3. Owing to their high mechanical properties, oxide films have a shield (protecting)

action, significantly reducing the operating stresses in subsurface layers [54].

Mild and severe surface oxidation has been introduced in dry sliding surfaces. The

distinction between these two surface oxidations lies in the sliding velocity, normal load,

area of covered surfaces, thickness, and strength of the layers [3, 55-57]. In a pin-on-disc

system, mild type of surface oxidation is encountered while the sliding speed exceeds

1m/s with a light load, or in case of lower speed with higher loads [3, 56]. The mild

surface oxidation characterized by thin, brittle and patchy oxide film. In contrast, a high

sliding speed (more than 10 m/s for steel), thick oxide film, and surface totally covered

12

by oxide film represent severe surface oxidation [3]. Heavily frictional heating at the tips of asperities causes oxide surface. Completely oxidized and thin layers of molten oxide are formed at the asperity contacts (Fig 2.4) [3]. Fig 2.5a and 2.5b show that a thin oxide film forms at the asperity contacts. Then, the thickness of film reaches to critical magnitude. Up to this level, thin film plays as a protective layer between metallic surfaces [3].
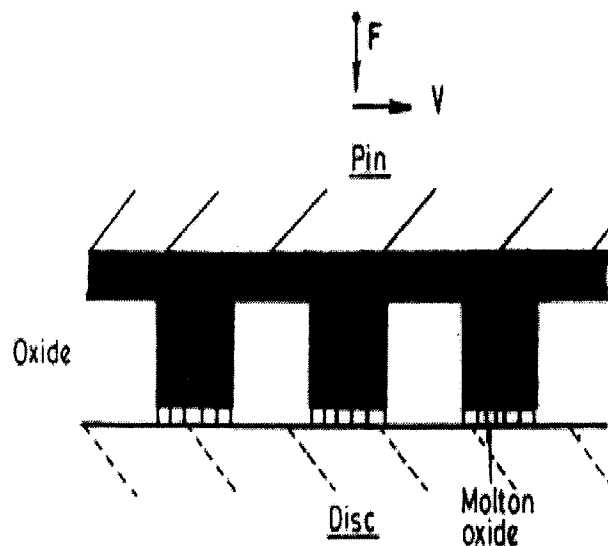
Fig. 2.4 Schematic representation of idealized severe-oxidational wear model [3].

13
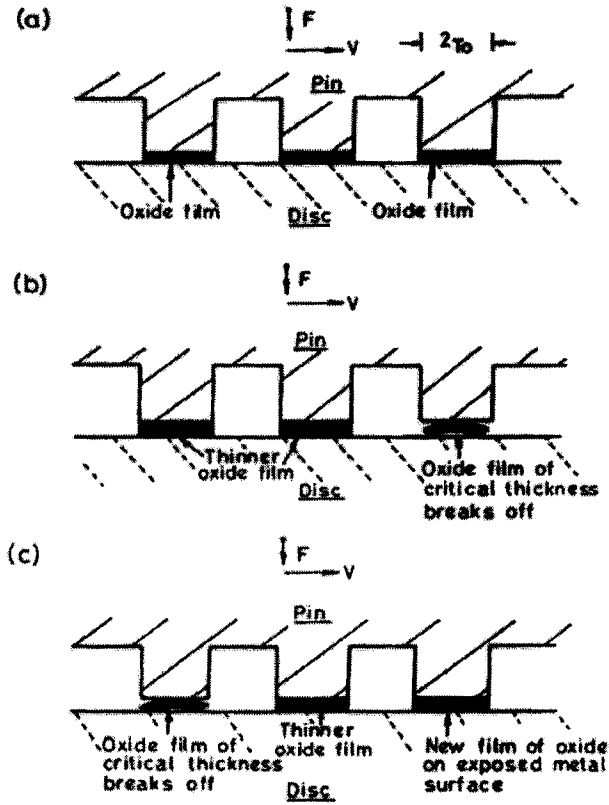
Fig. 2.5 Schematic representation of idealized mild-oxidational wear model [3].
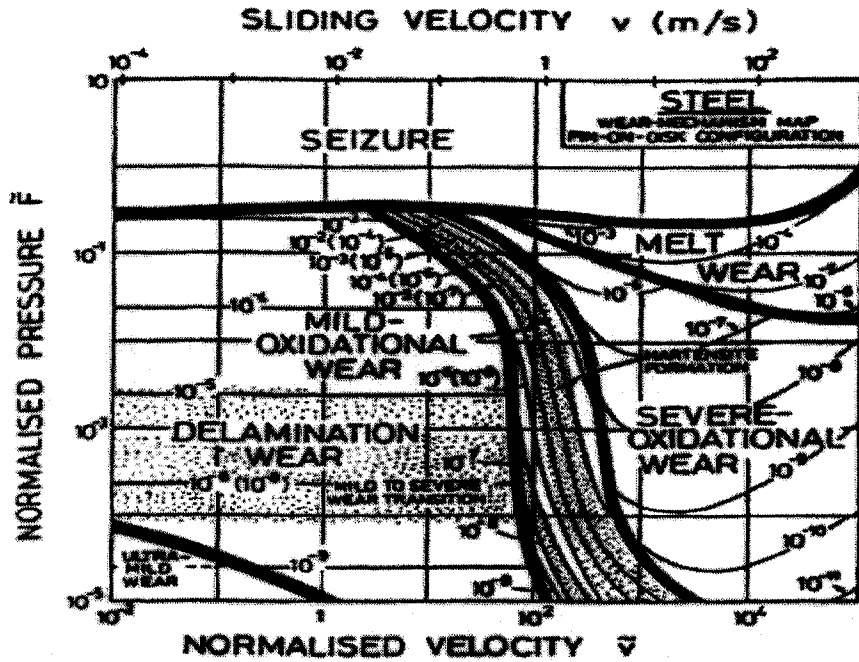
Fig. 2.6 The wear-mechanism map for a steel [3].

14

The empirical wear-mechanism map for steel can demonstrate a range of normalized velocity and normalized pressure (normal load) accompanied with sliding velocity. There are certain regions that mild-oxidational wear can occur, so can the severe-oxidational wear [3]. Fig 2.6 shows the region in wear-mechanism map occupied by oxidational wear.

2.3 Micro-abrasion wear for substrates and coatings

2.3.1 Introduction

To select materials with good wear resistance and thus durability of components and products is very important in industrial application. Surface engineering is an effective means to improve the wear property of bulk materials. To determine the wear performance of materials, traditional techniques such as pin-on-disc sliding wear test have been used successfully, but, particularly for thin hard coatings, it could be difficult to perform the test. The reason for this difficulty is that the coating thickness constrains the volume or depth of material that can be removed before the coating is perforated. Then only small amounts of wear can be tolerated for measuring the wear of the coating. Traditional methods of measurement such as mass loss become ineffective, and even techniques such as profilometry often cannot be used for components with normal engineering finishes as the depth of the wear damage is within the uncertainty of measurement caused by the original roughness of the surface [35].

Micro-abrasion test is a promising new technique for assessing the wear resistance of materials, especially coatings. It possesses many advantages over more conventional

15

abrasion tests including the ability to test small volumes of material and thin coatings, its perceived ease of use and the low cost of the test equipment, and its versatility. The test samples can be very small, as the size of the wear scar that is produced is small. This enables the technique to be used on small test coupons produced during the development of new coatings; as a technique suitable for quality control testing of coatings; and perform tests on coated components to check the quality [35].

2.3.2 Studies on the micro-abrasion test systems

As in any wear test method, many factors can affect the results of micro-abrasion test. Sevim and Eryurek [36] studied the effect of abrasive particle size on wear resistance in steels, and found that the wear resistance of non-heat-treated and heat-treated steels is a function of the abrasive particle size. Experimental investigation [37] of the effects of sample tilt angle and drive shaft groove width shows that both theses factors influence the stability of the rotation of the ball, and the shape of the abrasive slurry pool, which in turn affects the coefficient of friction in the wear scar area and the measured wear rate. Stachowiak et al. [38,41] have investigated the application of a ball-cratering (micro-abrasion) method to test three-body abrasive wear of bulk materials with large abrasive particles (particle size: 250-300μm). It was found that the surface roughness of the ball significantly affects the wear rates and the wear mechanisms of the metallic samples. The surface roughness of the ball steadily increased with testing time and was mainly affected by the angularity of abrasive particles. More angular particles produced higher ball surface roughness. The study also showed that the gradual increase in the ball surface roughness was responsible for the non-linearity of the wear rates with sliding time.

16

Three-body rolling wear dominated when the ball was smooth and the contribution of two-body grooving wear increased with increasing the ball roughness. Gee et al. [35] also studied the parameters affecting the miscro-abrasion test results. They found that the abrasive material, the size and the shape of the abrasive are important. As the load is increased there is a transition from a three-body rolling wear mechanism to a two-body grooving mechanism. Conversely, as the volume fraction of abrasive is increased, there is transition from two-body grooving to three-body rolling. These transitions can be shown by a wear mechanism map (Fig. 2.7). The wear volume (at constant sliding distance) is largely independent of sliding speed, but increases somewhat for very low speeds (Fig. 2.8a). For the free ball machine, the tendency of the ball to slip on the shaft increases as the speed increases. This can lead to an apparent decrease in wear as the ball speed increases (Fig. 2.8b) [35].
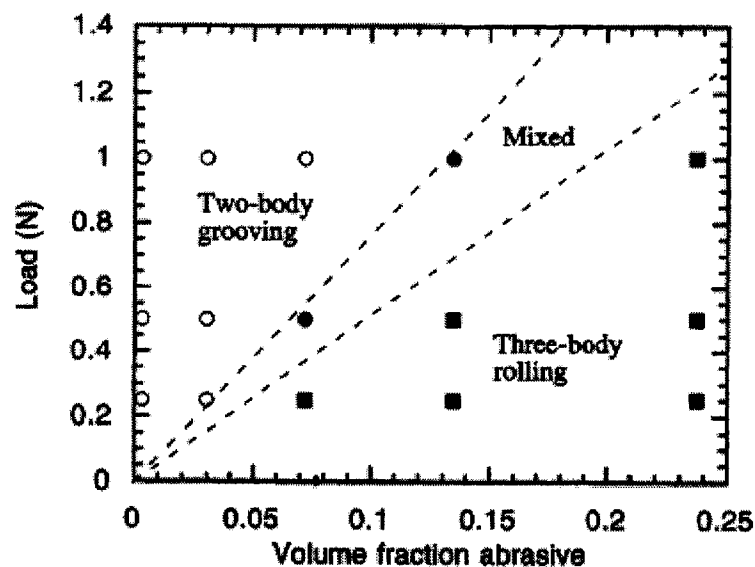
Fig. 2.7. Ball cratering wear mechanism map for tool steel sample with SiC abrasive [35].

17
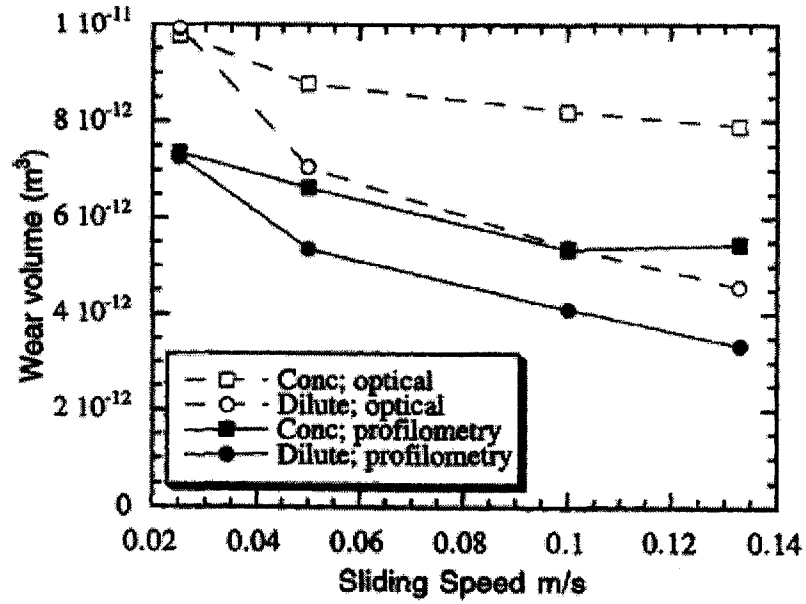
(a)
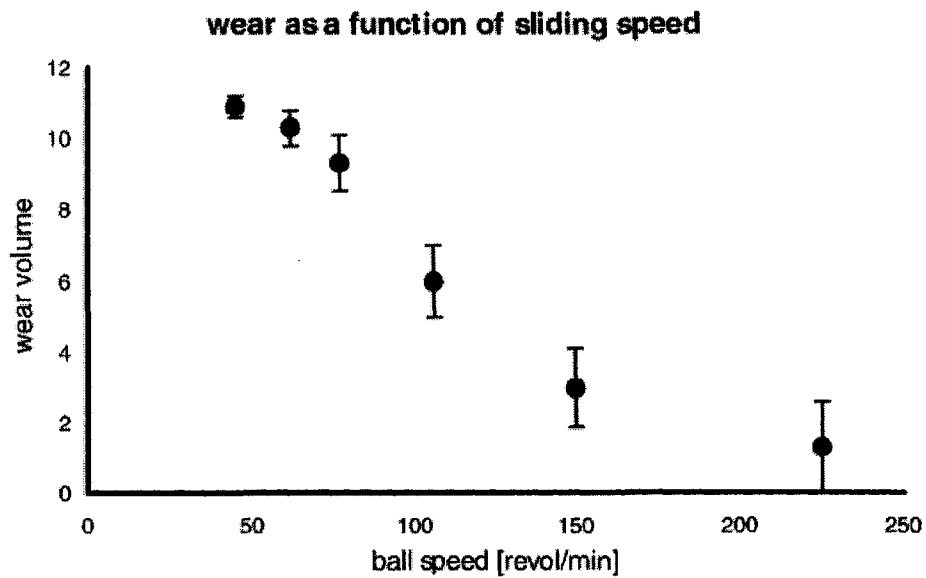
(b)

Fig. 2.8 Variation in wear volume with sliding speed: (a) for tool steel sample with fixed

ball system and 4 μm SiC suspension; (b) free ball single shaft machine with DLC

coating and 1 μm diamond suspension [35].

2.3.3 Wear rate calculation

In the micro-abrasion test abrasive slurry is drip-fed onto the contact between the ball and sample as shown in fig 2.9 [45]. By making a series of these craters (as illustrated in Fig. 2.10) and measuring the size of the scar dimensions, both coating and substrate wear coefficients Ks and Kc can be simultaneously determined from the test [45]. For bulk materials, the equation which is assumed to describe the abrasive wear is [35]

$$K = \frac{\pi b^4}{64R}\frac{1}{SN}$$

(2.2)

where S is the distance slid by the ball, N is the normal force on the sample, b is the diameter of the crater, R is the radius of the ball and k is the wear coefficient.

When perforation of the coating occurs, the following equation could be used [35]:

$$SN = \frac{1}{K_c}V_c + \frac{1}{K_s}V_s$$

(2.3)

where Kc and Ks are the wear coefficients of the coating and substrate, respectively, and Vc and Vs the measured wear volumes and SN the sliding distance multiplied by the applied load.
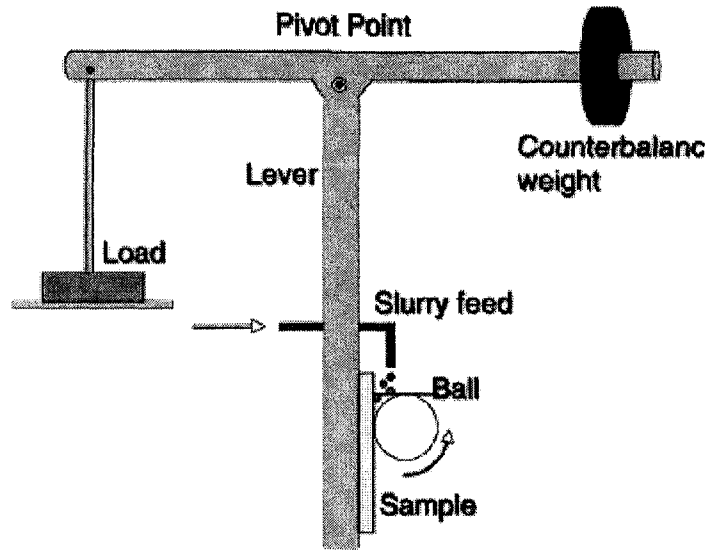
Fig. 2.9 Schematic layout illustrating the geometry of the micro-abrasion apparatus [45]
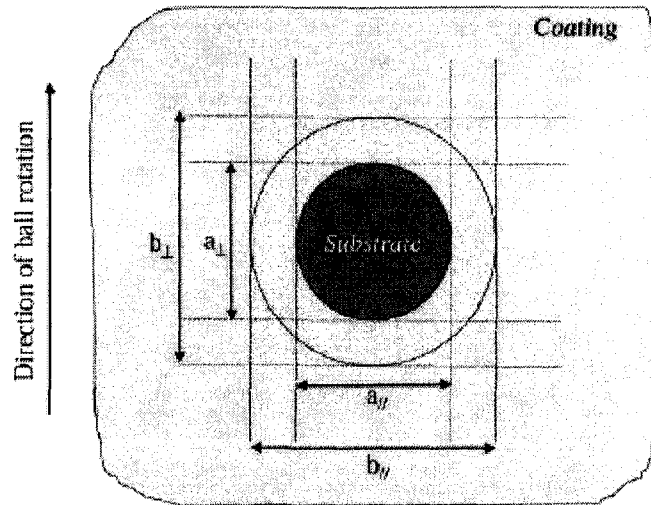
Fig. 2.10 Outer and inner diameters of the wear crater [45]

20

2.3.4 Micro-abrasion test for substrates and coatings

The new micro-abrasion wear test was proposed by Rutherford and Hutchings in the late 1990s [45]. Batista et al. [45] investigated the micro-abrasion wear performance of two duplex coatings: TiAlN and TiN. Single-layered TiAlN and TiN coatings were also tested to evaluate the effect of the duplex treatment on wear resistance. The wear coefficients of these coatings are listed in Table 2.1 [45].

Table 2.1 Wear coefficients and their 95% CI [45]

Specimen	k_c $(\times 10^{-13}\, m^3\, N^{-1}\, m^{-1})$	CI (95%) $(\times 10^{-13}\, m^3\, N^{-1}\, m^{-1})$	k_s $(\times 10^{-13}\, m^3\, N^{-1}\, m^{-1})$	CI (95%) $(\times 10^{-13}\, m^3\, N^{-1}\, m^{-1})$
Single-layered TiAlN coating	2.74	[2.59, 2.91]	13.20	[11.10, 16.40]
Duplex TiAlN coating	1.71	[1.61, 1.82]	20.60	[13.50, 33.00]
Single-layered TiN coating	7.27	[7.15, 7.39]	9.65	[9.54, 9.76]
Duplex TiN coating	4.12	[3.91, 4.35]	16.20	[14.90, 17.80]
Uncoated substrate	–	–	9.40	[9.00, 9.82]

The best micro-abrasion resistance was shown by the duplex TiAlN coating, followed by single-layered TiAlN, duplex TiN and single-layered TiN coatings. They also found that coating debris acts as an additional source of abradant particles in the SiC slurry, leading to higher abrasive wear in the substrate. The harder the coating debris, the more severe the abrasive wear in the substrate is [45].

Based another group of tests about the micro-abrasion wear property of duplex and non-duplex TiAlN, TiN and CrN coatings, Batista et al.[43] reported that the wear pattern change from surfaces characterized by grooves (uncoated substrate, single-layered TiN and CrN systems and duplex Cr-N system) to surfaces which exhibited multiply indented

21

surfaces (single-layered and duplex TiAlN systems), indicating a transition between wear mechanisms. This transition was found to be dependent on the ratio between the hardness of the abrasive particles and surface (coating) or subsurface hardness. If this ratio is decreased, it could be found the tendency of the abrasive particles to scratch the surface was reduced and the resistance to micro-scale abrasion was improved [43]. In terms of wear mechanism, a grooving wear mechanism was observed for a single-layered TiN coating and a mixed mechanism involving grooving and rolling wear was found to occur in a duplex TiN coating [46].

2.4 Coatings

2.4.1 Introduction

Many functional properties including wear properties can be optimized by applying suitable coatings to substrates [11]. In the second half of the 20th century, surface coatings have emerged for industrial application . In the late 1960s, TiC films deposited by CVD (chemical vapor deposition) on hard metal cutting tools appeared in the market. In 80s, the first PVD (physical vapor deposition) hard coatings were introduced to the market. Around 1980 TiN coatings deposited by CVD became commercially available [11]. At the same time drills and cutting inserts with a TiN and TiC overlayer, coated by PVD (ion plating) were produced. Around this time low friction coatings such as DLC (diamond-like carbon) deposited by PACVD (plasma activated chemical vapor deposition) and MoS2 deposited by PVD also appeared [11].

2.4.2 Improved performance of hard coatings

Various techniques are developed to change the properties of hard coatings. By adding different elements to a coating, defects (solid-solution hardening) as well as additional precipitations (precipitation hardening) and grain boundaries may be introduced into the coating, resulting in increased hardness. For example, the material hardness is increased by adding aluminum to TiN. The incorporation of smaller aluminum atoms into the lattice of TiN leads to a local tensile stress (lattice distortion) which contributes to the higher hardness. Another example is by introducing Al during the deposition process of TiN, the oxidation resistance increased from approximately 550 °C to 800 °C and additionally an increased hardness is observed. The enhanced oxidation resistance is a consequence of the formation of an aluminum-rich protective alumina passive layer at the surface [11]. The tribological behavior of the classical single layer coatings TiN and TiC could be improved by building multilayer structures. TiN/TiC, TiN/TiC/BN, TiN/TiC/B4C, TiN/TiVC/AlN, and TIN/TiC/SiC multilayer structures composed of 3-150 layers, exhibit a lower coefficient of friction as well as a longer edge life when applied on cutting tools [11]. It is also possible to deposit isotropic nanocomposite coatings consisting of crystallites, embedded in an amorphous matrix, with grain sizes in the nanometer range. In contrast to the multilayer structures, where any material combination can be obtained at any multilayer period, nanocomposites can only be deposited for certain material combinations. Additionally, the size of the crystallites can not be independently controlled by the deposition process, because it is essentially determined both by the properties of the materials and by the deposition conditions (temperature, plasma conditions, elemental concentrations, etc.). In the last decade some nanocomposite thin film systems, which show promising results for applications, have

23

been deposited and investigated [11]. The different techniques discussed above are shown in Figure 2.11.

alloyed	multilayer	isotropic multiphase
TiAlN	TiN/Al$_2$O$_3$/TiC	TiN/Si$_3$N$_4$
TiC$_x$N$_y$	TiN/TiCN/TiC	TiC/DLC
Ti-DLC	TiN/NbN	TiC/a-C
Si-DLC	TiN/VN	TiN/MoS$_2$
NiCoCrAlY	DLC/DLC	
	Ti-DLC/DLC	
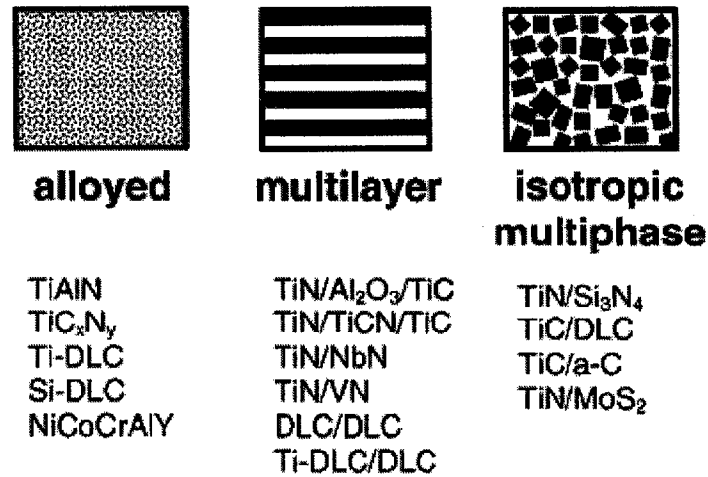
Fig. 2.11. Schematic representation of the structure of the different coatings [11].

2.4.3 TiN coating

As the first generation hard coating, TiN has been widely used and investigated [12-16, 19-22,24-25, 33-34, 43-50]. It is also the base coating for property improvement, no matter by alloying different elements into it, acting as one layer element of the multilayered coatings, or being the crystallites embedded in an amorphous matrix in nanocomposite coatings. It is widely used in the tool industry. Lim et al. [13] studied the effect of machining conditions on the flank wear of TiN-coated high speed steel tool inserts. Applying TiN coatings onto HSS tool inserts dramatically expands the range of feed rate and cutting speed. The extent of reduction in the measured wear rates depends strongly on the machining conditions. Three major dominant wear mechanisms for TiN-

24

coated HSS inserts were identified. The wear and wear mechanisms map are shown in Figs. 2.12 and 2.13 [18].
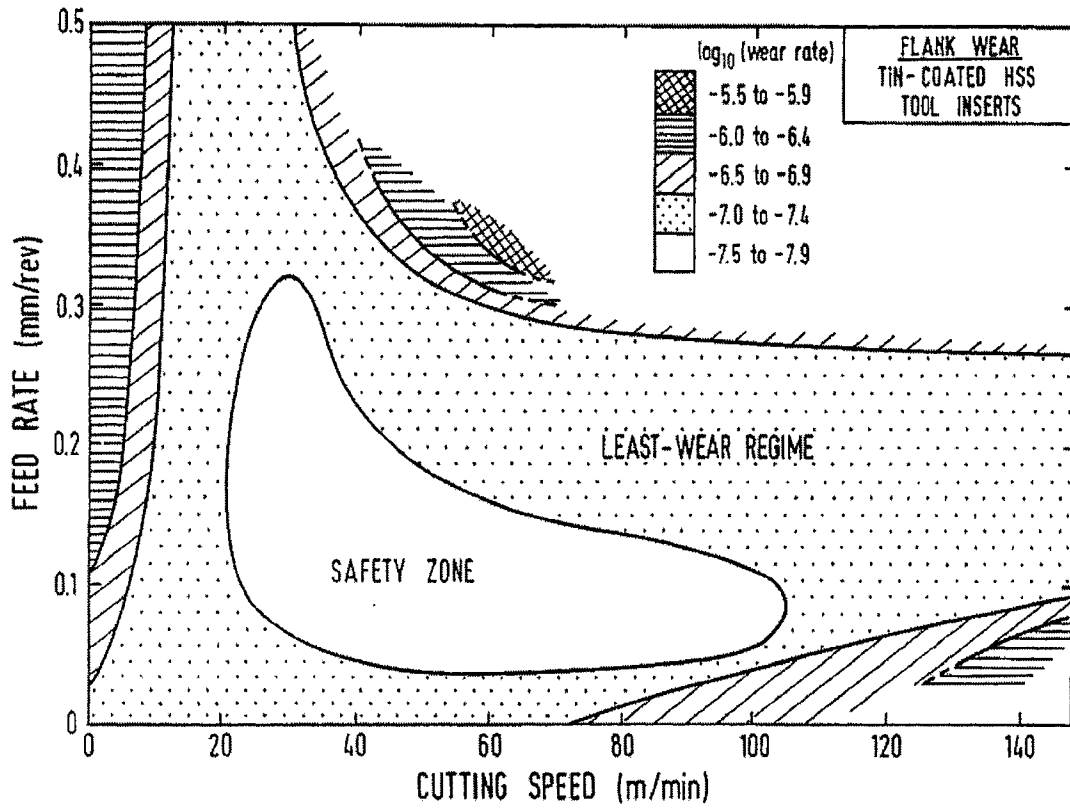
Fig. 2.12 Wear map for flank wear of TiN-coated HSS insets during dry turning operations [13].
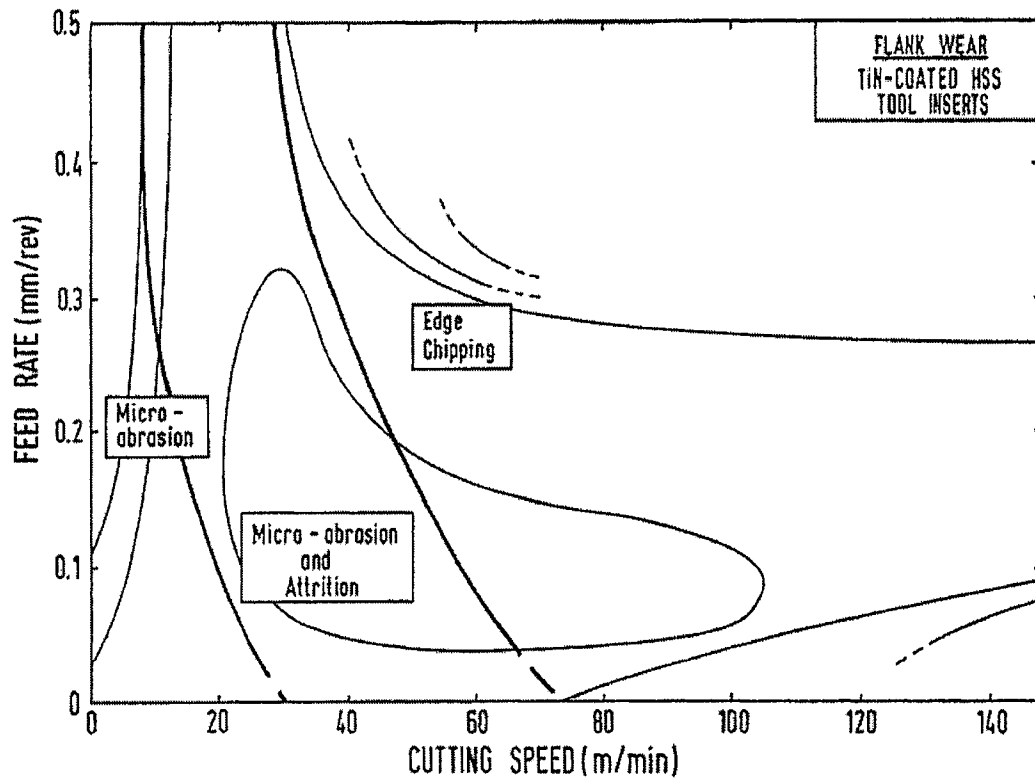
Fig. 2.13 Superimposition of the boundaries of the transition of dominant wear mechanisms onto the wear rate boundaries [13].

TiN coating is also a good benchmark to evaluate performance of other coatings [21, 24, 25, 34]. For example, Guu and Lin [21] compared the tribological characteristics of TiN and TiCN coatings. They investigated two different coatings with different layer thickness in terms of the friction coefficient, wear rate, adhesion strength, wear mechanism, microhardness, and effects of tribo-testing temperature and sliding speed on both the friction coefficient and wear rate.

2.4.4 The TiN/Si₃N₄ System

26

Efforts have been undertaken to codeposit silicon and titanium nitride based on the concept of incorporating stable oxide-forming elements (Al, Si, Hf, Cr, Zr, Nb) into TiN,. In contrast to TiAlN, TiZrN, and other single-phased hard materials, silicon cannot be substitutionally built in the lattice of TiN. In accordance with the Ti-Si-N phase diagram which does not show any stable ternary phase under equilibrium conditions, two-phase TiN/Si$_3$N$_4$ coatings form when silicon is added during deposition of TiN. The first coatings consisting of Ti-Si-N have been produced by CVD in 1982 [11].

The TiN-Si$_3$N$_4$ coatings produced by plasma-enhanced CVD method showed super high hardness of about 60 GPa at 15 at.-% silicon in the film while only X-ray signals from TiN were observed. In further tests these coatings were identified as nanocomposites consisting of TiN crystallites of about 4-7 nm (nc-TiN) surrounded by an amorphous Si$_3$N$_4$ (a-Si$_3$N$_4$) matrix. Such a nanocomposite is schematically illustrated in Figure 2.14 with TiN crystals embedded in an amorphous matrix of Si$_3$N$_4$. The hardness (and the crystallite size) is a distinct function of the silicon concentration in the film as can be seen in Figure 2.15, which compares results from various groups [11].
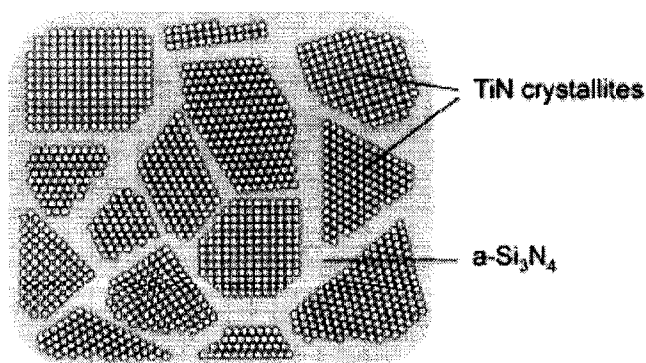
Fig. 2.14. Schematic representation of a nanocomposite consisting of a nanocrystalline phase embedded in an amorphous matrix [11].

27
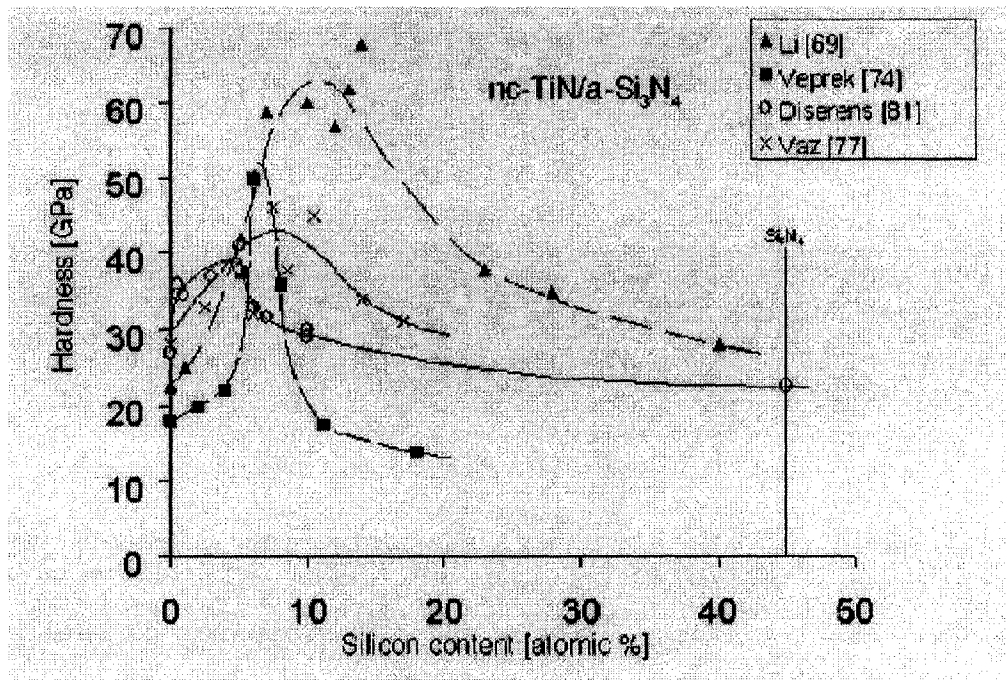
Fig. 2.15. Hardness of nc-TiN/a-Si3N4 nanocomposites as a function of the silicon content. Solid lines are for reactive PVD experiments, dashed lines are for PACVD films. The hardness maxima between 5 and 12 at.-% Si are obvious [11].

Nanocomposite thin films with improved properties are not restricted to the nitride systems alone. The incorporation of carbide particles into amorphous carbon (a-C:H, DLC) can produce so called "load-adaptive coatings", which exhibit high toughness and prolonged lifetime. The optical properties of a-C:H coatings have been adapted by the introduction of W and Cr as nanosize carbidic inclusions in the film. These coatings are applied, e.g., as selective absorber coatings for thermal solar energy conversion. An additional benefit can also be obtained by introducing materials with lubricating

28

properties such as MoS_2, C or DLC to a coating, either as top layer or as a composite coating as shown for example by Gilmore for the TiN/MoS_2, TiB_2/MoS_2, and TiB_2/C nanocomposite systems [11].

2.4.5 TiSiCN coatings

While the single phase hard coatings, such as TiN and TiC, are unlikely to provide the optimum properties. Three- component coating systems have been developed to achieve an increased combination of properties. Studies have shown that ternary component coatings can provide superior properties to binary coatings.

TiCN coatings have higher hardness and better wear resistance compared to TiN or TiC coatings. Studies have shown that TiCN is a solid solution of TiN and TiC and would incorporate the advantages and characteristics of both. The higher hardness value of TiCN coatings than that of TiN coatings was attributed to the solid-solution hardening by carbon atoms, and the better wear resistance could be attributed to its high microhardness and dense morphology [24-27].

Recently, quaternary TiSiCN coatings deposited by chemical vapor deposition (CVD), magnetron sputtering or hybrid deposition technique combining the arc ion plating and DC magnetron sputtering techniques have been studied and reported on [26-32]. For example, Jeon et al. [27] found that TiSiCN coating with a Si content of 8.9 at. % had a fine composite microstructure comprising nano-sized crystallites of TiCN surrounded by amorphous phase of Si_3N_4/SiC mixture. The micro-hardness value of the TiSiCN

29

coatings was much larger than that of TiCN coatings. In addition, the average friction coefficient of the TiSiCN coatings decreased with increasing Si content. However, comparing with the well used coatings like TiN, TiSiCN coatings are far from thoroughly investigated, especially their tribological properties with aluminium counterparts or in different environmental conditions, such as in coolant. It was also worth to notice that most of the PVD coatings studied only have a thickness of a few microns.

2.4.6 Coating deposition method-plasma enhanced magnetron sputtering (PEMS)

Compared to the common used coating deposition methods, such as cathodic arc vapor (plasma or arc ion plating) deposition , magnetron sputtering (or sputter ion plating) , and combined magnetron and arc processes, plasma enhanced magnetron sputter (PEMS) deposition is an improved version of conventional magnetron sputtering. It utilizes an electron source and a discharge power supply to generate plasma, independent of the magnetron plasma, in the entire vacuum system [49]. The PEMS technology has shown to produce much better TiN coatings for cutting applications [49, 58-59] and the superior performance of coatings can be attributed to the very fine (~60 nm) TiN microstructure that is formed due to the heavy ion bombardment [49, 60].

Fig. 2.16 is a schematic of the PEMS system. The PEMS technology uses an electron source (a heated filament, for instance) and a discharge power supply to generate plasma. This electron-source generated plasma is independent of the magnetron-generated plasma [49]. There are a number of advantages of this technique. First, during the substrate

30

sputter-cleaning, the magnetrons is not operated, while the electron-source generated plasma alone is sufficient to clean the substrate. In this way, deposition of the target material, which is of concern for conventional magnetron sputtering, will not occur and the cleaning of the sample surface is assured. Second, during the film deposition, the ion bombardment from the electron-source generated plasma is quite intense and the current density at the sample surfaces can be 25 times higher than that with the magnetron-generated plasma alone. Consequently, a high ion-to-atom ratio can be achieved [49].
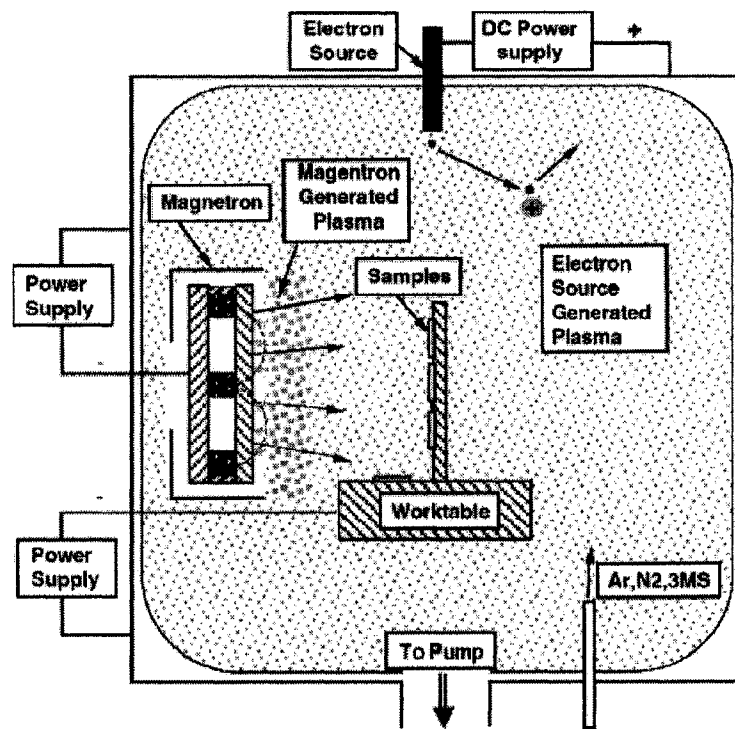
Fig.2.16. Schematic of plasma enhanced magnetron sputtering (PEMS). for the nanocomposite

31

2.5 Objectives of the study

In this study, five substrates materials 0050A, G3500, CarmoCast, CC2 and D2 were obtained from different suppliers. All these materials are good candidates for the selection of die materials. Two coatings TiN and TiSiCN were deposited by an innovative deposition process, plasma enhanced magnetron sputtering (PEMS), which was introduced in section 2.4.6. By using heavy ion bombardment prior to and during deposition to increase the coating adhesion and limit columnar growth, single-layered thick nitrides of ZrN, CrN, and TiN coatings up to about 80 μm and thick carbonitride coatings of ZrSiCN and TiSiCN about 30 μm could be obtained [49]. This technique was expected for the application of protecting turbine engine compressor blades, vanes and rotor blades in advanced aircraft and fluid pump impellers as well as piston rings for heavy-duty diesel engines [49]. These two TiN and TiSiCN coatings were selected as examples to explore super performance of materials other than that of the traditional ones such as the substrate materials. The performance of coatings in cutting coolant environment is also our interest. In this study, the TiN coating had a thickness of 47μm and the TiSiCN coating was 17μm thick. Besides the performance of materials, alternative testing means is also our interest to explore. The correlation between different testing methods is another good topic to discuss. The main purposes of this study could be summarized as follows:

(1) To evaluate the performance of substrate and coating materials from different suppliers.

(2) To analyze the hardness effect on wear performance of materials.

32

(3) To identify the wear mechanisms of materials (a) against different counterface materials; (b) under different load; (c) in different environments.

(4) Design and construct an alternative test system: micro-abrasion testing system.

(5) Explore the correlation between two abrasive wear test methods: (a) traditional pin-on-disc test with alumina pin; (b) innovative micro-abrasion test with alumina slurry.

CHAPTER 3 EXPERIMENTAL PROCEDURES

This chapter describes all the experimental procedures in the thesis. Three main parts are included.

3.1 Sliding wear for substrates

3.1.1 Preparation of substrates

Five kinds of tool substrate materials, namely 0050, G3500, CarmoCast, CC2 and D2 were obtained and slices ($25 \times 25 \times 5$ mm^3) were cut from them as samples for research purpose. All the slice samples were polished and then degreased with solvent, rinsed and cleaned with distilled water, finally dried. The surface roughness of the substrates is 0.1 ± 0.04 µm. The metallurgical photographs of the polished substrates were taken by using JEOL Scanning Electron Microscope (SEM) (Fig. 3.1). The composition limits of 0050A cast steel [4], G3500 cast iron [4], and D2 high-carbon, high-chromium, cold-work tool steel are listed in Tables 3.1, 3.2 and 3.3 respectively.

Table 3.1 Nominal Composition of 0050A cast steel

	Composition, wt%							
	C	Mn	Si	Cr	Mo	V	P	S
Cast Steel 0050A	0.4-0.5	0.9-1.2	0.2-0.5	0.8-1.1	0.35-0.5	≤1.5	≤0.045	≤0.05

34

Table 3.2 Nominal composition of G3500 cast iron

	Composition, wt%								
	C	Mn	Si	Cr	Ni	Mo	Cu	P	S
Cast Iron G3500	2.8-3.2	0.7-1.0	1.5-2.2	0.35-0.5	≤0.3	0.35-0.5	≤0.7	≤0.15	≤0.15

Table 3.3 Nominal composition of D2 high-carbon, high-chromium, cold-work tool steel

	Composition, wt%								
	C	Mn	Si	Cr	Ni	Mo	V	Cu	P
Tool Steel D2	1.4-1.6	≤0.6	≤0.6	11.0-13.0	≤0.3	0.7-1.2	≤1.1	≤0.25	0.03
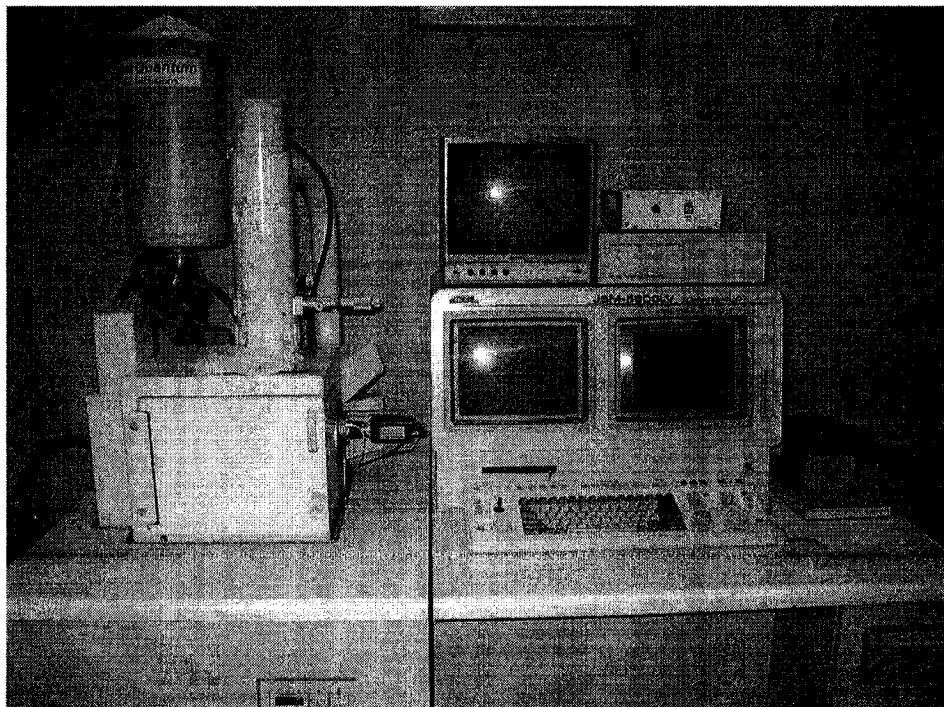
Fig. 3.1 JEOL Scanning Electron Microscope (SEM)

3.1.2 Characterization and tribological tests of 5 substrates
3.1.2.1 Substrates hardness tests

The Vicker hardness of the 5 substrates was measured using a Buehler microhardness tester (Fig. 3.2).
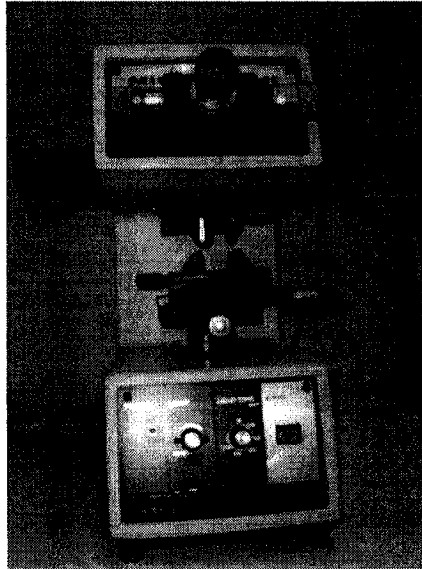
Fig. 3.2 Buehler microhardness tester

3.1.2.2 Tribological tests

The tribological properties of the 5 substrates were tested by use of a pin-on-disc tribometer (Sciland Pin/Disc Tribometer PCD-300A), (shown in Fig. 3.3) against alumina, aluminium and steel balls (diameter of spherical pin tips: 5.5mm) under different loads. The test conditions are detailed in Table 3.4. All the tests were performed at room temperature (20 ^{0}C), ~50% humidity, 0.1m/s sliding speed, and 250m sliding distance. The coefficient of friction (COF) was recorded by the tribometer during the tests. The wear track surface profile was measured using a Mitutoyo SJ-201P surface profiler (Fig. 3.4). The 2D and 3D wear track surface profiles were also measured using Wyko optical profiling system (Fig. 3.5).

36

Table 3.4 Pin-on-disc test conditions for 5 substrates:

0050A,G3500, Carmocast, CC2 and D2

Load and environment	Pin materials
5 N in air	Alumina
5N in air	Aluminium (6061)
5N in air	Steel (AISI 52100)
10N in air	Aluminium (6061)
15N in air	Steel (AISI 52100)
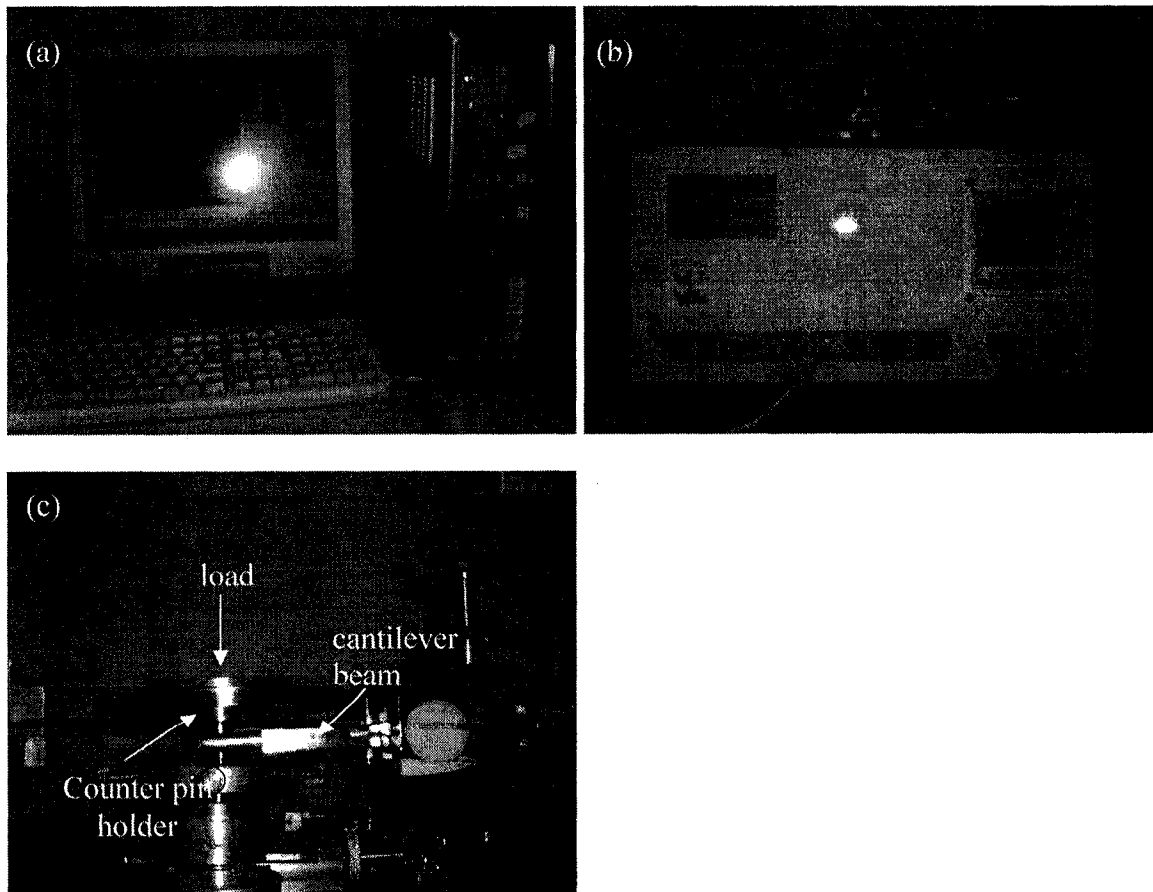
Fig. 3.3 Sciland Pin/Disc Tribometer PCD-300A system (a) data acquisition system (b) pin/disc tribometer (c)load cell and cantilever beam
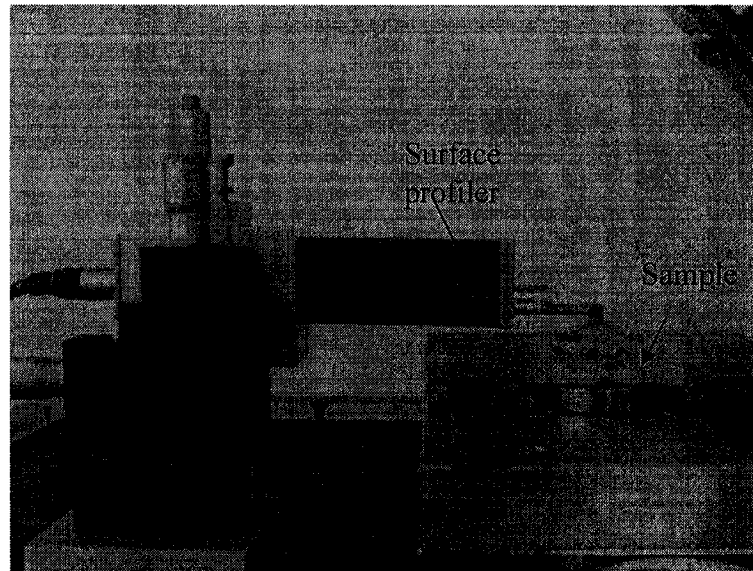
Fig. 3.4 Mitutoyo SJ-201P surface profiler
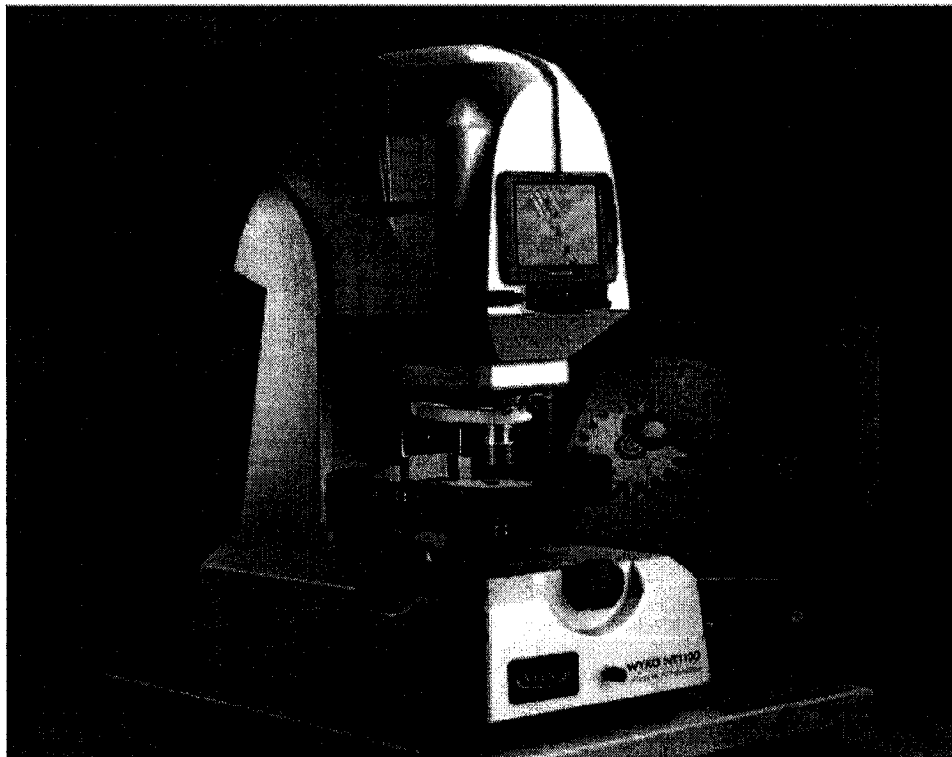
Fig. 3.5 Wyko optical profiling system

38

3.1.2.3 Wear morphology observation

The wear tracks of all samples were investigated by using SEM (Fig. 3.1) and Wyko optical profiling system (Fig. 3.5). Some of the wear tracks of worn counter parts were examined by using FEI Scanning Electron Microscope (SEM) with Energy Dispersive Spectroscopy (EDS) (Fig. 3.6).
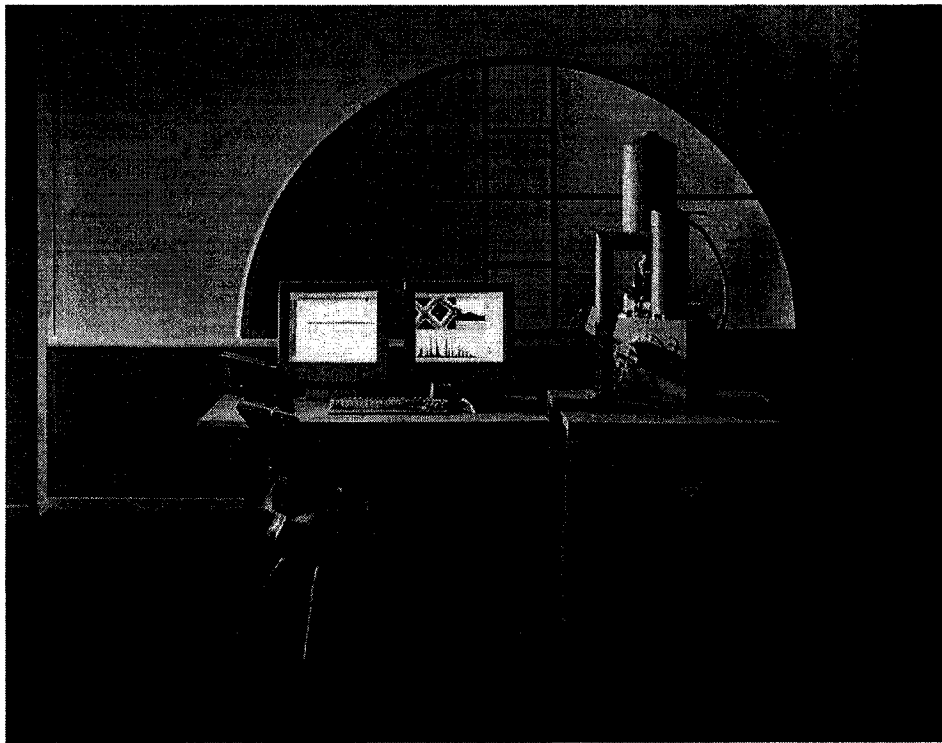
Fig. 3.6 FEI Scanning Electron Microscope (SEM) with Energy Dispersive Spectroscopy (EDS)

39
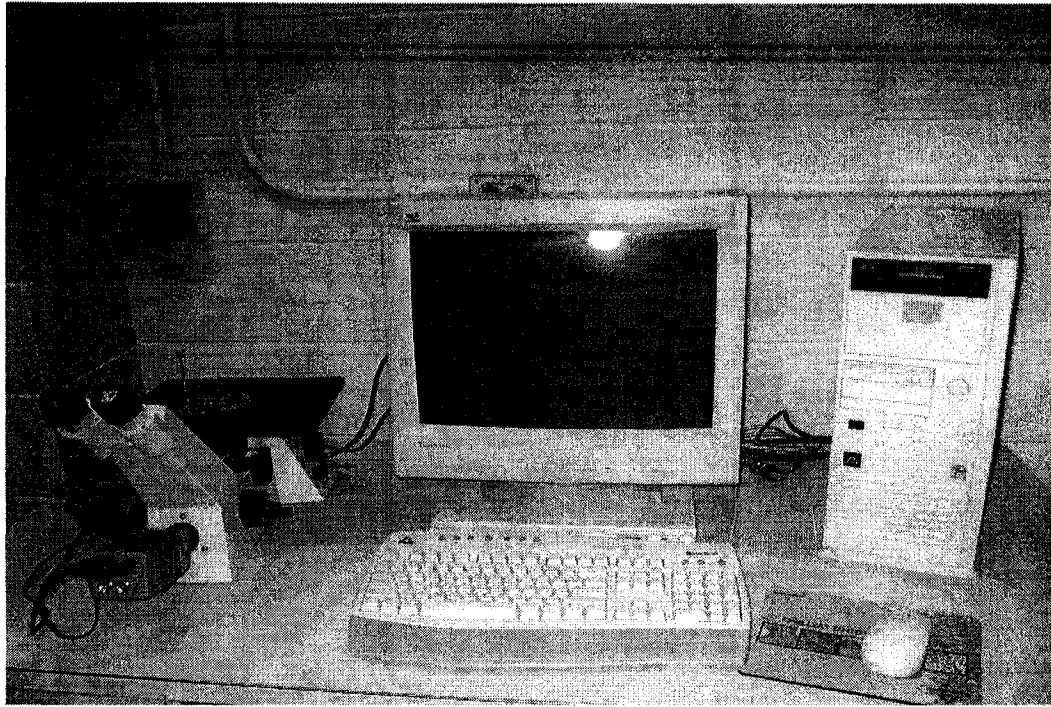
Fig. 3.7 Buehler optical microscope

3.2 Sliding wear for coatings

3.2.1 Coating deposition process

In the present study, one TiN coating and one TiSiCN coating were deposited on stainless steel testing coupons ($24.5\times24.5\times4$ mm) by a Plasma Enhanced Magnetron Sputtering (PEMS) process, which is discussed in detail in section 2,4.7. The process began with Ar (flow rate = 150sccm) sputter cleaning for 90-100 minutes; then a bond layer of Ti was deposited for 5 minutes at 4kW magnetron power. Subsequently, nitrogen (flow rate = 23 sccm) was admitted into the vacuum system while the Ti target power remained constant to form TiN. For TiSiCN, trimethylsilane (3MS) was also added to the vacuum system at a flow rate of 3 sccm. During the sputter cleaning, a discharge current of 20A was used first. When the process temperature (400°C) was reached, the current was reduced to 10A.

40

During the deposition, the discharge current remained at 10A. During the sputtering the bias on the part was 120V, and was reduced to 40V for film deposition. The detailed deposition parameters are given in Table 3.5.

Table 3.5 Process conditions for the TiN and TiSiCN coating samples

Sample	Sputter Cleaning		Film Deposition								
	Time (min)	I disch (A)	Time (h)	Temp (°C)	Pm (kW)	I bias (A)	I disch (A)	QN2 (sccm)	Q3MS (sccm)	Thick. (μm)
TiN	100	20-10	10	400	4	0.28	10	23	0	45
TiSiCN	90	20-10	5	400	4	0.22	10	23	3	17

3.2.2 Characterization and tribological tests of TiN and TiSiCN coatings

Scanning electron microscopy (SEM) was used to observe the morphology of the coating surface and cross-sectional microstructure of the samples. X-ray diffraction (XRD) was employed to study the phase structure of the coatings. The Hysitron Ubi 1 nanomechnical test instrument (Berkovich indenter, 6000μN load) was used for nanoindentation tests on the coatings. The coating hardness (H) and reduced elastic modulus (E) were measured and tabulated. The Rockwell hardness indentation method (testing load: 150 kg) was used to evaluate the adhesion strength of the coating layers. The resulting surface indentation fractures were examined by optical microscopy (Fig. 3.6).

A pin-on-disc tribometer (Fig. 3.3) was used to evaluate the tribological properties of the coatings at dry and coolant conditions with 5N normal load, 0.1 m/s (dry) and 0.05m/s (coolant) sliding speeds, 200 m sliding distance, and aluminium and alumina counterparts (diameter of spherical pin tips: 5.5mm). The test conditions are listed in Table 3.6. For the coolant testing conditions, the test coupons were immersed in regular workshop cutting coolant (Hangsterfer's S-500) to observe the lubricating and cooling effect. SEM was also used to observe the wear tracks as well as investigate the detailed wear mechanisms. The sliding wear test conditions for all the 5 substrates and 2 coatings are summarized in Table 3.7.

Table 3.6 Pin-on-disc test conditions for TiN and TiSiCN coatings

Load and environment	Pin materials
5 N in air	Alumina
5N in air	Aluminium (6061)
5N in coolant	Alumina
5N in coolant	Aluminium (6061)

42

Table 3.7 Pin-on-disc sliding wear test conditions for 5 substrates and 2 coatings

		Substrates					Coatings	
		0050	G3500	Carmo Cast	CC2	D2	TiN	TiSiCN
Load(N) and environment	Pin materials							
5N in air	Alumina	√	√	√	√	√	√	√
	Aluminium	√	√	√	√	√	√	√
	Steel	√	√	√	√	√		
10N in air	Aluminum	√	√	√	√	√		
15N in air	Steel	√	√	√	√	√		
5N in coolant	Alumina						√	√
	Aluminium						√	√

3.3 Micro-abrasion tests for substrates and coatings

To explore an alternative means to evaluate the abrasive wear property of materials, a micro-abrasion tester was designed, constructed and employed in this study.

3.3.1 Design and construction of micro-abrasion tester

3.3.1.1 Existing micro-abrasion test systems

43

Three variants of the test system have emerged. In all these three kinds of systems, wear is produced by pressing a rotating wheel or ball against the test sample, and introducing an abrasive suspension into the wear interface as shown in Fig. 3.8.

In the first system [35, 38, 41], a free ball is driven by friction force produced by a notched drive shaft as shown in Fig. 3.9a. Some uncertainty occurs in the speed of the ball because the ball is not connected with the driving shaft. The load can be varied by adjusting the angle of the sample holding plate. The disadvantage of this system is that when the angle is reduced to increase the normal load, there is an increasing tendency for the ball to slide up the sample giving non-spherical craters. A potential source of error in the normal load also exists due to the contribution to the effect of friction between the sample and ball which alters the effective weight of the ball. Another problem is for typical test balls, the maximum applied load that can be used is relatively small (about 0.4 N). There is also another type of free ball machine which uses a 30mm ball supported on grooves on two rotating shafts [35] (Fig. 3.9b). The sample is clamped into a pivoted arm with dead weight loading applied directly above the ball. The face of the sample is pressed against the top of the ball, and the load is applied and the range is from 0.5 to 5N. Again this test system has the problem of uncertainty in the speed of the ball because of the lack of the direct drive. However, the twin shaft system avoids the potential error in applied load due to friction between the ball and the test sample, and also enables higher test loads to be applied than with the first system. In the directly driven configuration [35, 37, 40] (Fig. 2c), the ball is driven directly a drive. This design also allows high normal load applied.

44
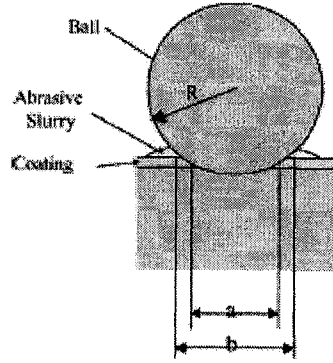
Fig. 3.8 Principle of micro-abrasion test

(a)

(b)

45
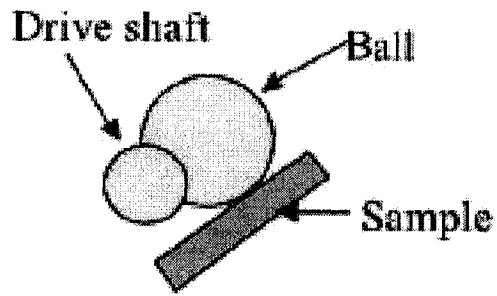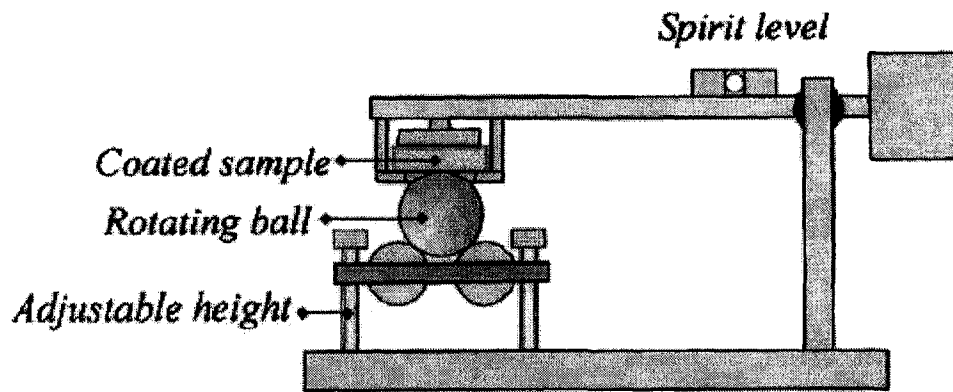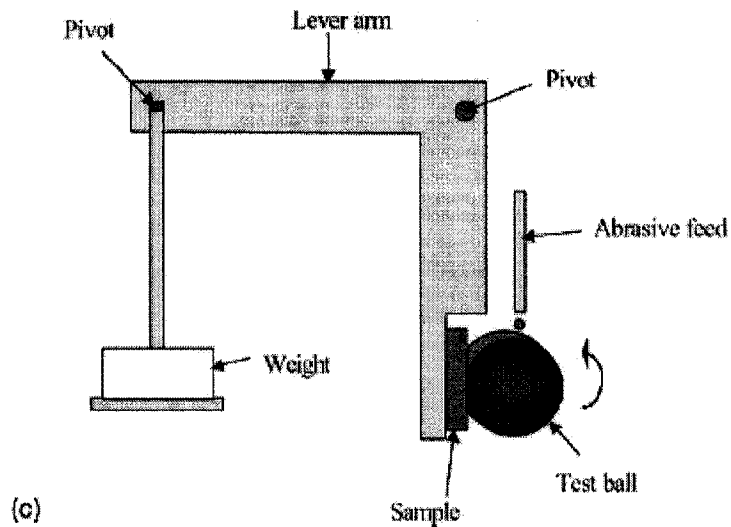
Fig. 3.9 Different micro-abrasion test systems (a) free ball-single shaft, (b) free ball-two shaft, (c) fixed ball.

3.3.1.2 Design features and parameters of micro-abrasion test system

To combine the advantages of the testing systems discussed above, we designed a system possessing the characteristics of the first and third systems as shown in Fig. 3.9. The system diagram is shown in Fig. 3.10. The design parameters [35-40] are listed in Table 3.8.
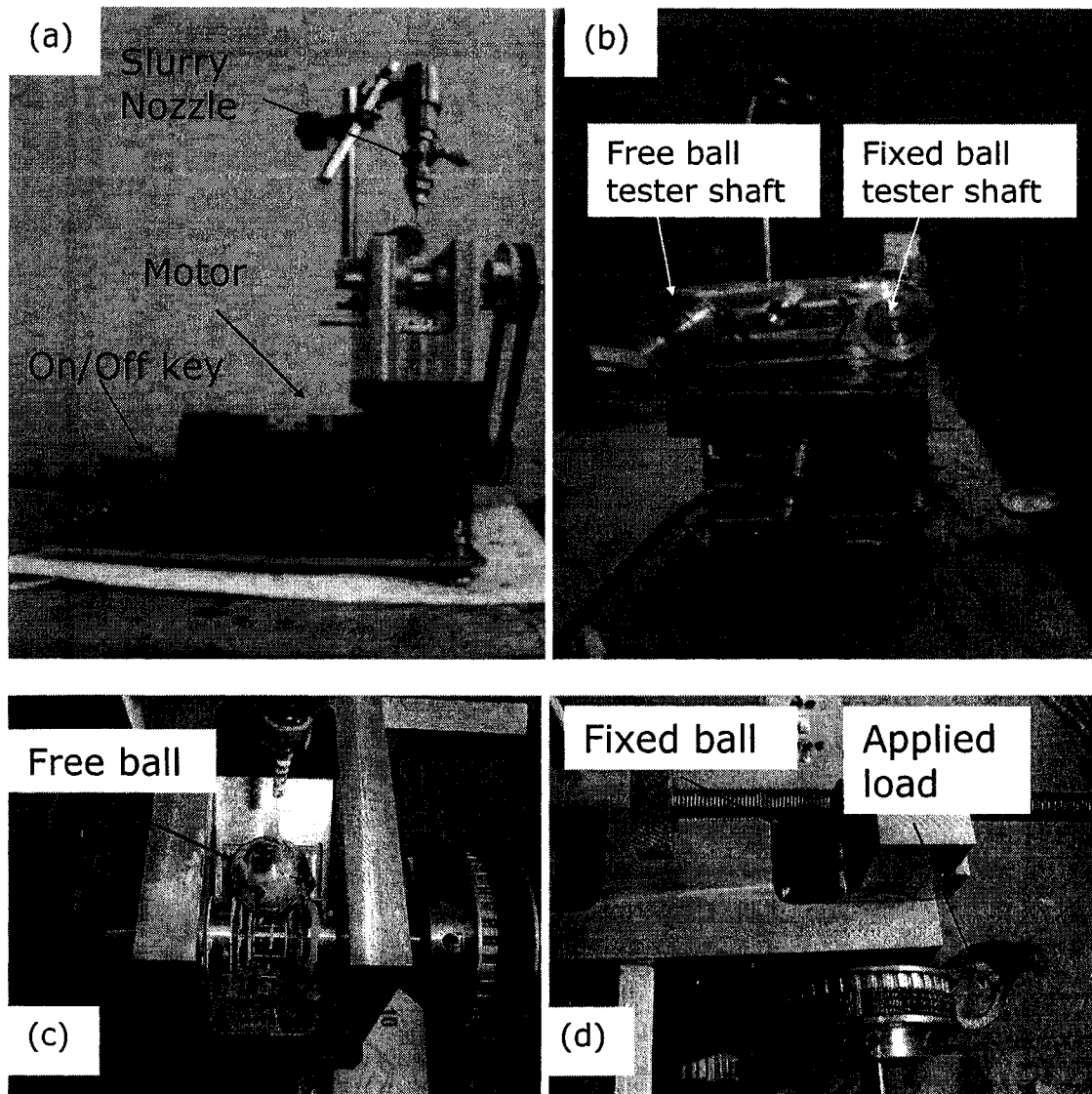
Fig. 3.10 Constructed micro-abrasion test system (a) side view, (b) front view, (c) details of the free ball-single shaft system, (d) details of the fixed ball system.

Table 3.8 Designed parameters for constructed micro-abrasion test system

Ball material	AISI 52100 bearing steel
Ball diameter (mm)	25.4mm
Ball hardness (Hv)	815±15
Ball weight (g)	63.6 (0.624N)
Motor rotation speed (rpm)	153
Abrasive slurry	5.0μm alumina water based suspension
Ball sliding speed (m/s)	0.2

3.3.2. Micro-abrasion wear test for substrates and coatings

The micro-abrasion wear property of substrates 0050A, G3500, CarmoCast, CC2 and D2 and coatings TiN and TiSiCN was tested by using the fixed ball system. The ball sliding speed was 0.2m/s (153 rpm) and the applied normal contact load was 4.0 N. The tests were carried out under dry sliding conditions. For each substrate sample, a set of two experiments was performed, corresponding to sliding distances of 24 m (306 revolutions) and 48m (612 rev.). For each coating sample, a set of two experiments was performed, corresponding to sliding distances of 48 m (612 revolutions) and 96m (1224 rev.). An optical microscope was used to measure the diameter of the wear crater (Fig. 3.7). The characteristics of the wear was studied by SEM (Fig. 3.1) and FEI Scanning Electron Microscope (SEM) with Energy Dispersive Spectroscopy (EDS) (Fig. 3.6). The micro-abrasion wear test conditions for all the 5 substrates and 2 coatings are summarized in Table 3.9.

48

For a wear crater of spherical geometry, the wear volume V can be calculated according to Eq. (3.1), where d is the crater diameter, and R the ball radius.

$$V = \pi d^4/64R \quad \text{for } d \ll R \tag{3.1}$$

Table 3.9 Micro-abrasion wear tests sliding distances for 5 substrates and 2 coatings

		Substrates					Coatings	
		0050A	G3500	Carmo Cast	CC2	D2	TiN	TiSiCN
Test method	Sliding distance (m)							
Fixed ball	24	√	√	√	√	√		
	48	√	√	√	√	√	√	√
	96						√	√

49

CHAPTER 4 EXPERIMENTAL RESULTS AND

DISCUSSION I: SLIDING WEAR OF SUBSTRATES

In this chapter, the surface morphology and tribological properties of the substrates are analyzed.

4.1 SEM observation of morphology of substrates

Figs. 4.1 to 4.5 show the morphology of substrate 0050, G3500, CarmoCast, CC2 and D2 respectively before tribological testing. From Fig. 4.2, needle shaped graphite particles were observed on the surface of the G3500 substrate, indicated by arrows in the Figure. Graphite can be expected to act as a lubricant at the beginning stage of the wear.
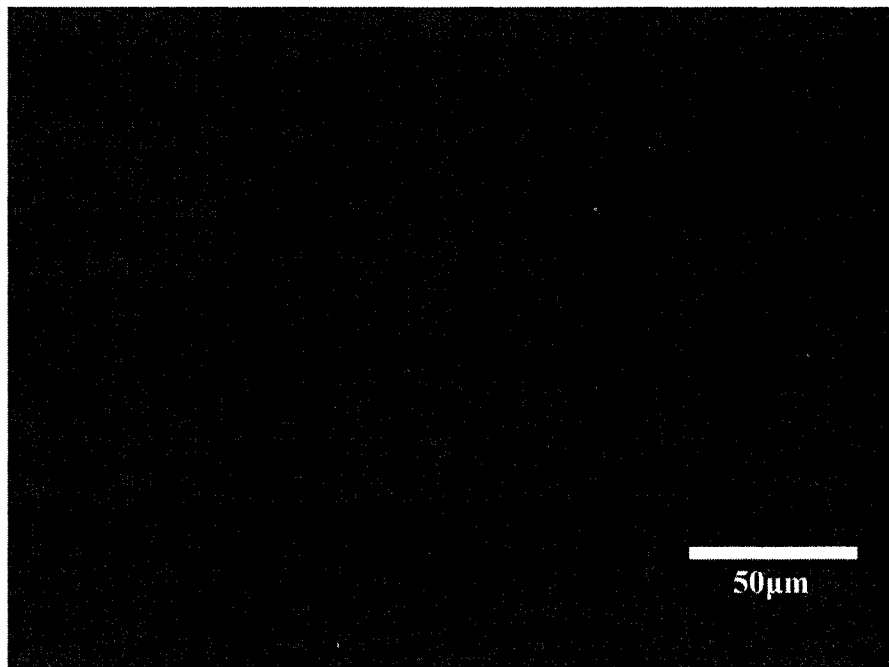
Fig. 4.1 SEM image of the 0050A substrate, 500×

50
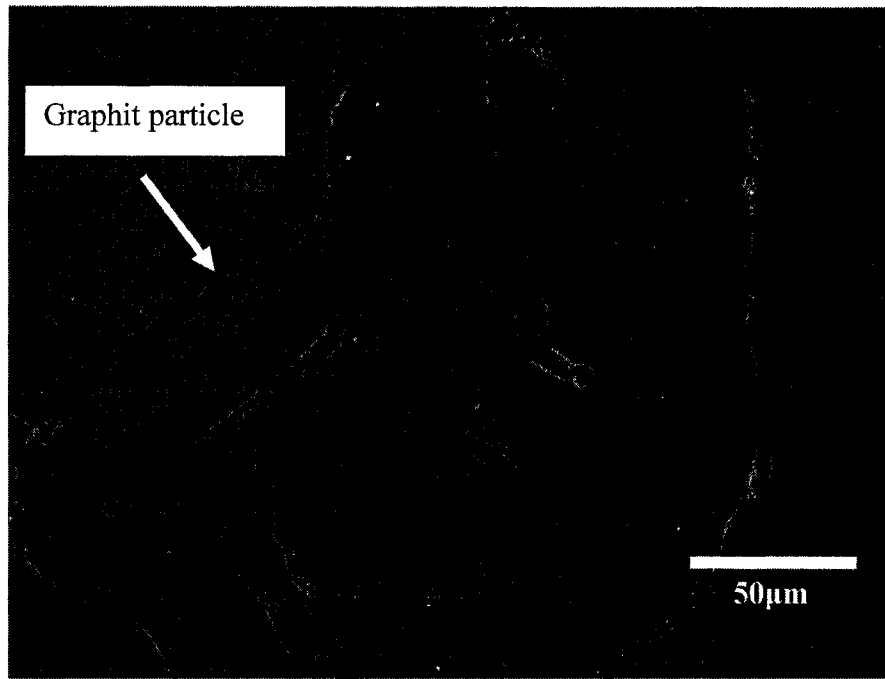
Fig. 4.2 SEM image of the G3500 substrate, 500×
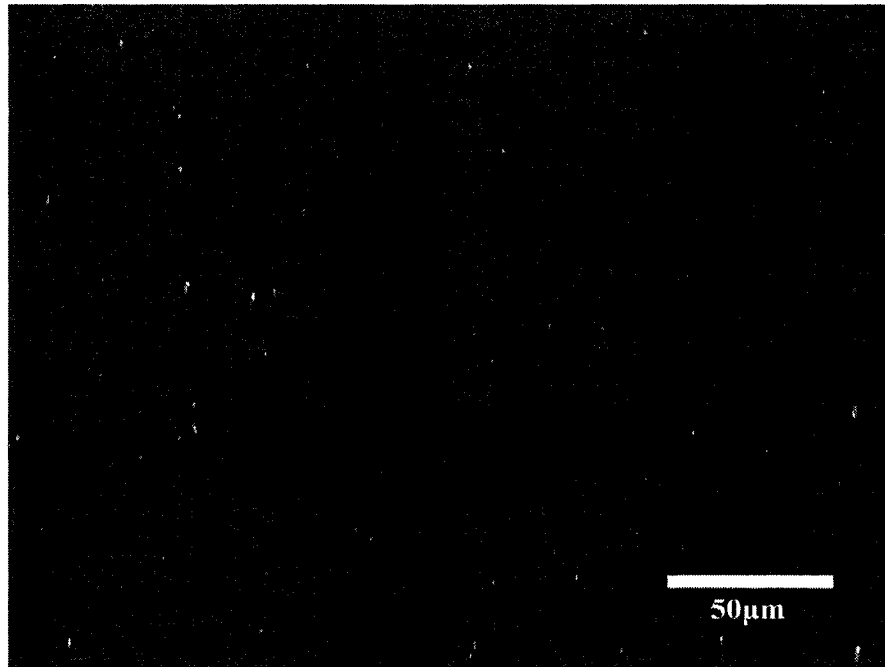
Fig. 4.3 SEM image of the CarmoCast substrate, 500×

51
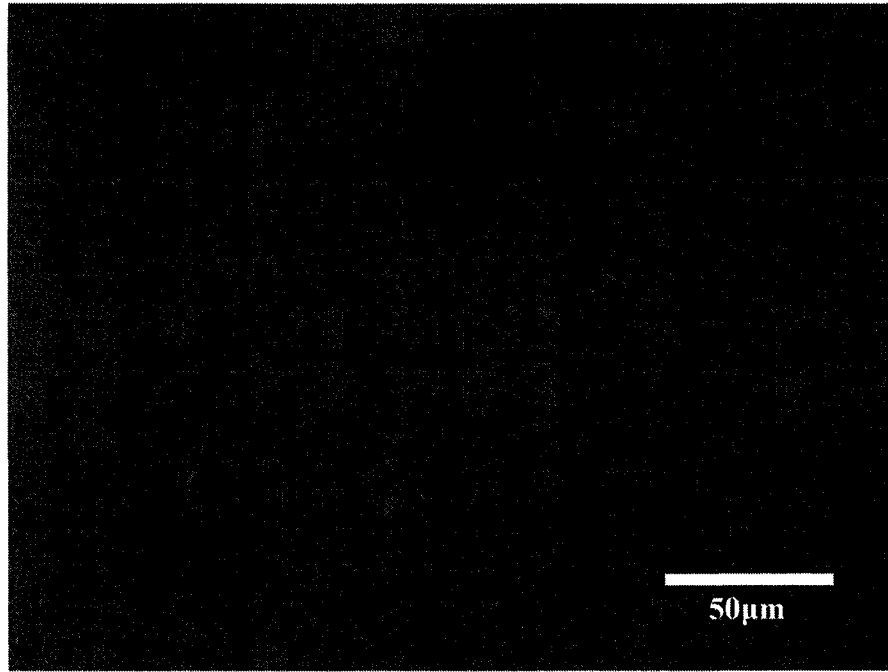
Fig. 4.4 SEM image of the CC2 substrate, 500×
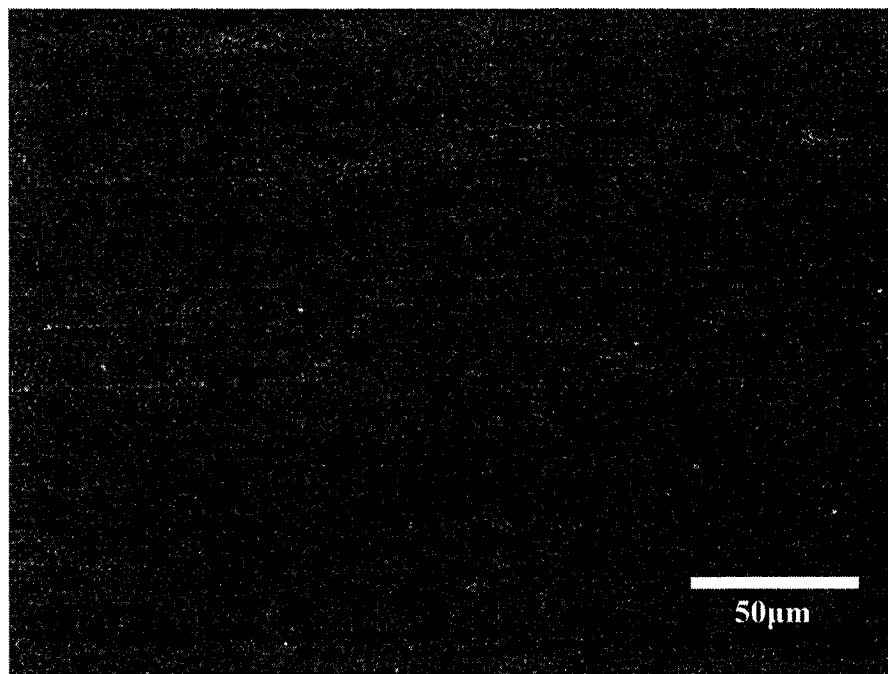
Fig. 4.5 SEM image of the D2 substrate, 500×

52

4.2 Hardness tests

The hardness of the substrates was measured on the substrate surface by a Vickers hardness tester. Although the quenching hardening process was done under a similar condition by another independent supplier, the substrates have different hardness. The values of hardness are shown in Fig. 4.6. 0050A displayed the highest hardness and G3500 showed the lowest hardness.

	0050A	G3500	CarmoCast	CC2	D2
Hv	803	293	513	600	702
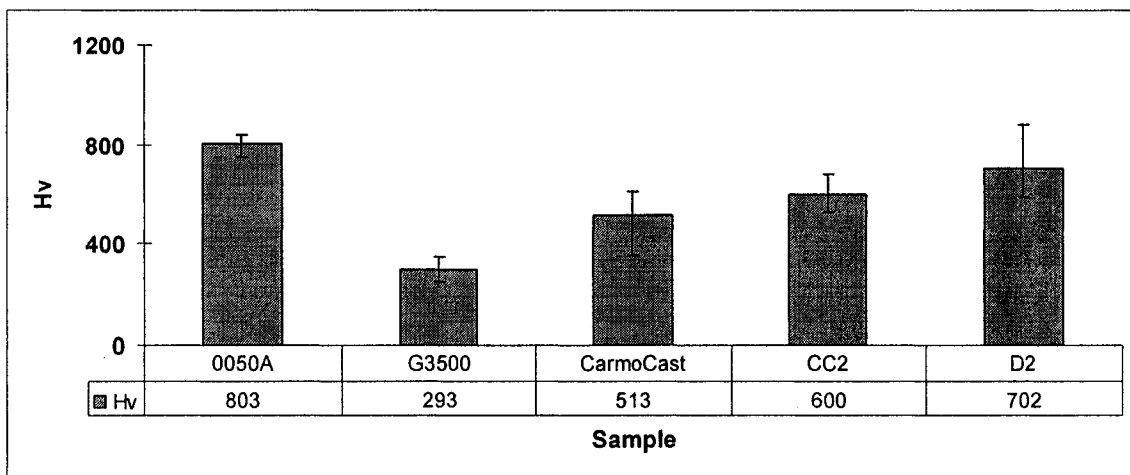
Fig. 4.6 Hardness of 5 substrates of 0050A, G3500, CarmoCast, CC2 and D2

4.3 COF (Coefficient of friction) and Wear Rate in Pin-on-disc tests

Fig. 4.7 and Fig. 4.8 show tribological properties of the tested samples against alumina pin, aluminium pin, steel pin under 5N load, against aluminium pin under 10N load and against steel pin under 15N load. The values of coefficient of friction (COF) and wear rate are presented in Figs. 4.7 and 4.8.

COF	0050A	G3500	CarmoCast	CC2	D2
▨ Alumina -5N	0.6	0.7	0.9	0.75	0.69
■ Aluminium-5N	0.55	0.55	0.6	0.45	0.6
□ Steel -5N	0.6	0.45	0.6	0.6	0.5
□ Aluminium-10N	0.45	0.5	0.6	0.45	0.55
■ Steel-15N	0.8	0.65	0.8	0.7	0.6
			Sample		
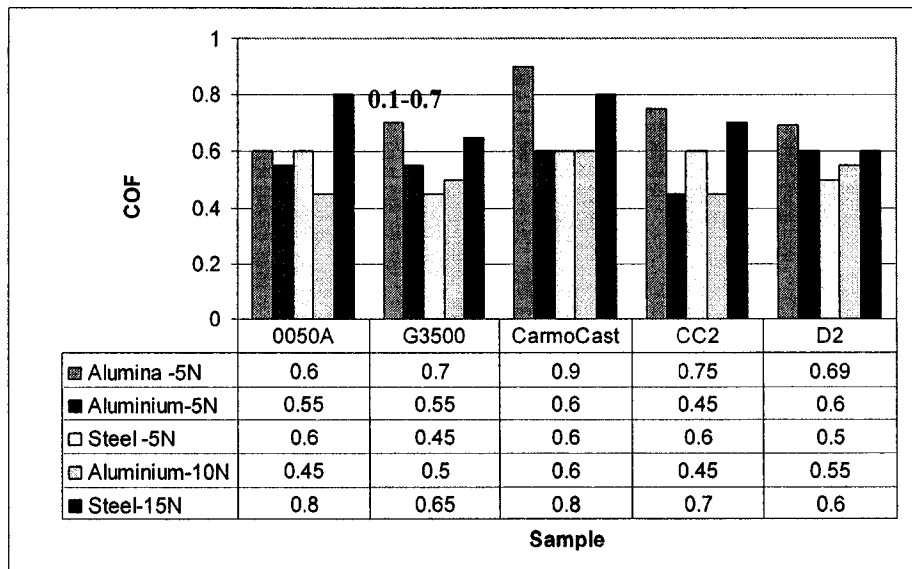
Fig. 4.7 COF of 5 substrates (0050A, G3500, CarmoCast, CC2 and D2) against alumina pin, aluminium pin, steel pin under 5N load, against aluminium pin under 10N load and against steel pin under 15N load

Wear Rate ($10^3 \mu m^3/Nm$)	0050A	G3500	CarmoCast	CC2	D2
▨ Alumina -5N	13.2	8.1	12.7	12.5	6.7
■ Aluminium-5N	3.8	7.6	4.1	4.9	1.5
□ Steel -5N	1.1	0.7	5.1	2.5	0.5
□ Aluminium-10N	3.9	6.7	7.9	3.6	4.7
■ Steel-15N	4.1	14	11.1	5.7	3.1
			Sample		
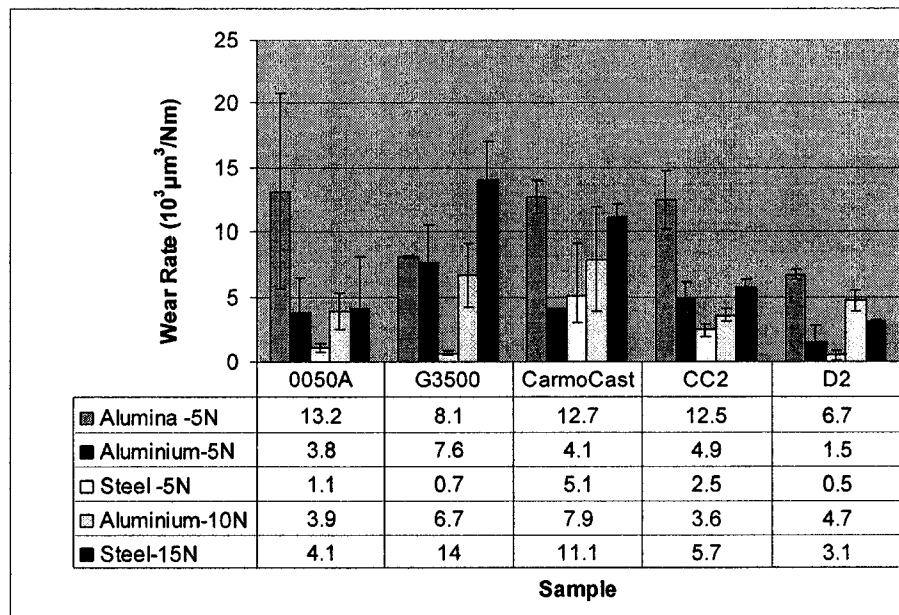
Fig. 4.8 Wear rate of 5 substrates (0050A, G3500, CarmoCast, CC2 and D2) against alumina pin, aluminium pin, steel pin under 5N load, against aluminium pin under 10N load and against steel pin under 15N load

54

4.4 Results and discussion of pin-on-disc tests against alumina pin under 5N load

4.4.1 COF (Coefficient of friction) and Wear Rate

Fig. 4.9 shows the COF, wear rate and hardness and of substrates against alumina pin under 5N load. The substrates perform the coefficient of friction from the range of 0.6 to 0.9. CarmoCast substrate showed the highest COF and 0050A displayed the lowest COF. G3500 substrate displays two stages of friction. At the first stage, the graphite particles act as a lubricant to reduce the resistance for friction, so the substrate shows a very low COF of 0.1 at the beginning of the sliding test. After the wear out of the graphite, the COF increases dramatically from 0.1 to 0.7. Though G3500 has low hardness, it has relative low wear rate and this may benefit from the lubricating effect of graphite particles. 0050A has the highest value of hardness; however, it also exhibits the highest wear rate, probably due to the brittle martensite phase. For CarmoCast, CC2 and D2, the harder one has the better wear resistance. D2 has the lowest wear rate.

55

COF, Wear Rate & Hardness vs Alumina- 5N
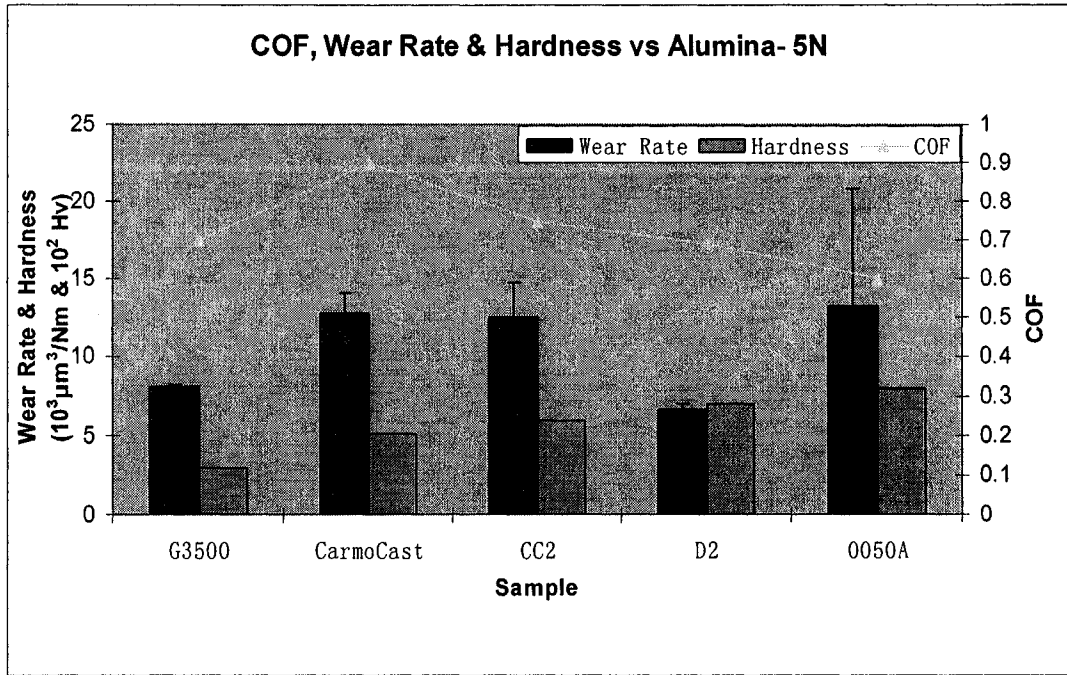
Fig. 4.9 COF, wear rate and hardness of 5 substrates (G3500, CarmoCast, CC2, D2and 0050A) against alumina pin under 5N load

4.4.2 3D Wyko profile images of wear tracks

Fig. 10 shows 3D Wyko profile images of substrates wear tracks after pin-on-disc tests against alumina pin under 5 N load. From these images we can see that D2 demonstrate a narrow and smooth wear track

56

(a) 0050-AO-5N

1.2 mm

0.9

(b) G3500-AO-5N

1.2 mm

0.9

57

(c) CarmoCast-AO-5N
1.2 mm
0.9

(d) CC2-AO-5N
1.2 mm
0.9

58

Fig. 4.10 3D Wyko profile images of substrates sliding wear tracks against alumina pin under 5N load: (a) 0050A, (b) G3500, (c) CarmoCast, (d) CC2 and (e) D2

4.4.3 SEM images of wear tracks

Figs. 4.11 to 4.15 show the SEM images of wear tracks on substrates of 005A, G3500, CarmoCast, CC2 and D2 after pin-on-disc test against alumina pins under 5N load of 250m sliding distance. Materials peeling could be observed for all substrate materials. Servere wear could be found on 0050A, CarmoCast and CC2, and these substrates exhibit high wear rates when the wear tracks were measured using surface profile meter. Fatigue cracking and peeling could be found on the wear track of G3500. Abrasive wear dominates under this test conditon.

59

Fig. 4.11 SEM images of wear track on 0050A substrate after pin-on-disc test against alumina pins under 5N load with 250m sliding distance (a) 50×, (b) 500×

Fig. 4.12 SEM images of wear track on G3500 substrate after pin-on-disc test against alumina pins under 5N load with 250m sliding distance (a) 50×, (b) 500×

Fig. 4.13 SEM images of wear track on CarmoCast substrate after pin-on-disc test against alumina pins under 5N load with 250m sliding distance (a) 50×, (b) 500×

60

Fig. 4.14 SEM images of wear track on CC2 substrate after pin-on-disc test against alumina pins under 5N load with 250m sliding distance (a) 50×, (b) 500×

Fig. 4.15 SEM images of wear track on D2 substrate after pin-on-disc test against alumina pins under 5N load with 250m sliding distance (a) 50×, (b) 500×

4.5 Results and discussion of pin-on-disc tests against aluminium pin under 5N load

4.5.1 COF (Coefficient of friction) and Wear Rate

61

Fig. 4.16 shows the COF, wear rate and hardness of substrates against aluminium pin under 5N load. The substrates show the coefficient of friction from the range of 0.45 to 0.55. CarmoCast substrate showed the highest COF which can be attributed to its lower hardness and CC2 displayed the lowest COF. All the substrates have much lower wear rate than those against alumina pins under 5 N. Unlike the performance against alumina pin, G3500 has the highest wear rate which could be counted on its low hardness and it seems that it doesn't benefit from the lubricating effect of graphite particles. Considering the error of measurement, the overall anti-wear performance for G3500, CarmoCast, CC2 and D2 has the tendency that the harder material has the better wear resistance. 0050A displays higher wear rate than D2, probably due to its brittle martensitic phase. D2 presents the lowest wear rate.
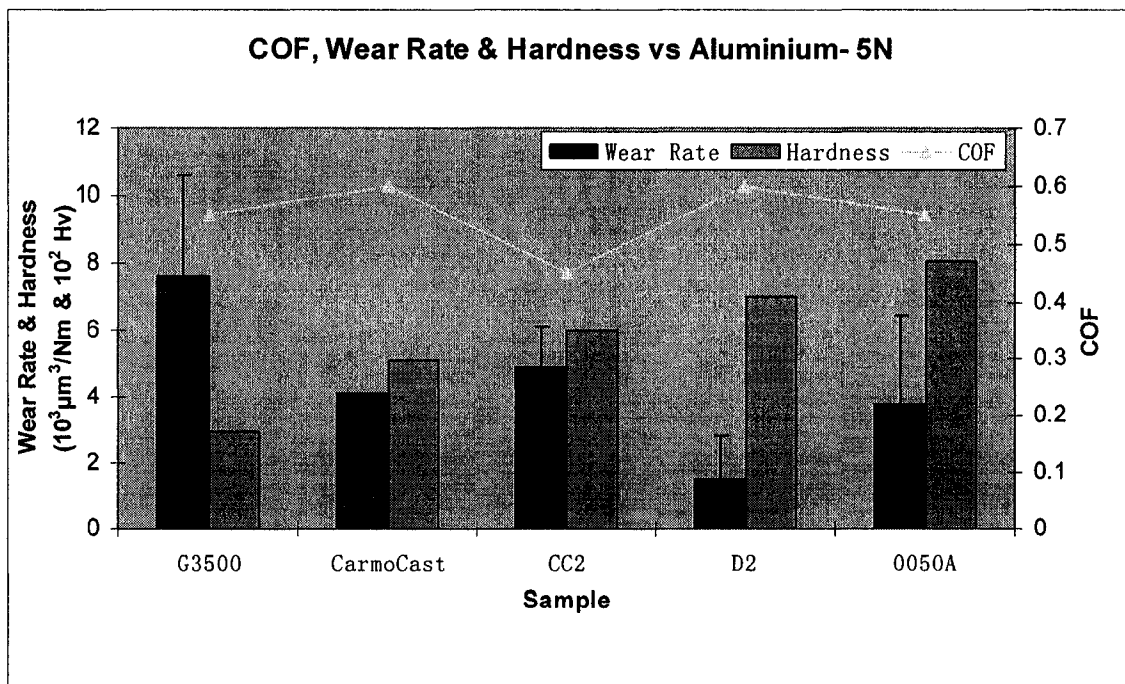
Fig. 4.16 COF, wear rate and hardness of 5 substrates (G3500, CarmoCast, CC2, D2 and 0050A,) against aluminium pin under 5N load

4.5.2 3D Wyko profile images of wear tracks

Fig. 4.17 shows 3D Wyko profile images of substrates wear tracks after pin-on-disc tests against aluminium pin under 5 N load. Compared to wear tracks against alumina pin, these wear tracks display wider and shallower appearances.

2.5 mm

0050-Al-5N

2.5 mm

G3500-Al-5N

63

CarmoCast-Al-5N

(d)

CC2-Al-5N

64
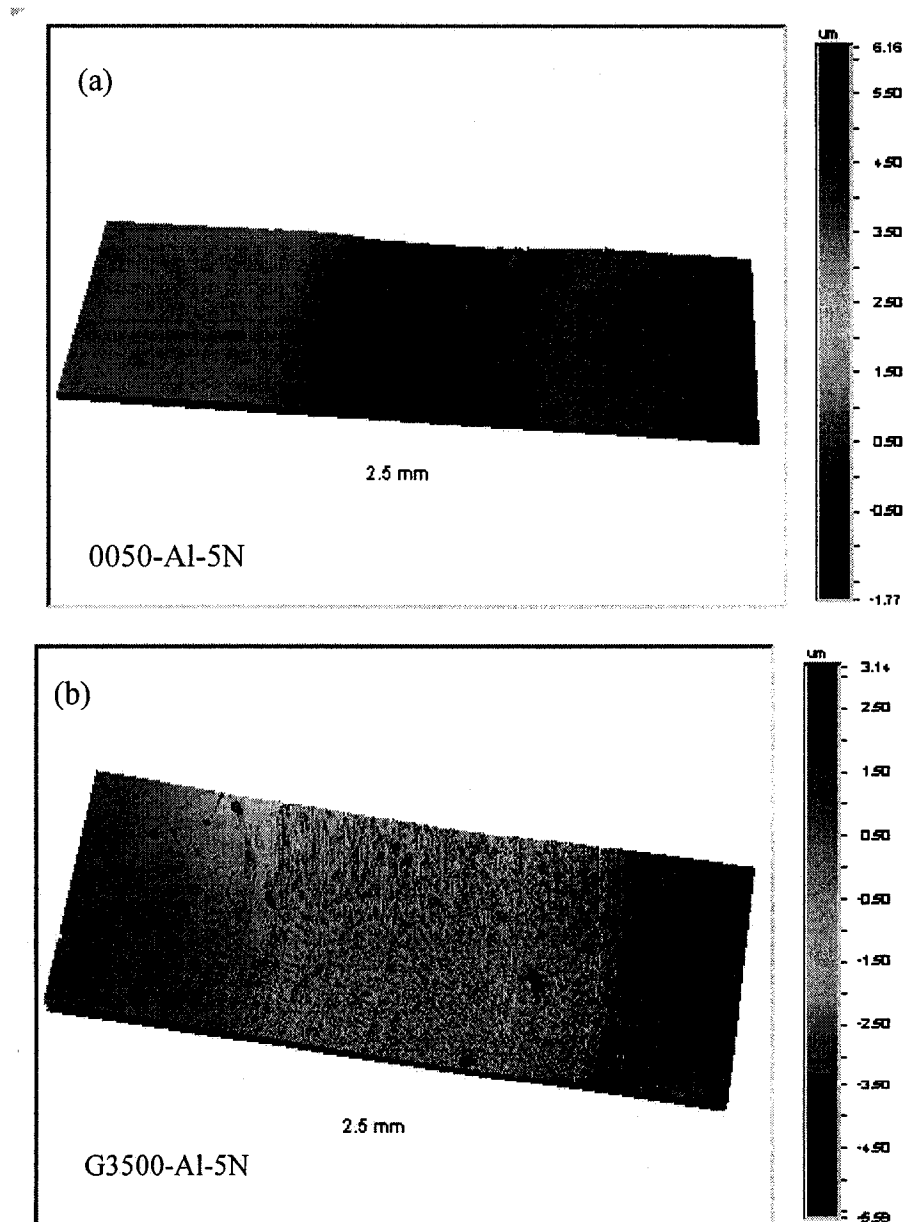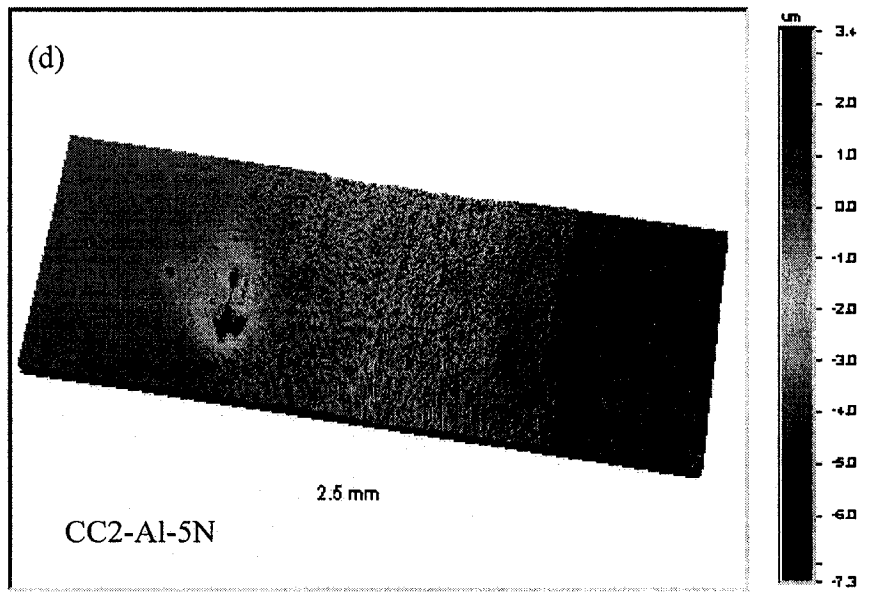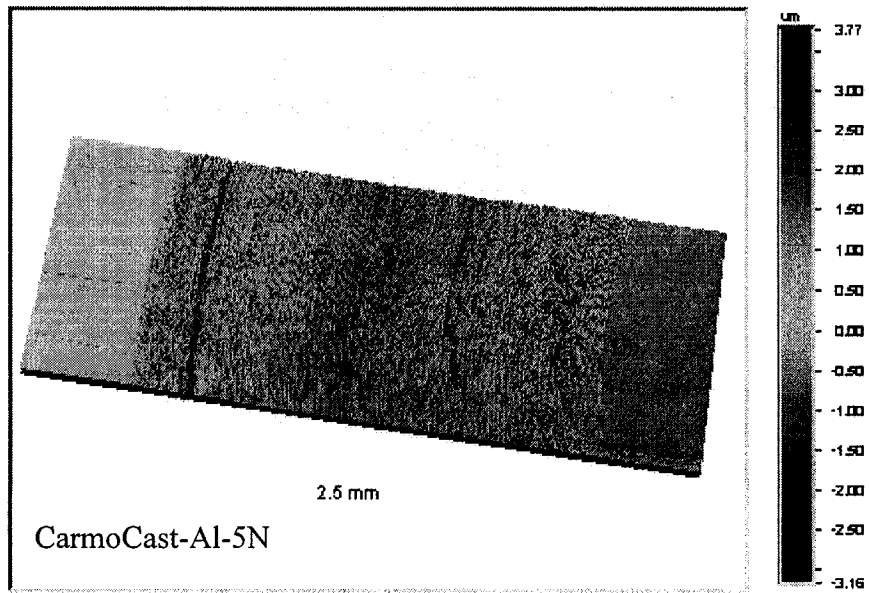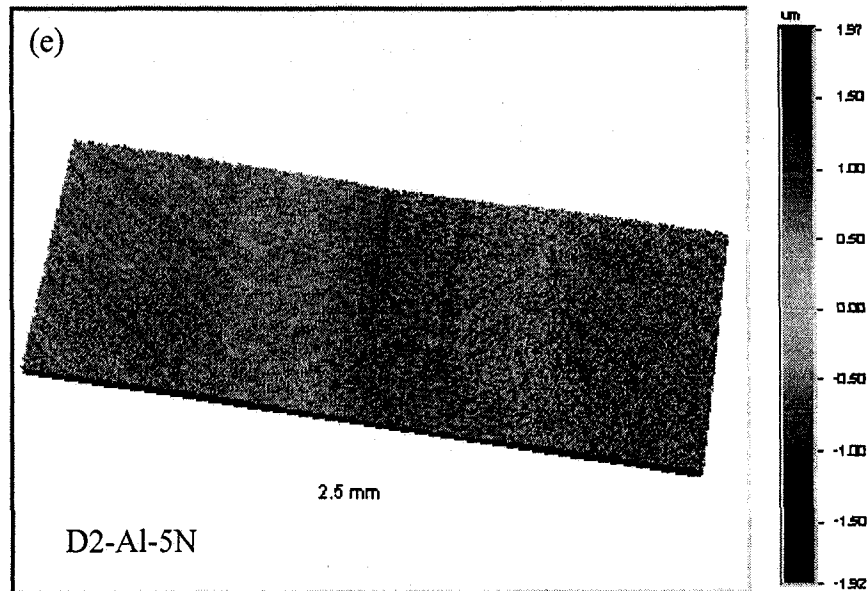
Fig. 4.17 3D Wyko profile images of substrates sliding wear tracks against alumina pin under 5N load: (a) 0050A, (b) G3500, (c) CarmoCast, (d) CC2 and (e) D2

4.5.3 SEM images of wear tracks

Figs. 4.18 to 4.22 show the SEM images of wear tracks on substrates of 005A, G3500, CarmoCast, CC2 and D2 after pin-on-disc test against aluminium pins under 5N load with 250m sliding distance. Compared with the wear tracks presented in Figs. 4.11 to 4.15 for tests against alumina pins, the wear tracks on substrates of 0050A, G3500, CarmoCast, CC2 and D2 after pin-on-disc test against aluminium pins are much wider and smother. This is consistent with the much lower wear rate for each substrate against aluminium pin compared with the wear rate obtained for respective substrate against alumina pin. And on all these wear tracks, transferred materials can be observed. D2 presents a smooth wear track and high hardness could be one of the reasons. Adhesive wear dominates under this test condition.

65
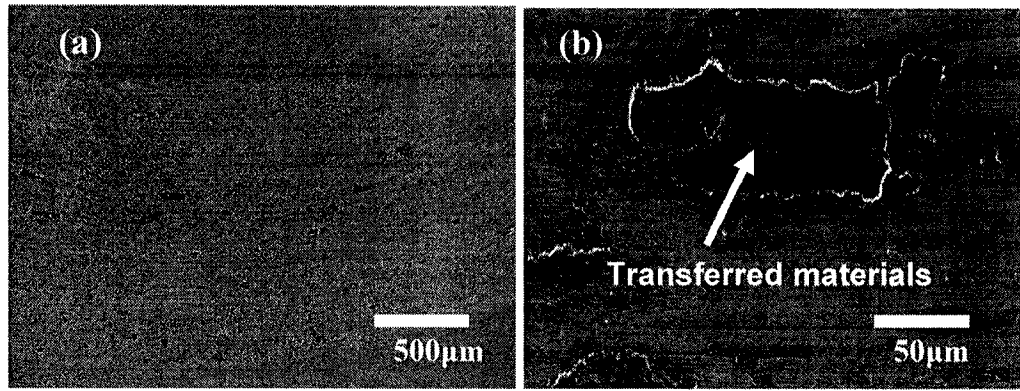
Fig. 4.18 SEM images of wear track on 0050A substrate after pin-on-disc test against aluminium pins under 5N load with 250m sliding distance (a) 50×, (b) 500×
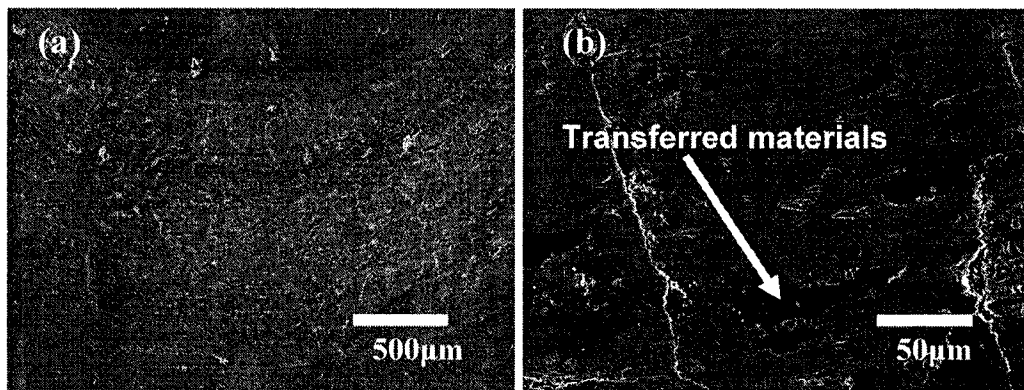
Fig. 4.19 SEM images of wear track on G3500 substrate after pin-on-disc test against aluminium pins under 5N load with 250m sliding distance (a) 50×, (b) 500×

Fig. 4.20 SEM images of wear track on CarmoCast substrate after pin-on-disc test against aluminium pins under 5N load with 250m sliding distance (a) 50×, (b) 500×

66

Fig. 4.21 SEM images of wear track on CC2 substrate after pin-on-disc test against aluminium pins under 5N load with 250m sliding distance (a) 50×, (b) 500×

Fig. 4.22 SEM images of wear track on D2 substrate after pin-on-disc test against aluminium pins under 5N load with 250m sliding distance (a) 50×, (b) 500×

4.6 Results and discussion of pin-on-disc tests against aluminium pin under 10N load

4.6.1 COF (Coefficient of friction) and Wear Rate

Fig. 4.23 shows the COF, wear rate and hardness of substrates against aluminium pin under 10N load. The substrates perform the coefficient of friction from the range of 0.45 to 0.6. CarmoCast substrate shows the highest COF and wear rate while CC2 display the

lowest COF and wear rate. Similar to the performance against alumina under 5 N and unlike the performance against aluminium pin under 5 N load, G3500 did not exhibit the highest wear rate due to its lowest hardness and it seems that it could benefit more from the lubricating effect of graphite particles under higher Hertz contact pressure. For CarmoCast, D2 and 0050A, the anti-wear performance has the tendency that the harder the material is the better wear resistance it has. CC2 presents the lowest wear rate.
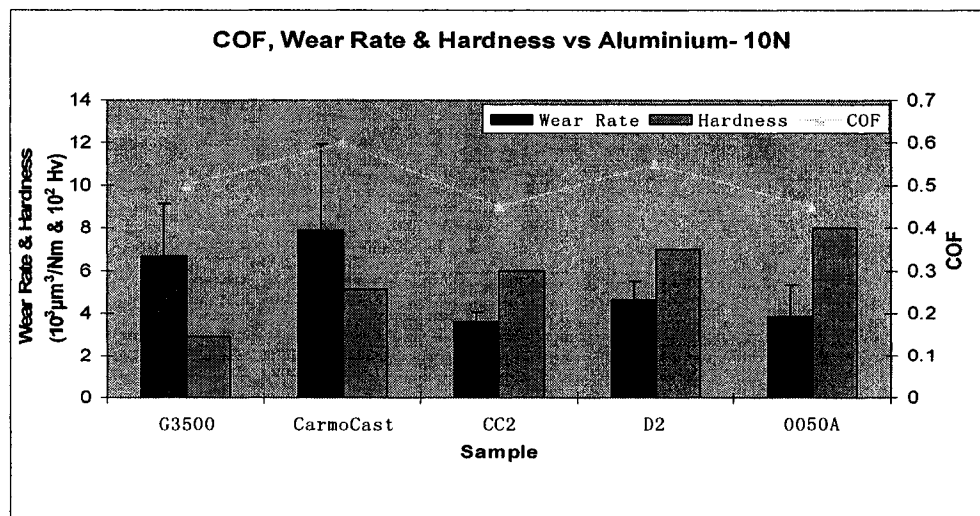
Fig. 4.23 COF and Wear Rate of 5 substrates (0050A, G3500, CarmoCast, CC2 and D2) against aluminium pin under 10N load

4.6.2 3D Wyko profile images of wear tracks

Fig. 4.24 shows 3D Wyko profile images of substrates wear tracks after pin-on-disc tests against aluminium pin under 10 N load. Compared to wear tracks of substrates against aluminium pin under 5N load, these wear tracks display severer wear.

68

(a)

2.5 mm

0050-Al-10n

(b)

2.5 mm

G3500-Al-10n

(c)

CarmoCast-Al-10n
1.2 mm

0.9

(d)

CC2-Al-10n
2.5 mm

70
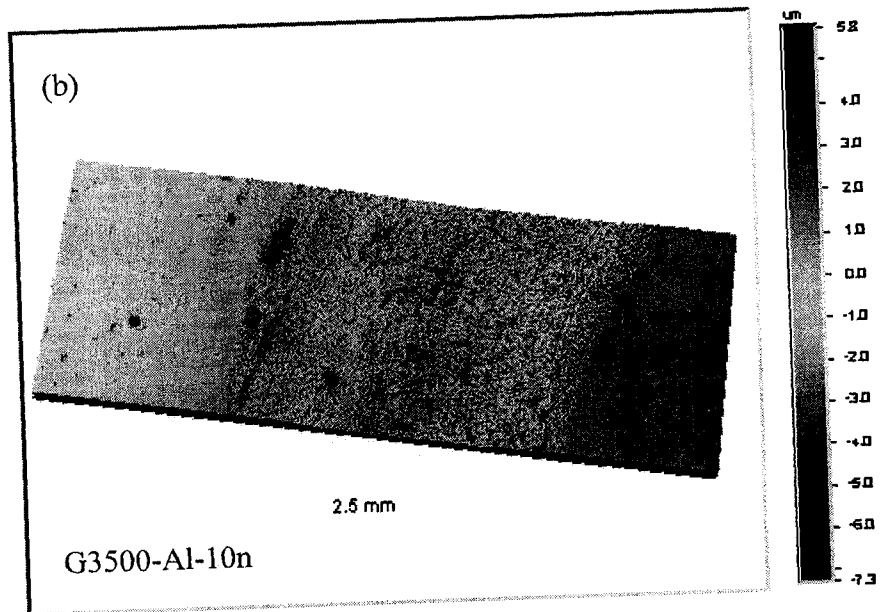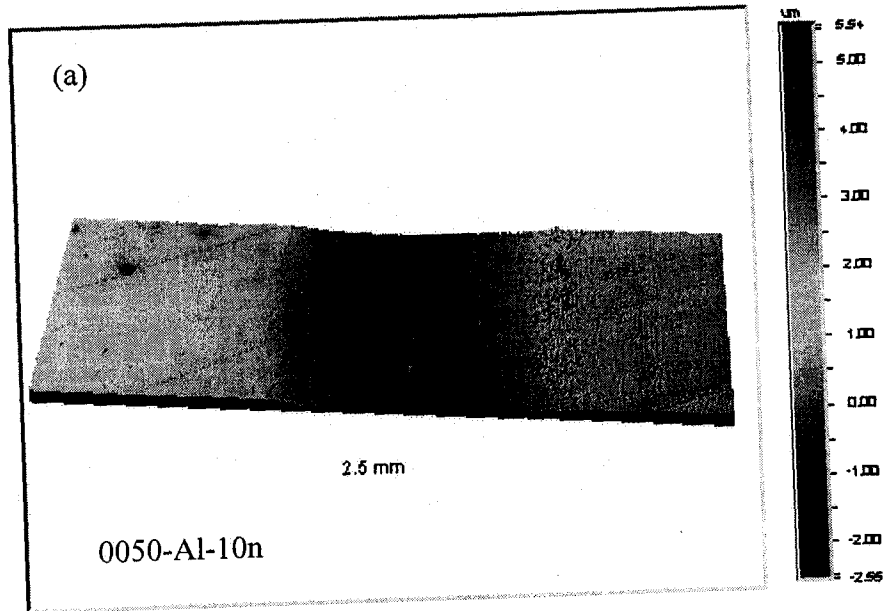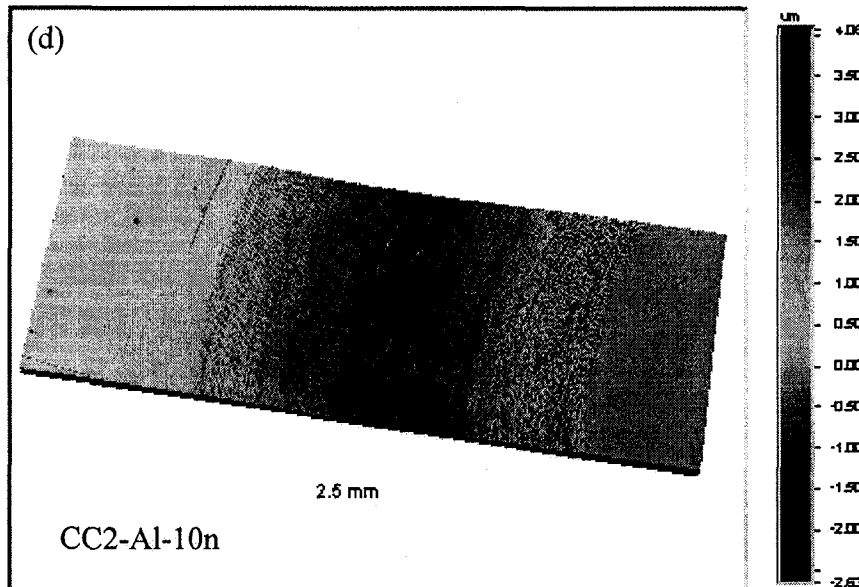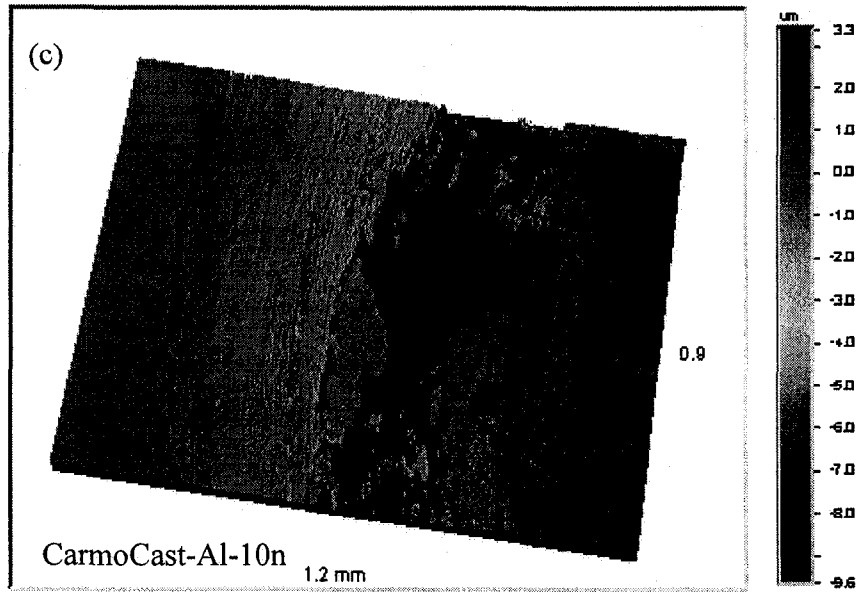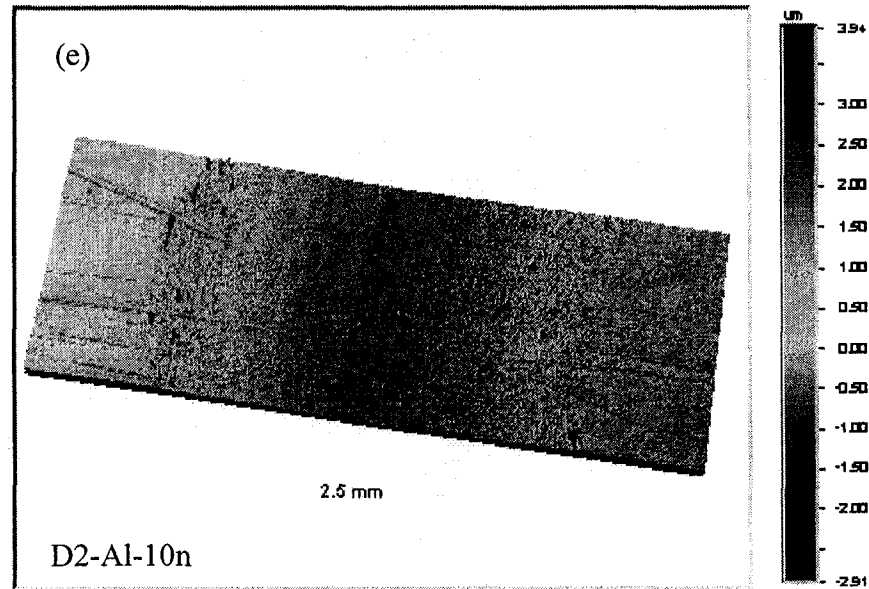
Fig. 4.24 3D Wyko profile images of substrates sliding wear tracks against alumina pin under 10N load: (a) 0050A, (b) G3500, (c) CarmoCast, (d) CC2 and (e) D2

4.6.3 SEM images of wear tracks

Figs. 4.25 to 4.29 show the SEM images of wear tracks on substrates of 005A, G3500, CarmoCast, CC2 and D2 after pin-on-disc test against aluminium pins under 10N load with 250m sliding distance. Compared with the wear tracks presented in Figs. 4.18 to 4.22 at tests against aluminium pins under 5N load, these wear tracks present severer wear and more transferred materials can be observed. Adhesive wear dominated under this test condition.

71
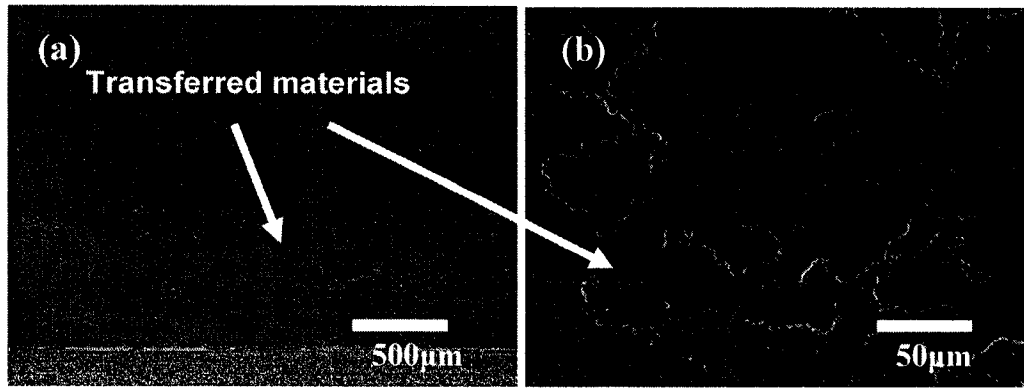
Fig. 4.25 SEM images of wear track on 0050A substrate after pin-on-disc test against aluminium pins under 10N load with 250m sliding distance (a) 50×, (b) 500×
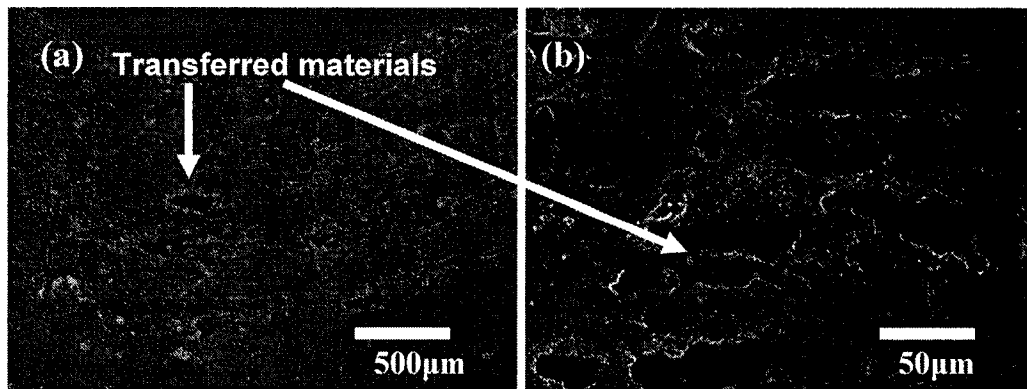
Fig. 4.26 SEM images of wear track on G3500 substrate after pin-on-disc test against aluminium pins under 10N load with 250m sliding distance (a) 50×, (b) 500×

Fig. 4.27 SEM images of wear track on CarmoCast substrate after pin-on-disc test against aluminium pins under 10N load with 250m sliding distance (a) 50×, (b) 500×

72

Fig. 4.28 SEM images of wear track on CC2 substrate after pin-on-disc test against aluminium pins under 10N load with 250m sliding distance (a) 50×, (b) 500×

Fig. 4.29 SEM images of wear track on D2 substrate after pin-on-disc test against aluminium pins under 10N load with 250m sliding distance (a) 50×, (b) 500×

4.7 Results and discussion of pin-on-disc tests against steel pin under 5N load

4.7.1 COF (Coefficient of friction) and Wear Rate

Fig. 4.30 shows the COF, wear rate and hardness of substrates against steel pin under 5N load. The substrates perform the coefficient of friction from the range of 0.45 to 0.6. 0050A, CarmoCast andCC2 substrates show similar higher COF. G3500 shows the

73

lowest COF. All the substrates except CarmoCast exhibit lower wear rate than those against alumina and aluminium pins respectively under 5N load. Similar to the performance against alumina under 5 N and against aluminium pin under 10 N, and unlike the performance against aluminium pin under 5 N load, G3500 exhibits low wear rate which could be attributed to the lubricating effect of graphite. 0050A exhibits the highest hardness, however, it displays higher wear rate than D2, probably due to its brittle martensite phase. For CarmoCast, CC2 and D2, the anti-wear performance has the tendency that the harder the material is the better wear resistance it has. D2 exhibits the lowest wear rate.
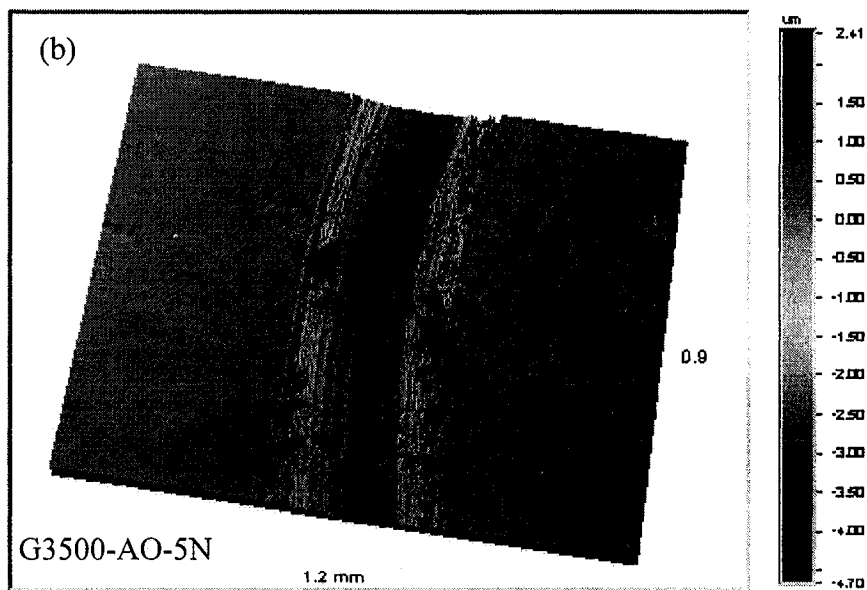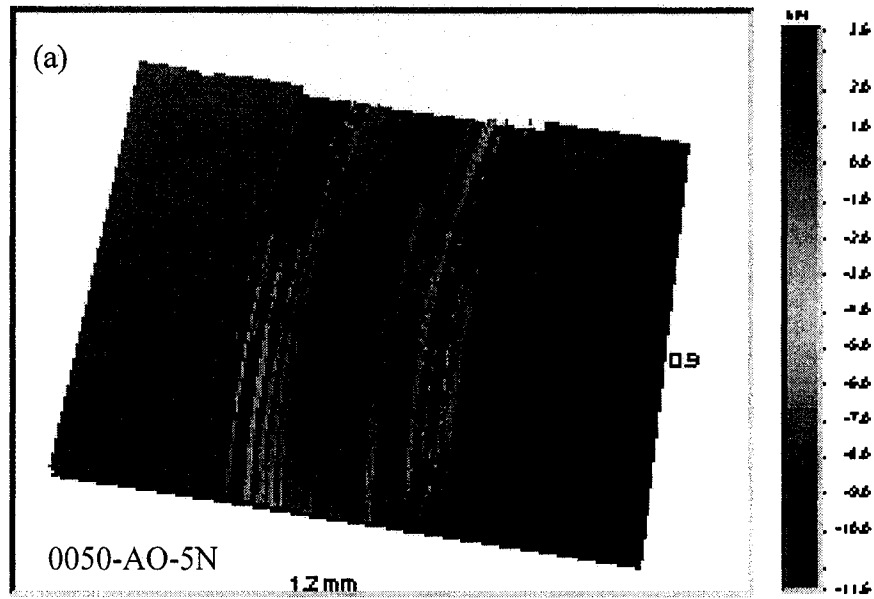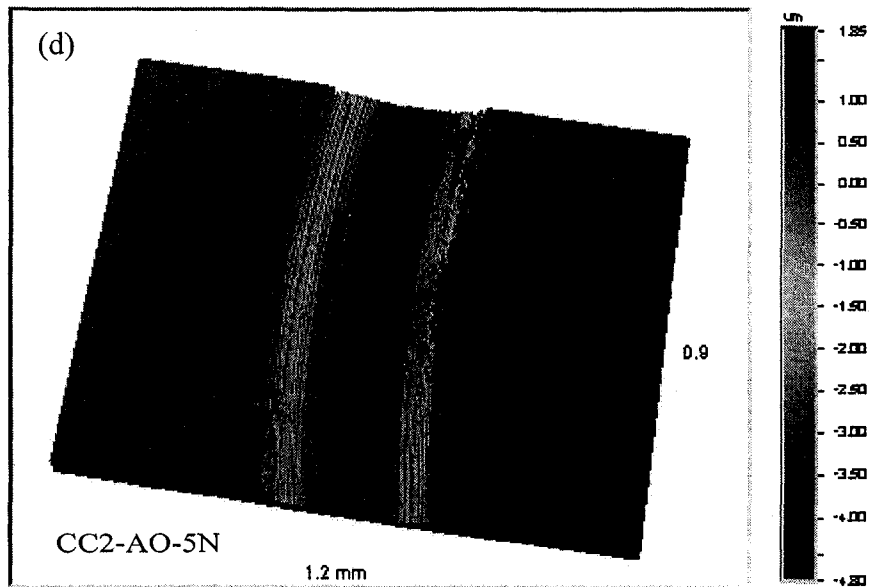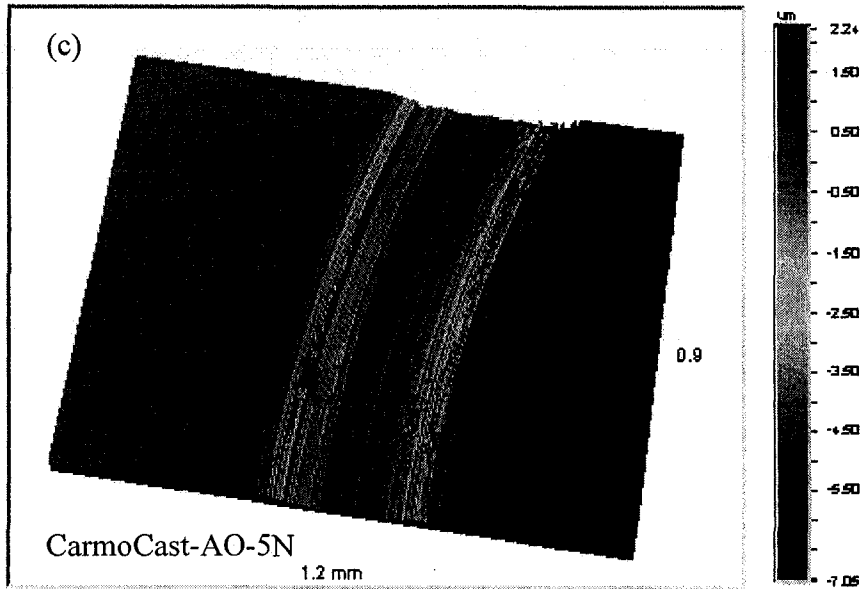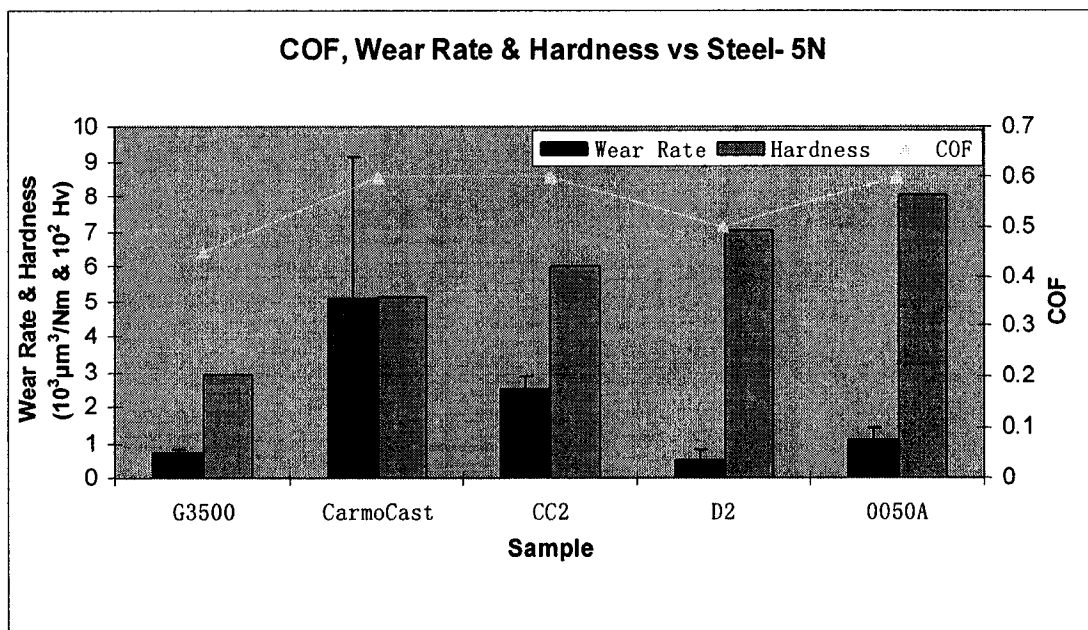

Fig. 4.30 COF, wear rate and hardness of 5 substrates (G3500, CarmoCast, CC2, D2 and 0050A,) against steel pin under 5N load

4.7.2 3D Wyko profile images of wear tracks

74

Fig. 4.31 shows 3D Wyko profile images of substrates wear tracks after pin-on-disc tests against steel pin under 5N load. Compared to wear tracks against alumina pin and aluminium pin under 5N load, these wear tracks show rougher appearances which demonstrate the existence of transferred materials.

75

(b)

G3500-S-5n

1.2 mm

0.9

um
3.1
1.0
-1.0
-3.0
-5.0
-7.0
-9.0
-11.0
-13.0
-15.4

(c)

CarmoCast-S-5n

1.2 mm

0.9

um
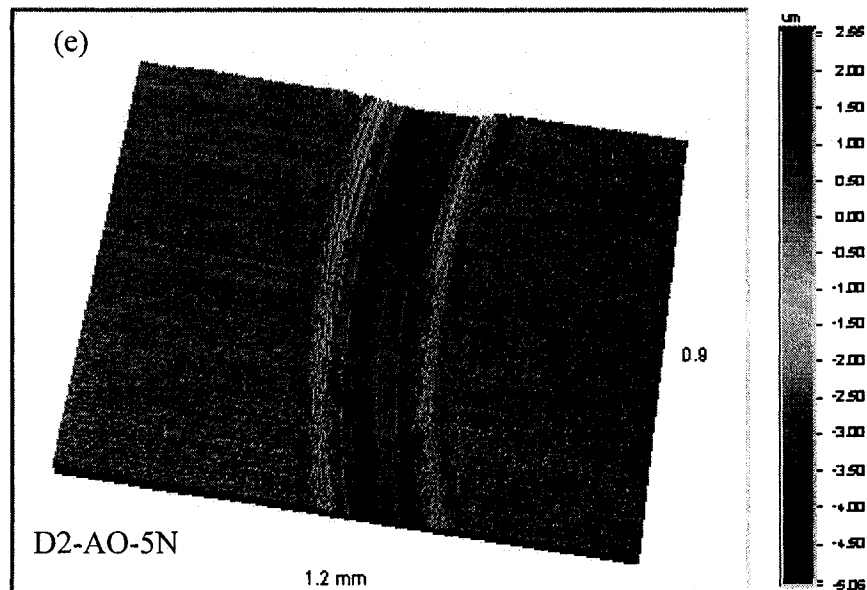1.59
1.00
0.00
-1.00
-2.00
-3.00
-4.00
-5.00
-6.00
-7.12

76
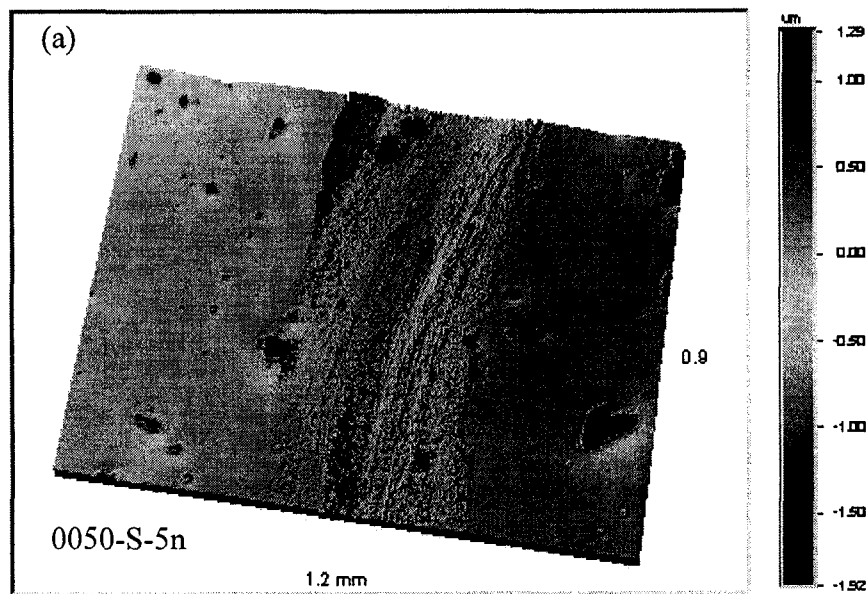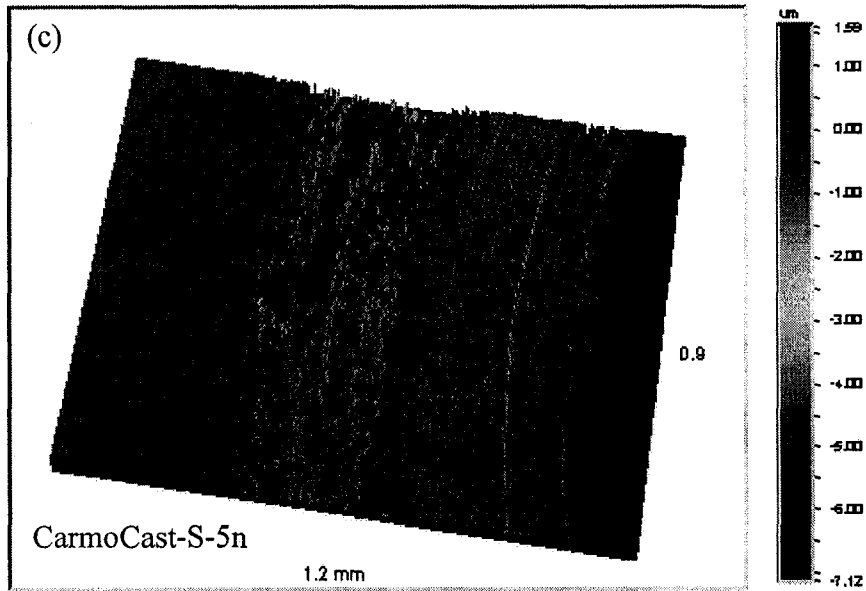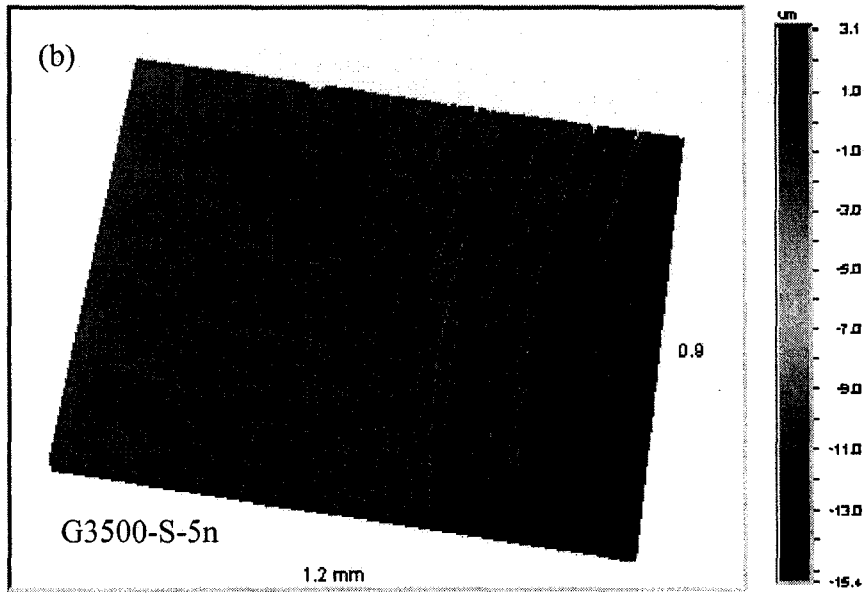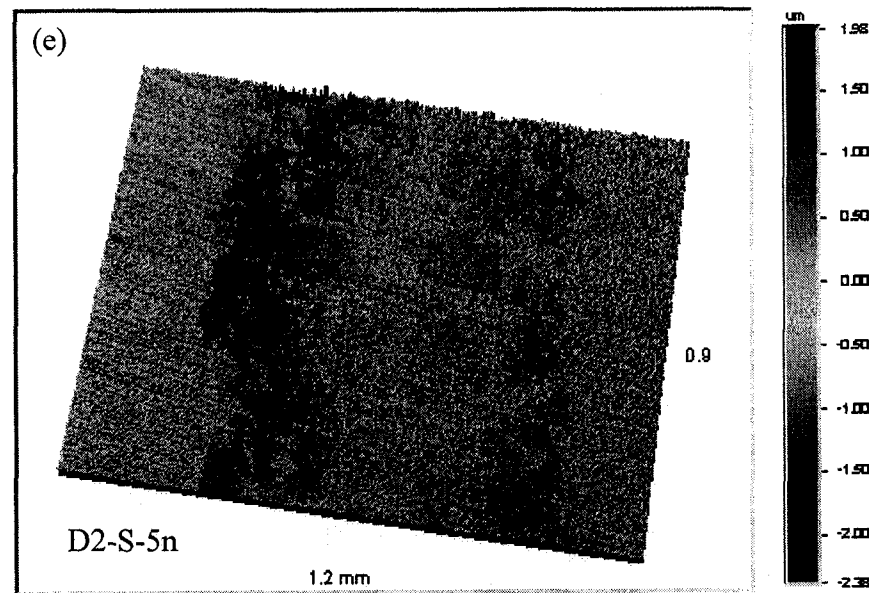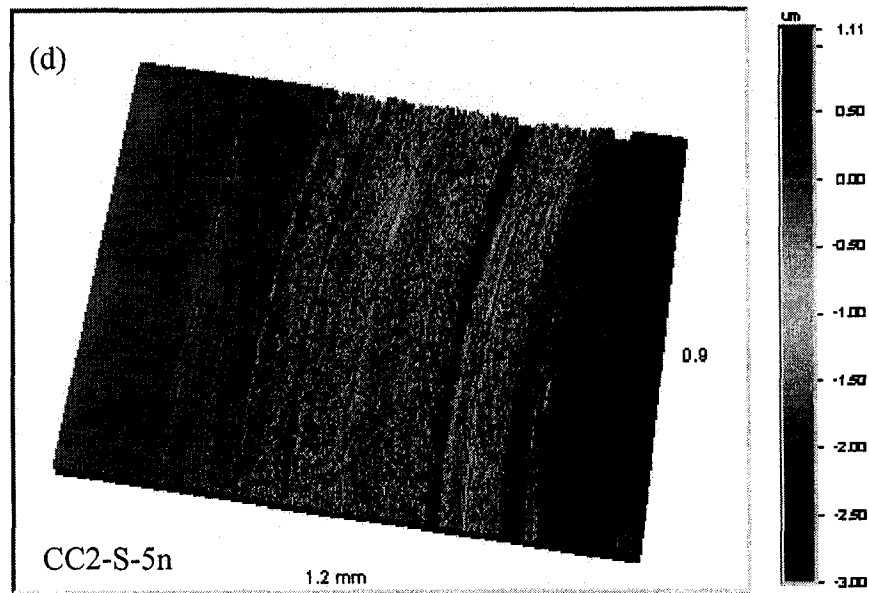
Fig. 4.31 3D Wyko profile images of substrates sliding wear tracks against steel pin under 5N load: (a) 0050A, (b) G3500, (c) CarmoCast, (d) CC2 and (e) D2

77

4.7.3 SEM images of wear tracks

Figs. 4.32 to 4.36 show the SEM images of wear tracks on substrates of 005A, G3500, CarmoCast, CC2 and D2 after pin-on-disc test against steel pins under 5N load with 250m sliding distance. Compared with the wear tracks presented in Figs. 4.14 to 4.18 at tests against alumina pins, wear tracks against steel pins are wider. Compared with the wear tracks presented in Figs. 4.18 to 4.22 for tests against aluminium pins under a 5N load, the wear tracks against steel pins present more transferred materials. This suggests that adhesive wear dominates under this test condition. It appears that CarmoCast has the widest and roughest wear track. Similar to the performance against alumina and aluminium pin under 5N load, D2 presents the best wear resistance. Adhesive wear dominates.
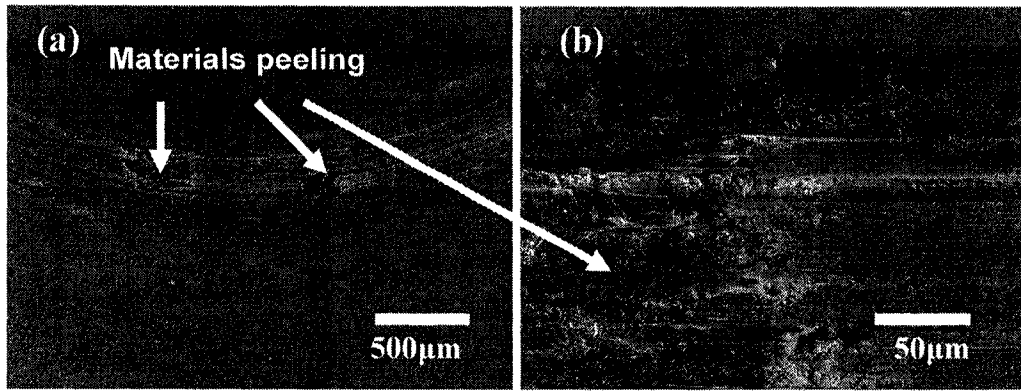

Fig. 4.32 SEM images of wear track on 0050A substrate after pin-on-disc test against steel pins under 5N load with 250m sliding distance (a) 50×, (b) 500×
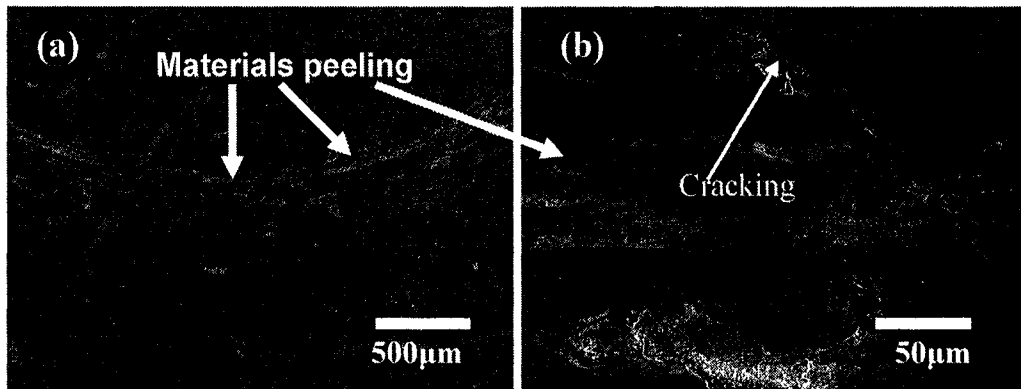
Fig. 4.33 SEM images of wear track on G3500 substrate after pin-on-disc test against steel pins under 5N load with 250m sliding distance (a) 50×, (b) 500×
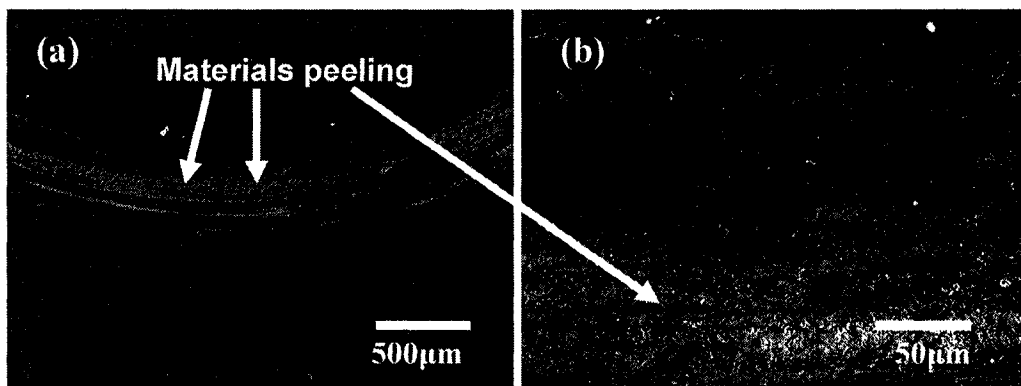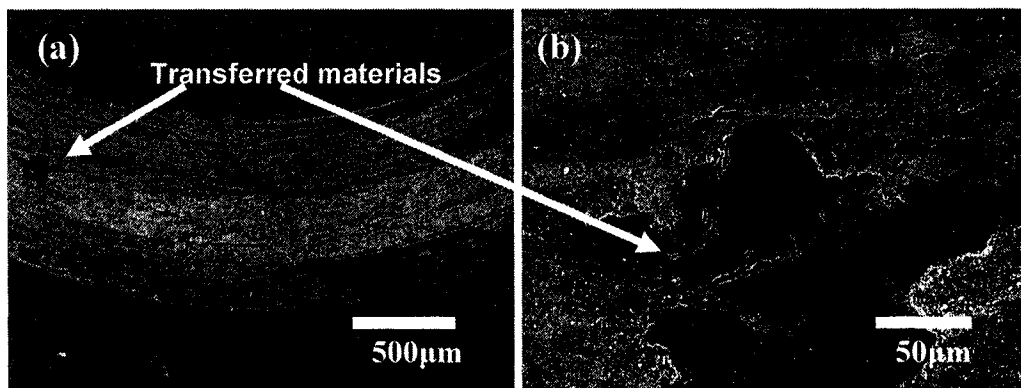

Fig. 4.34 SEM images of wear track on CarmoCast substrate after pin-on-disc test against steel pins under 5N load with 250m sliding distance (a) 50×, (b) 500×
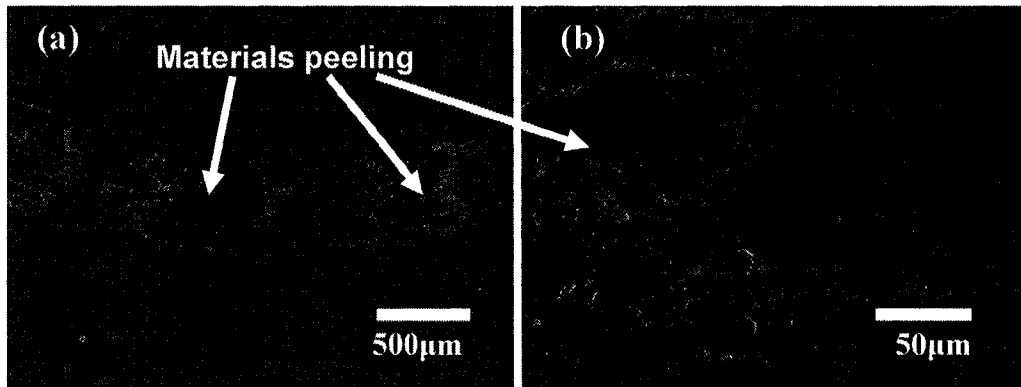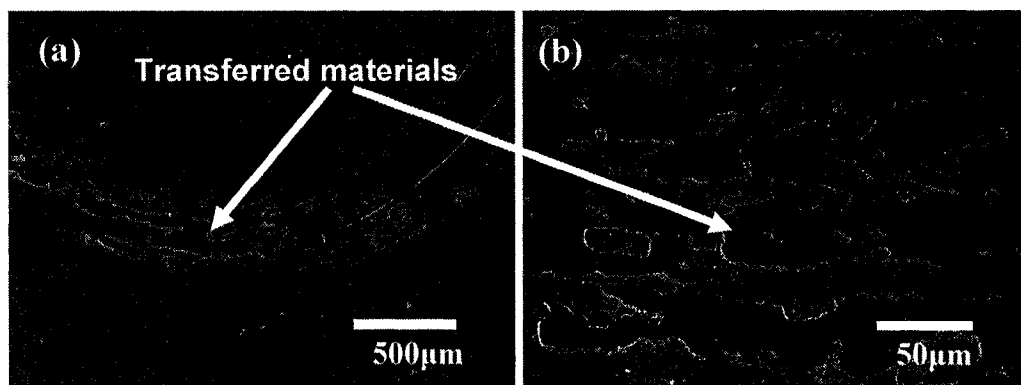

Fig. 4.35 SEM images of wear track on CC2 substrate after pin-on-disc test against steel pins under 5N load with 250m sliding distance (a) 50×, (b) 500×
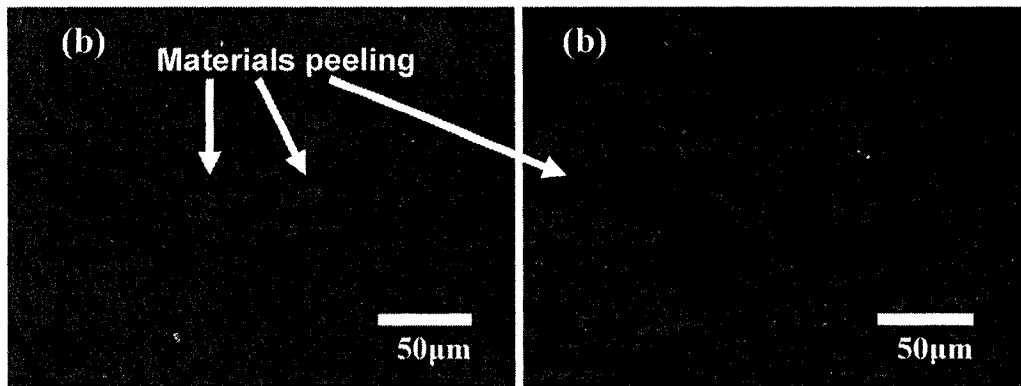
79

Fig. 4.36 SEM images of wear track on D2 substrate after pin-on-disc test against steel pins under 5N load with 250m sliding distance (a) 50×, (b) 500×

4.8 Results and discussion of pin-on-disc tests against steel pin under 15N load

4.8.1 COF (Coefficient of friction) and Wear Rate

Fig. 4.37 shows the COF, wear rate and hardness of substrates against steel pin under 15N load. The substrates show the coefficient of friction from the range of 0.6 to 0.8. 0050A and CarmoCast substrates show similar higher COF. D2 presents the lowest COF. G3500 has the highest wear rate. All substrates exhibit higher wear rate compared with the tests against steel pins under 5N load. Unlike the performance against alumina under 5 N, against aluminium pin under 10 N and against steel under 5N, and similar to the performance against aluminium pin under 5 N load, G3500 exhibit the highest wear rate due to its lowest hardness. From the wear performance of G3500 against different counterpart materials and under different load, it can be concluded that the graphite

80

particles take effect only under some conditions. If the Hertz contact pressure is as low as against aluminium under 5N load or as high as against steel pin under 15N, the graphite can not make too much different with the wear performance of G3500. Only under conditions like against alumina under 5N, against aluminium pin under 10N and against steel under 5N, the lubricating effect or wear reduction effect could be obviously observed. For G3500, CarmoCast, CC2 and D2, the harder material has the better wear resistance. Though 0050A has the highest value of hardness, it displays higher wear rate than D2, probably due to its brittle martensite phase. D2 exhibits the lowest wear rate.

COF,Wear Rate & Hardness vs Steel-15N
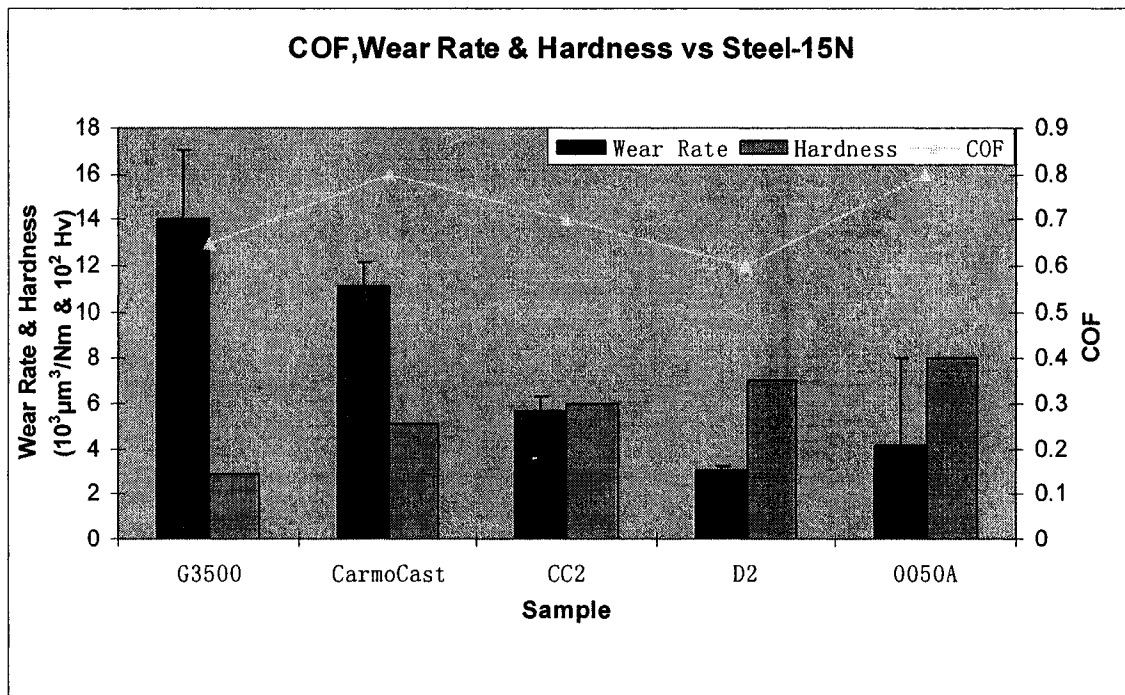
Fig. 4.37 COF, wear rate and hardness of 5 substrates (G3500, CarmoCast, CC2, D2 and 0050A,) against steel pin under 15N load

4.8.2 3D Wyko profile images of wear tracks

81

Fig. 4.38 shows 3D Wyko profile images of substrates wear tracks after pin-on-disc tests against steel pin under 15N load. Unlike the phenomena for substrates against steel pin under 5N load, material transfer occurring during the sliding wear process under low load is eliminated or becomes less under high load.

(a)

2.5 mm

0050-S-15N

(b)

2.5 mm

G3500-S-15N

82

(c)

2.5 mm

CarmoCast-S-15N

(d)

2.5 mm

CC2-S-15N

83
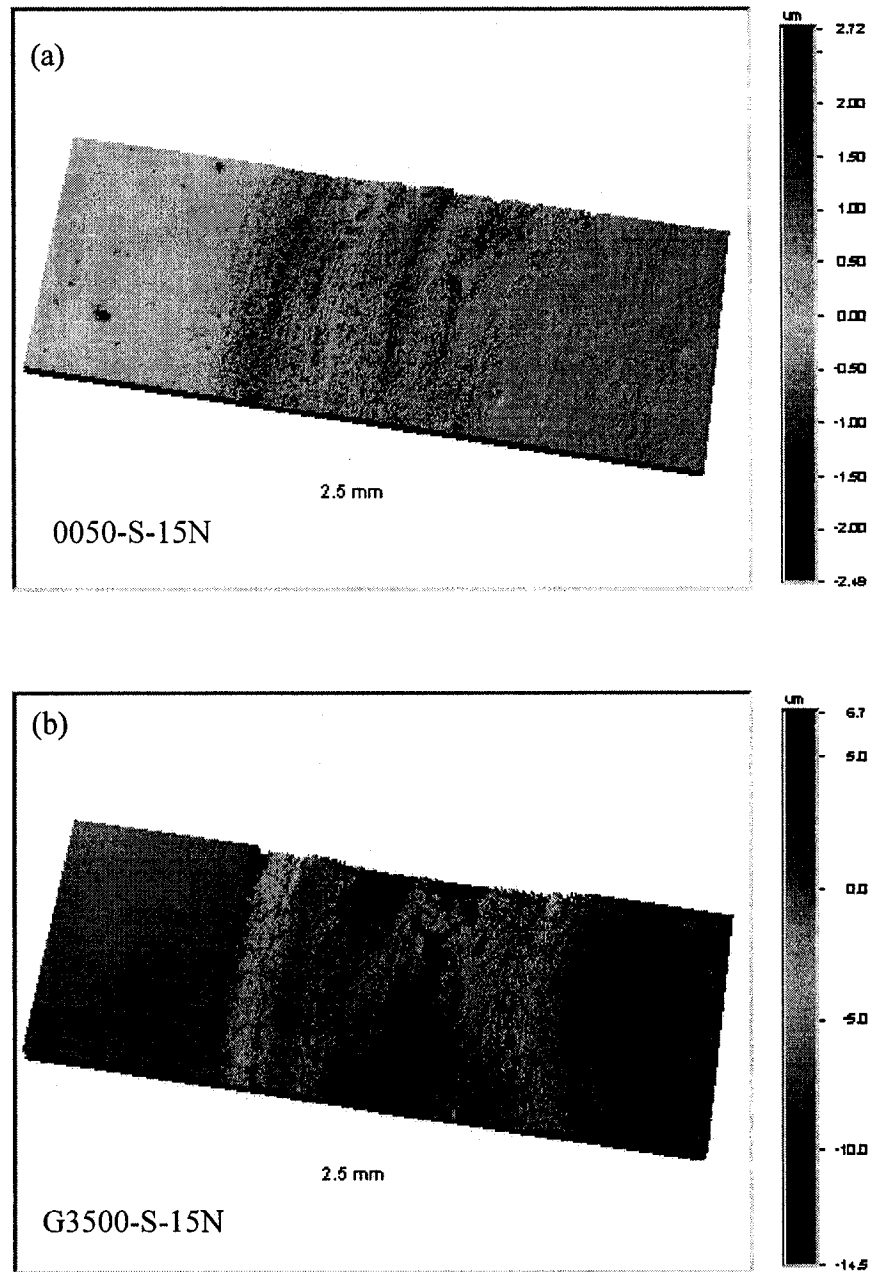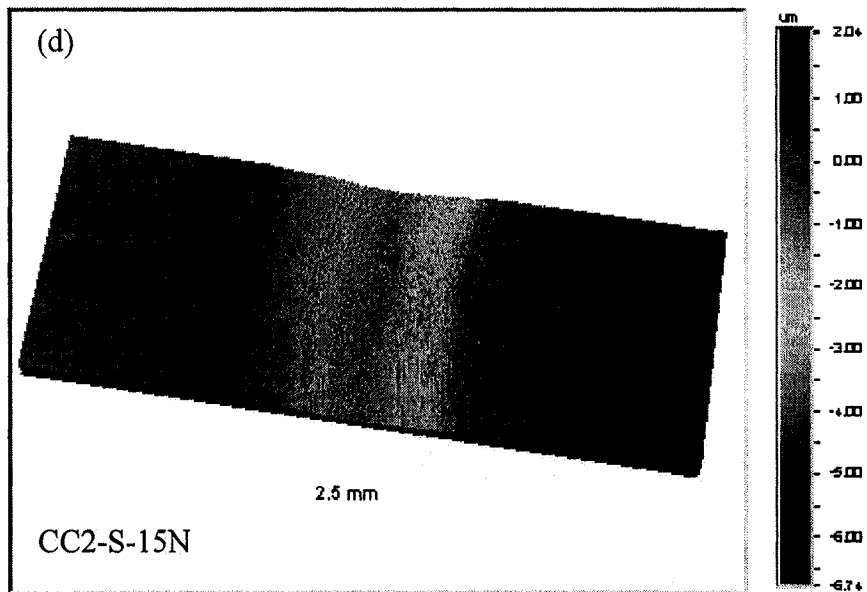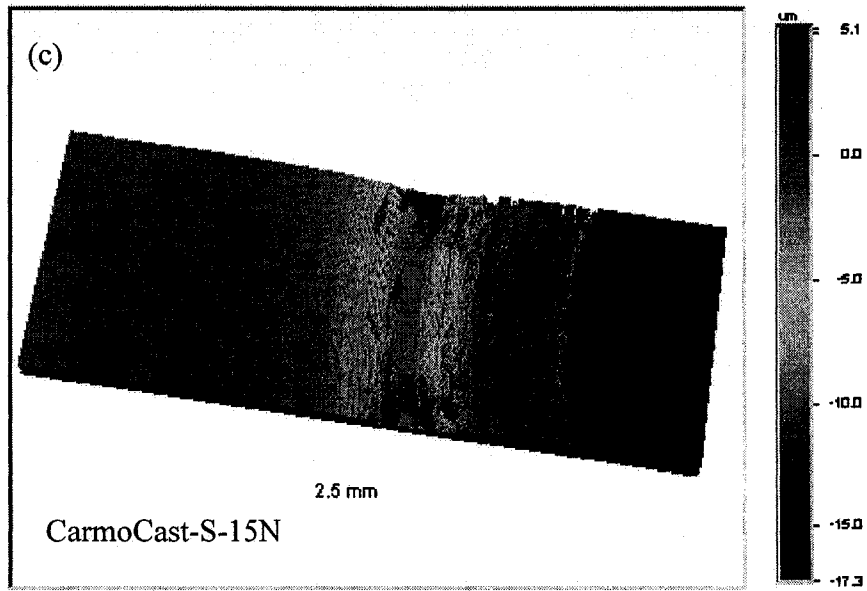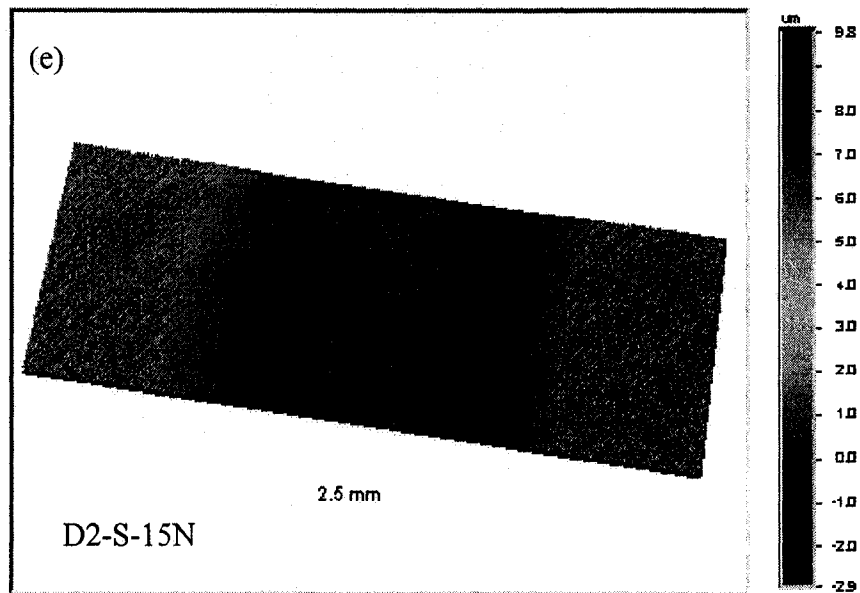
Fig. 4.38 3D Wyko profile images of substrates sliding wear tracks against steel pin under 15N load: (a) 0050A, (b) G3500, (c) CarmoCast, (d) CC2 and (e) D2

4.8.3 SEM images of wear tracks

Figs. 4.39 to 4.43 show the SEM images of wear tracks on substrates of 005A, G3500, CarmoCast, CC2 and D2 after pin-on-disc test against steel pins under 15N load with 250m sliding distance. Compared with the wear tracks presented in Figs. 4.32 to 4.36 at tests against steel pins under 5N load, these wear tracks present less transferred materials, which means the material transfer occurring during the sliding wear process under low load is reduced under high load. This suggests that delamination wear or fatigue wear dominates under this test condition. Small amount of transferred materials could be observed on the wear track surfaces of 0050A and CC2. Cracks and peeling of materials are shown on the wear track of G3500. D2 presents the best wear resistance performance because it shows a smooth wear track surface.

84
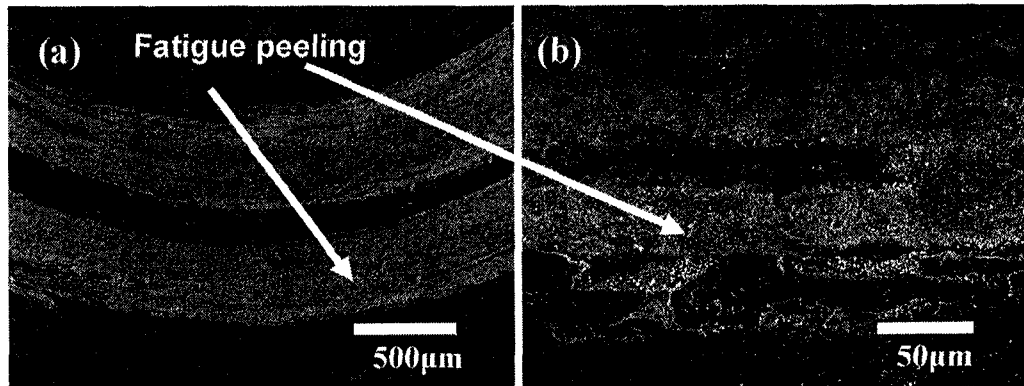
Fig. 4.39 SEM images of wear track on 0050A substrate after pin-on-disc test against

steel pins under 15N load with 250m sliding distance (a) 50×, (b) 500×
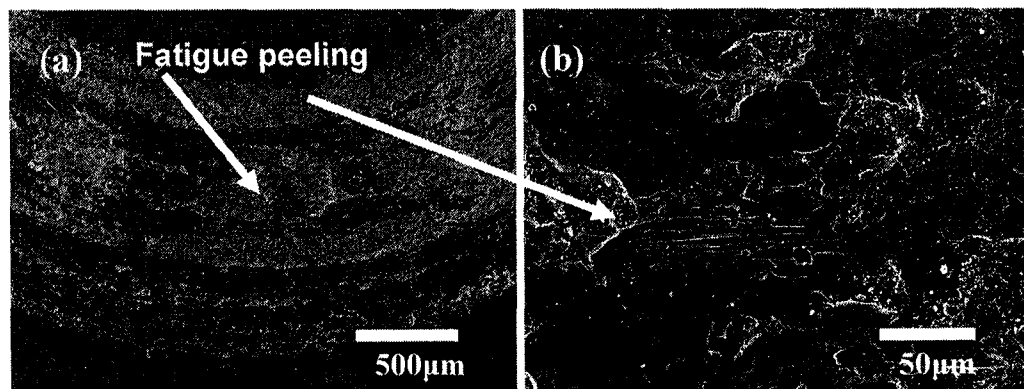
Fig. 4.40 SEM images of wear track on G3500 substrate after pin-on-disc test against

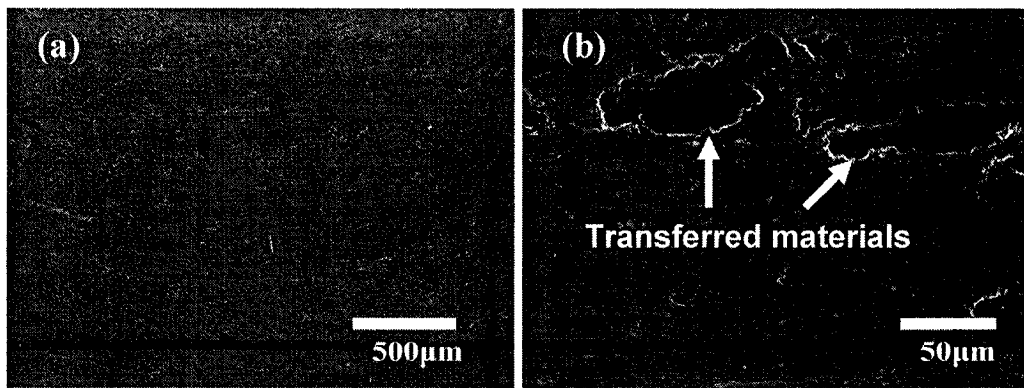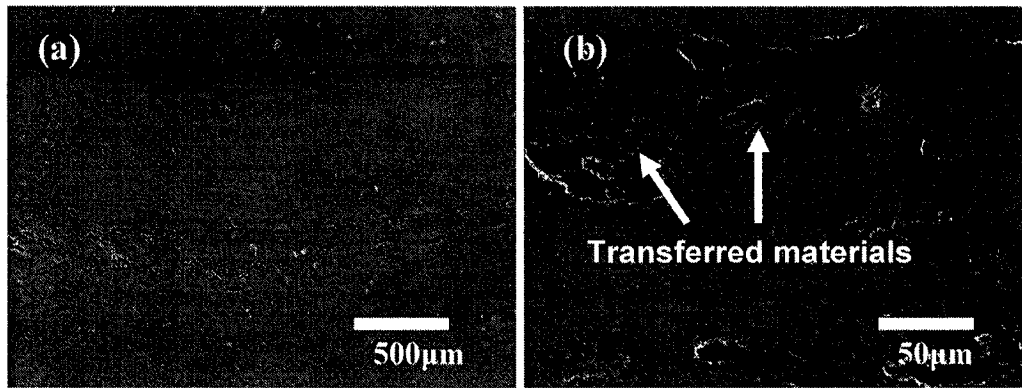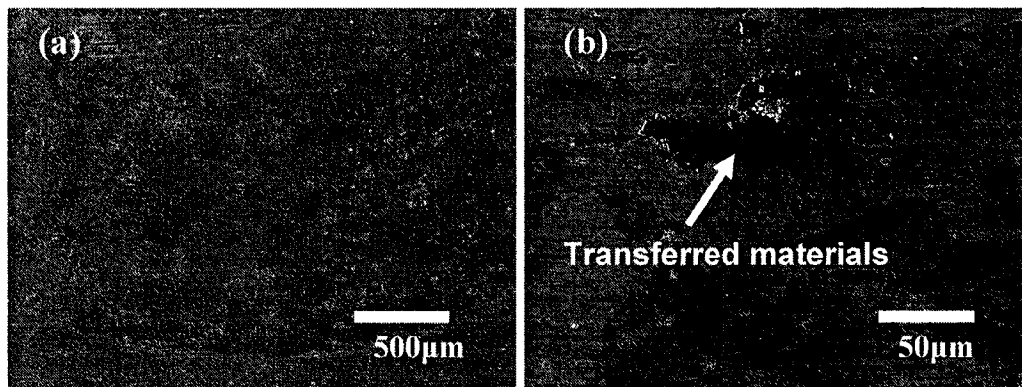steel pins under 15N load with 250m sliding distance (a) 50×, (b) 500×
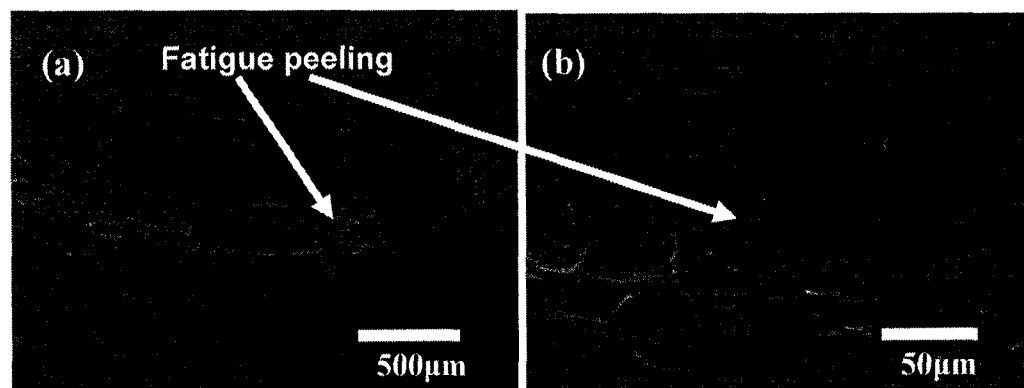
Fig. 4.41 SEM images of wear track on CarmoCast substrate after pin-on-disc test against

steel pins under 15N load with 250m sliding distance (a) 50×, (b) 500×
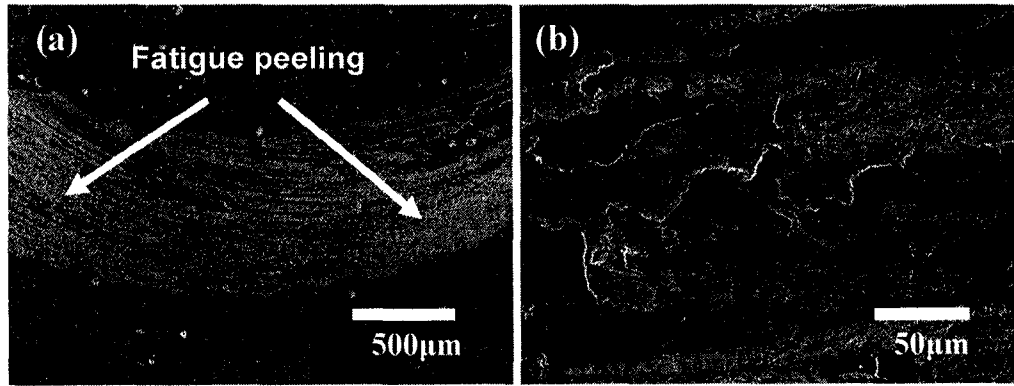
Fig. 4.42 SEM images of wear track on CC2 substrate after pin-on-disc test against steel

pins under 15N load with 250m sliding distance (a) 50×, (b) 500×
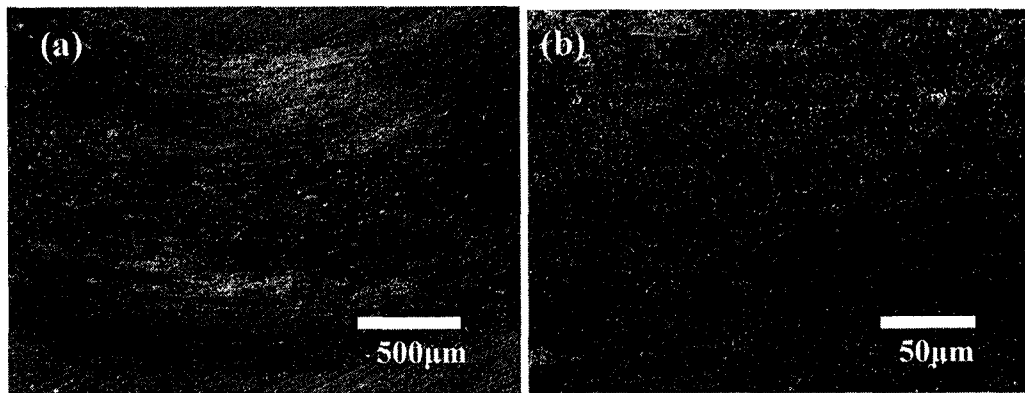
Fig. 4.43 SEM images of wear track on D2 substrate after pin-on-disc test against steel

pins under 15N load with 250m sliding distance (a) 50×, (b) 500×

4.9 Wear of counter pins against G3500 under different loads

Figs. 4.44 and 4.45 show the SEM images of wear scar on steel pin after pin-on-disc test

against G3500 under 5N and 15N load, respectively, with 250m sliding distance.

Obviously, the steel pin against G3500 under 15N load has larger wear scar than the one

under 5N load. Figs. 4.46 and 4.47 show the SEM images of wear scar on aluminium pin

after pin-on-disc test against G3500 under 5N and 10N load, respectively, with 250m

sliding distance. It shows that the aluminium pin against G3500 under 10N load has more wear than the one under 5N load. Back transferred materials could be found on the aluminium pin against G3500 under 5N load. The phenomenon of materials peeling happened on the aluminium pin against G3500 under 10N load. So with the increase of the applied normal load, the wear to the counterparts increases.
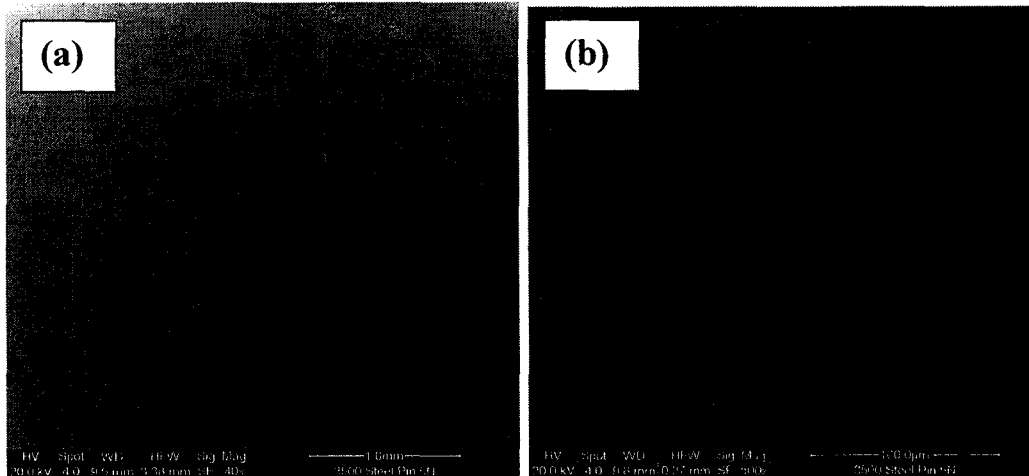
Fig. 4.44 SEM images of wear scar on steel pin after pin-on-disc test against G3500 under 5N load with 250m sliding distance (a) 40×, (b) 500×
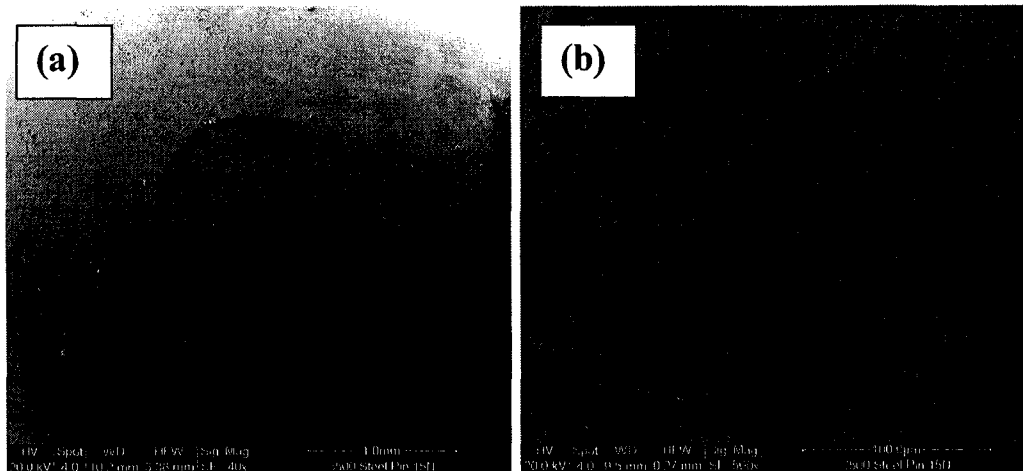
Fig. 4.45 SEM images of wear scar on steel pin after pin-on-disc test against G3500 under 15N load with 250m sliding distance (a) 40×, (b) 500×

87
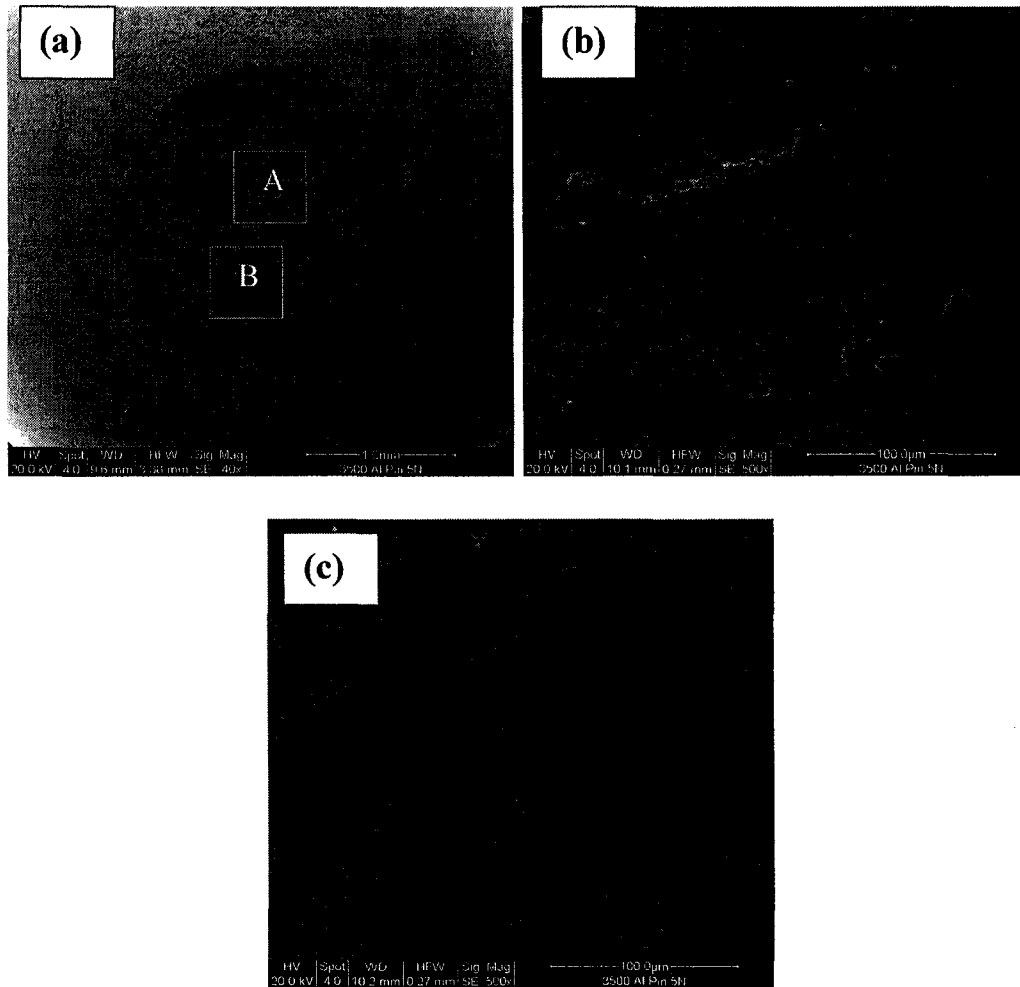
Fig. 4.46 SEM images of wear scar on aluminium pin after pin-on-disc test against G3500 under 5N load with 250m sliding distance (a) 40×, (b) area A, 500×, (c) area B, 500×
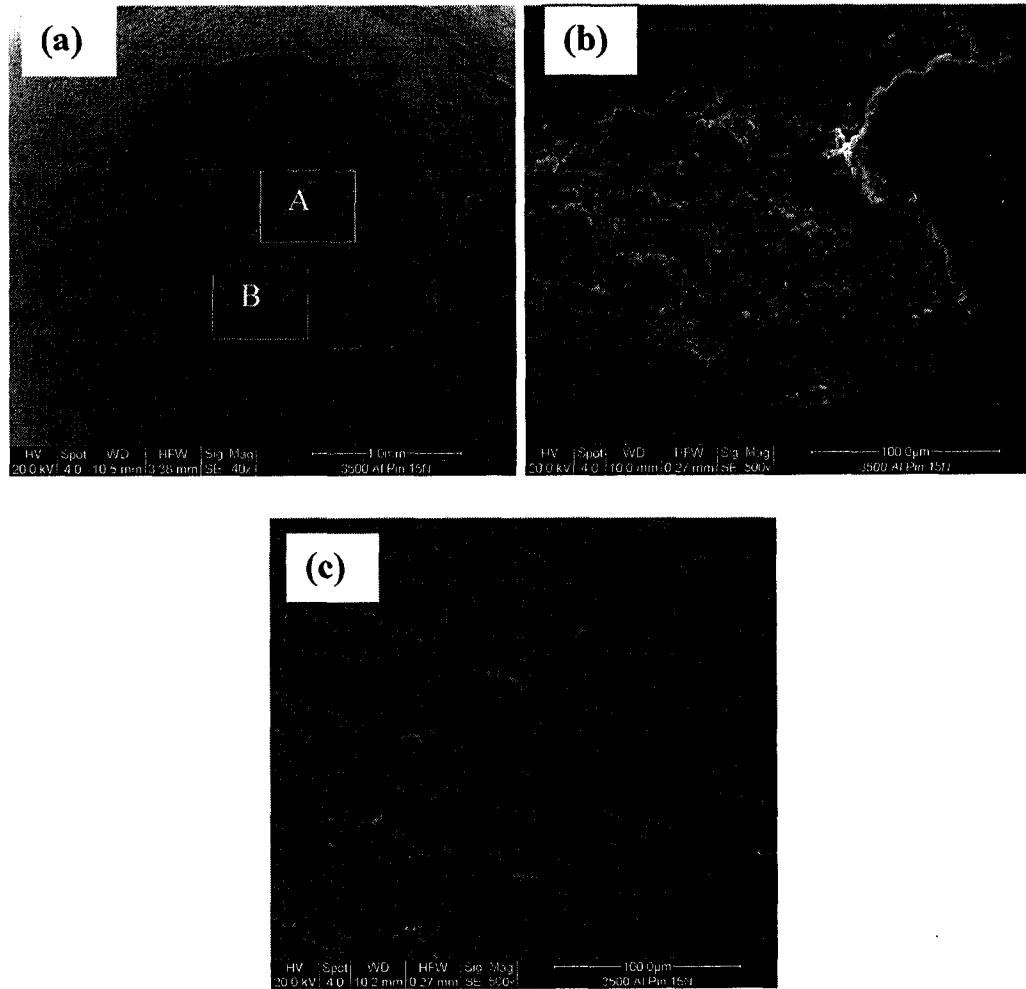
Fig. 4.47 SEM images of wear scar on aluminium pin after pin-on-disc test against G3500 under 10N load with 250m sliding distance (a) 40×, (b) area A, 500×, (c) area B, 500×

4.10 EDX analysis for substrates and counter pins

4.10.1 EDX analysis for G3500 substrate

Figs. 4.48 to 4.64 are EDX analysis results of selected locations on substrate G3500. Fig. 4.48 display EDX analysis of G3500 substrate. Figs. 4.49 and 4.50 show EDX analysis of selected areas of wear track on G3500 after pin-on-disc test against alumina pins under 5N load with 250m sliding distance. It could be found that some areas on the wear track are oxidized. Figs 4.51 and 4.52 are EDX analysis of wear track on G3500 substrate after pin-on-disc test against aluminium pin under 5N load. Transferred oxidized aluminium material from the counter pin could be found on the wear track surface but no oxide is found on the areas not covered by transferred aluminum. Figs 4.53 to 4.56 are EDX analysis of wear track on G3500 substrate after pin-on-disc test against aluminium pin under 10N load. The test results are quite similar to those against aluminium under 5N load. Transferred oxidized aluminium material from the counter pin could be found on the wear track surface but no oxide is found on the areas not covered by transferred aluminum. The only difference seems that more aluminium materials are transferred from the pin under 10N load than those under 5N load. Figs 4.57 and 4.60 are EDX analysis of wear track on G3500 substrate after pin-on-disc test against steel pin under 5N load. Transferred oxidized iron from the counter pin could be found on the wear track surface and some oxides are found on some areas not covered by transferred materials. Figs 4.61 to 4.64 are EDX analysis of wear track on G3500 substrate after pin-on-disc test against steel pin under 15N load. Transferred oxidized iron from the counter pin could be found on the wear track surface and also some oxides are found on some areas not covered by transferred materials.

90
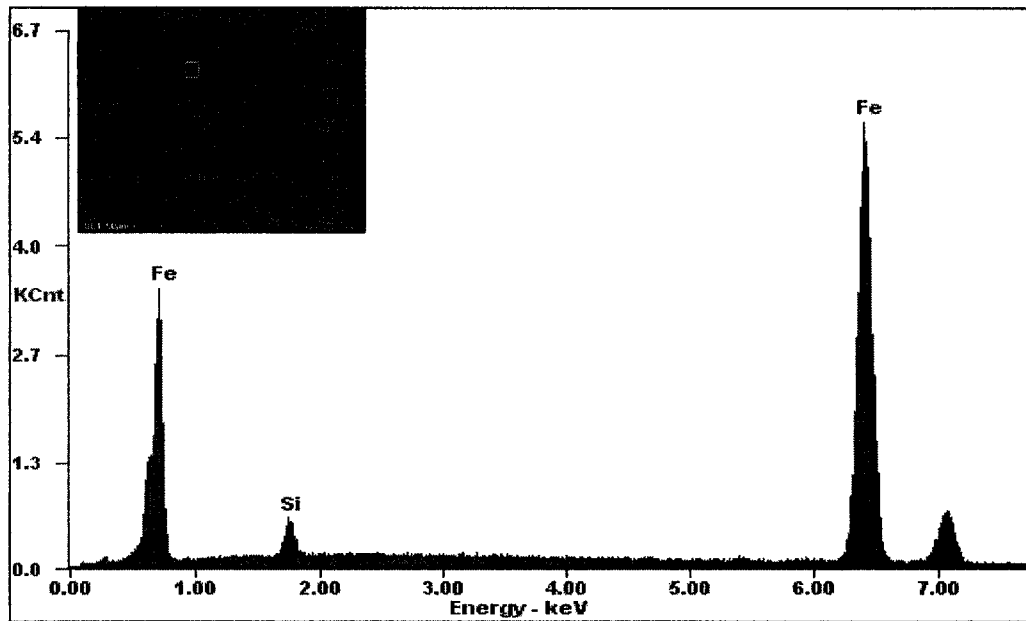
Fig. 4.48 EDX analysis of selected location as shown in the SEM image of G3500

substrate
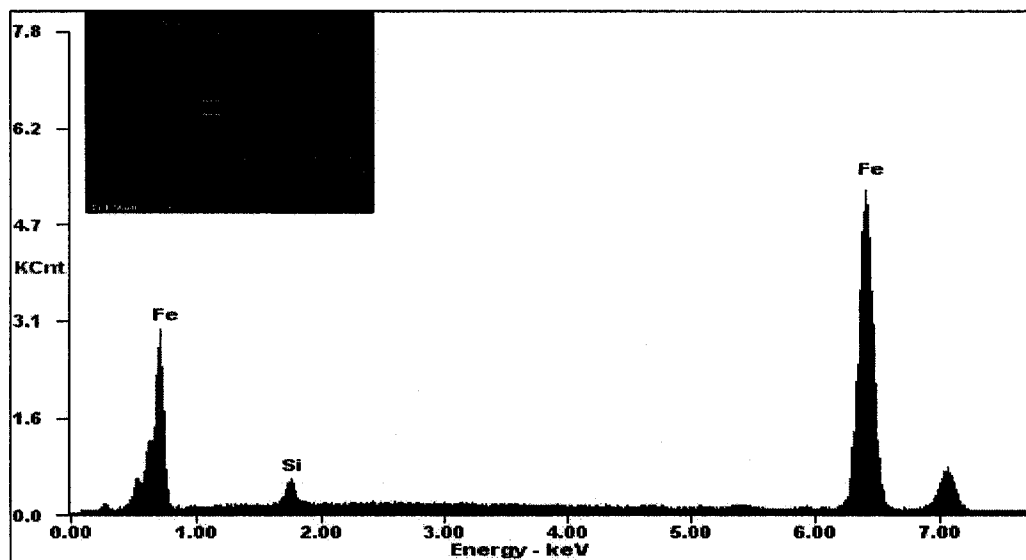
Fig. 4.49 EDX analysis of selected location 1 as shown in the SEM image of wear track

on G3500 substrate after pin-on-disc test against alumina pins under 5N load with 250m
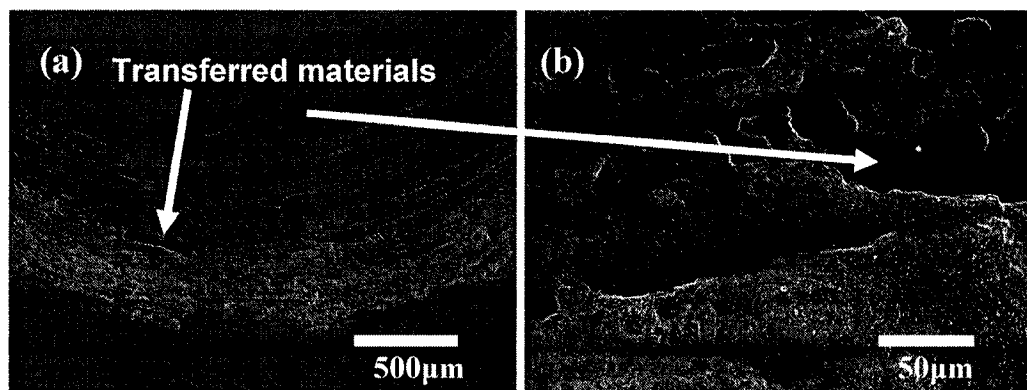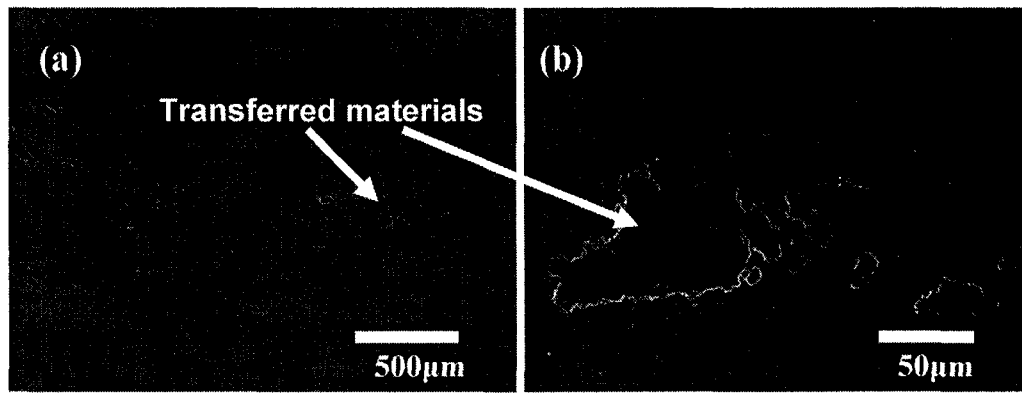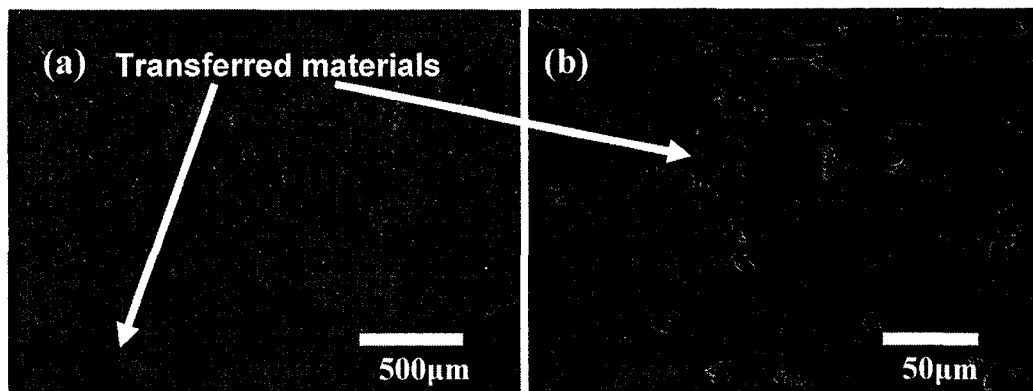
sliding distance

91
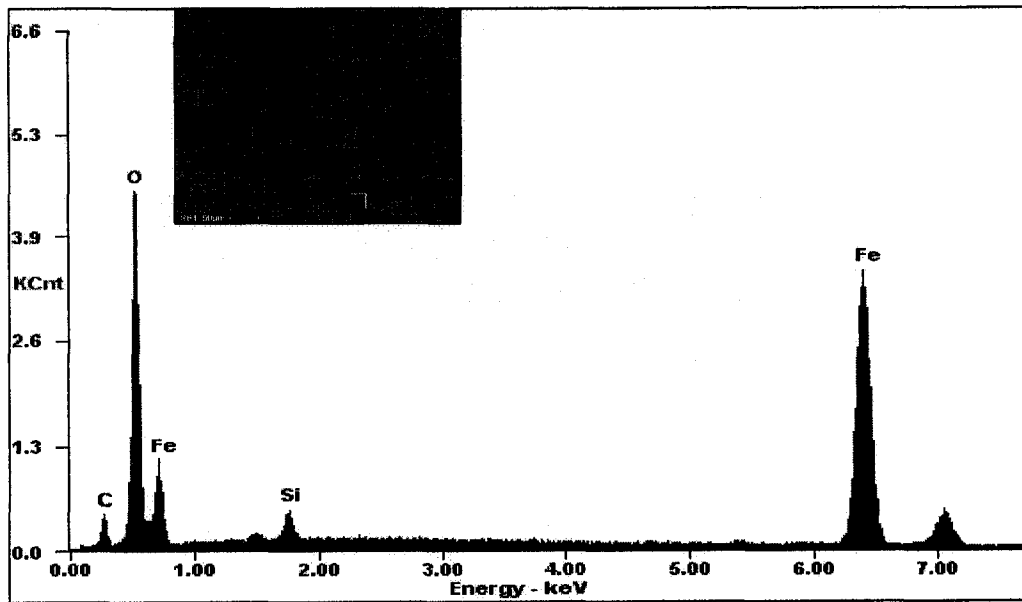
Fig. 4.50 EDX analysis of selected location 2 as shown in the SEM image of wear track

on G3500 substrate after pin-on-disc test against alumina pins under 5N load with 250m
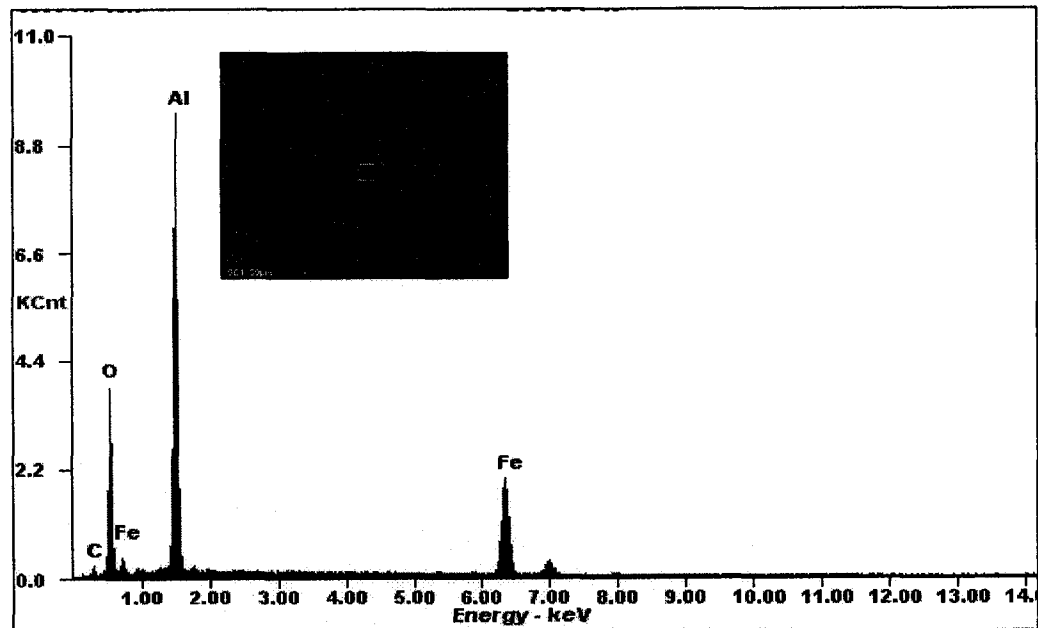
sliding distance

Fig. 4.51 EDX analysis of selected location 1 as shown in the SEM image of wear track

on G3500 substrate after pin-on-disc test against aluminium pins under 5N load with

250m sliding distance

92
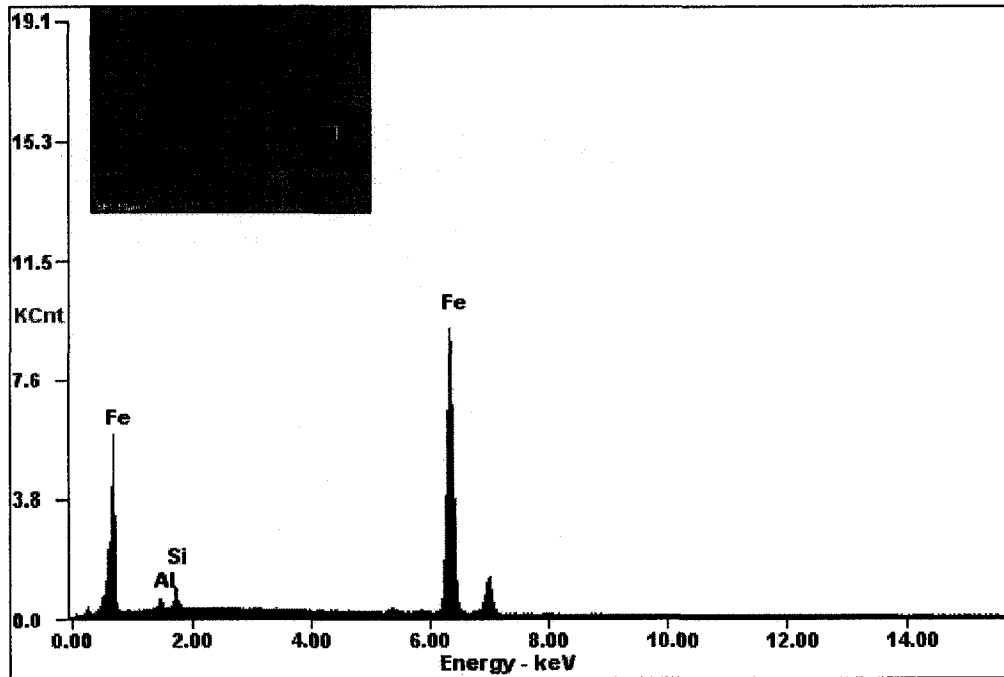
Fig. 4.52 EDX analysis of selected location 2 as shown in the SEM image of wear track on G3500 substrate after pin-on-disc test against aluminium pins under 5N load with 250m sliding distance
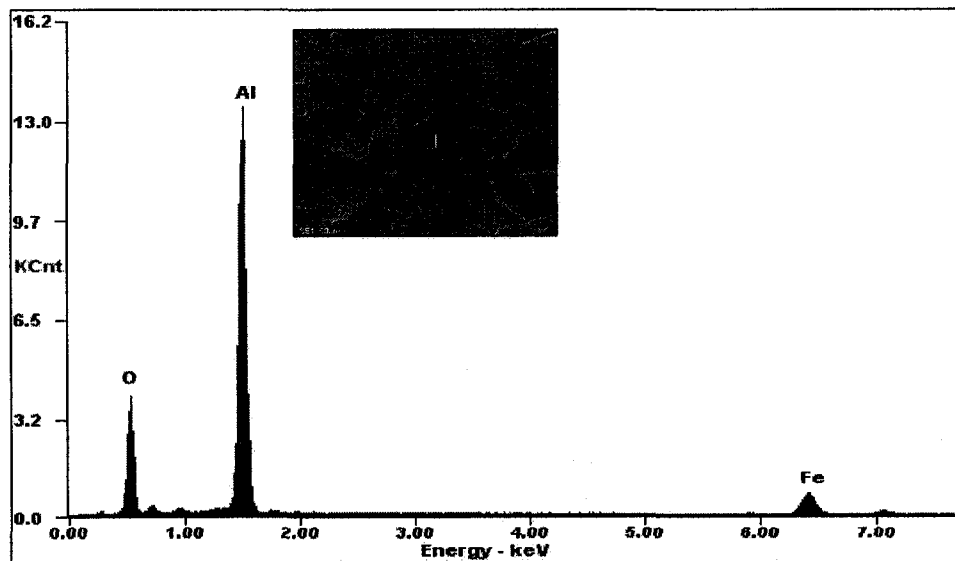
Fig. 4.53 EDX analysis of selected location 1 as shown in the SEM image of wear track on G3500 substrate after pin-on-disc test against aluminium pins under 10N load with 250m sliding distance

93
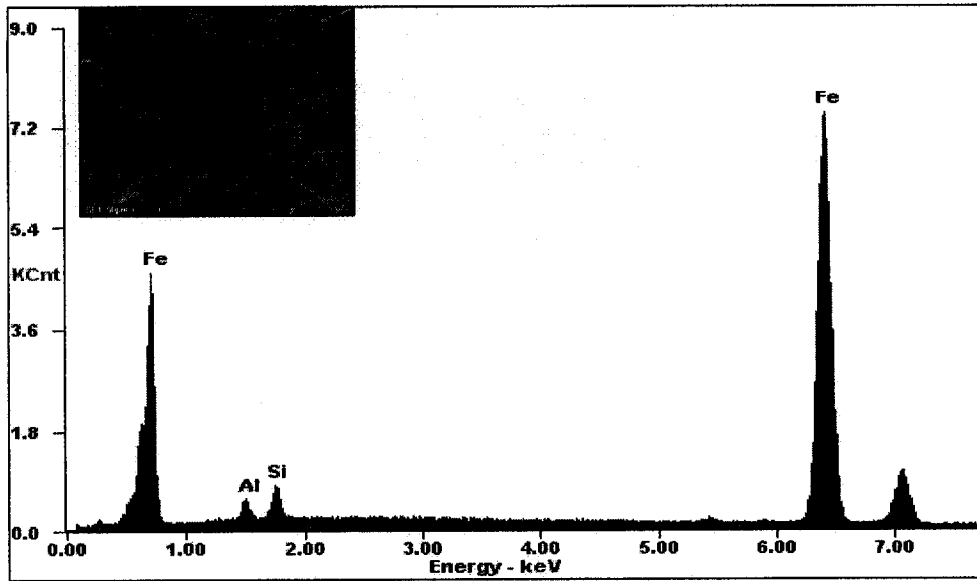
Fig. 4.54 EDX analysis of selected location 2 as shown in the SEM image of wear track on G3500 substrate after pin-on-disc test against aluminium pins under 10N load with 250m sliding distance
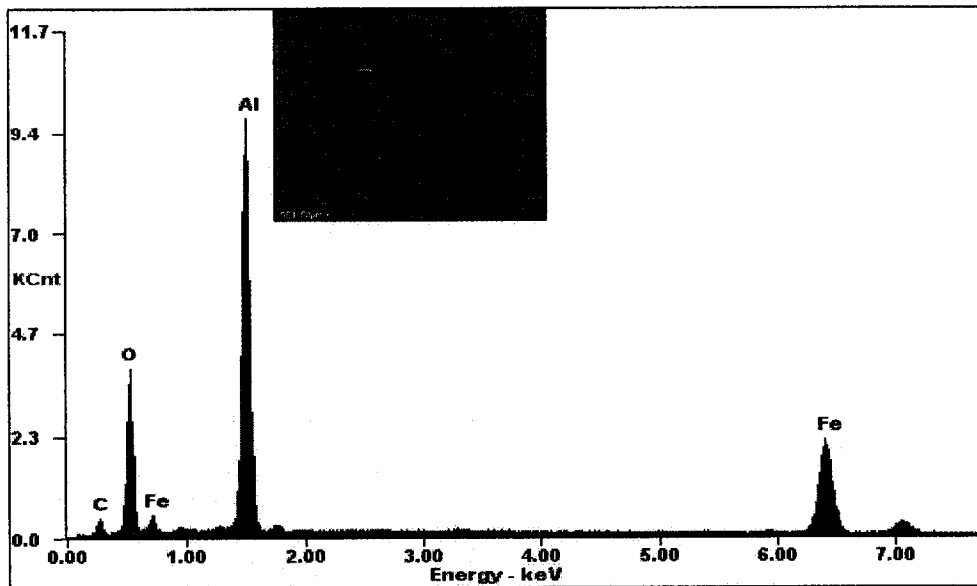
Fig. 4.55 EDX analysis of selected location 3 as shown in the SEM image of wear track on G3500 substrate after pin-on-disc test against aluminium pins under 10N load with 250m sliding distance
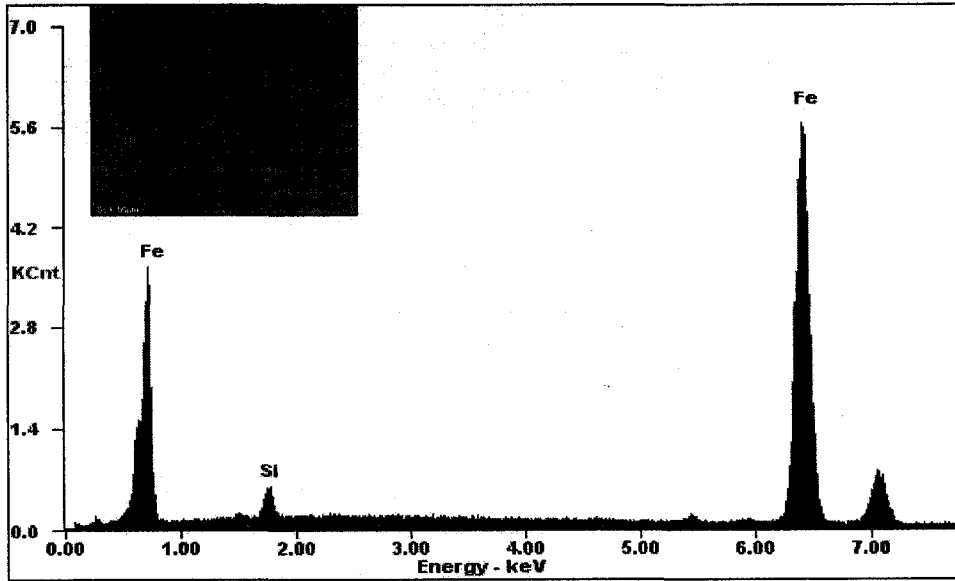
Fig. 4.56 EDX analysis of selected location 4 as shown in the SEM image of wear track on G3500 substrate after pin-on-disc test against aluminium pins under 10N load with 250m sliding distance
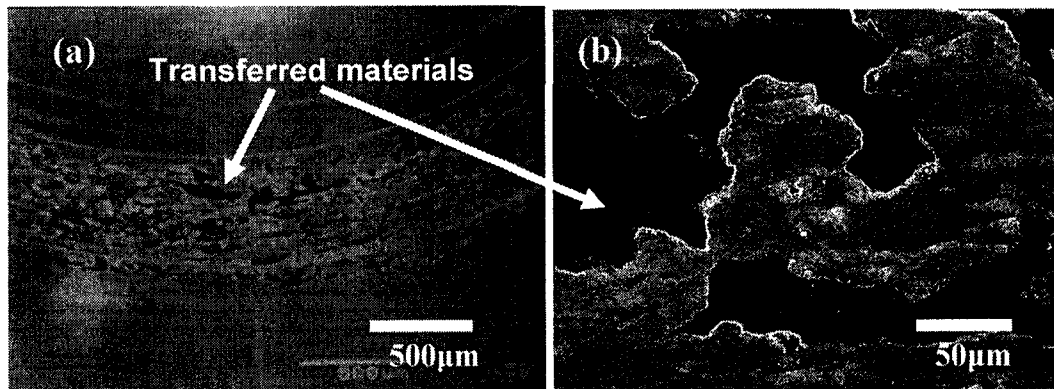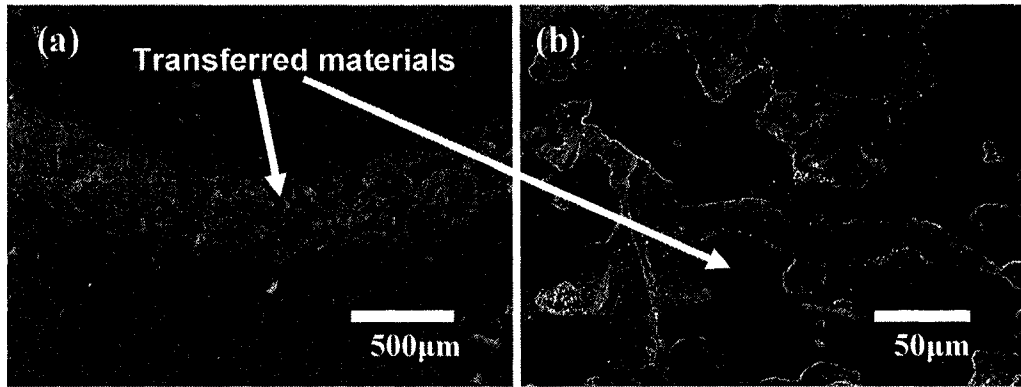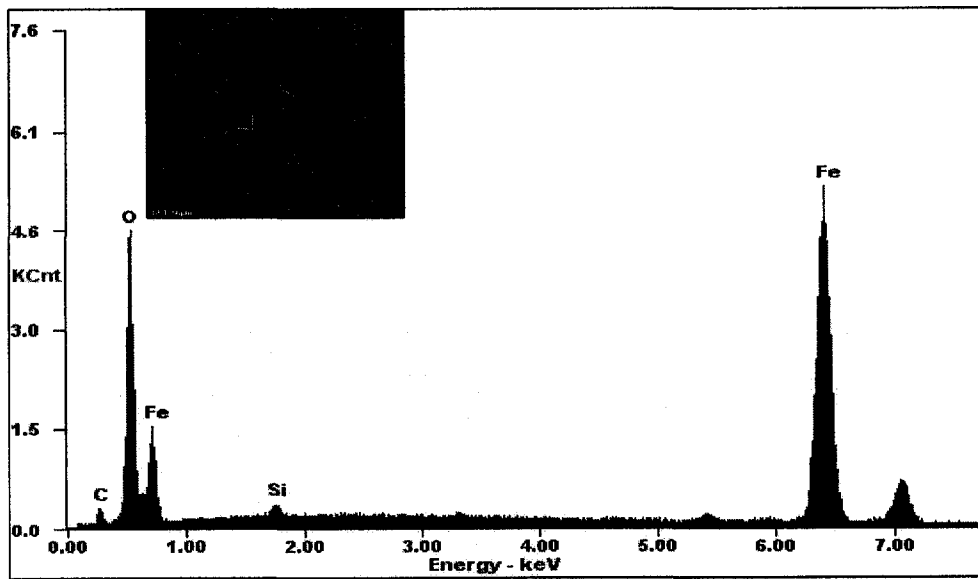

Fig. 4.57 EDX analysis of selected location 1 as shown in the SEM image of wear track on G3500 substrate after pin-on-disc test against steel pin under 5N load with 250m sliding distance

Fig. 4.58 EDX analysis of selected location 2 as shown in the SEM image of wear track on G3500 substrate after pin-on-disc test against steel pin under 5N load with 250m sliding distance
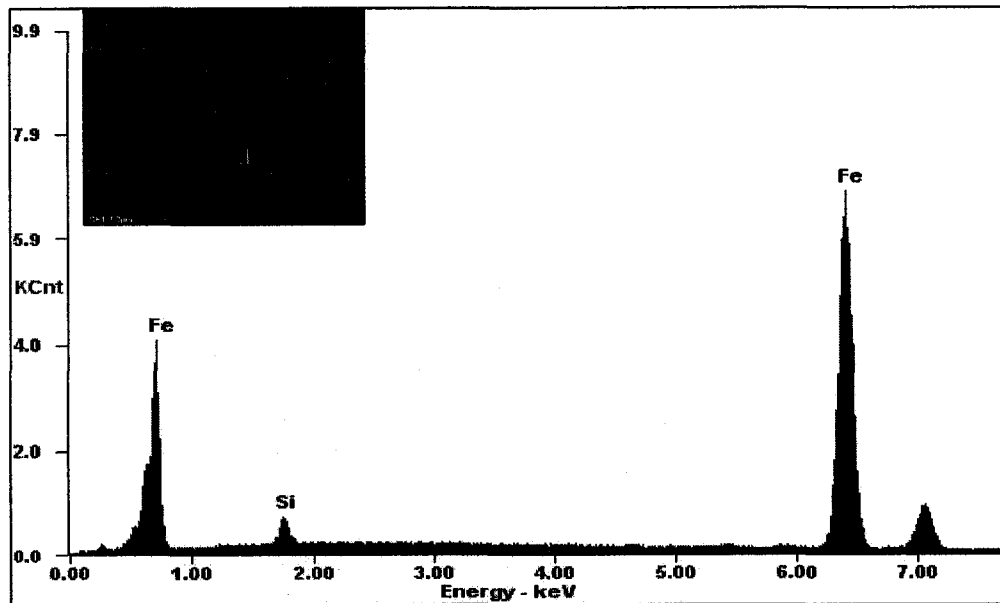
Fig. 4.59 EDX analysis of selected location 3 as shown in the SEM image of wear track on G3500 substrate after pin-on-disc test against steel pin under 5N load with 250m sliding distance

96
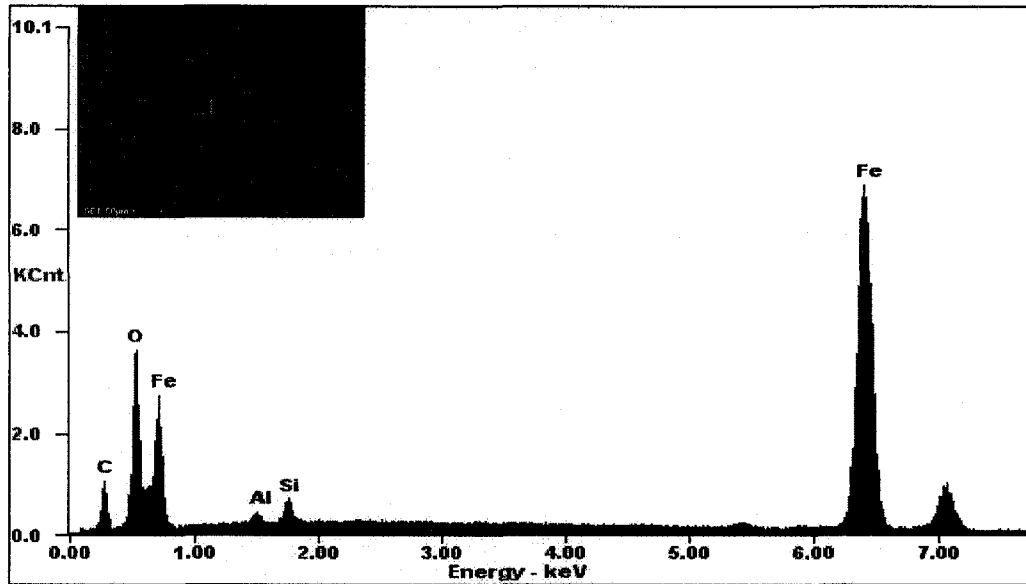
Fig. 4.60 EDX analysis of selected location 4 as shown in the SEM image of wear track on G3500 substrate after pin-on-disc test against steel pin under 5N load with 250m sliding distance
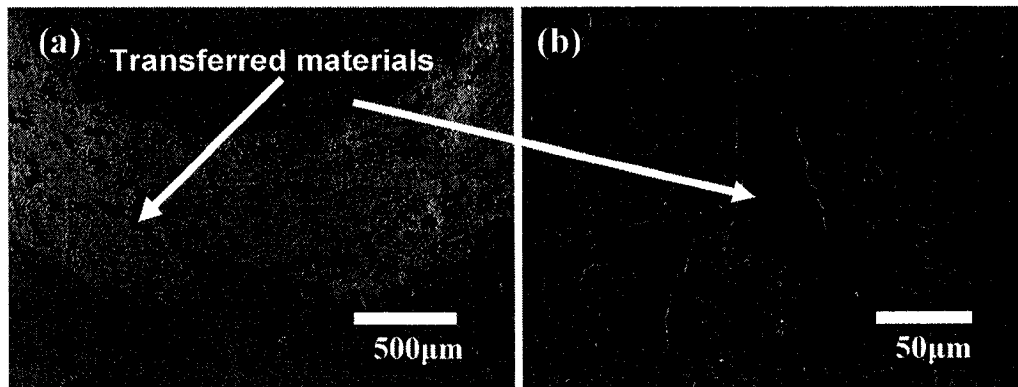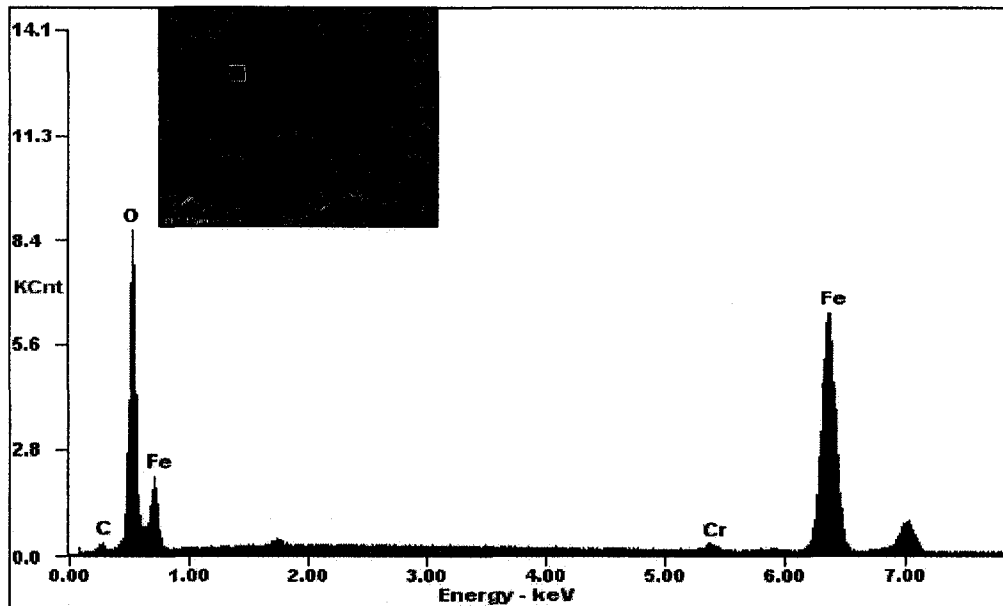

Fig. 4.61 EDX analysis of selected location 1 as shown in the SEM image of wear track on G3500 substrate after pin-on-disc test against steel pin under 15N load with 250m sliding distance

97
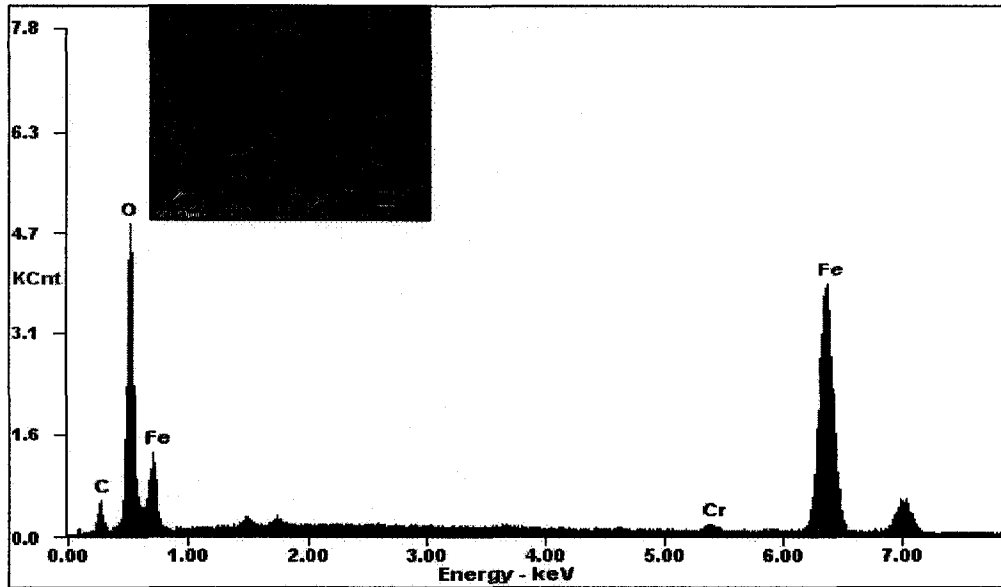
Fig. 4.62 EDX analysis of selected location 2 as shown in the SEM image of wear track on G3500 substrate after pin-on-disc test against steel pin under 15N load with 250m sliding distance
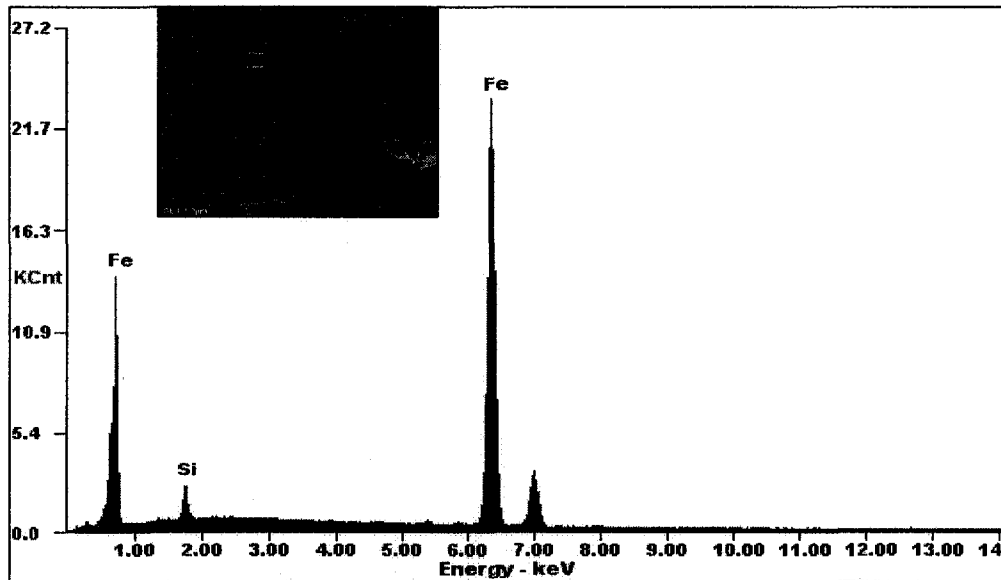
Fig. 4.63 EDX analysis of selected location 3 as shown in the SEM image of wear track on G3500 substrate after pin-on-disc test against steel pin under 15N load with 250m sliding distance

98
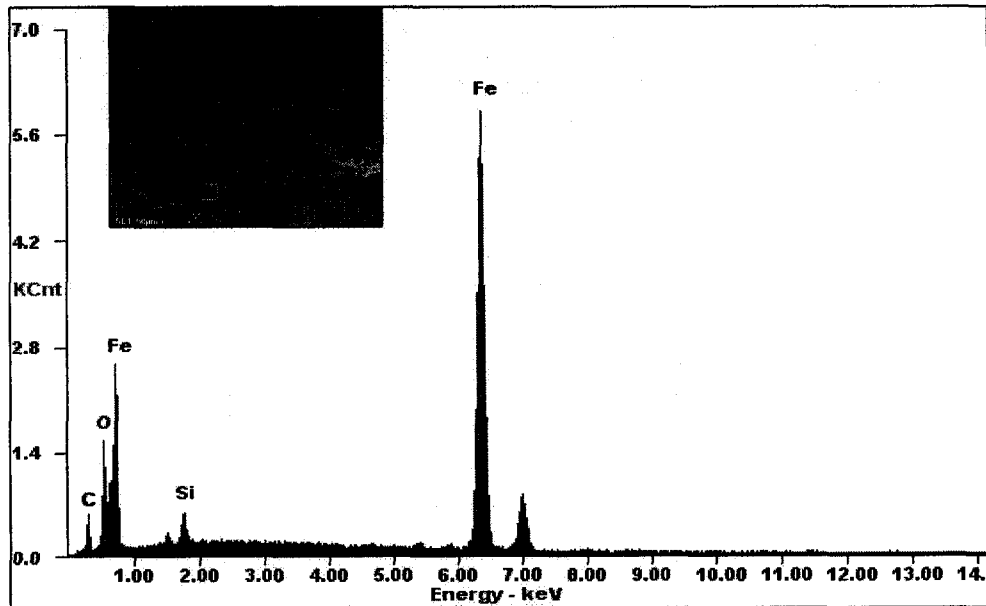
Fig. 4.64 EDX analysis of selected location 4 as shown in the SEM image of wear track

on G3500 substrate after pin-on-disc test against steel pin under 15N load with 250m

sliding distance

4.10.2 EDX analysis for CC2 substrate

Figs. 4.65 to 4.82 are EDX analysis results of selected locations on substrate G3500. Fig.

4.65 display EDX analysis of CC2 substrate. Figs. 4.66 and 4.67 show EDX analysis of

selected areas of wear track on CC2 substrate after pin-on-disc test against alumina pins

under 5N load with 250m sliding distance. No oxides are found on the wear track surface.

Figs 4.68 and 4.69 are EDX analysis of wear track on CC2 substrate after pin-on-disc test

against aluminium pin under 5N load. Transferred oxidized aluminium material from the

counter pin could be found on the wear track surface but no oxide is found on the areas

not covered by transferred aluminum. Figs 4.70 to 4.73 are EDX analysis of wear track

on CC2 substrate after pin-on-disc test against aluminium pin under 10N load. The test

results are quite similar to those against aluminium pin under 5N load. Transferred

99

oxidized aluminium material from the counter pin could be found on the wear track surface but no oxides are found on the areas not covered by transferred aluminum. The only difference seems that more aluminium materials are transferred from the pin under 10N load than those under 5N load. Figs 4.74 to 4.77 are EDX analysis of wear track on CC2 substrate after pin-on-disc test against steel pin under 5N load. Transferred oxidized iron from the counter pin could be found on the wear track surface but no oxides are found on the areas not covered by transferred materials. Figs 4.78 to 4.83 are EDX analysis of wear track on CC2 substrate after pin-on-disc test against steel pin under 15N load. Transferred oxidized iron from the counter pin could be found on the wear track surface and some oxides are found on some areas not covered by transferred materials.
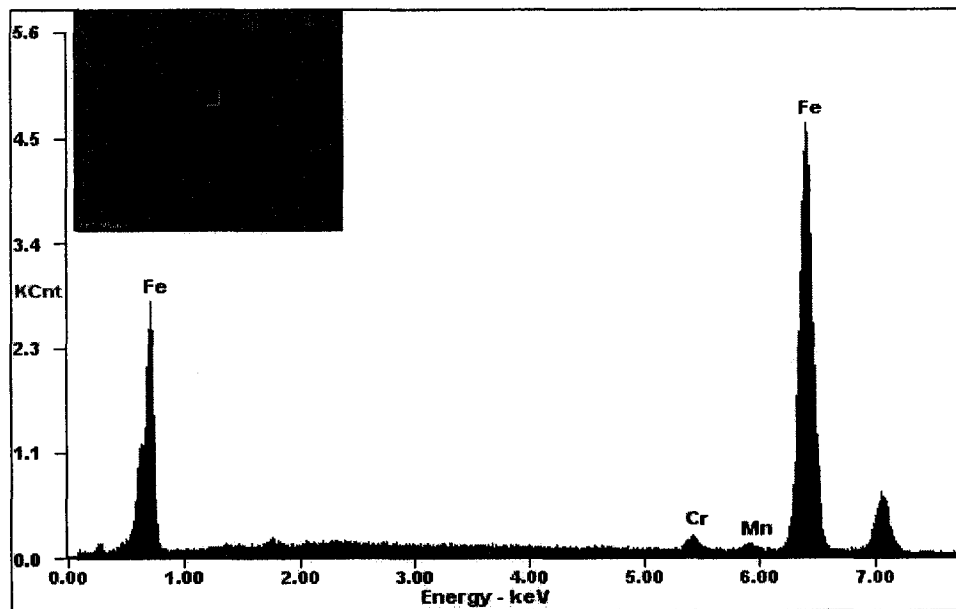
Fig. 4.65 EDX analysis of selected location as shown in the SEM image of CC2 substrate
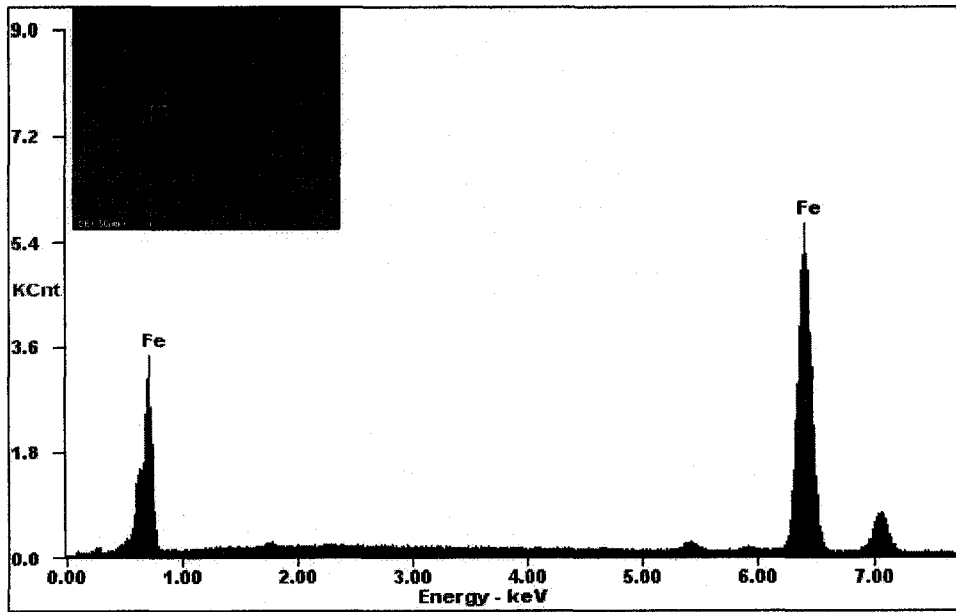
Fig. 4.66 EDX analysis of selected location 1 as shown in the SEM image of wear track on CC2 substrate after pin-on-disc test against alumina pins under 5N load with 250m sliding distance
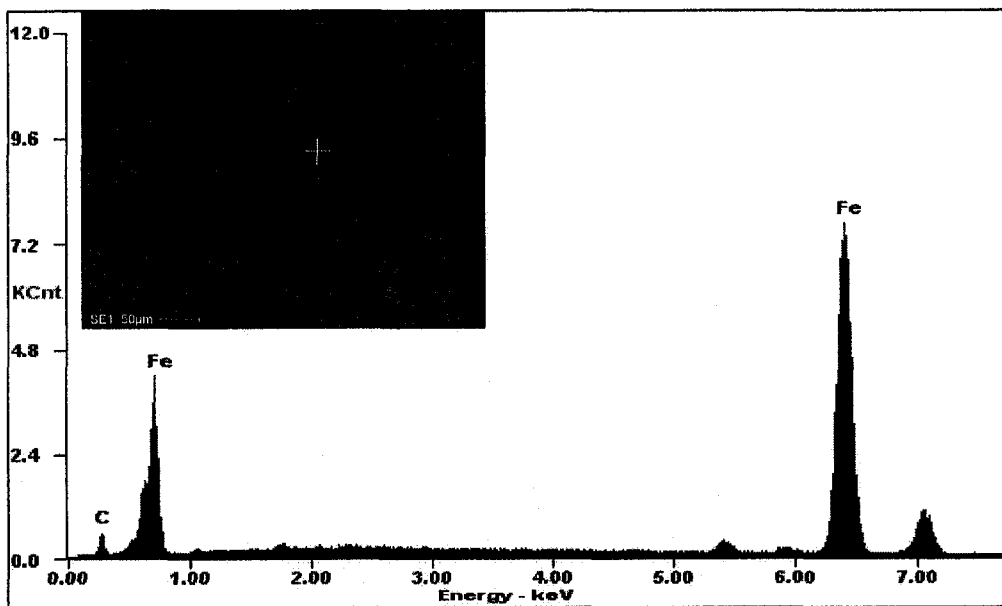
Fig. 4.67 EDX analysis of selected location 2 as shown in the SEM image of wear track on CC2 substrate after pin-on-disc test against alumina pins under 5N load with 250m sliding distance
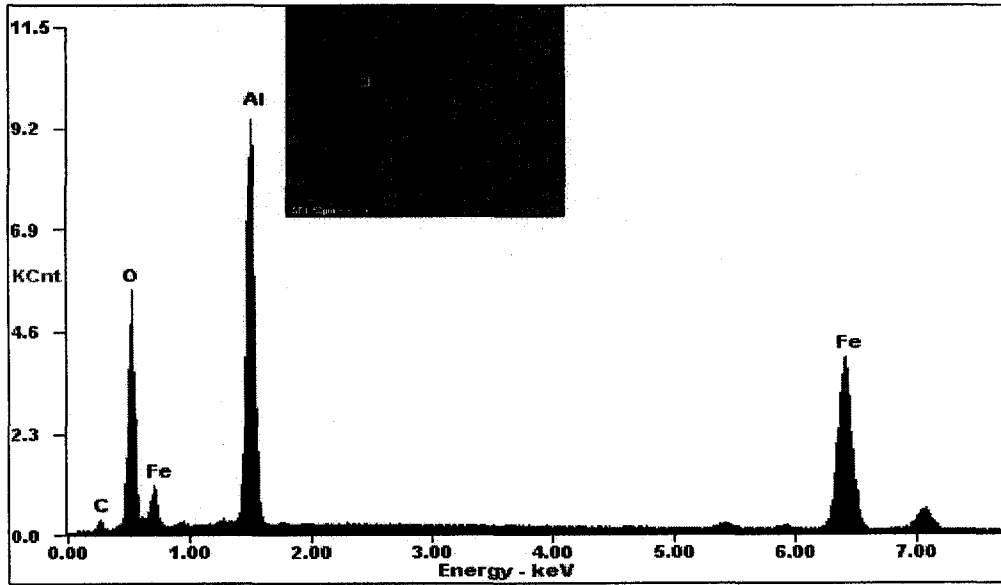
Fig. 4.68 EDX analysis of selected location 1 as shown in the SEM image of wear track on CC2 substrate after pin-on-disc test against aluminium pins under 5N load with 250m sliding distance
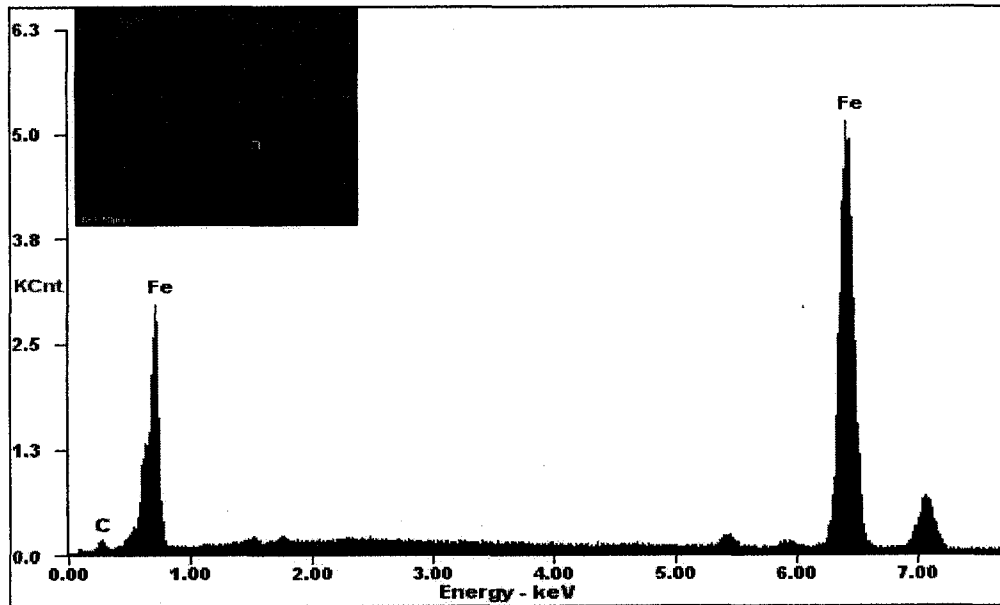

Fig. 4.69 EDX analysis of selected location 2 as shown in the SEM image of wear track on CC2 substrate after pin-on-disc test against aluminium pins under 5N load with 250m sliding distance
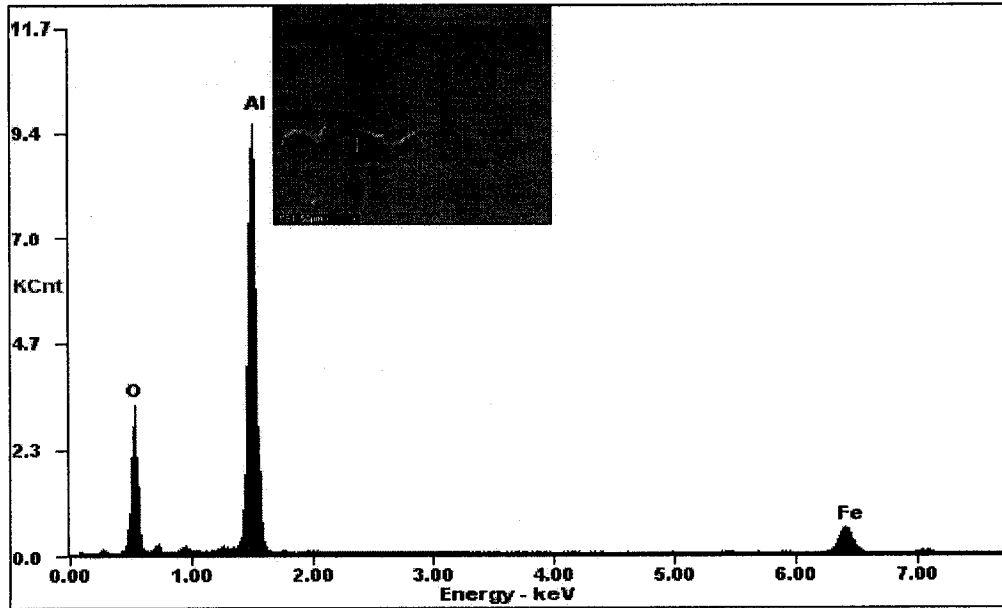
Fig. 4.70 EDX analysis of selected location 1 as shown in the SEM image of wear track on CC2 substrate after pin-on-disc test against aluminium pins under 10N load with 250m sliding distance
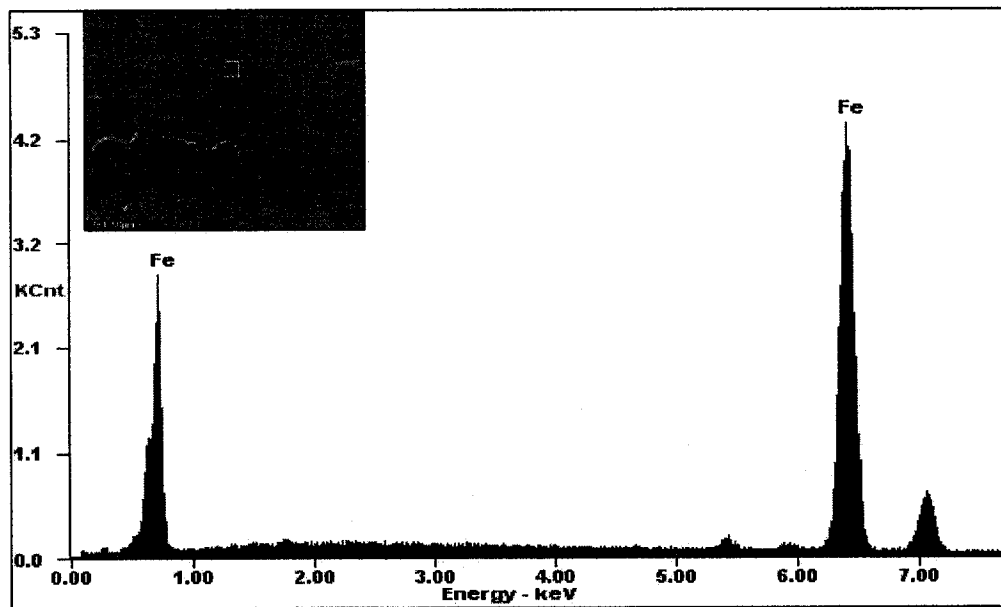

Fig. 4.71 EDX analysis of selected location 2 as shown in the SEM image of wear track on CC2 substrate after pin-on-disc test against aluminium pins under 10N load with 250m sliding distance
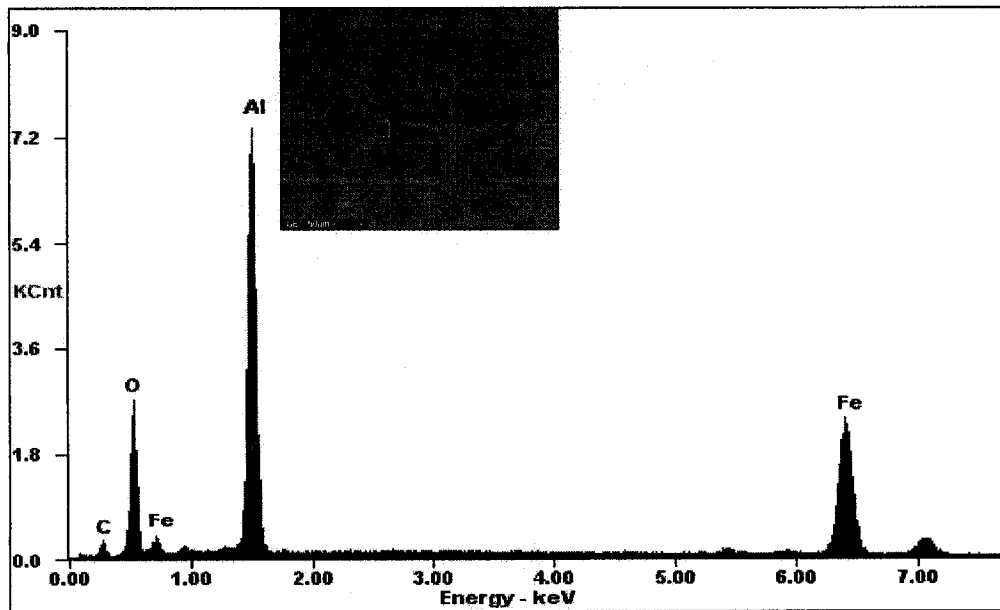
Fig. 4.72 EDX analysis of selected location 3 as shown in the SEM image of wear track
on CC2 substrate after pin-on-disc test against aluminium pins under 10N load with
250m sliding distance
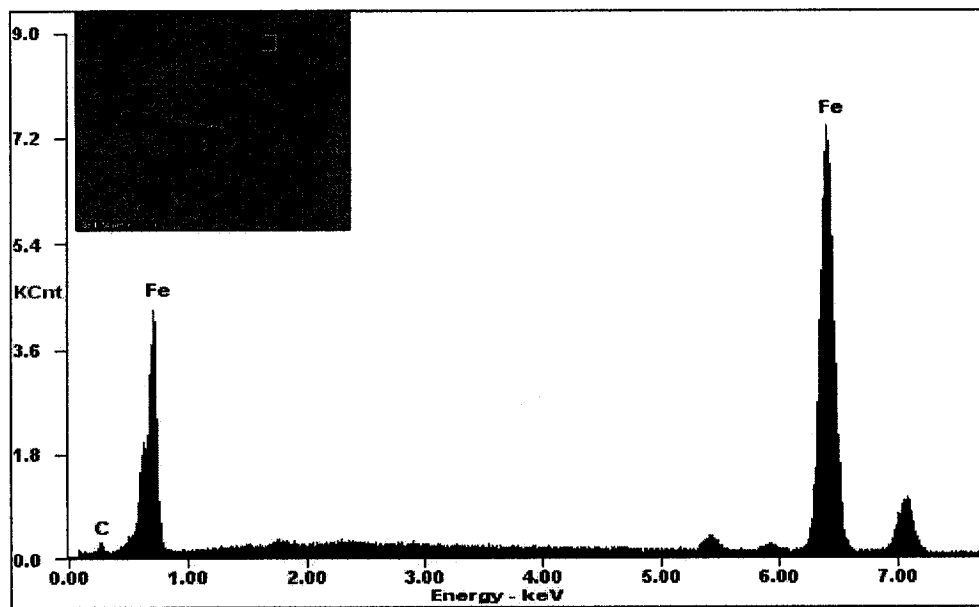
Fig. 4.73 EDX analysis of selected location 4 as shown in the SEM image of wear track
on CC2 substrate after pin-on-disc test against aluminium pins under 10N load with
250m sliding distance

104
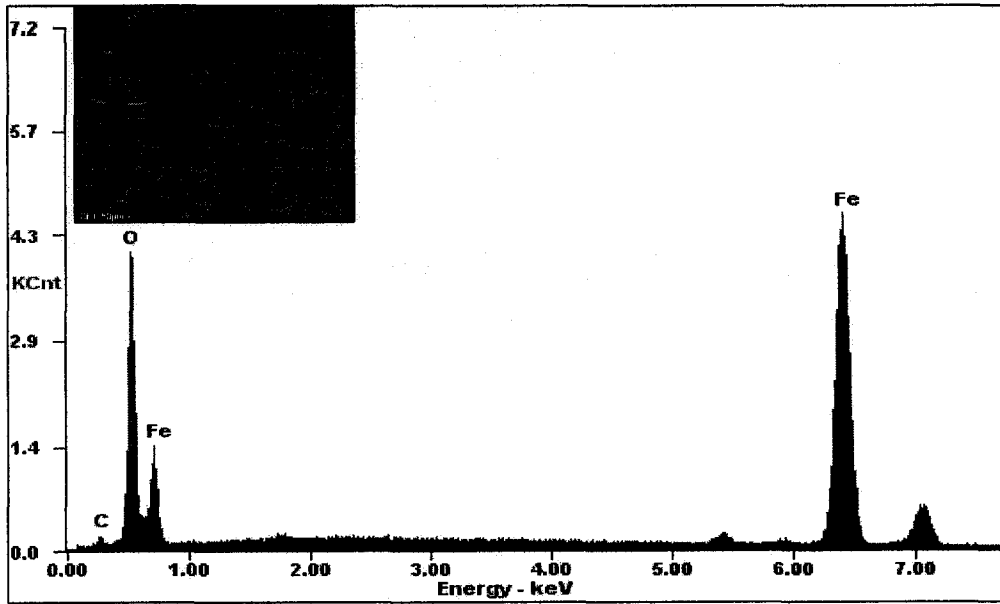
Fig. 4.74 EDX analysis of selected location 1 as shown in the SEM image of wear track on CC2 substrate after pin-on-disc test against steel pin under 5N load with 250m sliding distance
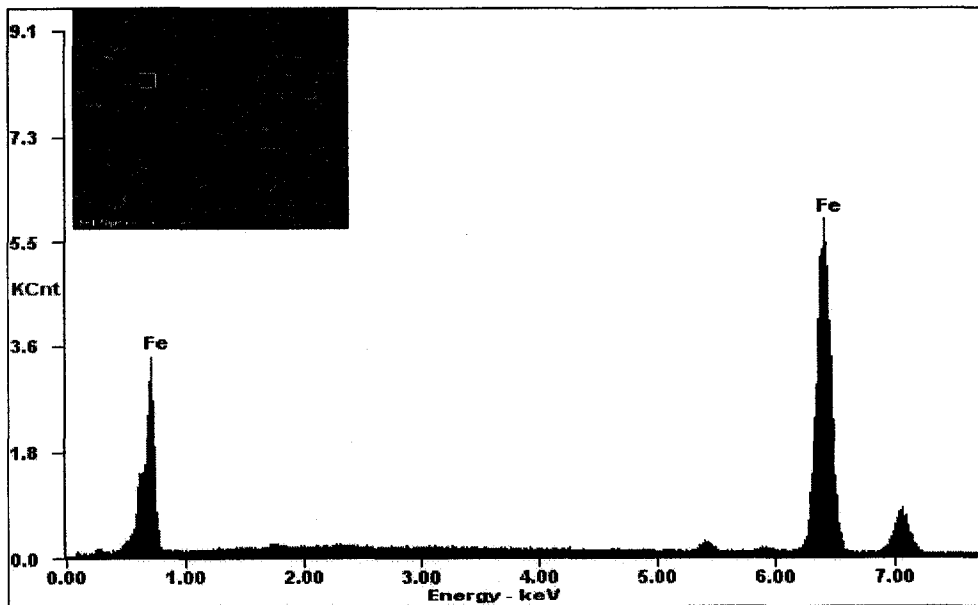
Fig. 4.75 EDX analysis of selected location 2 as shown in the SEM image of wear track on CC2 substrate after pin-on-disc test against steel pin under 5N load with 250m sliding distance

105
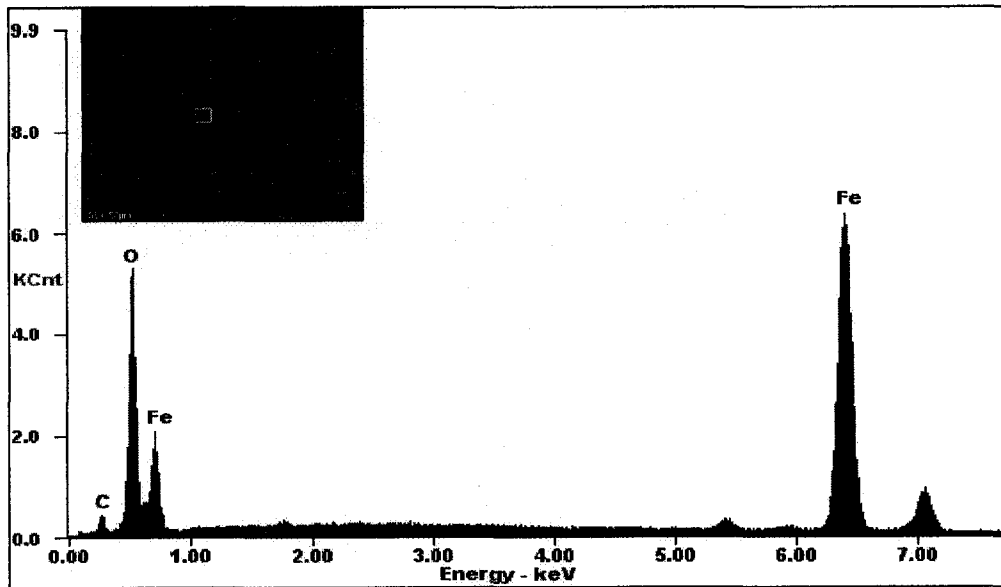
Fig. 4.76 EDX analysis of selected location 3 as shown in the SEM image of wear track

on CC2 substrate after pin-on-disc test against steel pin under 5N load with 250m sliding
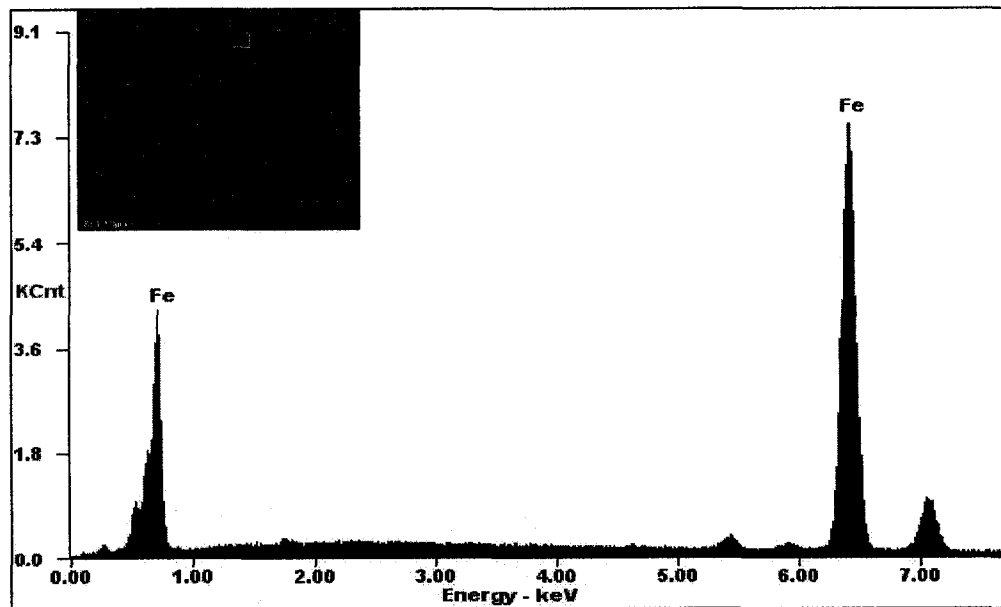
distance

Fig. 4.77 EDX analysis of selected location 4 as shown in the SEM image of wear track

on CC2 substrate after pin-on-disc test against steel pin under 5N load with 250m sliding
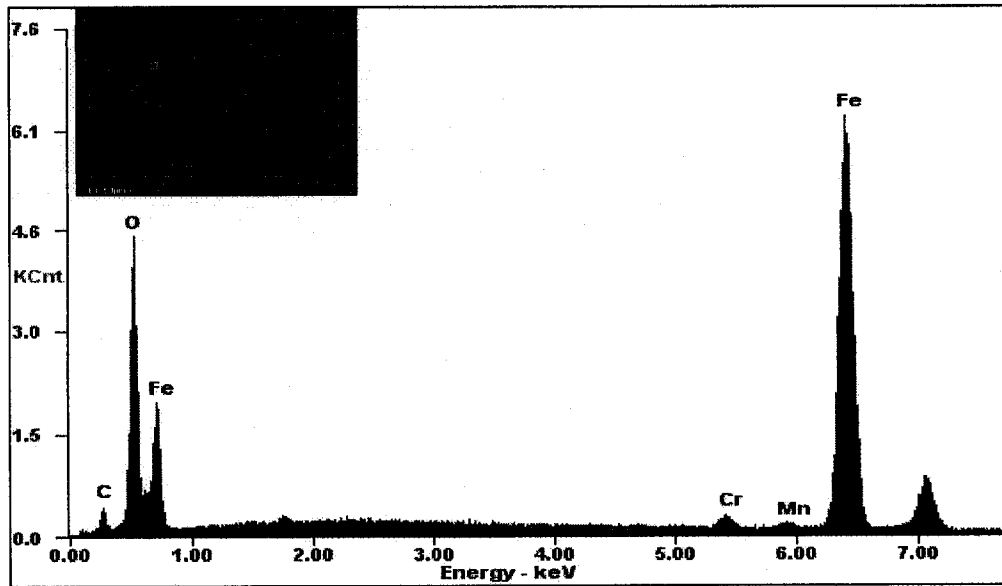
distance

Fig. 4.78 EDX analysis of selected location 1 as shown in the SEM image of wear track on CC2 substrate after pin-on-disc test against steel pin under 15N load with 250m sliding distance
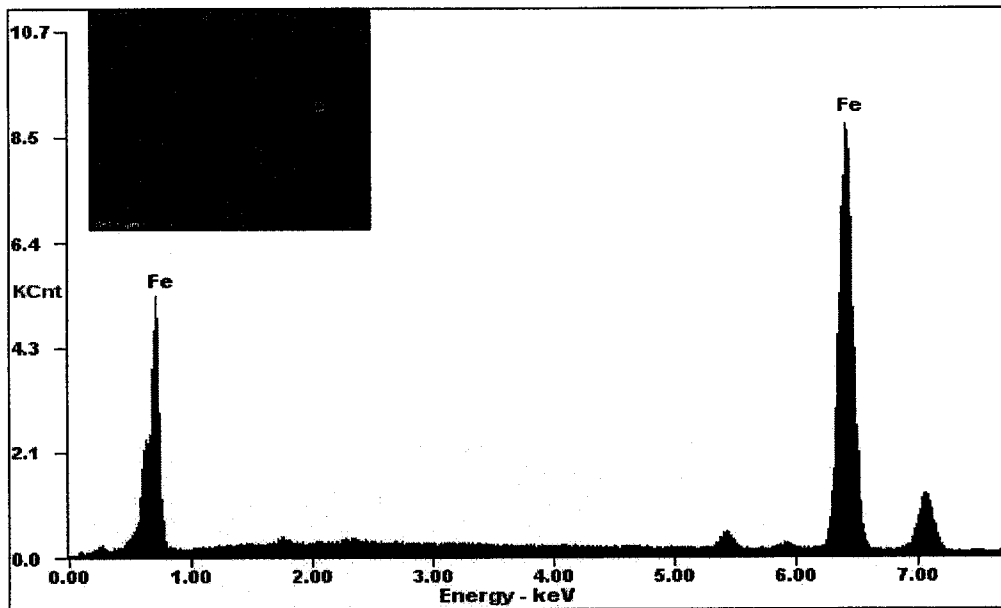
Fig. 4.79 EDX analysis of selected location 2 as shown in the SEM image of wear track on CC2 substrate after pin-on-disc test against steel pin under 15N load with 250m sliding distance

107
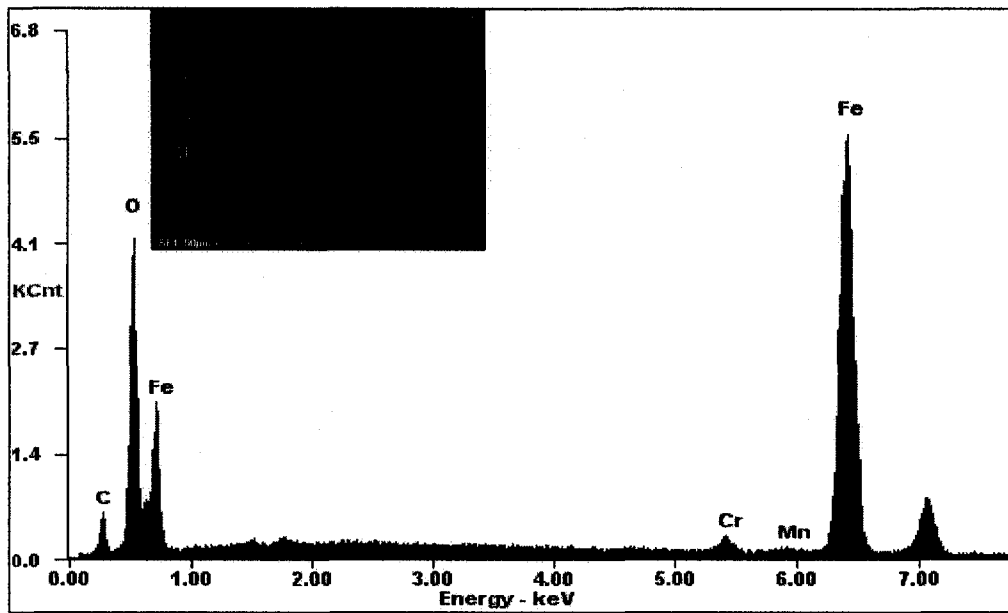
Fig. 4.80 EDX analysis of selected location 3 as shown in the SEM image of wear track on CC2 substrate after pin-on-disc test against steel pin under 15N load with 250m sliding distance
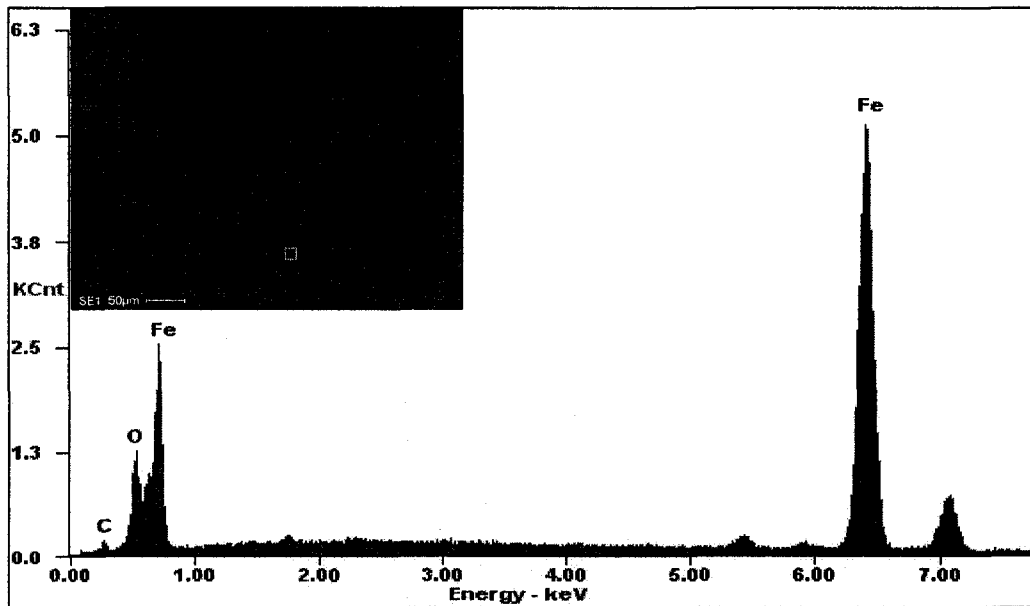
Fig. 4.81 EDX analysis of selected location 4 as shown in the SEM image of wear track on CC2 substrate after pin-on-disc test against steel pin under 15N load with 250m sliding distance

108
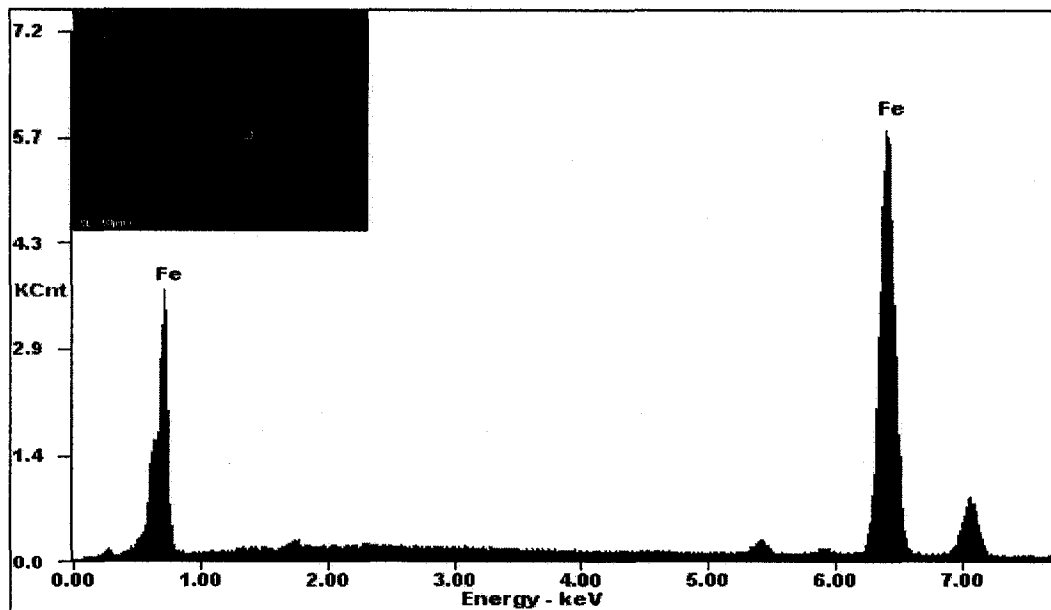
Fig. 4.82 EDX analysis of selected location 5 as shown in the SEM image of wear track on CC2 substrate after pin-on-disc test against steel pin under 15N load with 250m sliding distance

4.10.3 EDX analysis of counter pins

Figs. 4.83 to 4.95 are EDX analysis of wear scars on counter pins after pin-on-disc test against G3500 under 5N load with 250m sliding distance. Figs. 4.83 to 4.85 show EDX analysis of wear scar on aluminium pin after pin-on-disc test against G3500 under 5N with 250m sliding distance. It could be found that all the tested areas are oxidized. Back transferred oxidized aluminium materials with higher degree of oxidation could be found on the wear scar surface. Figs. 4.86 to 4.89 show EDX analysis of wear scar on aluminium pin after pin-on-disc test against G3500 under 10N with 250m sliding distance. All the tested areas are oxidized with higher degree of oxidation than that of under 5N load. Peeling of materials could be found on the wear scar surface. Figs. 4.90 and 4.91 show EDX analysis of wear scar on steel pin after pin-on-disc test against G3500 under

109

5N with 250m sliding distance. Some areas are oxidized but no back transferred materials could be found. Figs. 4.92 to 4.95 show EDX analysis of wear scar on steel pin after pin-on-disc test against G3500 under 15N with 250m sliding distance. The test results are quite similar to those under 5N load. Some areas are oxidized but no back transferred materials could be found.
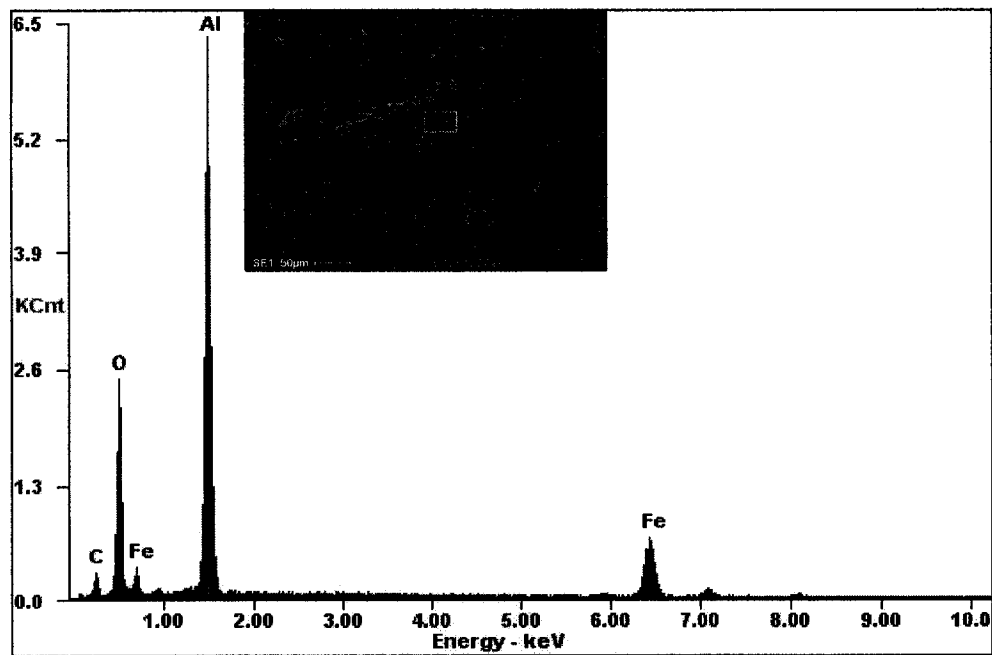
Fig. 4.83 EDX analysis of selected location 1 as shown in the SEM image of wear scar on aluminium pin after pin-on-disc test against G3500 under 5N load with 250m sliding distance

110
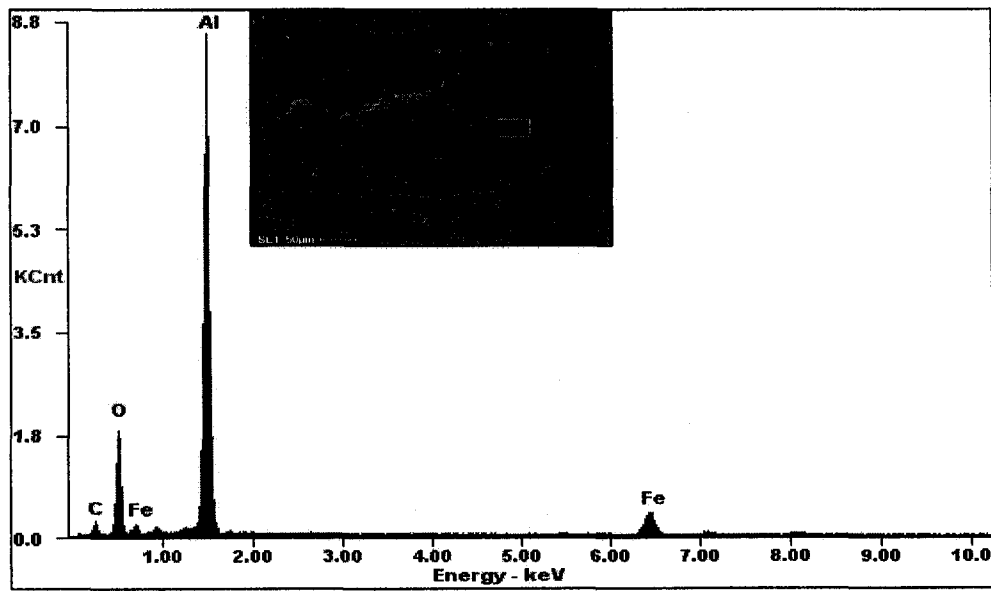
Fig. 4.84 EDX analysis of selected location 2 as shown in the SEM image of wear scar on aluminium pin after pin-on-disc test against G3500 under 5N load with 250m sliding distance
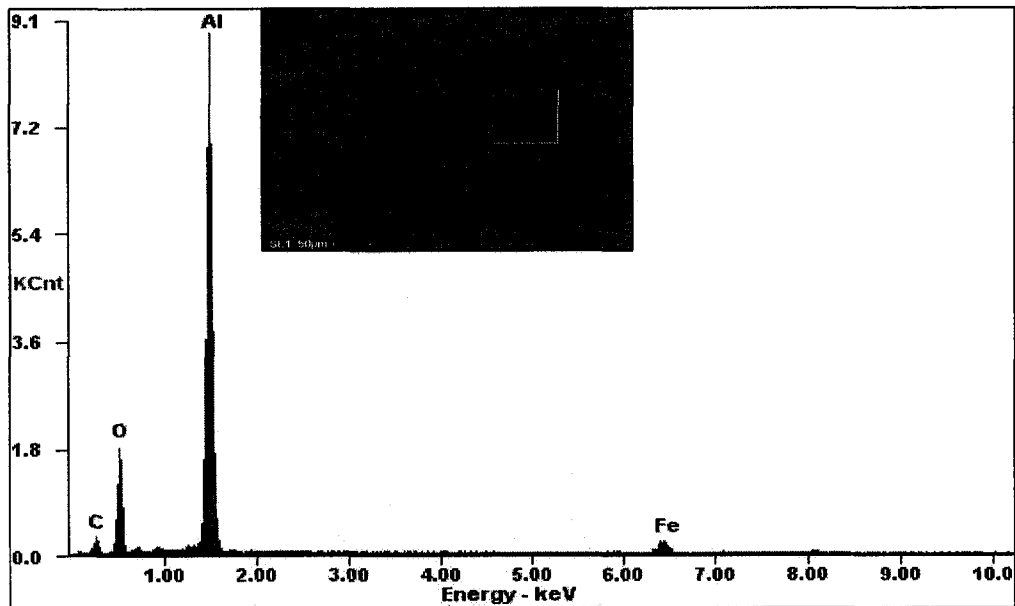
Fig. 4.85 EDX analysis of selected location 3 as shown in the SEM image of wear scar on aluminium pin after pin-on-disc test against G3500 under 5N load with 250m sliding distance

111
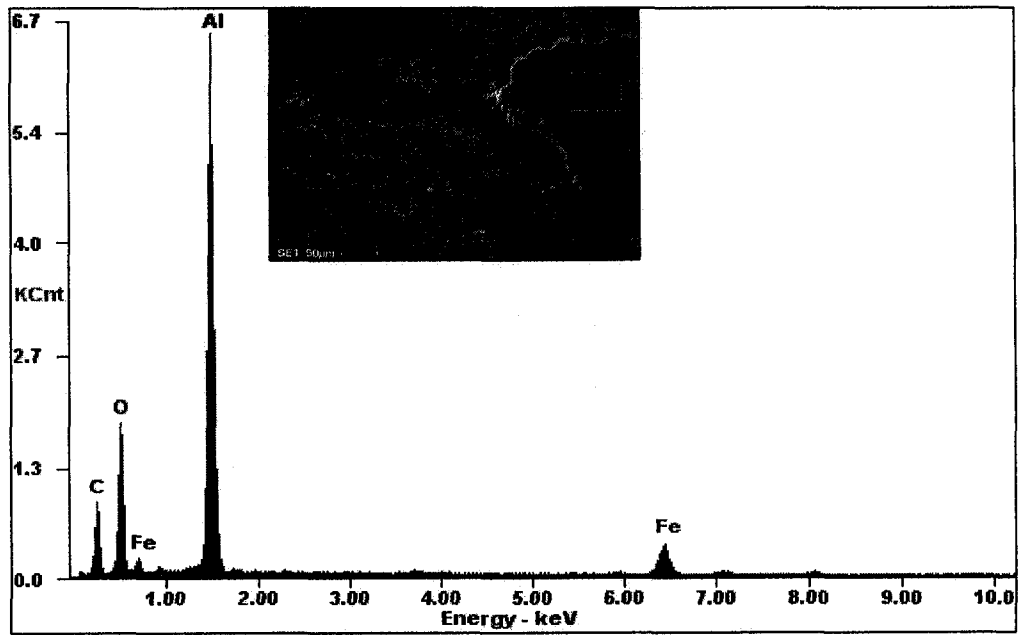
Fig. 4.86 EDX analysis of selected location 1 as shown in the SEM image of wear scar on aluminium pin after pin-on-disc test against G3500 under 15N load with 250m sliding 3500-Alpin-15N-1
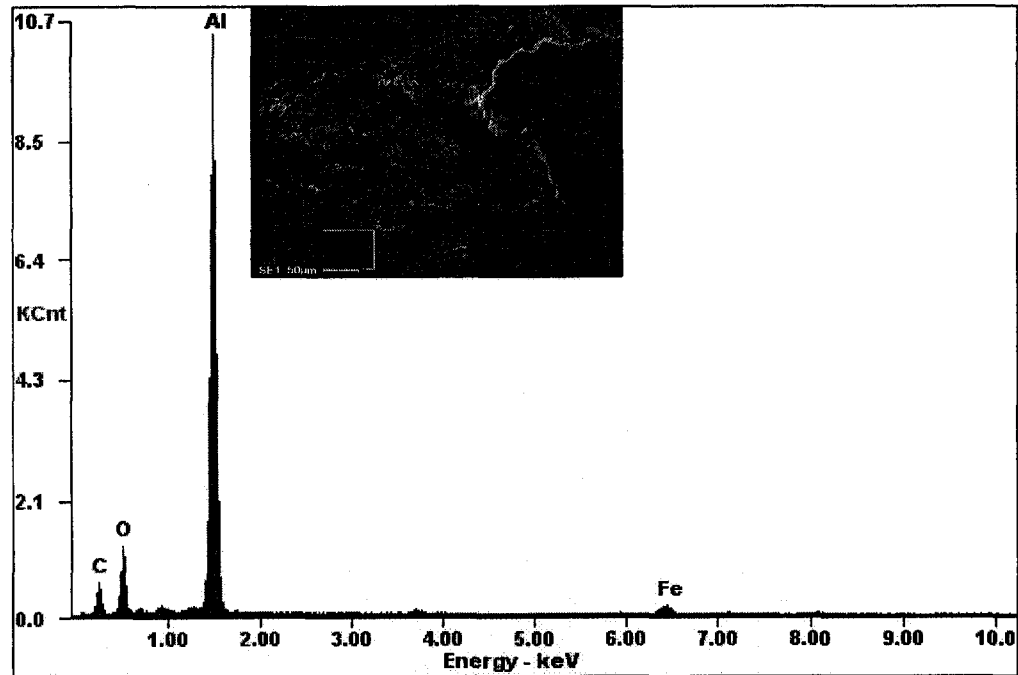
Fig. 4.87 EDX analysis of selected location 2 as shown in the SEM image of wear scar on aluminium pin after pin-on-disc test against G3500 under 15N load with 250m sliding

112
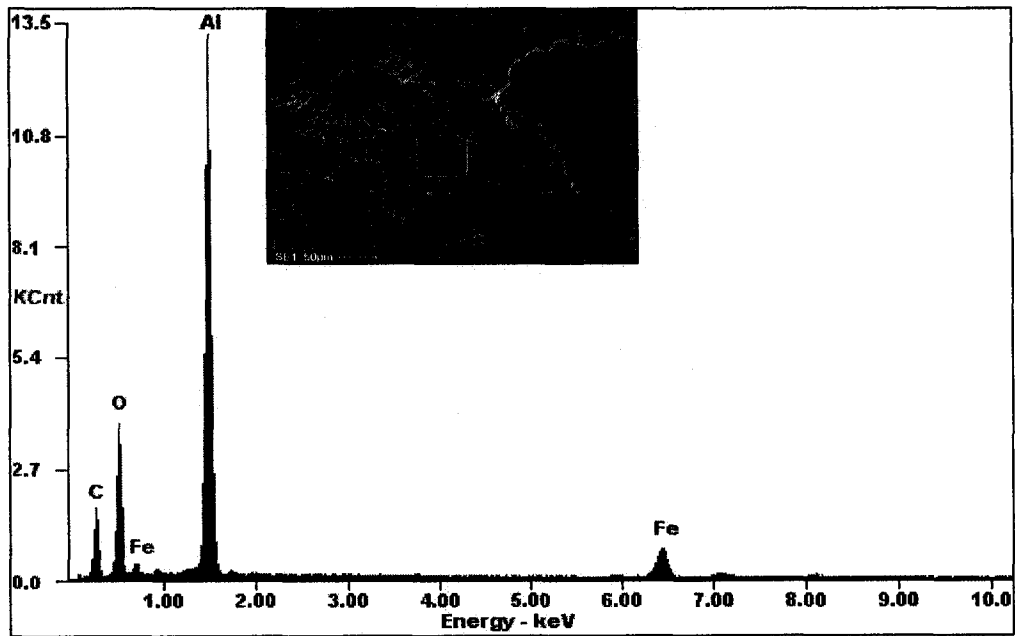
Fig. 4.88 EDX analysis of selected location 3 as shown in the SEM image of wear scar on aluminium pin after pin-on-disc test against G3500 under 15N load with 250m sliding distance
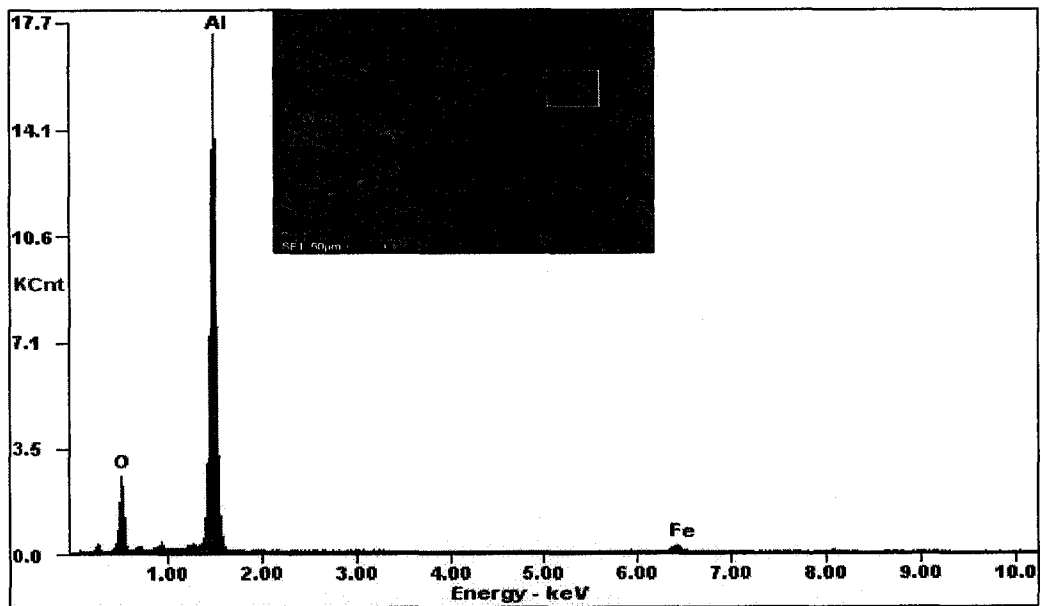
Fig. 4.89EDX analysis of selected location 4 as shown in the SEM image of wear scar on aluminium pin after pin-on-disc test against G3500 under 15N load with 250m sliding distance

113
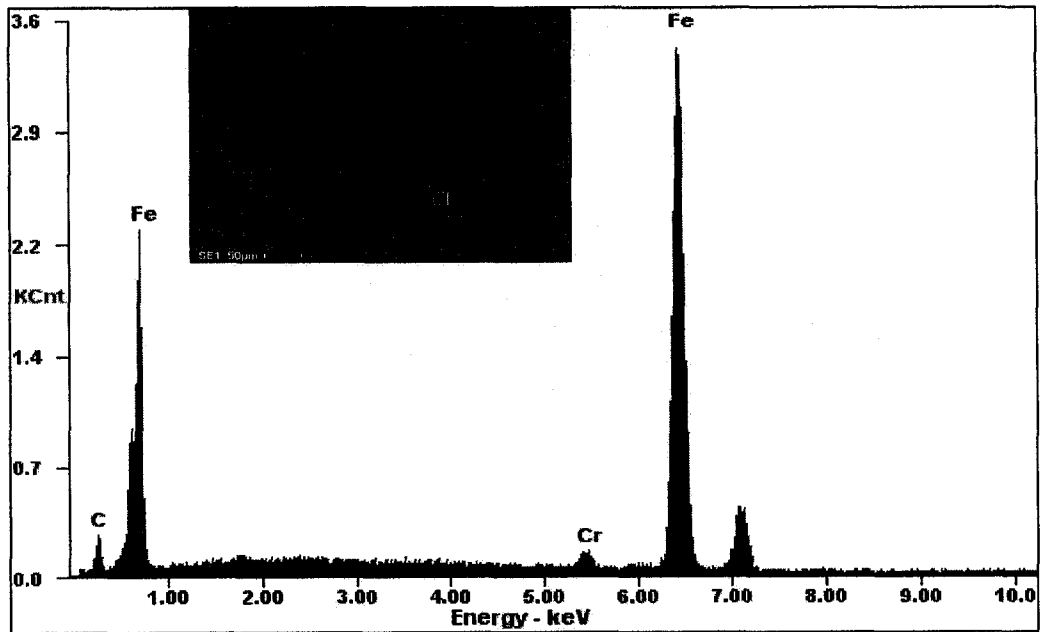
Fig. 4.90 EDX analysis of selected location 1 as shown in the SEM image of wear scar on

steel pin after pin-on-disc test against G3500 under 5N load with 250m sliding distance
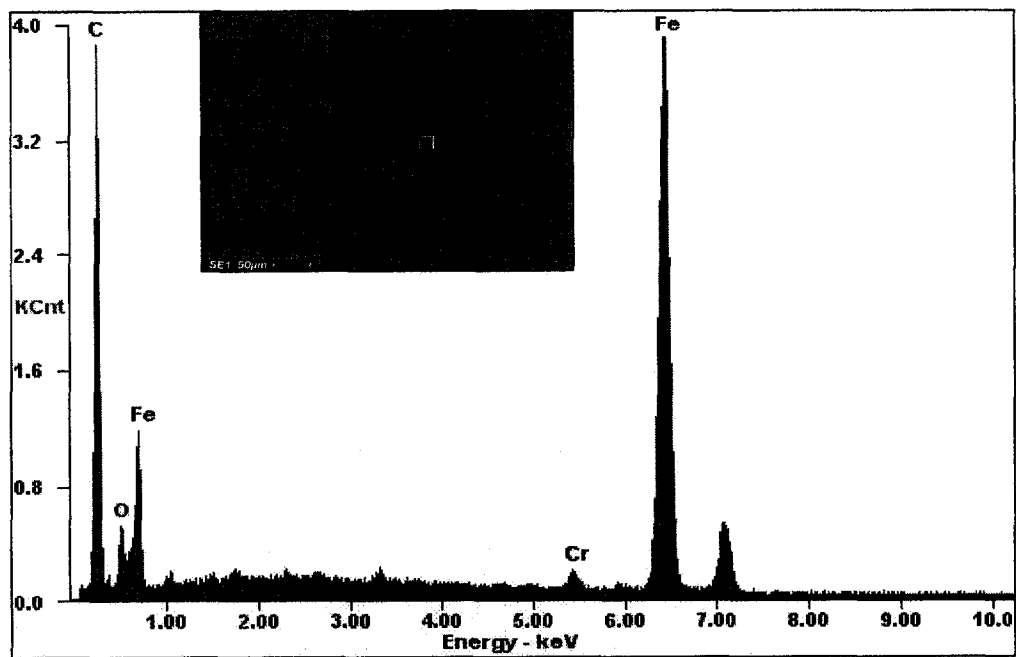
Fig. 4.91 EDX analysis of selected location 2 as shown in the SEM image of wear scar on

steel pin after pin-on-disc test against G3500 under 5N load with 250m sliding distance

114
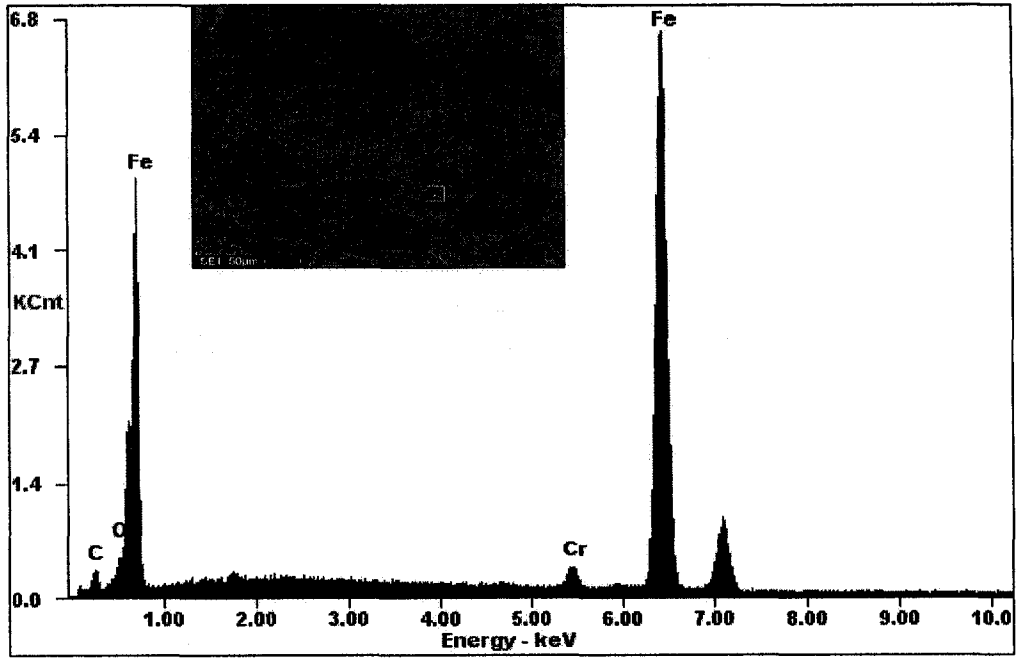
Fig. 4.92 EDX analysis of selected location 1 as shown in the SEM image of wear scar on steel pin after pin-on-disc test against G3500 under 15N load with 250m sliding distance
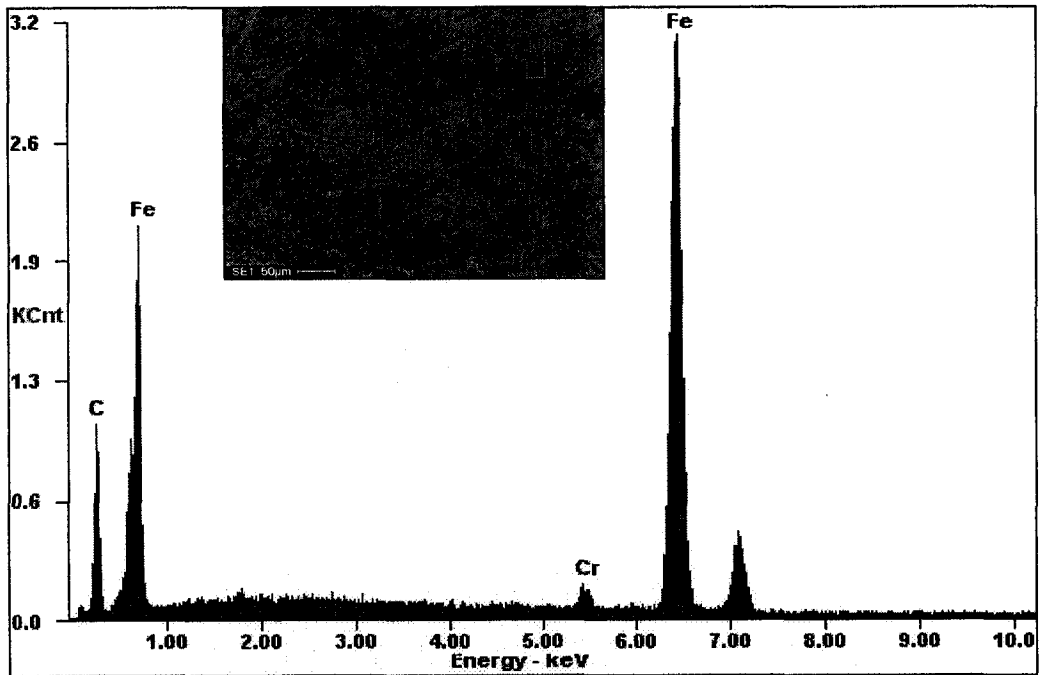
Fig. 4.93 EDX analysis of selected location 2 as shown in the SEM image of wear scar on steel pin after pin-on-disc test against G3500 under 15N load with 250m sliding distance

115
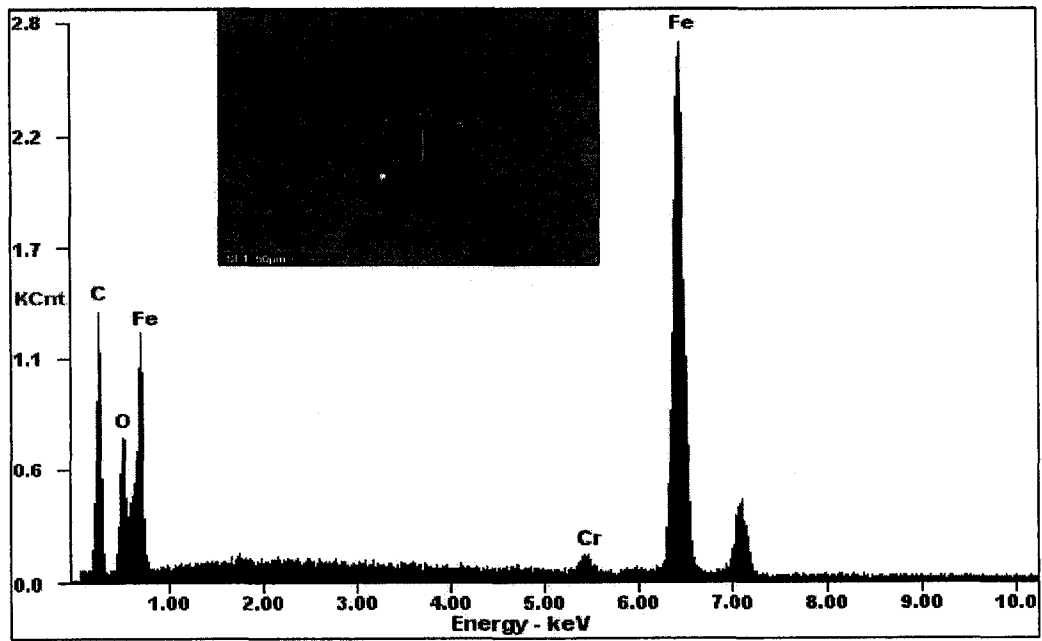
Fig. 4.94 EDX analysis of selected location 3 as shown in the SEM image of wear scar on

steel pin after pin-on-disc test against G3500 under 15N load with 250m sliding distance
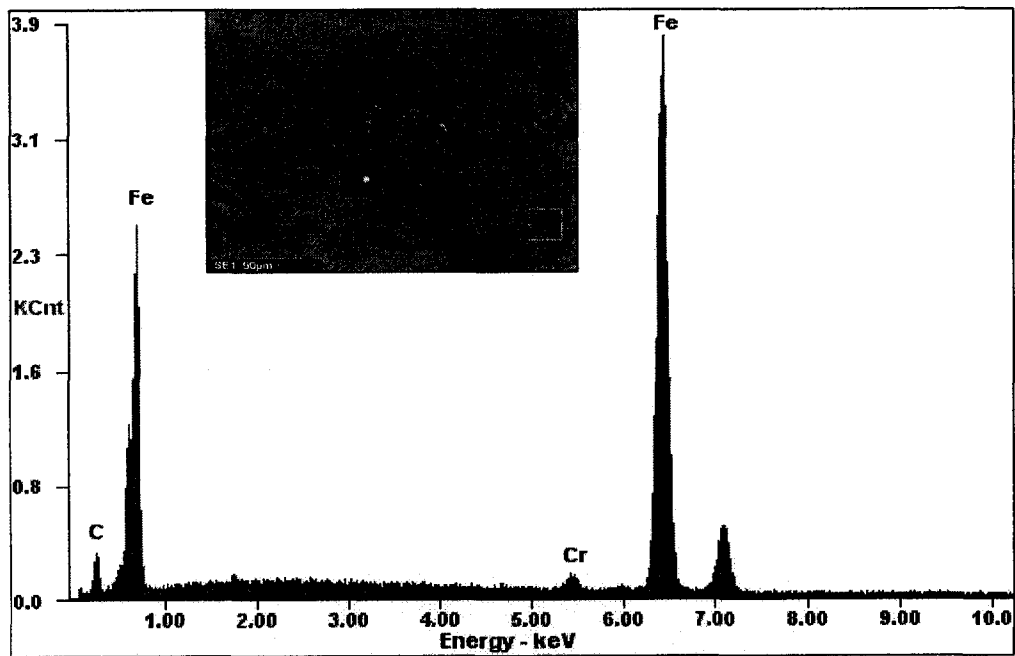
Fig. 4.95 EDX analysis of selected location 4 as shown in the SEM image of wear scar on

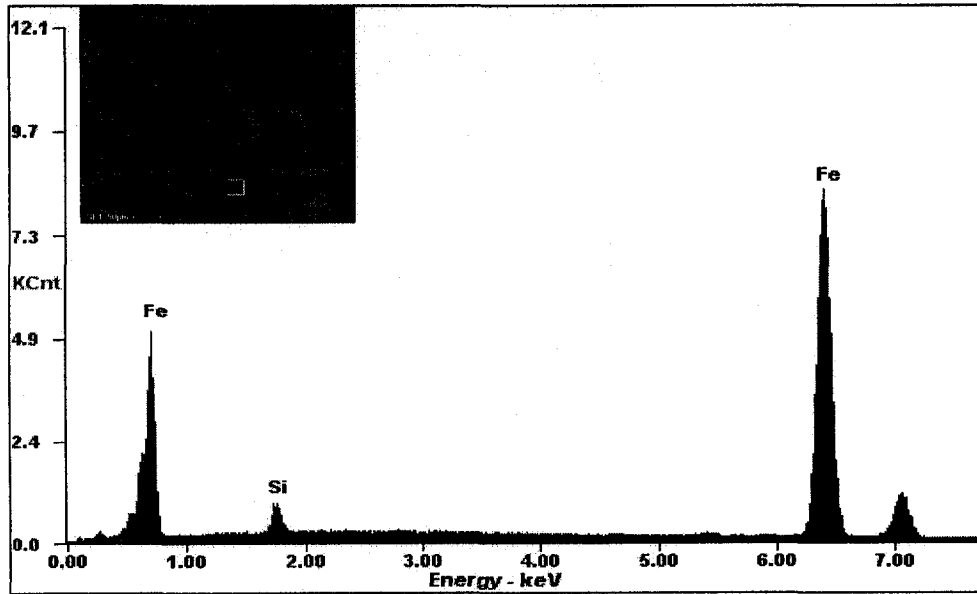steel pin after pin-on-disc test against G3500 under 15N load with 250m sliding distance

3500-Steelpin-15N-4

116

4.11 Materials transfer resistant performance of substrates

According to previous analysis, adhesive wear dominated for all the substrate materials under the test conditions of against aluminium pins under 5N and 10N load and against steel pins under 5N load. As one of the main applications for all these substrate materials is for die materials, it is quite useful to evaluate the materials transfer resistance property for the substrates, especially the materials transfer resistance property to aluminium and steel, which are two kinds of materials that are widely used in automotive industry. Fig. 4.96 (a), (b) and (c) collected all the SEM images for wear tracks of substrates after pin-on-disc tests against aluminum pins under 5N and 10N load and against steel pins under 5N load and (d) evaluated the ranking of the materials transfer resistance for 5 substrates (5- least transferred materials, excellent materials transfer resistance; 1-most transferred materials, fair materials transfer resistance). It appears that D2 exhibits the best materials transfer resistance either against aluminium or against steel.

(a)

(b)

117

(c)

Materials Transfer Resistance Index

vs Al under 5N ■ vs Al under 10N □ vs steel under 5N
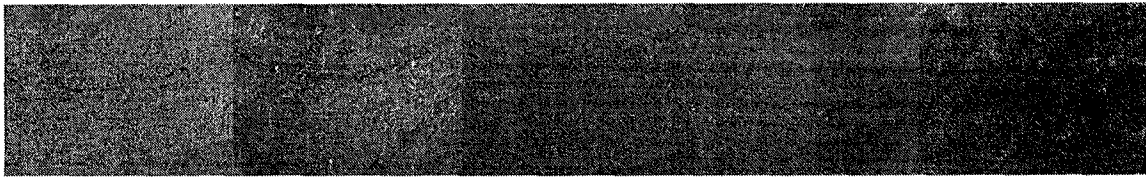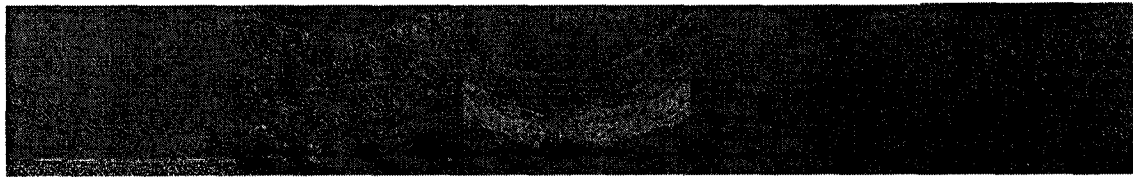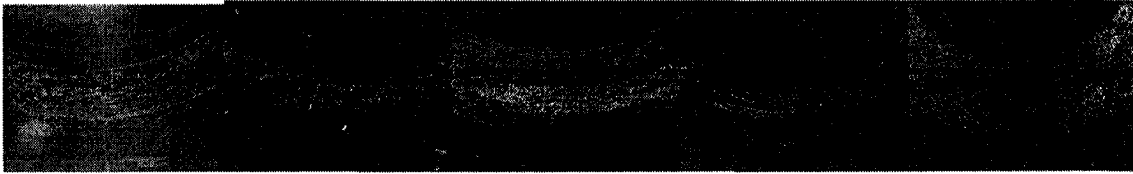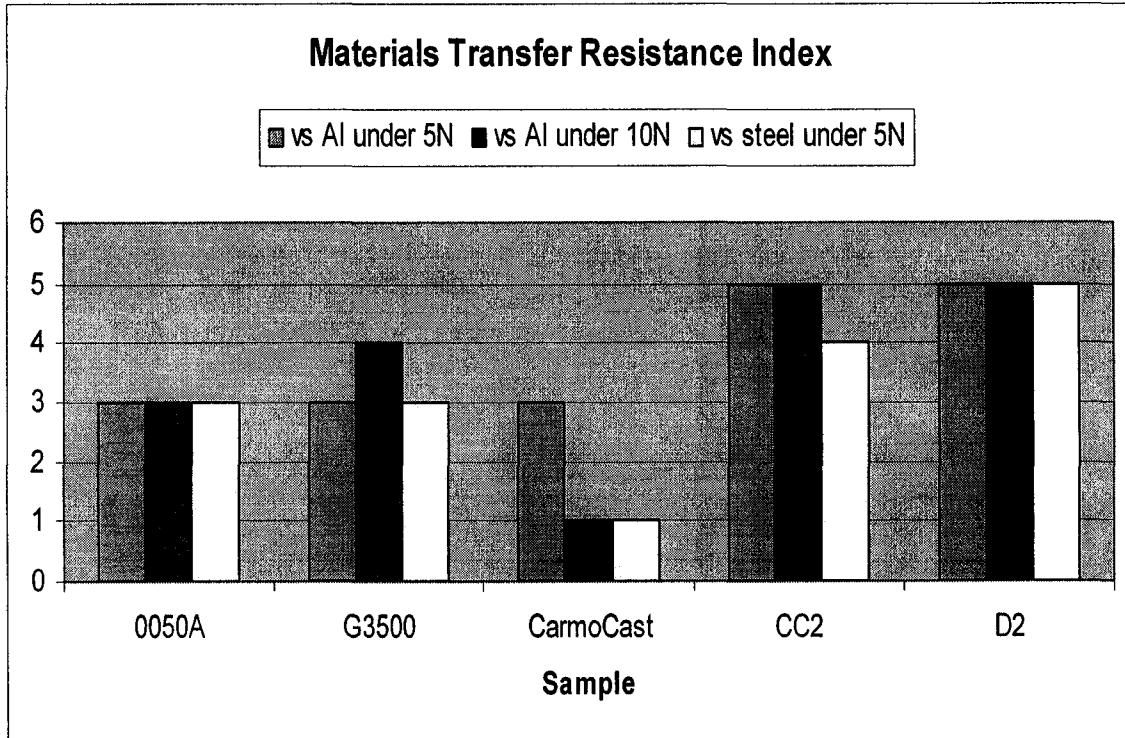
(d)

Fig. 4.96 (a), (b) and (c) SEM images for wear tracks of substrates (from left to right) 0050A, G3500, CarmoCast, CC2 and D2 after pin-on-disc tests (a) against aluminium pins under 5N load, (b) against aluminium pins under 10N load, (c) against steel pins under 5N load; (d) Materials transfer resistance index (5-the best, 1-the worst) for substrates of 0050A, G3500, CarmoCast, CC2 and D2 based on wear tracks SEM images observation after pin-on-disc tests against aluminium pins under 5N load, against aluminium pins under 10N load and against steel pins under 5N load.

118

4.12 Summary

The sliding wear performance of 5 substrates was studied. The following conclusions were made:

(1) For the wear performance of substrates against alumina pins under 5N load: Though G3500 has a low hardness, it has a relatively low wear rate and this may arise from the lubricating effect of the graphite particles. 0050A has the highest value of hardness; however, it also exhibits the highest wear rate, probably due to the brittle martensite phase. For CarmoCast, CC2 and D2, the harder one has the better wear resistance. D2 shows the lowest wear. Abrasive wear mechanisms dominate.

(2) For the wear performance of substrates against aluminium pin under 5N load: All the substrates have much lower wear rate than those against alumina pins under 5 N. Unlike the performance against alumina pin, G3500 has the highest wear rate which could be attributed to its low hardness and it seems that it doesn't benefit from the lubricating effect of graphite particles. Considering the error of measurement, the overall anti-wear performance for G3500, CarmoCast, CC2 and D2 has the tendency that the harder material has the better wear resistance. Though it is harder, 0050A displays higher wear rate than D2, probably due to it brittle martensitic phase. D2 presents the lowest wear rate. Adhesive wear mechanisms dominate.

(3) For the wear performance of substrates against aluminium pin under 10N load: Similar to the performance against alumina under 5 N and unlike the performance against aluminium pin under 5 N load, G3500 did not exhibit the highest wear rate due to its lowest hardness and it seems that it could benefit more from the lubricating effect of graphite particles under this test condition. For CarmoCast, D2 and 0050A, the harder material has the better wear resistance. CC2 presents the lowest wear rate. Adhesive wear mechanisms dominate.

(4) For the wear performance of substrates against steel pin under 5N load: All the substrates except CarmoCast exhibit lower wear rate than those against alumina and aluminium pins respectively under 5N load. Similar to the performance against alumina under 5 N and against aluminium pin under 10 N, and unlike the performance against aluminium pin under 5 N load, G3500 exhibits the lowest wear rate which could also be attributed to the lubricating effect of graphite. 0050A exhibits the highest hardness, however, it displays a higher wear rate than D2, probably due to its brittle martensite phase. For CarmoCast, CC2 and D2, the harder material has the better wear resistance. D2 exhibits the lowest wear rate. Adhesive wear mechanisms dominate.

(5) For the wear performance of substrates against steel pin under 15N load: All substrates exhibit higher wear rate compared with the tests against steel pins under 5N load. Unlike the performance against alumina under 5 N, against aluminium pin under 10 N and against steel under 5N, and similar to the performance against aluminium pin under 5 N load, G3500 exhibit the highest wear rate due to its lowest hardness. For G3500, CarmoCast, CC2 and D2, the

anti-wear performance has the tendency that the harder the material is the better wear resistance it has. Though 0050A has the highest value of hardness, it displays higher wear rate than D2, probably due to its brittle martensite phase. D2 exhibits the lowest wear rate. Fatigue wear or delamination wear mechanism dominates.

(6) The graphite particles of G3500 take effect only under some conditions. If the Hertz contact pressure is too low as against aluminium under 5 N load or too high as against steel pin under 15N, the graphite can not make too much different with the wear performance of G3500. Only under conditions like against alumina under 5 N, against aluminium pin under 10 N and against steel under 5N, the lubricating effect or wear reduction effect could be obviously observed. It seems that when the contact pressure is low, the wear is slight and only happens on the surface and graphite particles as a solid lubricant do involve in the wear process; when the contact pressure is high enough, the graphite will be worn out quickly, and it loses lubricating effects. However, for the Al at 5N load, transferred Al may cover the graphite on G3500 surface, resulting in no existence of solid lubricant. Thus, only when the contact pressure is within a certain range, the lubricating effect of graphite could be obviously observed.

(7) From the EDX analysis for G3500 substrate: Some oxidation occurs on the wear surface after pin-on-disc test against alumina pin under 5N load. After pin-on-disc tests against aluminium pin under 5N and 10N load, no oxidation occurs on the wear track surface, however, the oxidized aluminium transferred from the pin could be found on the wear track surface. Some oxidation occurs on some area of

121

the wear track surface as well as transferred oxidized iron from the counter pin could be found on the wear track surface after pin-on-disc tests against steel pin under 5 and 15N load.

(8) From the EDX analysis for CC2 substrate: No oxidation occurs on the wear track surface after pin-on-disc test against alumina pin under 5N load; After pin-on-disc tests against aluminium pin under 5N and 10N load, no oxidation occurs on the wear track surface, however, oxidized aluminium transferred from the pins could be found on the wear track surface. No oxidation occurs on the wear track surface, however, oxidized iron transferred from the counter pin could be found on the wear track surface after pin-on-disc tests against steel pin under 5N load. Some oxidation occurs on some area of the wear surface as well as transferred oxidized iron from the counter pin could be found on the wear track surface after pin-on-disc tests against steel pin under15N load.

(9) From the EDX analysis of wear scars on counter pins after pin-on-disc test against G3500: All the tested areas of aluminium pins are oxidized after pin-on-disc tests against G3500 under 5N and 10N load. Some areas of steel pins are oxidized after pin-on-disc tests against G3500 under 5N and 15N.

(10) In terms of the materials transfer resistance performance, D2 is the best either against aluminium or against steel under the present test conditions.

(11) D2 has the best wear resistant performance in general.

(12) Although the quenching hardening process was done under a similar condition by another independent supplier, the substrates appear to have different hardness.

122

Since the substrates have different hardness, the ranking of performance may not

reflect the real performance of products from the suppliers,

CHAPTER 5 EXPERIMENTAL RESULTS AND

DISCUSSION II: SLIDING WEAR OF COATINGS

5.1 SEM observation and XRD analysis

Figure 5.1 are the scanning electron microscopy (SEM) images of the TiN coating and the TiSiCN coating, showing the surface morphology of coatings on the surfaces (1a, 1b,) and on the cross-sections (1c, 1d). For the thick TiN (thickness 45μm) coating, some macro particles on the surface (Figure 1a) and large upside-down conical shaped structure on the cross-section (Figure 1c) were observed. It was generally considered that these macro particles were unfavorable to the properties of coating [33]. For the TiSiCN (thickness 17μm) coating (Figure 1b, 1d), its surface is smooth and there are some droplets on it, possibly occurred on the late stage of deposition; large granular grained structure can be observed on the coating surface, which seems to duplicate the microstructure of stainless steel substrate, probably not by epitaxial growth but by recrystallization; the cross-sectional image shows that TiSiCN coating has a denser and finer microstructure, which could be expected to lead to improved coating properties.
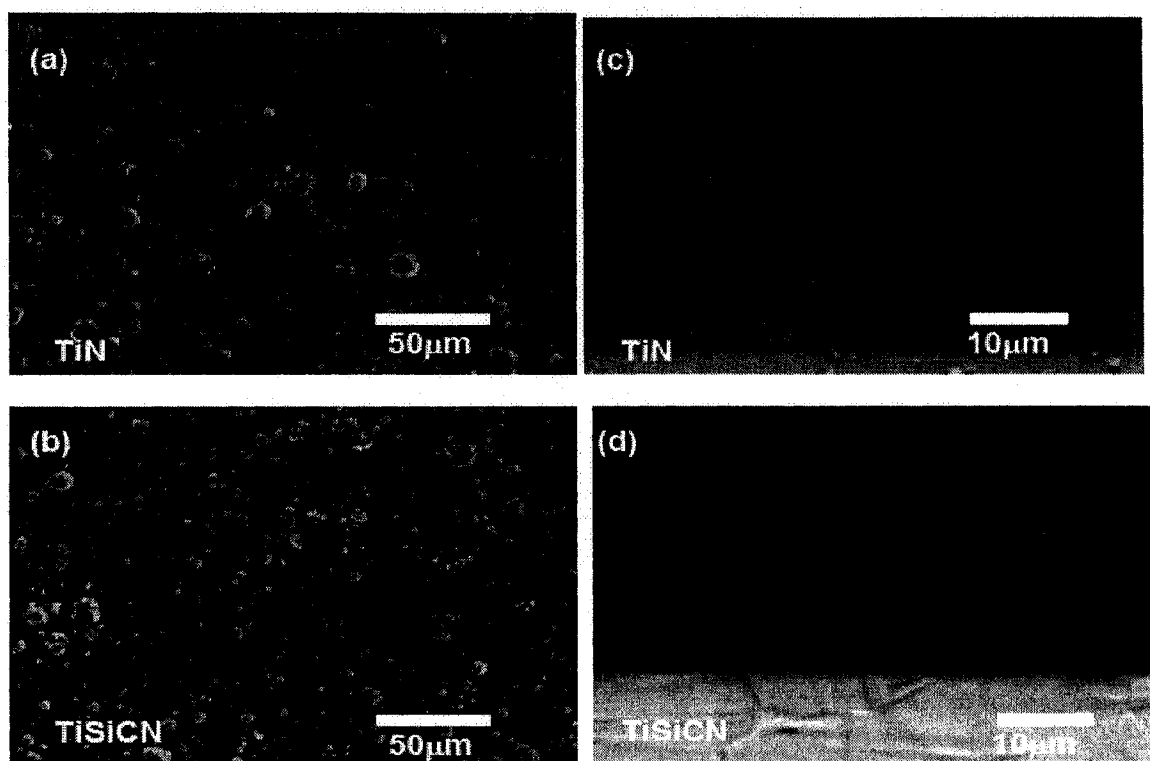
Fig.5.1 SEM images of the surfaces (a, b) and cross sections (c, d) of TiN and TiSiCN coating samples.

Figure 5.2 shows the XRD patterns for the TiN and TiSiCN coating samples. The XRD pattern for TiSiCN coating displayed TiN and TiC structures, corresponding to (111), (200) and (220) planes of TiN, and (311), (400) and (420) planes of TiC. Although XRD results did not show any crystalline Si_3N_4 phase, the possibility that Si_3N_4 could exist in amorphous form was expected [29]. Ma et al. [28, 29] reported a TiSiCN coating system dominated by TiN structure with plane orientation of (200), while with the increase of Si content, the TiSiCN coatings had some mixed plane orientations (TiN and TiC) of (111), (220) and (200). Kuo et al. [31, 32] also found some TiSiCN coating systems dominated by cubic TiC structure or by both TiN and $TiN_{0.3}$ structures.

125
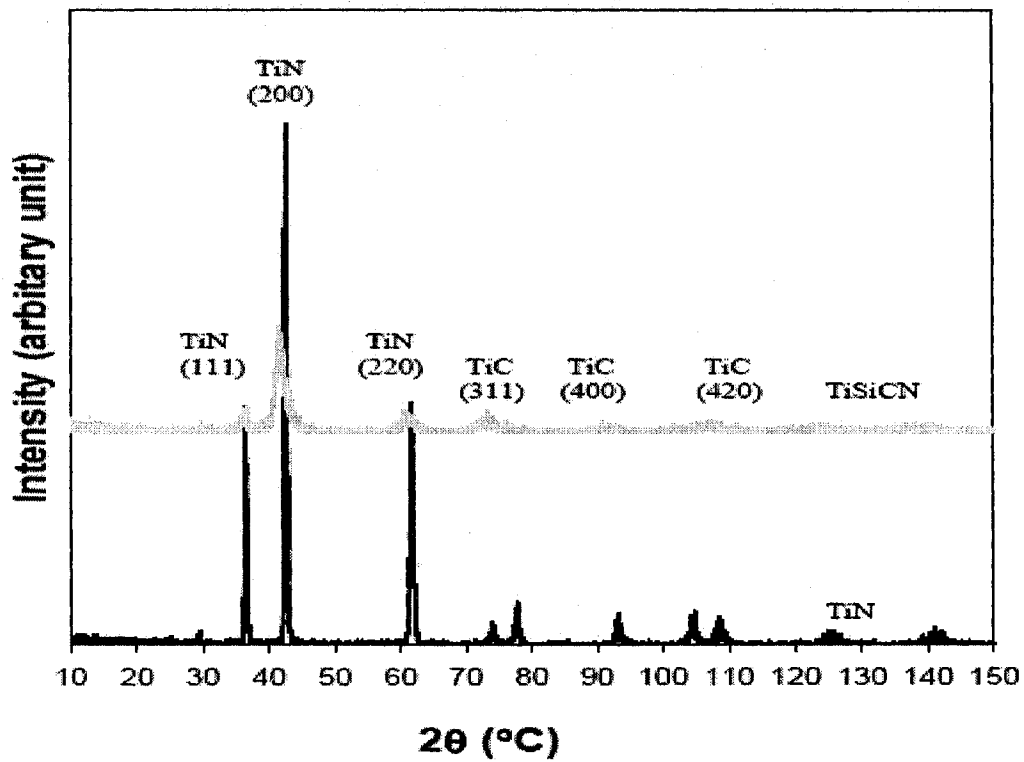
Figure 5.2 X-ray diffraction (XRD) patterns of TiN and TiSiCN coatings.

5.2 Hardness and coating adhesion tests

Figure 5.3 shows the nanoindentation force-displacement curves of the two coatings. Hardness (H) and elastic modulus (E) were determined using the Oliver-Pharr data analysis method [61]. The TiSiCN coating exhibited higher hardness and lower elastic modulus than the TiN coating.

126
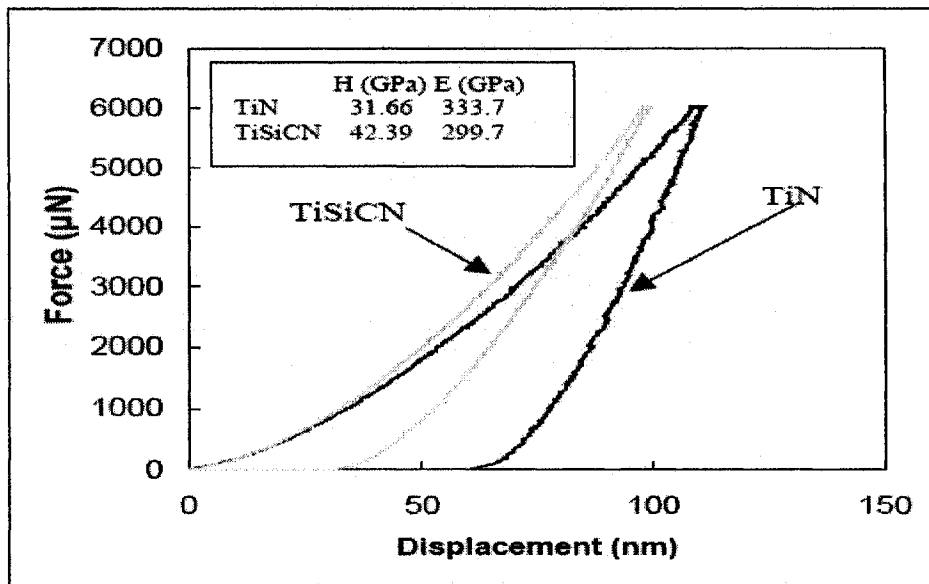
Figure 5.3 Force-displacement curves of TiN and TiSiCN coatings at nanoindentation tests.

The adhesive strength is considered to be the force needed to separate the coatings from the substrate. The indentation tests were conducted on a Rockwell hardness tester, applying a hardened steel ball to the surfaces of the samples with 150kg load [62]. The resulted damages to the coating around the indentation were examined using optical microscopy and are shown in Figure 5.4. The degree of the coating cracking is used to determine the adhesion property as ranked from HF1 to HF5. HF1 means no crack occurred, while HF5 indicates severe spalling on the coating surface. The coatings of TiN and TiSiCN could be evaluated as HF1 and HF1/HF2, respectively. Thus, both of the two coatings exhibited a good adhesion property, although the studied coatings in this project are much thicker than the commercially used PVD coatings.

127
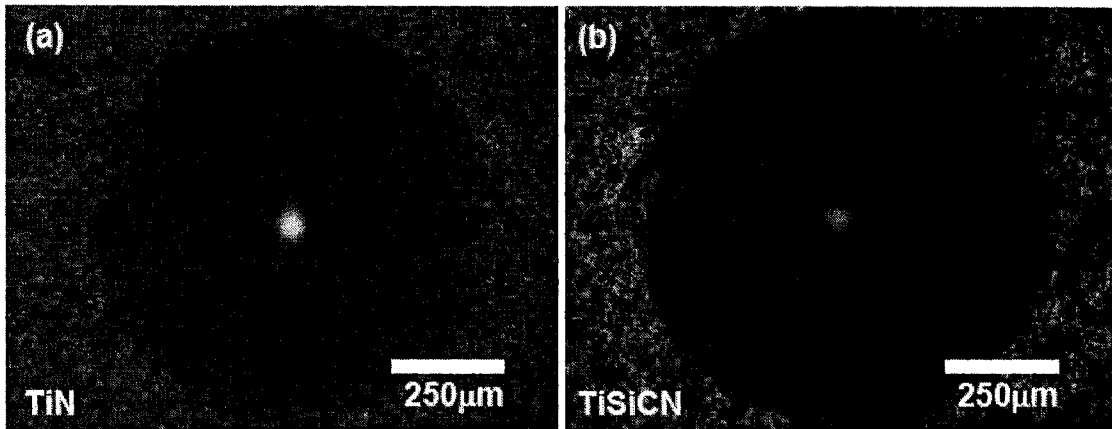
Figure 5.4 Surface failures due to indentation tests for adhesion evaluation of (a)TiN and (b) TiSiCN coating samples.

5.3 Pin-on-disc tests

Figures 5.5 and 5.6 show tribological properties of the various testing samples with and without applications of the lubricating and cooling coolant against aluminium and alumina counterface materials. The values of wear rate and coefficients of frictions (C.O.F) are also presented in Figures 5.5 and 5.6.

	aa	aoa	ac	aoc
▣ TiN	519.8	50.8	0	51.2
☐ TiSiCN	281.9	110.9	0	43.3

Samples
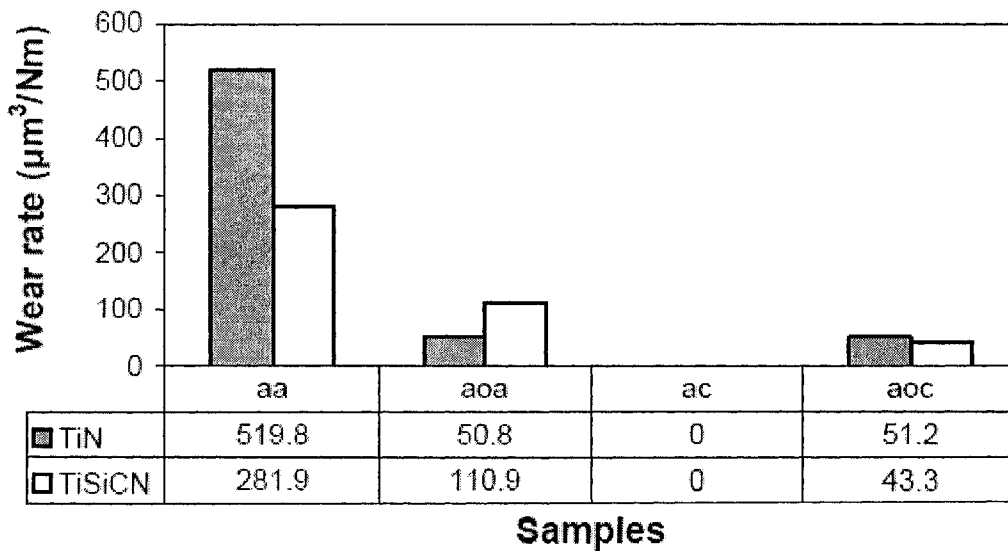
Figure 5.5 Wear rates of TiN and TiSiCN coatings against aluminium counterparts in air, alumina counterparts in air, aluminium counterparts in coolant and alumina counterparts in coolant.

128

Samples	aa	aoa	ac	aoc
■ TiN	0.8	0.32	0.12	0.15
□ TiSiCN	0.6	0.28	0.25	0.24
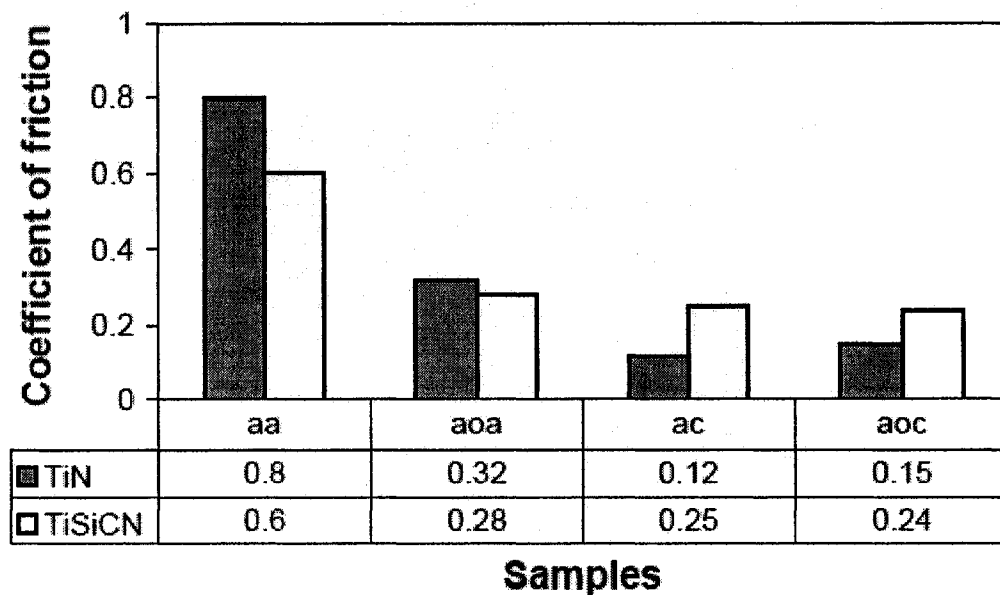
Figure 5.6 Coefficient of friction of TiN and TiSiCN coatings against aluminium counterparts in air, alumina counterparts in air, aluminium counterparts in coolant and alumina counterparts in coolant.

In air, the TiSiCN coating exhibited lower wear rate and lower C. O. F than the TiN coating when tested against aluminum pins, while it exhibited higher wear rate and lower C. O. F than the TiN coating when tested against alumina balls. It was also noted that aluminium counterparts caused both coatings to have larger wear rate and larger C. O. F. in air. Comparing with the wear property of substrates, it can be found that the wear rate of TiSiCN against alumina in air under 5N is only about one-sixtieth of the wear rate of D2 (the smallest among 5 substrates) against alumina in air under 5N load. This shows that the abrasive wear rates for both coatings are much smaller than the abrasive wear rates of substrates.

129

On the other hand, to evaluate the tribological properties of the coatings in different environmental conditions, cutting coolant was used in the present study. Hangsterfer's S-500 cutting fluid is a water soluble oil, which is comprised of petroleum or mineral oil, emulsifiers and other additives. Improved cooling capabilities and good lubrication due to the blending of oil and water could be achieved by using this kind of coolant. The coolant could provide protective oil films between the coatings and the counterparts, which could be expected to improve the wear resistance and the coefficient of friction for the coatings [63].

As seen in Figures 5.5 and 5.6, coolant played a role as expected. After using a coolant, the wear resistance and C. O. F were generally improved for both coatings. Compared with the wear properties of the coatings tested in the air, the wear property of the coatings in the coolant testing conditions was totally different. The wear rates of two coatings against aluminiun pins (negligible as shown by number "0" in the table) were smaller, instead of larger, than those against alumina balls. This demonstrated that the coolant could prevent the adhesive wear which dominated the wear behavior of coatings against soft aluminium pins in air as discussed later on.

It was worth to notice that as a comparison reference, the TiN coating observed in this study had a better tribological properties (wear resistance and C.O.F.) than other TiN coating samples we had on hand.

130

5.4 SEM study of wear behavior

Figure 5.7 shows SEM images for wear tracks of two coatings tested in air against aluminium counterparts (a, b) and against alumina counterparts (c, d). It could be observed that for each coating, the wear track against aluminium counterpart was wider and rougher than that against alumina one. Materials transferring from the aluminium pin to the localized areas on the coating surface could also be observed. For the wear tracks against alumina pins, TiN exhibits wider wear track and TiSiCN shows some surface fatigue which results materials peeling as shown in Fig. 5.7d. This will help to explain the reason why TiSiCN exhibit higher wear rate than TiN when tested against alumina in air. Another possibility could also help is that the coating debris can act as an additional source of abradant particles in the sliding wear, leading to higher abrasive wear. The harder the coating debris, the more severe the abrasive wear in coating [45]. Material transferring and polishing are the main wear mechanisms for both coatings when tested against aluminium under 5N load in air. Polishing is the dominate mechanism for TiN coating when tested against alumina under 5N load in air. Polishing and surface fatigue are the dominant wear mechanisms for TiSiCN coating tested against alumina pin under 5N load in air.

Figure 5.8 and Figure 5.9 show SEM images for wear tracks on TiN and TiSiCN coatings surfaces after pin-on-disc tests in coolant against aluminium counterpart and alumina counterpart. Comparing with the wear tracks on coating surfaces after tests in air shown in Figure 5.7, the wear tracks in Figure 5.8 and 5.9 are much smoother, indicating that the coolant provided a lubricant film and eliminated adhesive wear for coatings against

131

aluminium pins. Considering the effect of counterparts in coolant, since the Hertz contact stress was higher for the rigid alumina ball/coating contact than that for the soft aluminium pin/coating contact system, the wear scar was more observable on Figure 5.8 (b) and Figure 5.9 (b) than that on Figure 5.8 (a) and Figure 5.9 (a). Surface polishing is the dominant wear mechanism for both coatings when tested in coolant, either against aluminium or alumina under a 5N load.
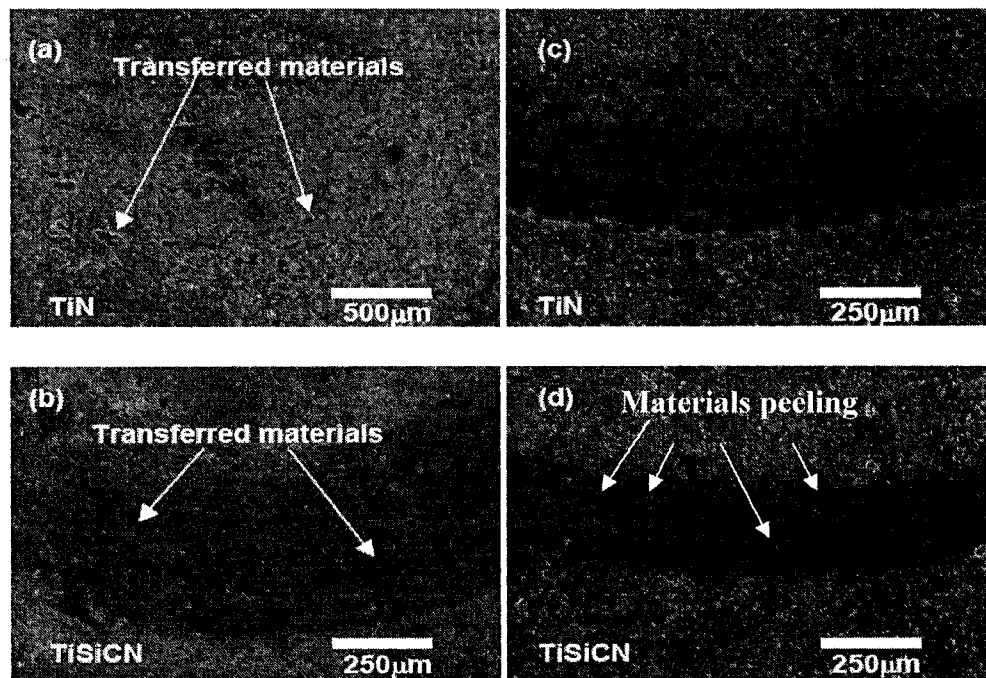
Figure 5.7 SEM images for wear tracks on TiN and TiSiCN coating surfaces after pin-on-disc tests in air against aluminium counterparts (a, b) and alumina counterparts (c, d).

132
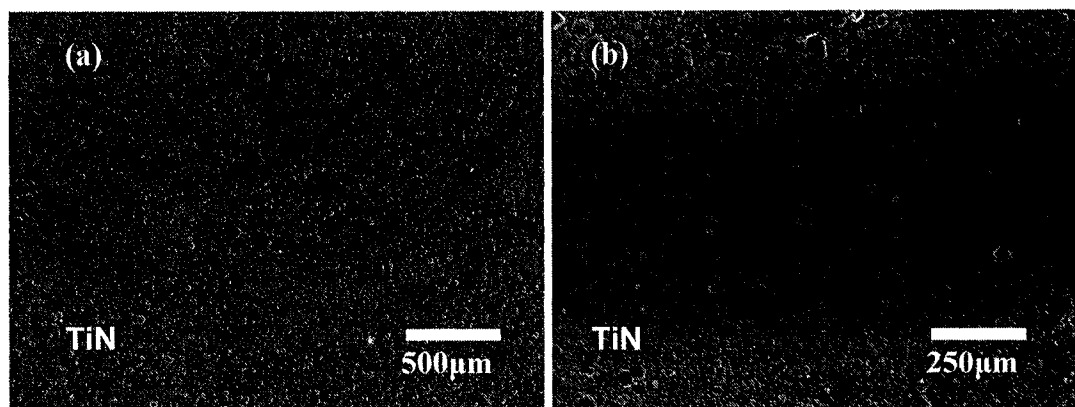
Figure 5.8 SEM images for wear tracks on TiN coating surface after pin-on-disc tests in coolant against (a) aluminium counterpart and (b) alumina counterpart.
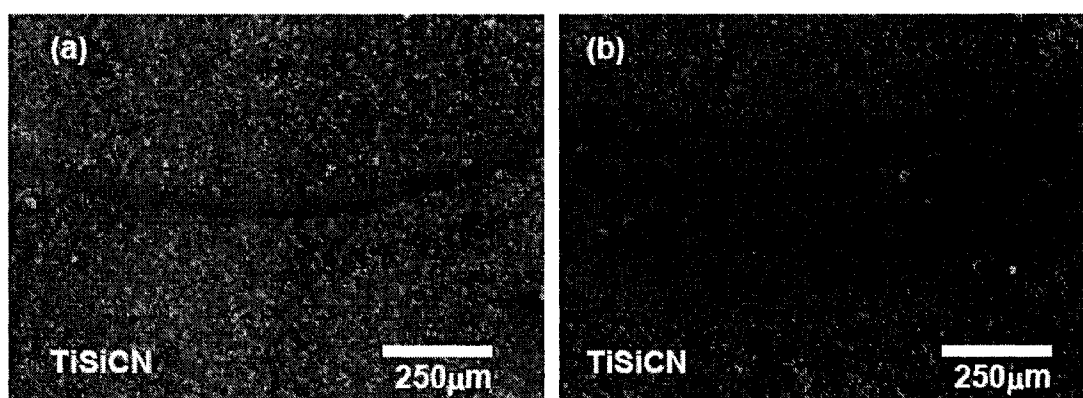
Figure 5.9 SEM images for wear tracks on TiSiCN coating surface after pin-on-disc tests in coolant against (a) aluminium counterpart and (b) alumina counterpart.

5.5. Summary

(1) Very thick TiN and TiSiCN coatings (17-45μm) were successfully deposited onto stainless steel substrates by a Plasma Enhanced Magnetron Sputtering (PEMS) deposition technique.

(2) Both of the coatings had a high interface adhesion strength.

(3) In air, the TiSiCN coating exhibited a lower wear rate and a lower C. O. F than the TiN coating when tested against an aluminum pin, while it exhibited a higher wear rate and a lower C. O. F than the TiN coating when tested against an alumina ball. The aluminium pin also caused both TiN and TiSiN coatings to have a larger wear rate and larger C. O. F in air.

(4) In a coolant, the wear rates of the coatings against the aluminiun pin (negligible) were smaller, instead of larger, than those against the alumina ball.

(5) The cutting coolant could provide a lubricant effect and thus reduce the adhesive wear between the coating and the counterpart, which led to decreased wear rate and reduced coefficient of friction (C. O. F).

(6) Material transfer and polishing are the main wear mechanisms for both coatings when tested against aluminium under 5N load in air.

(7) Polishing is the dominate mechanism for TiN coating when tested against alumina under 5N load in air. Polishing and surface fatigue are the dominant wear mechanisms for TiSiCN coating tested against alumina pin under 5N load in air.

(8) Surface polishing is the dominant wear mechanism for both coatings when tested in coolant, either against aluminium or alumina under 5N load.

(9) The abrasive wear rates for both coatings are much smaller than the wear rates for substrates. The wear rate of TiSiCN (which is greater than TiN) against alumina in air under 5N is only about one-sixtieth of the wear rate of D2 (the smallest among 5 substrates) against alumina in air under 5N load.

134

CHAPTER 6 EXPERIMENTAL RESULTS AND

DISCUSSION II: MICRO-ABRASION WEAR OF

SUBSTRATES AND COATNGS

In this chapter, the micro-abrasion wear of substrates and coatings will be studied.

6.1 Micro-abrasion wear of substrates

6.1.1 Micro-abrasion wear rate of substrates

Fig. 6.1 shows the micro-abrasion wear rate and hardness for substrates of 0050A, G3500, CarmoCast, CC2 and D2 with sliding distance of 24m and 48m. D2 displayed the best micro-abrasion wear resistance due to its high hardness. With a shorter sliding distance (24m), G3500 exhibit good wear resistance which is similar to its behavior against alumina under 5N load in the pin-on-disc sliding wear test. The reason could be the lubricant effect of graphite. Interestingly, comparing with the wear rate in the sliding wear test shown in Fig. 6.2, it could be found that the substrates perform similar relative micro-abrasion wear resistance in the group. This result suggests that micro-abrasion wear test method is an effective alternative measure for abrasive wear test for materials.

Wear Rate & Hardness

24m **48m** ···▲··· Hardness

Sample	0050A	G3500	CarmoCa	CC2	D2
24m	217.01	146.14	260.84	249.31	131.54
48m	252.66	243.17	293.42	216.3	142.55
Hardness	803	293	513	600	702

Fig. 6.1 Micro-abrasion wear rate and hardness for substrates of 0050A, G3500, CarmoCast, CC2 and D2 with sliding distance of 24m and 48m.
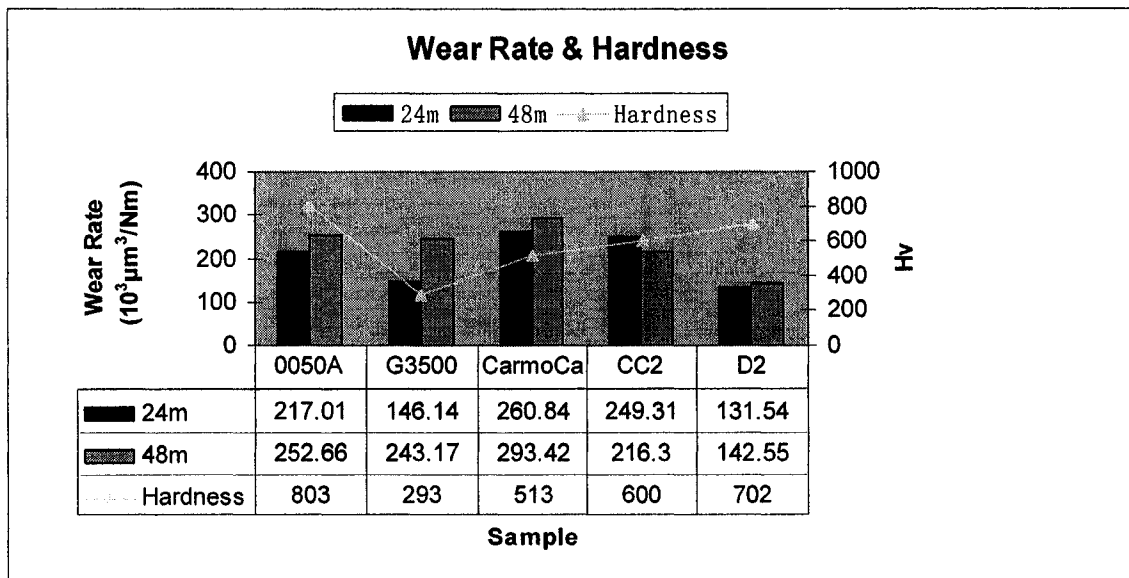
Wear Rate & Hardness

Sliding Wear Rate **Micro-abrasion Wear Rate** ···▲··· Hardness
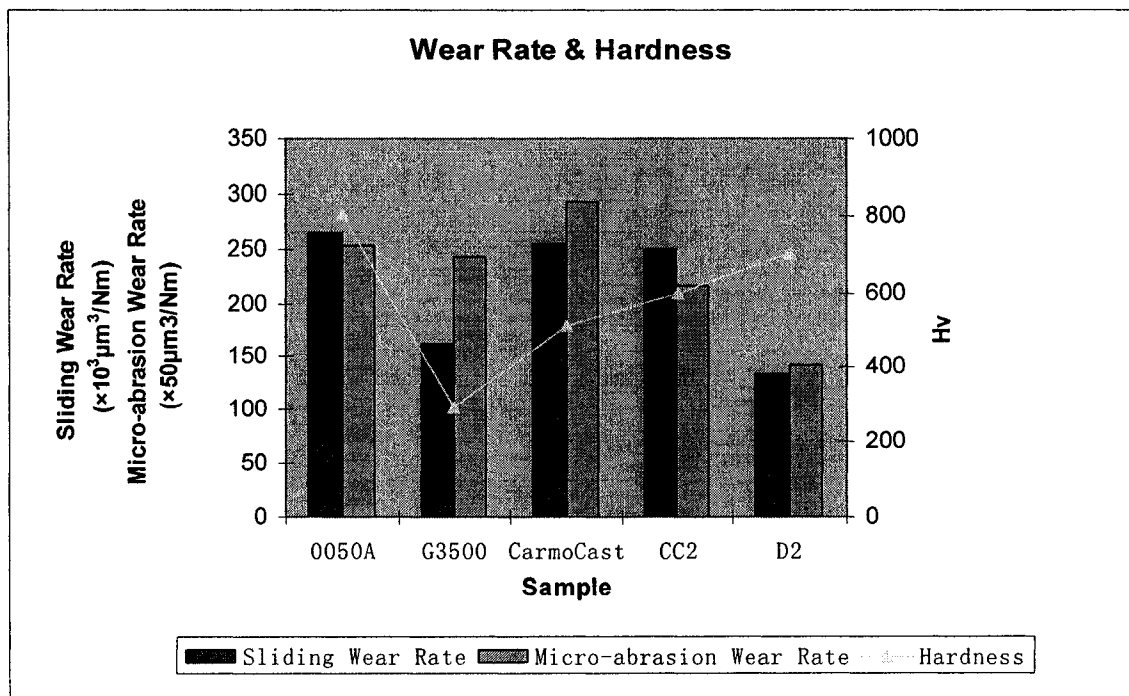
Fig. 6.2 Abrasive sliding wear rate after pin-on-disc tests (against alumina pins under 5N /250m), micro-abrasion wear rate after micro-abrasion wear tests (with alumina slurry under 4N/48m) and hardness for substrates 0050A, G3500, CarmoCast, CC2 and D2.

136

6.1.2 SEM observation for micro-abrasion wear behaviors of substrates

Figs. 6.3 to 6.12 are SEM images of wear scars on the substrates of 0050A, G3500, CarmoCast, CC2 and D2 after micro-abrasion testing under a 4N load with 24m and 48m sliding distance. Microploughing is the dominant interaction between the abrasive particles and the substrates surfaces. The white particles appearing on the images were determined by EDX analysis to be alumina particles coming from the slurry.

Fig. 6.3 SEM images of wear scar on 0050A substrate after micro-abrasion test under 4N load with 24m distance (a) 50×, (b) 500×
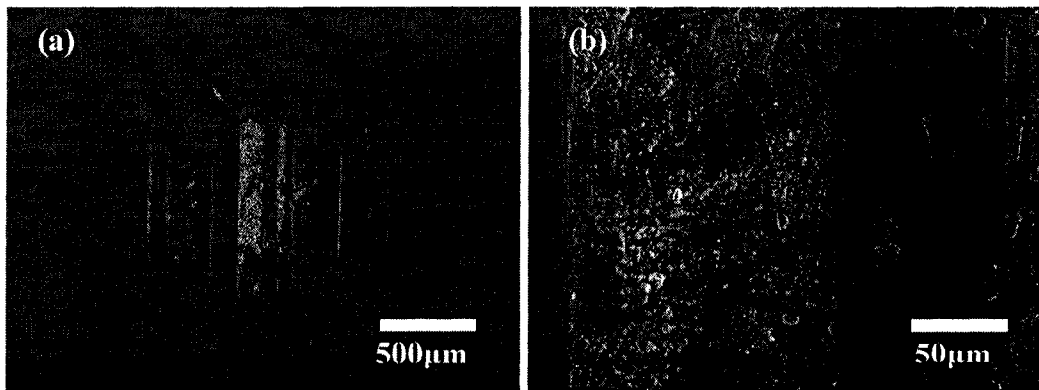
Fig. 6.4 SEM images of wear scar on G3500 substrate after micro-abrasion test under 4N load with 24m distance (a) 50×, (b) 500×

137
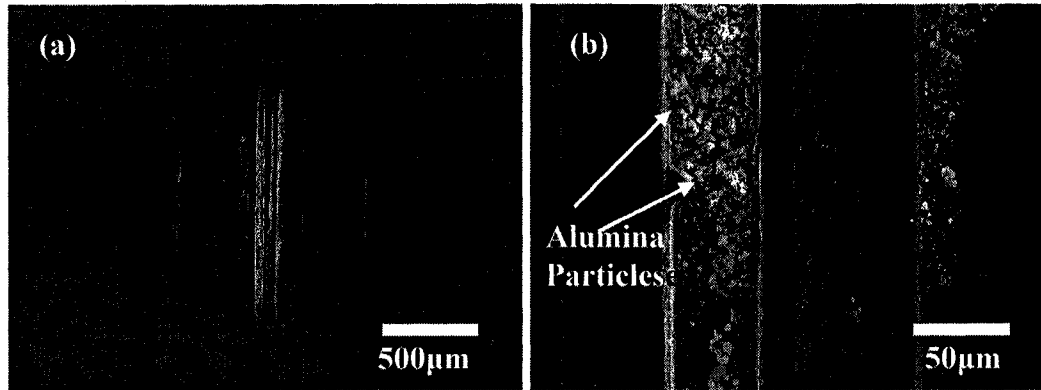
Fig. 6.5 SEM images of wear scar on CarmoCast substrate after micro-abrasion test under 4N load with 24m distance (a) 50×, (b) 500×
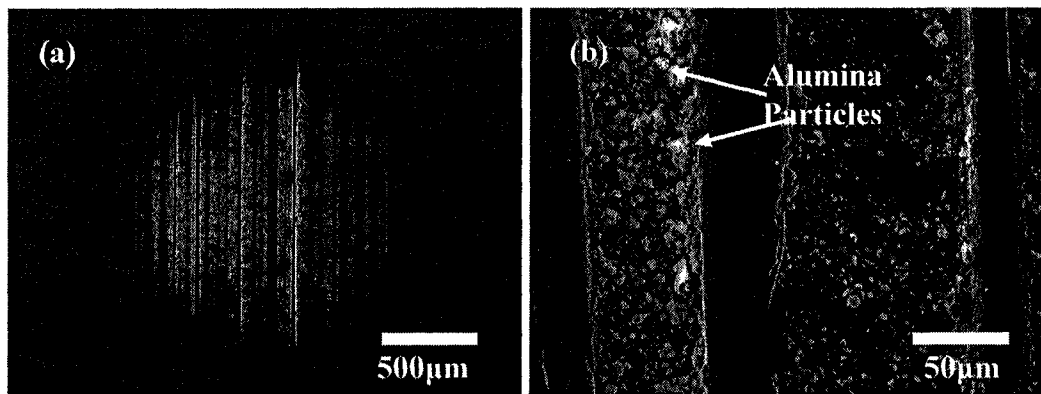
Fig. 6.6 SEM images of wear scar on CC2 substrate after micro-abrasion test under 4N load with 24m distance (a) 50×, (b) 500×
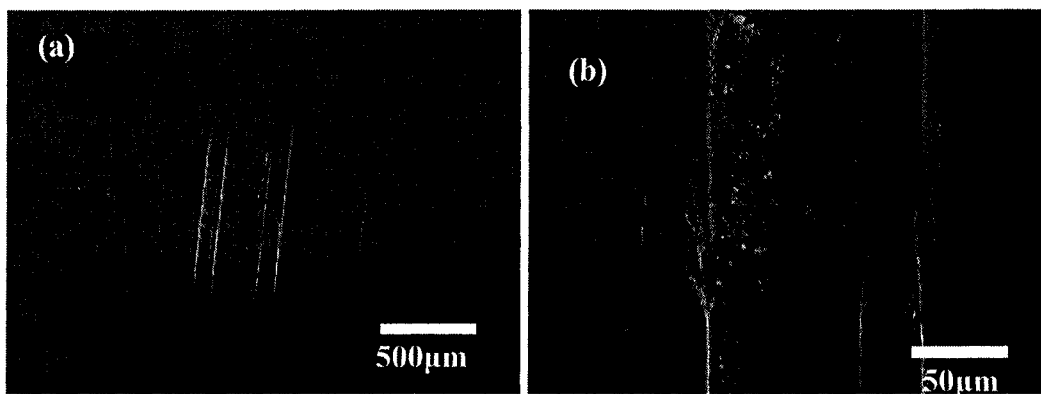
Fig. 6.7 SEM images of wear scar on D2 substrate after micro-abrasion test under 4N load with 24m distance (a) 50×, (b) 500×

138
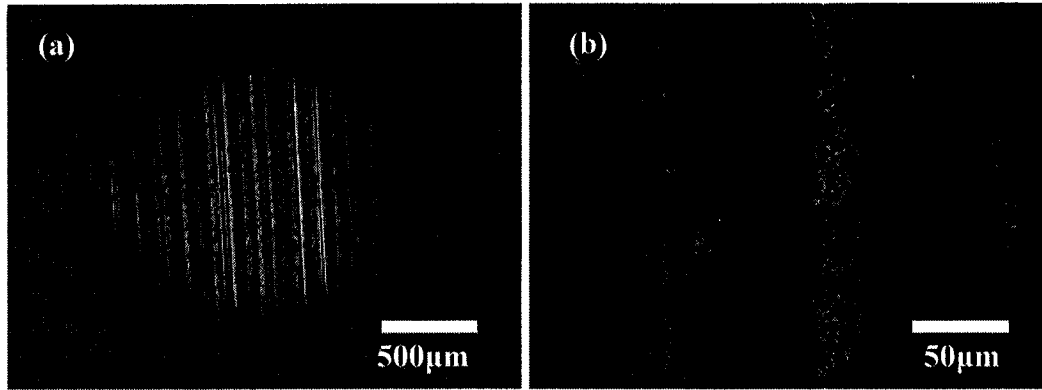
Fig. 6.8 SEM images of wear scar on 0050A substrate after micro-abrasion test under 4N load with 48m distance (a) 50×, (b) 500×
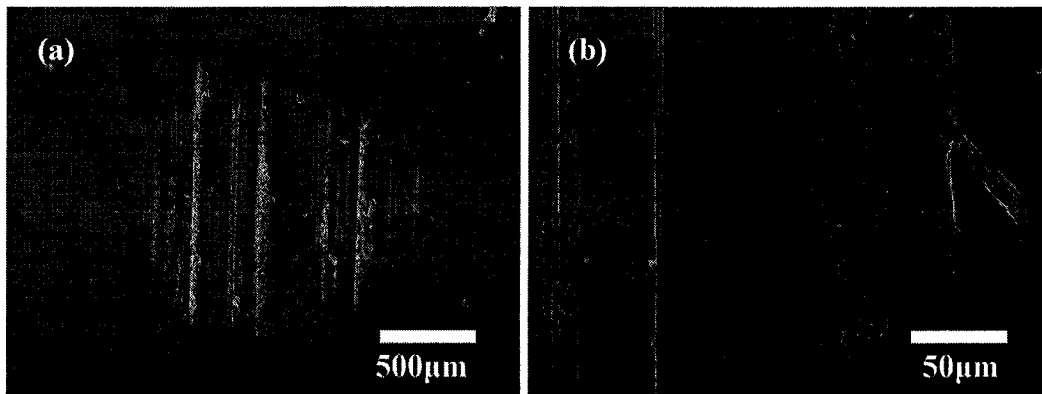
Fig. 6.9 SEM images of wear scar on G3500 substrate after micro-abrasion test under 4N load with 48m distance (a) 50×, (b) 500×
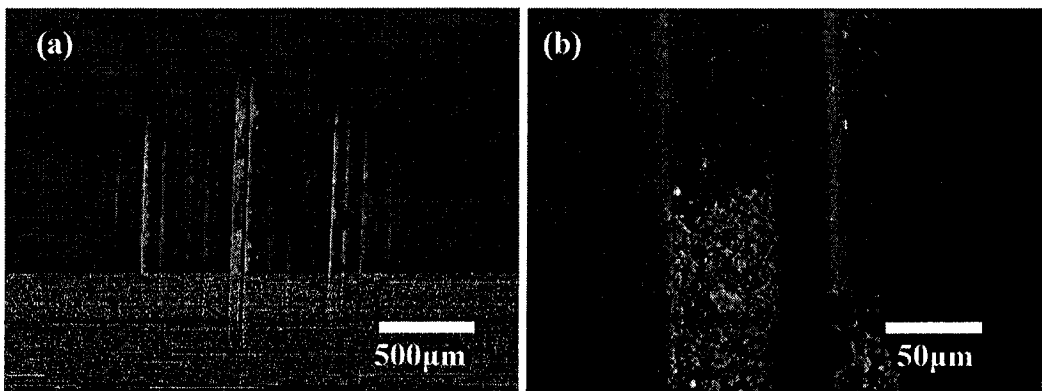
Fig. 6.10 SEM images of wear scar on CarmoCast substrate after micro-abrasion test under 4N load with 48m distance (a) 50×, (b) 500×

139
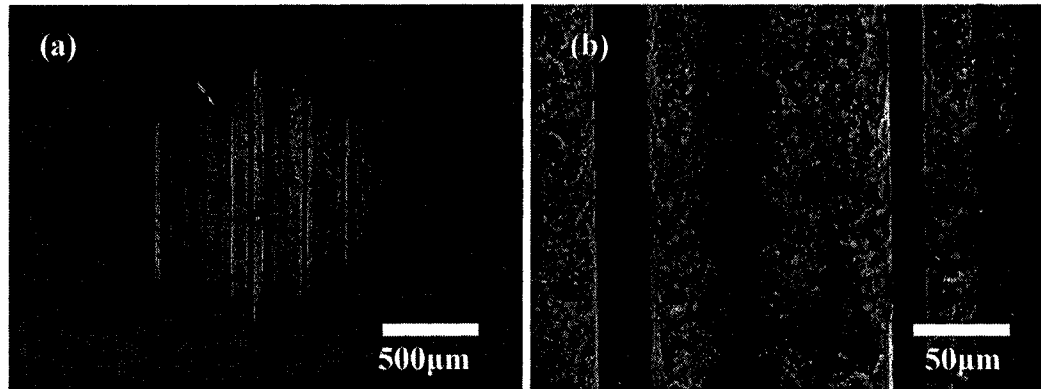
Fig. 6.11 SEM images of wear scar on CC2 substrate after micro-abrasion test under 4N

load with 48m distance (a) 50×, (b) 500×
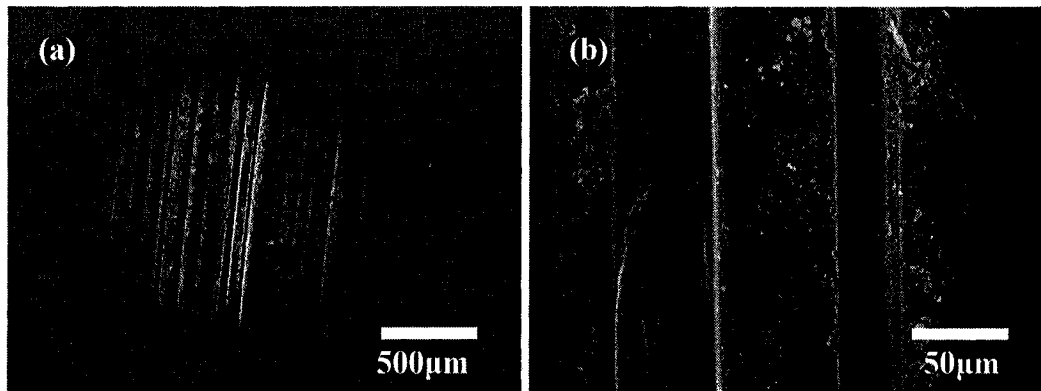
Fig. 6.12 SEM images of wear scar on D2 substrate after micro-abrasion test under 4N

load with 48m distance (a) 50×, (b) 500×

6.1.3 Surface profiles of wear scars on the 5 substrates

Figs 6.13 to 6.22 are surface profiles (maximum cross-section vertical to the sliding

direction) of wear scars on the 5 substrates after micro-abrasion test under 4N load after 2

minutes (24m distance) and 4 miniutes (48m distance). The dimensions of the wear scars

and the wear rates are summarized in Table 6.1. D2 exhibits the smallest wear scar and so

the smallest wear rate and CarmoCast has the deepest wear groove.

0050A-2min
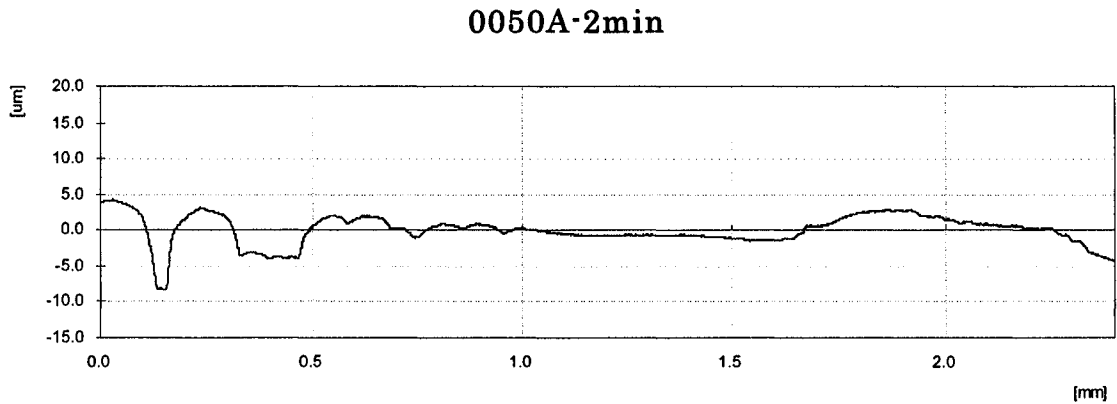
Fig. 6.13 Surface profile (maximum cross-section vertical to the sliding direction) of

wear scar on 0050A substrate after micro-abrasion test under 4N load after 2 minutes

(24m distance)

G3500-2min
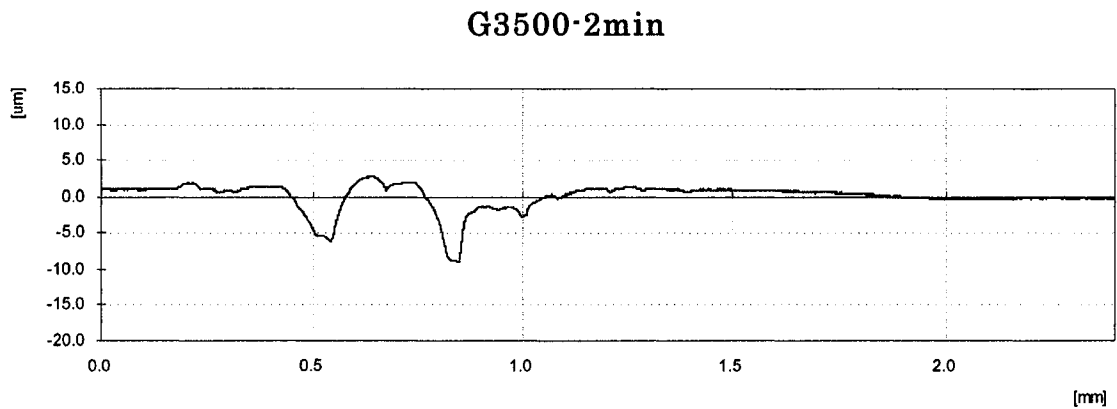
Fig. 6.14 Surface profile (maximum cross-section vertical to the sliding direction) of

wear scar on G3500 substrate after micro-abrasion test under 4N load after 2 minutes

(24m distance)

141

CarmoCast-2min

Fig. 6.15 Surface profile (maximum cross-section vertical to the sliding direction) of wear scar on CarmoCast substrate after micro-abrasion test under 4N load after 2 minutes (24m distance)

CC2-2min
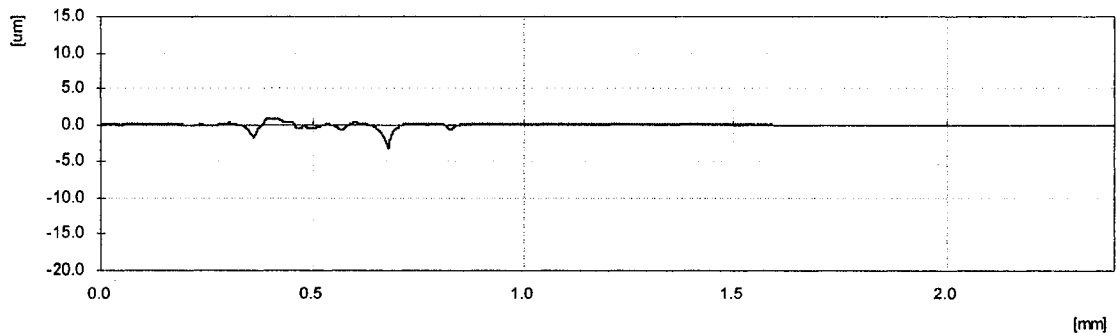
Fig. 6.16 Surface profile (maximum cross-section vertical to the sliding direction) of wear scar on CC2 substrate after micro-abrasion test under 4N load after 2 minutes (24m distance)

142

D2-2min
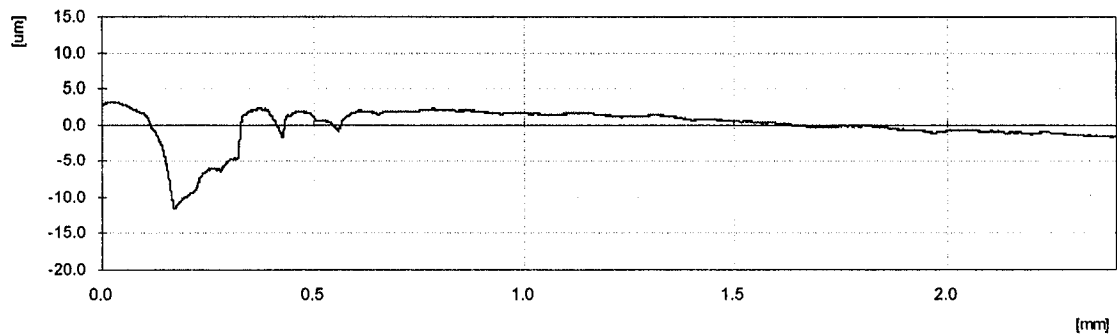
Fig. 6.17 Surface profile (maximum cross-section vertical to the sliding direction) of wear scar on D2 substrate after micro-abrasion test under 4N load after 2 minutes (24m distance)

0050A-4min
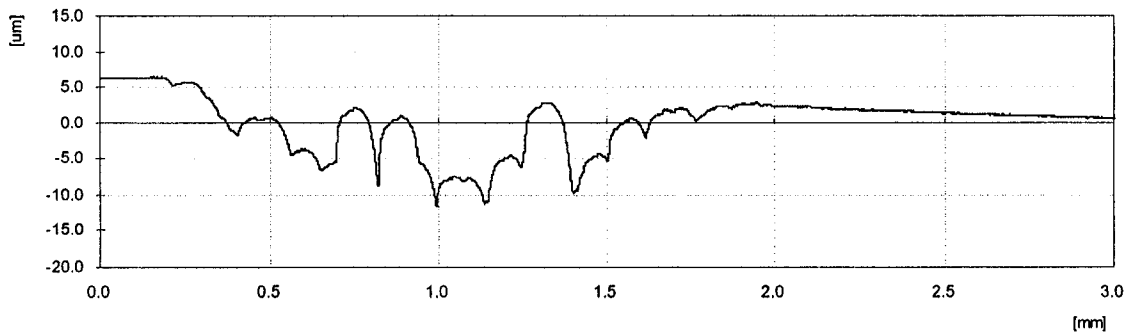
Fig. 6.18 Surface profile (maximum cross-section vertical to the sliding direction) of wear scar on 0050A substrate after micro-abrasion test under 4N load after 4 minutes (48m distance)

143

G3500-4min
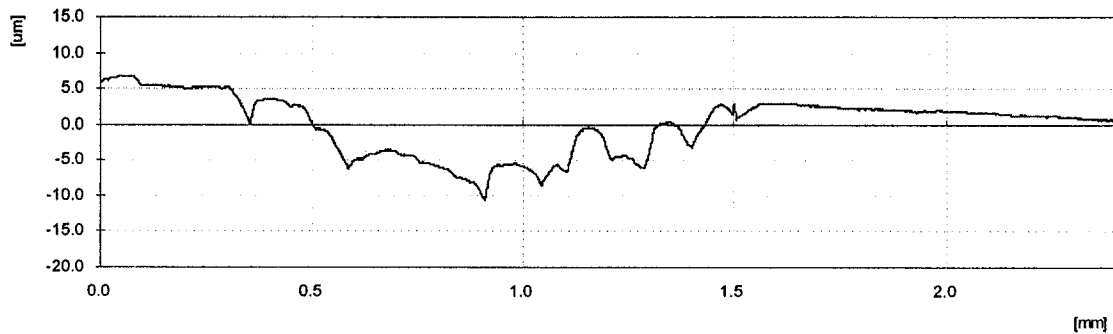
Fig. 6.19 Surface profile (maximum cross-section vertical to the sliding direction) of wear scar on G3500 substrate after micro-abrasion test under 4N load after 4 minutes (24m distance)

CarmoCast-4min
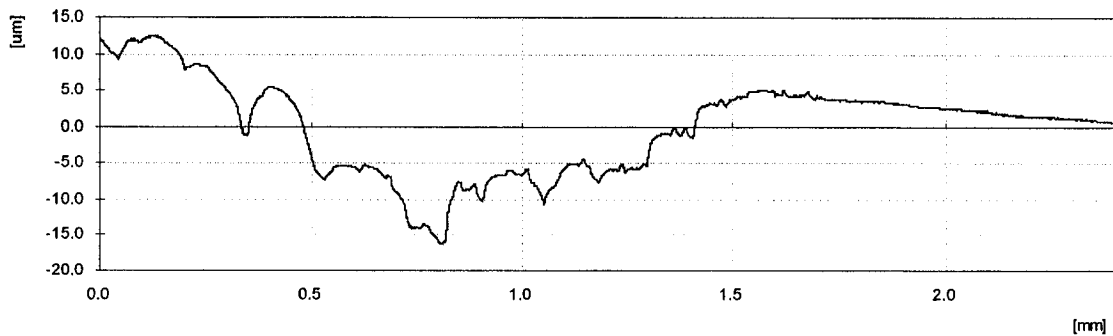
Fig. 6.20 Surface profile (maximum cross-section vertical to the sliding direction) of wear scar on CarmoCast substrate after micro-abrasion test under 4N load after 4 minutes (48m distance)

144

CC2-4min
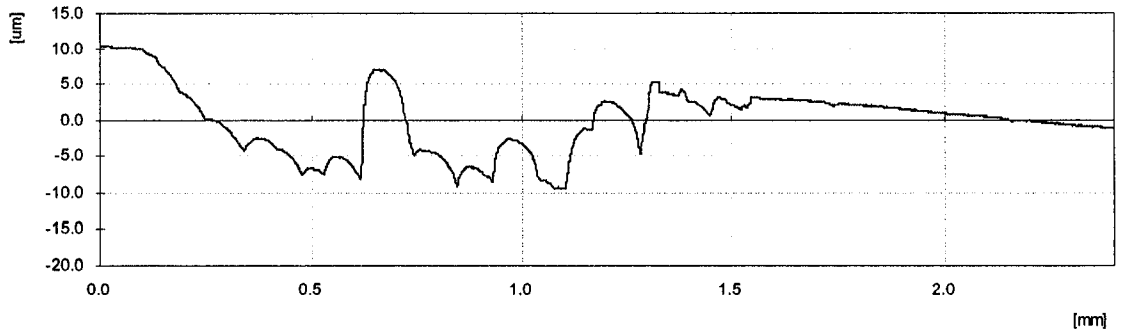
Fig. 6.21 Surface profile (maximum cross-section vertical to the sliding direction) of wear scar on CC2 substrate after micro-abrasion test under 4N load after 4 minutes (48m distance)

D2-4min
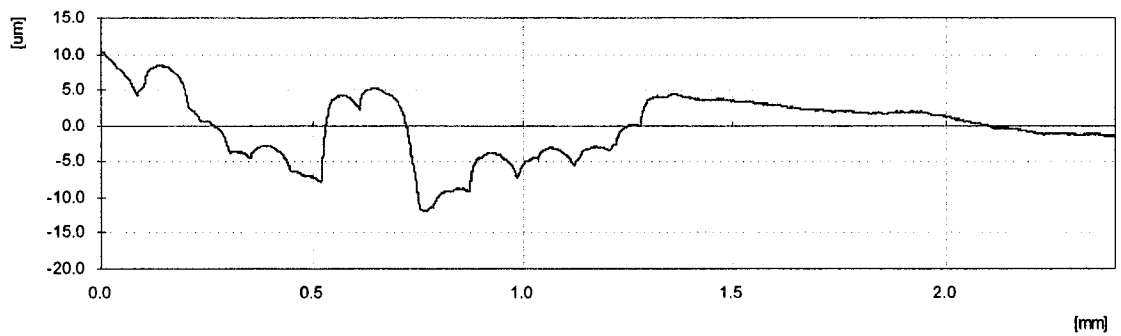
Fig. 6.22 Surface profile (maximum cross-section vertical to the sliding direction) of wear scar on D2 substrate after micro-abrasion test under 4N load after 2 minutes (24m distance)

145

Table 6.1 Dimensions of wear scars and wear rates of substrates after

micro-abrasion testing at 24m and 48m sliding distance under a 4N load

	Average Diameter (mm)		largest Depth (μm)		Wear Rate ($10^3 \mu m^3$/Nm)	
Sliding distance(m)	24m	48m	24m	48m	24m	48m
0050A	1.52	4.76	8.21	11.42	133.4	155.3
G3500	1.38	3.21	8.92	10.17	89.8	149.5
CarmoCast	1.59	5.73	5.95	15.28	160.3	180.4
CC2	1.57	5.47	3.13	8.79	153.2	132.9
D2	1.34	2.89	11.5	11.9	80.9	87.6

6.2 Micro-abrasion wear of coatings

6.2.1 SEM observation for micro-abrasion wear behaviors of coatings

Figs. 6.23 to 6.26 are SEM images of wear scars on the TiN and TiSiCN coatings after

micro-abrasion test under 4N load at 48m and 96m sliding distance. For the TiN coating,

microploughing is the dominant interaction between the abrasive particles and the coating

surfaces. For TiSiCN coating, cracks and server material peeling could be observed on

the wear scar surface, which shows that delamination or surface fatigue wear is the main

wear mechanism. The deepest depth of the cracked crater is about 2μm, which is much

less than the thickness of the coating (17μm). This result is consistent with the

performance observation for TiSiCN coating after pin-on-disc test against alumina under

5N in air.

146
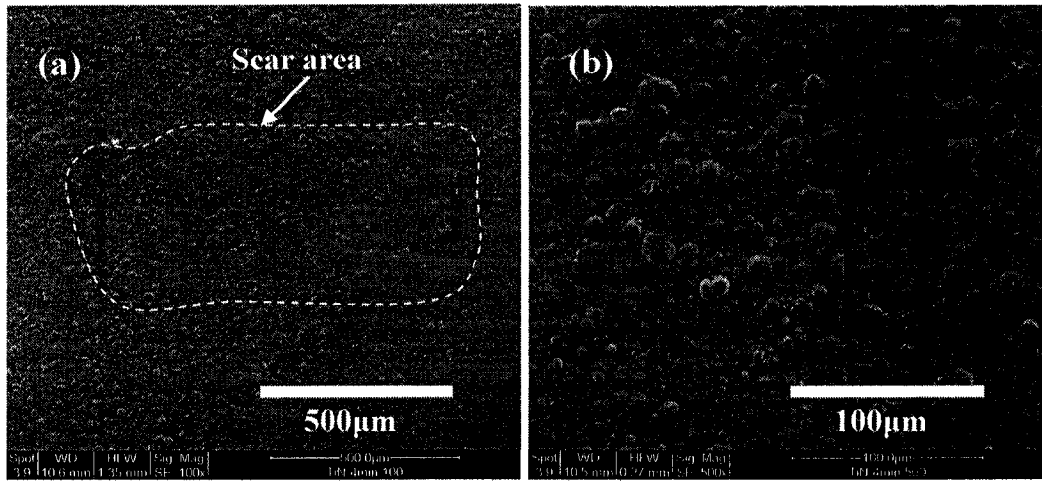
Fig. 6.23 SEM images of wear scar on TiN coating after micro-abrasion test under 4N load with 48m distance (a) 100×, (b) 500×
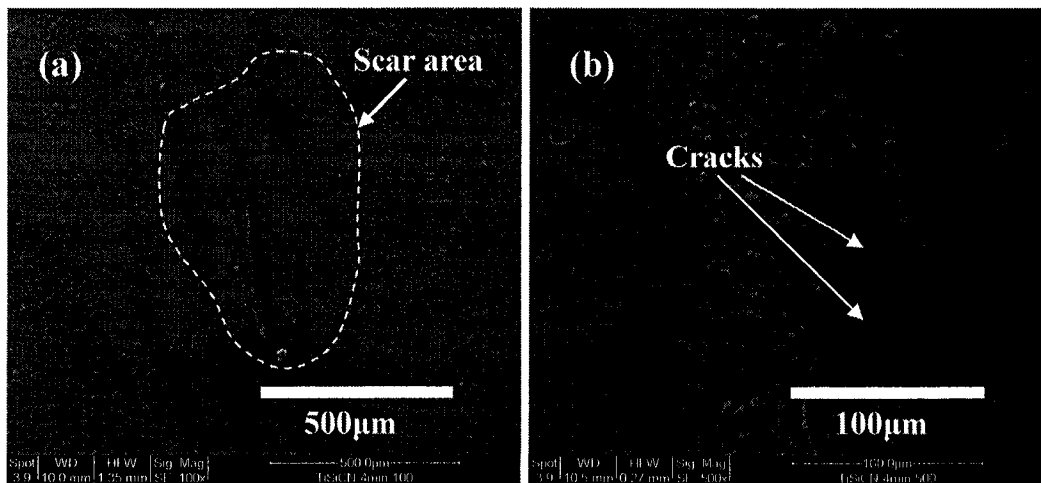
Fig. 6.24 SEM images of wear scar on TiSiCN coating after micro-abrasion test under 4N load with 48m distance (a) 100×, (b) 500×
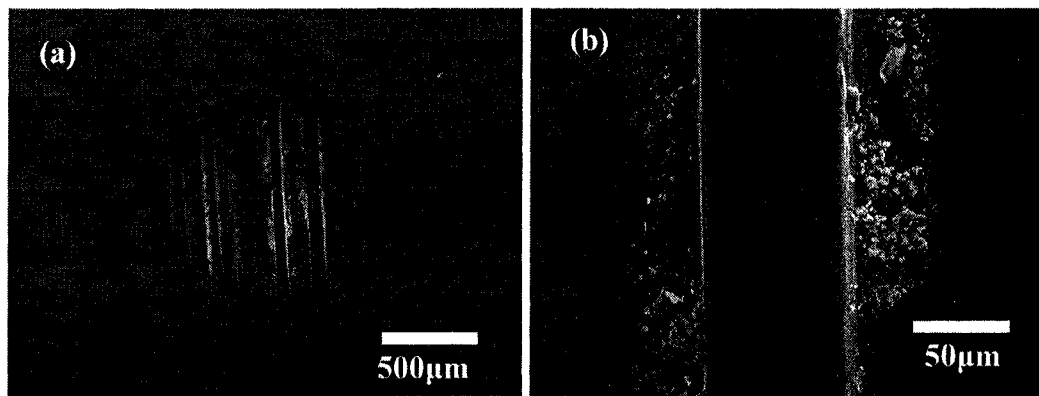
147
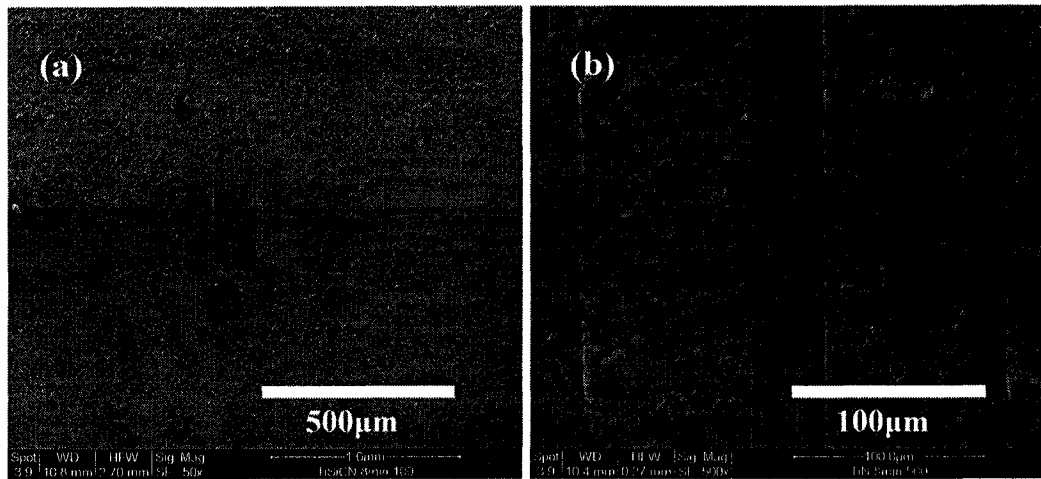
Fig. 6.25 SEM images of wear scar on TiN coating after micro-abrasion test under 4N load with 96m distance (a) 100×, (b) 500×
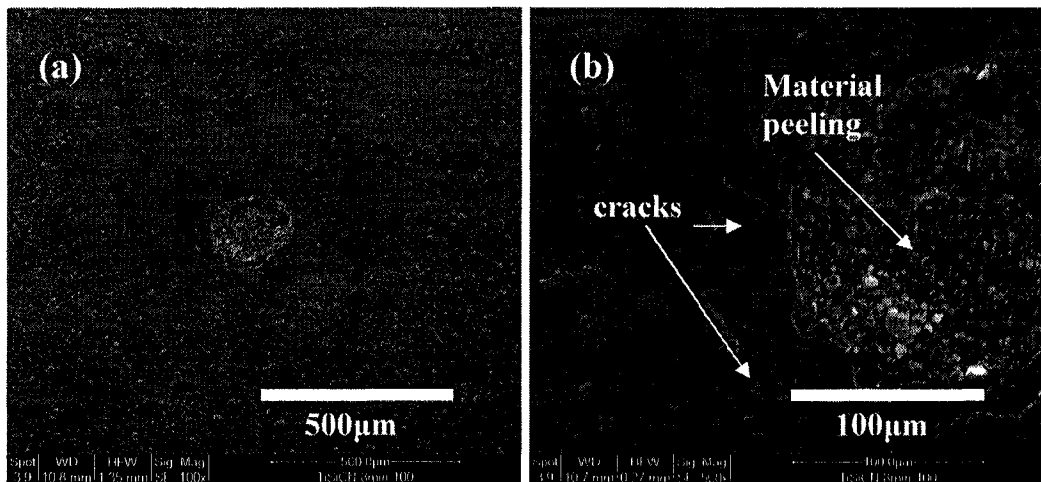
Fig. 6.26 SEM images of wear scar on TiSiCN coating after micro-abrasion test under 4N load with 96m distance (a) 100×, (b) 500×

6.2.2 Micro-abrasion wear rate of coatings

Fig. 6.27 shows the micro-abrasion wear rate of TiN and TiSiCN coatings only basing on the size of the wear scars occurring on the micro-abrasion wear test. It appears that

TiSiCN exhibit good abrasive wear resistance. But, the conclusion that TiSiCN has better abrasive wear resistance seems simple if the surface fatigue wear shown in Fig. 6.26 was considered. Obviously, by observing the real wear situation shown in Fig. 6.25 and 6.26, TiN has a better wear performance. This result is consistent with the result from the sliding wear test with alumina counterpart in air.

Wear Rate & Hardness

	Wear Rate	Hardness
■ Wear Rate	11.06	1.82
Hardness	31.66	42.39
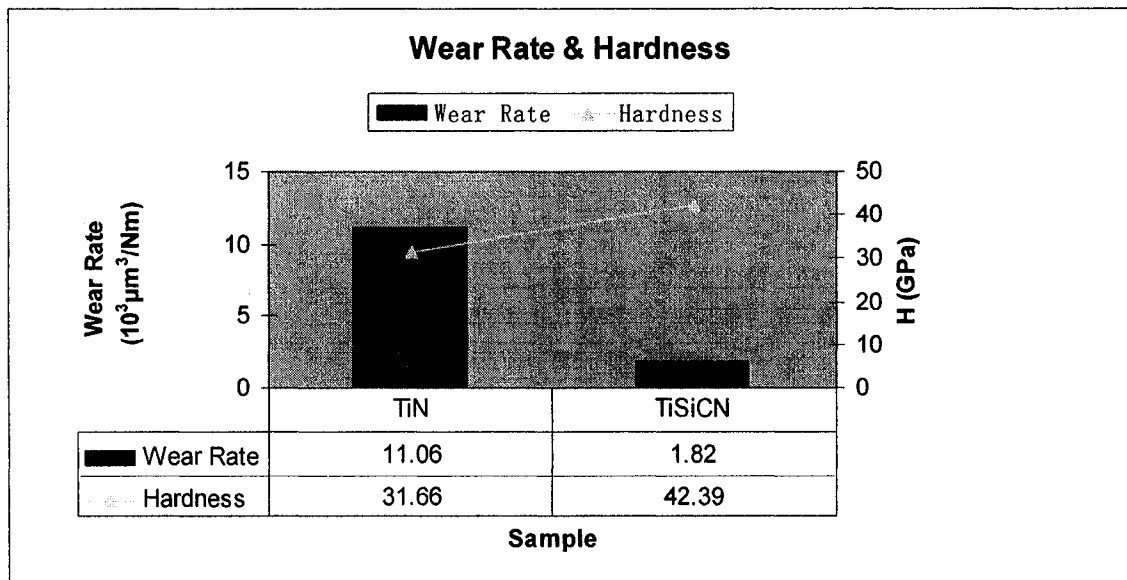
Fig. 6.27 Micro-abrasion wear rate of TiN and TiSiCN coatings with sliding distance of 96m and their hardness.

6.3 Summary

6.3.1 Micro-abrasion wear of substrates

(1) D2 displays the best micro-abrasion wear resistance due to its high hardness.

(2) At a shorter sliding distance (24m), G3500 exhibited good wear resistance which is similar to its behavior against alumina under 5N load in the pin-on-disc sliding wear test. This is attributed to the lubricating effect of graphite.

149

(3) Compared with the wear behavior in the sliding wear test, the substrates shows similar ranking of the micro-abrasion wear resistance in the group. This result suggests that micro-abrasion wear test method is an effective alternative measure for abrasive wear test for materials.

6.3.2 Micro-abrasion wear of coatings

(1) For TiN coating, microploughing is the dominant interaction between the abrasive particles and the coating surfaces.

(2) For TiSiCN coating, cracks and server material peeling could be observed on the wear scar surface, which shows that delamination or surface fatigue wear is the main wear mechanism. This result is consistent with the performance observation for TiSiCN coating after pin-on-disc test against alumina under 5N in air.

(3) TiN has a better micro-abrasion wear resistance than TiSiCN. This result is consistent with the result from the sliding wear test with alumina counterpart in air.

150

CHAPTER 7 SUMMARY AND RECOMMENDATION FOR

FUTURE WORK

In this thesis, five substrates materials 0050A, G3500, CarmoCast, CC2 and D2 are collected from different suppliers. All these materials are good candidates for the selection of die materials. Two coatings TiN and TiSiCN with thickness of 17μm and 47μm were deposited by an innovative deposition process, plasma enhanced magnetron sputtering (PEMS). These two coatings were selected as examples to explore improved wear performance of materials other than that of the traditional ones such as the substrate materials. In this study, the wear performance of substrates and coatings are comparatively investigated. Besides the performance of materials, an alternative testing means is explored. The correlation between two testing methods is also studied.

7.1 Sliding wear for substrates

The sliding wear performance of 5 substrates 0050A, G3500, CarmoCast, CC2 and D2 are comparatively studied. Following results could be concluded:

7.1.1 Hardness, counterpart and load effects on wear performance and wear mechanism

(1) For the wear performance of substrates against alumina pin under 5N load: Though G3500 has low hardness, it has relative low wear rate and this may benefit from the lubricating effect of graphite particles. 0050A has the highest value of hardness; however, it also exhibits the highest wear rate, probably due to the brittle martensite phase. For CarmoCast, CC2 and D2, the harder one has the better wear resistance. D2 presents the lowest wear. Abrasive wear mechanism dominates.

(2) For the wear performance of substrates against aluminium pin under 5N load: All the substrates have much lower wear rate than those against alumina pins under 5N. G3500 has the highest wear rate which could be counted on its low hardness. For G3500, CarmoCast, and D2, the harder material has the better wear resistance. Though it is harder, 0050A displays higher wear rate than D2, probably due to it brittle martensitic phase. D2 present the lowest wear rate. Adhesive wear mechanism dominates.

(3) For the wear performance of substrates against aluminium pin under 10N load: G3500 does not exhibit the highest wear rate due to its lowest hardness and it seems that it could benefit more from the lubricating effect of graphite particles under this test condition. For CarmoCast, D2 and 0050A, the anti-wear performance has the tendency that the harder the material is the better wear resistance it has. CC2 presents the lowest wear rate, probably due to a least chemical affinity to the aluminium pin. Adhesive wear mechanism dominates.

(4) For the wear performance of substrates against steel pin under 5N load: All the substrates except CarmoCast exhibit lower wear rate than those against alumina

152

and aluminium pins respectively under 5N load. G3500 exhibit low wear rate which could be attributed to the lubricating effect of graphite. 0050A exhibits the highest hardness, however, it displays higher wear rate than D2, probably due to its brittle martensite phase. For CarmoCast, CC2 and D2, the anti-wear performance has the tendency that the harder the material is the better wear resistance it has. D2 exhibits the lowest wear rate. Adhesive wear mechanism dominates.

(5) For the wear performance of substrates against steel pin under 15N load: All substrates exhibit higher wear rate compared with the tests against steel pins under 5N load. G3500 exhibit the highest wear rate due to its lowest hardness. For G3500, CarmoCast, CC2 and D2, the anti-wear performance has the tendency that the harder the material is the better wear resistance it has. Though 0050A has the highest value of hardness, it displays higher wear rate than D2, probably due to its brittle martensite phase. D2 exhibits the lowest wear rate. Fatigue wear or delamination wear mechanism dominates.

7.1.2 Graphite effect

(6) The effect of graphite of G3500 as a lubricant can be observed only under some conditions. If the Hertz contact pressure is as low as against aluminium under 5 N load or as high as against steel pin under 15N, the graphite can not make much difference to the wear performance of G3500. Only under conditions like against alumina under 5N, against aluminium pin under 10N and against steel under 5N, the lubricating effect or wear reduction effect could be obviously observed. It

153

seems that when the contact pressure is low, the wear is slight and only happens on the surface and graphite particles as a solid lubricant do involve in the wear process; when the contact pressure is high enough, the graphite will be worn out quickly, and it loses lubricating effects. However, for the Al at 5N load, transferred Al may cover the graphite on G3500 surface, resulting in no existence of solid lubricant. Thus, only when the contact pressure is within a certain range, the lubricating effect of graphite could be obviously observed.

7.1.3 Tribochemical effects

(7) From the EDX analysis for G3500 substrate: Some oxidation occurs on the wear surface after pin-on-disc test against alumina pin under 5N load. After pin-on-disc tests against aluminium pin under 5N and 10N load, no oxidation occurs on the wear track surface, however, the oxidized aluminium transferred from the pin could be found on the wear track surface after pin-on-disc tests against aluminium pin under 5N and 10N load. Some oxidation occurs on some area of the wear track surface as well as transferred oxidized iron from the counter pin could be found on the wear track surface after pin-on-disc tests against steel pin under 5 and 15N load.

(8) From the EDX analysis for CC2 substrate: No oxidation occurs on the wear track surface after pin-on-disc test against alumina pin under 5N load; After pin-on-disc tests against aluminium pin under 5N and 10N load, no oxidation occurs on the wear track surface, however, oxidized aluminium transferred from the pins could be found on the wear track surface. No oxidation occurs on the wear track surface,

however, oxidized iron transferred from the counter pin could be found on the wear track surface after pin-on-disc tests against steel pin under 5N load. Some oxidation occurs on some area of the wear surface as well as transferred oxidized iron from the counter pin could be found on the wear track surface after pin-on-disc tests against steel pin under15N load.

(9) From the EDX analysis of wear scars on counter pins after pin-on-disc test against G3500: All the tested areas of aluminium pins are oxidized after pin-on-disc tests against G3500 under 5N and 10N load. Some areas of steel pins are oxidized after pin-on-disc tests against G3500 under 5N and 15N.

7.1.4 Materials transfer effects

(10) In terms of the materials transfer resistance performance, D2 is the best either against aluminium or against steel under the testing conditions.

7.1.5 Supplier effects

(11) D2 has the best wear resistant performance in general.

(12) Although the quenching hardening process was done under a similar condition by another independent supplier, the substrates appear to have different hardness. Since the substrates have different hardness, the ranking of performance may not reflect the real performance of products from the suppliers.

7.2 Sliding wear for coatings

(1) Very thick TiN and TiSiCN coatings (17-45μm) were successfully deposited onto stainless steel substrates by Plasma Enhanced Magnetron Sputtering (PEMS) deposition technique.

(2) Both of the coatings had a high interface adhesion strength.

(3) In air, the TiSiCN coating exhibited a lower wear rate and a lower C. O. F than the TiN coating when tested against an aluminum pin, while it exhibited a higher wear rate and a lower C. O. F than the TiN coating when tested against an alumina ball. The aluminium pin also caused both TiN and TiSiN coatings to have a larger wear rate and larger C. O. F in air.

(4) In coolant, the wear rates of the coatings against the aluminiun pin (negligible) were smaller, instead of larger, than those against the alumina ball.

(5) The cutting coolant could provide a lubricant effect and thus reduce the adhesive wear between the coating and the counterpart, which led to decreased wear rate and reduced coefficient of friction (C. O. F).

(6) Material transfer and polishing are the main wear mechanisms for both coatings when tested against aluminium under 5N load in air.

(7) Polishing is the dominate mechanism for TiN coating when tested against alumina under 5N load in air. Polishing and surface fatigue are the dominant wear mechanisms for TiSiCN coating tested against alumina pin under 5N load in air.

(8) Surface polishing is the dominant wear mechanism for both coatings when tested in coolant, either against aluminium or alumina under 5N load.

(9) The abrasive wear rates for both coatings are much smaller than the wear rates for substrates. The wear rate of TiSiCN (which is greater than TiN) against alumina

156

in air under 5N is only about one-sixtieth of the wear rate of D2 (the smallest among 5 substrates) against alumina in air under 5N load.

Table 7.1 summarizes the wear mechanism (WM), wear resistance (WR) and material transfer resistance (MTR) for 5 substrates and 2 coatings against different counterparts under different loads in different environment conditions.

7.3 Micro-abrasion wear for substrates and coatings

7.3.1 Micro-abrasion wear test system design and construction

(1) The micro-abrasion wear test system is successfully designed and constructed.

(2) The system can automatically apply slurry under controlled flow dripping rate and can operate in free-ball and fixed ball loading modes.

(3) The system can be used to investigate micro-abrasive wear of substrate materials and coatings.

7.3.2 Micro-abrasion wear of substrates

(4) D2 displays the best micro-abrasion wear resistance due to its high hardness.

(5) With shorter distance (24m), G3500 exhibit good wear resistance which is similar to its behavior against alumina under 5N load in the pin-on-disc sliding wear test. The reason could be attributed to the lubricant effect of graphite.

(6) Comparing with the abrasive wear behavior in the sliding wear test, it could be found that the substrates have a similar performance in micro-abrasion wear tests.

157

7.3.3 Micro-abrasion wear of coatings

(4) For TiN coating, microploughing is the dominant interaction between the abrasive particles and the coating surfaces.

(5) For TiSiCN coating, cracks and server material peeling could be observed on the wear scar surface, which shows that delamination or surface fatigue wear is the main wear mechanism. This result is consistent with the performance observation for TiSiCN coating after pin-on-disc test against alumina under 5N in air.

(6) TiN has a better third-body micro-abrasion wear resistance than TiSiCN. This result is consistent with the result from the sliding wear test with alumina counterpart in air.

. 7.4 Recommendation for future work

(1) Since the tested substrate materials have different hardness and the hardness was found to have a significant influence on wear properties of substrates, it is necessary to minimize the influence of hardness on wear performance through the use of appropriate hardening process to obtain similar hardness for all substrates in the future study.

(2) By using the fixed ball micro-abrasion tester, the normal load applied on the samples can be adjusted. The micro-abrasion wear performance under different loads is a good subject for further study.

(3) TiSiCN coating has a higher hardness than TiN, however, TiSiCN coating shows a higher wear rate. The influence of toughness on wear performance and the technology to increase the toughness of coating will be of interest.

158

(4) The economy factor should be considered in the future to evaluate the overall performance of materials from different suppliers.

Table 7.1 Wear mechanism (WM), wear resistance (WR) and material transfer resistance (MTR) for 5 substrates and 2 coatings against different counterparts under different loads in different environment conditions

Pin/load	Alumina/5N		Al/5N			Al/10N			Steel/5N			Steel/15N	
	WM	WR	WM	WR	MTR	WM	WR	MTR	WM	WR	MTR	WM	WR
0050A	abrasive wear	fair	adhesive wear	good	good	adhesive wear	good	good	adhesive wear	excellent	good	fatigue wear	good
G3500		good		fair	good		fair	good		excellent	good		fair
CarmoCast		fair		good	good		fair	fair		fair	fair		fair
CC2		fair		good	excellent		good	excellent		good	excellent		good
D2		good		excellent	excellent		good	excellent		excellent	excellent		excellent

	Alumina/5N in air		Al/5N in air			Alumina/5N in coolant		Al/5N in coolant	
	WM	WR	WM	WR	AWR	WM	WR	WM	WR
TiN coating	polishing	Excellent	material transfer	good	good	polishing	excellent	polishing	excellent
TiSiCN coating	Polishing + surface fatigue wear	good	material transfer +polishing	excellent	excellent	polishing	excellent	polishing	excellent

REFERENCES

[1] K.H. Zum Gahr, Microstructure and wear of materials, Elsevier, New York 1987.

[2] A.R. Riahi, A.T.Alpas, Wear map for grey cast iron, Wear 255 (2003) 401-409.

[3] S. Lim, M.F. Ashby, Wear mechanism maps, Acta Metall. 35 (1987) 1-24.

[4] X. Nie, L. Wang, Z.C. Yao, L. Zhang, F. Cheng, Surf. & Coat. Technol. 200(2005) 1745-1750.

[5] J.J. Jeong, B.Y. Jeong, M.H. Kim, C. Lee, Surf. Coat. Technol. 150 (2002) 24.

[6] J. Baranowska, Surf. Coat. Technol. 100– 101 (1998) 271.

[7] C.X. Li, T. Bell, Wear 256 (2004) 1144.

[8] A.L. Yeroklin, X. Nie, A. Leyland, S.J. Dowey, A. Matthews, Surf. Coat. Technol. 122 (1999) 73.

[9] X. Nie, Q.K. Hao, J.M. Wei, J. Wuhan Univ. Technol. Mater. Sci. Edit. 11 (1996) 28.

[10] X. Nie, C. Tsotsos, A. Wilson, A.L. Yerokhin, A. Leyland, A. Matthews, Surf. Coat. Technol. 139 (2001) 135.

[11] Roland Hauert, Jorg Patscheider, Advanced Engineering Materials, 2000, 2, No5, 247-259

[12] C. Subramanian, K. N. Strafford, T.P. Wilks, L.P. Ward, J. Mater. Proc, Technol. 56 (1996) 385-397

[13] S.C. Lim, C.Y.H. Lim, K.S. Lee, Wear 181-183 (1995) 901-912

[14] W. Heinke, A. Leyland, A. Matthews, G. Berg, C. Friedrich, E. Broszeit, Thin solid Films 270 (1995) 431-438

[15] S. Wilson, A.T. Alpas, Surf. Coat. Technol. 94-95 (1997) 53-59

[16] K.L. Rutherford, S.J. Bull, E.D. Doyle, I.M. Hutchings, Surf. Coat. Technol. 80 (1996) 176-180

[17] D.V. Shtansky, E.A. Levashov, A.N. sheveiko, J.J. Moore, J. Mater. Synth. Proc. Vol. 6, No. 1, 1998, 61-72

[18] C. Rebholz, J.M. Schneider, A.A. Voevodin, J. Steinebrunner, C. Charitidis, S. Logothetidis, A. Leyland, A. Matthews, Surf. Coat. Technol. 113 (1999) 126-133

[19] V. Imbeni, C. Martini, E. Lanzoni, G. Poli, I.M. Hutchings, Wear 251 (2001) 997-1002

[20] S. Wilson, A.T. Alpas, Surf. Coat. Technol. 120-121 (1999) 519-527

[21] Y.Y. Guu, J.F. Lin, Surf. Coat. Technol. 85 (1996) 146-155

[22] S. PalDey, S.C. Deevi, Materials Science and Engineering A342 (2003) 58-79

[23] T. Polcar, R. Novak, P. Siroky, Wear 260 (2006) 40-49

[24] Y.L. Su, S.H. Uao, Z.L. Leu, C.S. Wei, C.T. Wu, Wear 213 (1997) 165-174

[25] T. Polcar, T. Kubart, R. Novak, L. Kopecky, P. Siroky, Surf. Coat. Technol. 193 (2005) 192-199

[26] D. V. Shtansky, E. A. Levashov, A. N. Sheveiko, J.J. Moore, J. Mater. Synth. Proc. Vol. 6. No. 1 (1998) 61-72

[27] J.H. Jeon, S.R. Choi, W.S. Chung, K.H. Kim, Surf. Coat. Technol. 188-189 (2004) 415-419

[28] D. Ma, S. Ma, K. Xu, Surf. Coat. Technol., 200 (2005) 382-386

[29] D. Ma, S. Ma, H. Dong, K. Xu and T. Bell, Thin Solid Films 496 (2006) 438-444

[30] D.H. Kuo, K.W. Huang, Thin Solid Films 394 (2001) 72-80

[31] D.H. Kuo, K.W. Huang, Thin Solid Films 394 (2001) 81-89

[32] D.H. Kuo, K.W. Huang, Thin Solid Films 419 (2002) 11-17

[33] F. Lang, Z. Yu, Surf. Coat. Technol. 145 (2001) 80-87

[34] F. Zhou, C. M. Suh, S.S. Kim, R. Murakami, Tribo. Lett. 13 (2002) 173-178

[35] M.G. Gee, A. Gant, I. Hutchings, R. Bethke, K. Schiffman, K. van Acker, S. Poulat, Y. Gachon, J. von Stebut, Wear 255 (2003) 1-13

[36] I. Sevim, I.B. Eryurek, Materials and Design 27 (2006) 173-181

[37] C. Leroy, K.I. Schiffmann, K. van Acker, J. von Stebut, Surf. Coat. Technol. 200 (2005) 153-156

[38] G. B. Stachowiak, G.W. Stachowiak, J.M. Brandt, Tribo. Int. 39 (2006) 1-11

[39] K. Adachi, I.M. Hutchings, Wear 258 (2005) 318-321

164

[40] K. Bose, R.J.K. Wood, Wear 258 (2005) 322-332

[41] G.B. Sta chowiak, G.W. Stachowiak, Wear 256 (2004) 600-607

[42] C.K.N. Oliveira, R.M. Munoz Riofano, L.C. Casteletti, Surf. Coat. Technol. 200
(2006) 5140-5144

[43] J.C.A Batista, C. Godoy, A. Matthews, Tribo. Int.35 (2002) 363-372

[44] K.L. Rutherford, I.M. Hutchings, Surf. Coat. Technol. 79 (1996) 231-239

[45] J.C.A Batista, A. Matthews, C. Godoy, Surf. Coat. Technol. 142-144 (2001) 1137-
1143

[46] J.C.A Batista, M.C. Joseph, C. Godoy, A. Matthews, Wear 249 (2002) 971-979

[47] R.C. Cozza, D.K. Tanaka, R.M. Souza, Surf. Coat. Technol. 201 (2006) 4242-4246

[48] T. Polcar, T. Kubart, R. Novak, L, Kopecky, P. Siroky, Surf. Coat. Technol. 193
(2005) 192-199

[49] R. Wei, E. Langa, C. Rincon, J.H. Arps, Surf. Coat. Technol. 201 (2006) 4453-4459

[50] W. Feng, D.Yan, J. He, G. Zhang, G. Chen, W. Gu, S. Zhang, Appl. Sur. Sci. 243 (2005) 204-213

[51] M.J. Neale, Tribology handbook, 2nd edition, Butterworth-Heinemann, Oxford 1995

[52] I. M. Hutchings, Tribology: friction and wear of engineering materials, London: CRC Press, 1992

[53] J. Zhang , A.T. Alpas, Acta Mater, 45 (1997) 513-528

[54] I.I. Garbar, Tribo. Int. 35 (2002) 749-755

[55] H. So, Wear 184 (1995) 161-167

[56] H. So, D.S. Yu, C.Y. Chuang, Wear 253 (2002) 1004-1015

[57] S.C. Lim, Tribo. Int. 35 (2002) 717-723

[58] J.N. Matossian, R. Wei, J. Vajo, G. Hunt, M. Gardos, G. Chambers, L. Soucy, D. Oliver, L. Jay, C.M. Tylor, G. Alderson, R. Komanduri, A. Perry, Surf. Coat. Technol. 108–109 (1998) 496.

[59] R.Wei, J.J. Vajo, J.N. Matossian, M.N. Gardos, Surf. Coat. Technol. 158–159 (2002) 465.

[60] S.V. Fortuna, Y.P. Sharkeev, A.P. Perry, J.N. Matossian, A. Shuleopov, Thin Solid Films 377–378 (2000) 512.

[61] W.C. Oliver, G.M. Pharr, J. Mater. Res. 7(1992)1564

[62] K. Taube, Quality management of Tribological Coatings – Properties and Testing Methods, Mat.-wiss. u. Werkstofftech. 31 (2000) 616-624

o   [63] Y.L. Su, W.H. Kao, Wear 223 (1998) 119-130

LIST OF PUBLICATIONS AND CONFERENCE

PRESENTATIONS RESULTING FROM THIS WORK

Publications resulting from this work:

H. Xu, X. Nie, R. Wei, "Tribological Behavior of a TiSiCN coating tested in air and coolant", Surface & Coatings Technology 201 (2006) 4236-4241

Conference presentations resulting from this work:

H. Xu, X. Nie, R. Wei, "Tribological Behavior of a TiSiCN coating tested in air and coolant", 33rd International Conference on Metallurgical Coatings and Thin Films (ICMCTF), San Diego, California, U.S.A., May 1-5, 2006,

VITA AUCTORIS

NAME: Hua Xu

PLACE OF BIRTH: Jilin, China

YEAR OF BIRTH: 1968

EDUCATION: Tsinghua University, China

                     1985-1990, B. Sc

                     Beijing University of Astronautics and Aerospace, China

                     1990-1993, M. A. Sc

                     University of Windsor, Canada

                     2005-2007, M. A. Sc